



## **TESIS DOCTORAL**

### **Rational design of high performance lithium iron phosphate positive electrodes with conducting polymer for lithium-ion batteries**

(Diseño racional de electrodos positivos de alto rendimiento de fosfato de litio y hierro con polímero conductor para baterías de ión litio)

Presentada por:  
**Daniel Cíntora Juárez**

Directores:

**Dr. José Luis Tirado Coello**  
*Catedrático de Universidad*

**Dr. Carlos Pérez Vicente**  
*Profesor Contratado Doctor*

**Dr. Shahzada Ahmad**  
*Investigador Abengoa Research*

DEPARTAMENTO DE QUÍMICA INORGÁNICA E INGENIERÍA QUÍMICA  
UNIVERSIDAD DE CÓRDOBA, 2016

TITULO: *Rational design of high performance lithium iron phosphate positive electrodes with conducting polymer for lithium-ion batteries (Diseño racional de electrodos positivos de alto rendimiento de fosfato de litio y hierro con polímero conductor para baterías de ión litio)*

AUTOR: *Daniel Cíntora Juárez*

---

© Edita: Servicio de Publicaciones de la Universidad de Córdoba. 2016  
Campus de Rabanales  
Ctra. Nacional IV, Km. 396 A  
14071 Córdoba

[www.uco.es/publicaciones](http://www.uco.es/publicaciones)  
[publicaciones@uco.es](mailto:publicaciones@uco.es)

---





**TÍTULO DE LA TESIS:**

Rational design of high performance lithium iron phosphate positive electrodes with conducting polymer for lithium-ion batteries

(Diseño racional de electrodos positivos de alto rendimiento de fosfato de litio y hierro con polímero conductor para baterías de ión litio)

**DOCTORANDO:**

Daniel Cíntora Juárez



## INFORME RAZONADO DEL/DE LOS DIRECTOR/ES DE LA TESIS

José Luis Tirado Coello, Catedrático, Carlos Pérez Vicente, Profesor Contratado Doctor, ambos miembros del Departamento de Química Inorgánica e Ingeniería Química de la Universidad de Córdoba, y el Dr. Shahzada Ahmad, Investigador de Abengoa Research (Sevilla) informan que la Tesis Doctoral presentada por

**Daniel Cíntora Juárez**, titulada

*Rational design of high performance lithium iron phosphate positive electrodes with conducting polymer for lithium-ion batteries*

*(Diseño racional de electrodos positivos de alto rendimiento de fosfato de litio y hierro con polímero conductor para baterías de ión litio)*

se ha realizado, dentro del Programa de Doctorado Materiales y Energía en el laboratorio de Química Inorgánica de la Universidad de Córdoba durante el desarrollo de un contrato según el artículo artículo 52 de los Estatutos de la Universidad de Córdoba con Abengoa Research, titulado *Nuevos materiales fosfatos para los cátodos de baterías de iones alcalinos de alto rendimiento*, con el que se ha contratado a **Daniel Cíntora Juárez**, y cuya selección tuvo en cuenta una adecuada formación previa del doctorando en el campo de investigación en el que se encuadra el trabajo, al haber realizado el Máster Erasmus Mundus *Materials for Energy Storage and Conversion (MES-C)*. La presente memoria reúne, a juicio de los directores, los requisitos exigidos, y ha dado lugar a más de tres artículos publicados en revistas científicas incluidas en el primer cuartil de la relación de revistas del ámbito de la especialidad con índice de calidad relativo y en tres de los cuales el doctorando es primer autor. Los directores informan además de la buena actitud y dedicación del doctorando a la Tesis, el alto grado de especialización que le han conferido las actividades experimentales, análisis de resultados y extracción razonada de conclusiones en un campo de gran actualidad, como ha sido el objeto de su trabajo, orientado hacia el desarrollo de materiales avanzados para el almacenamiento de energía.

Por todo ello, se autoriza la presentación de la tesis doctoral.

Córdoba, 8 de marzo de 2016

Firma de los directores



Fdo.: José L. Tirado Coello Fdo.: Carlos Pérez Vicente Fdo.: Shahzada Ahmad



Informe según el Journal Citation Reports para los artículos publicados incluidos en la presente memoria

Los artículos incluidos en la presente memoria fueron publicados en revistas cuya información de impacto se obtuvo del *Journal Citation Reports* de ISI web of Knowledge para el año 2014. La información se presenta en la siguiente tabla:

Journal	Impact factor	Category	Total Journals In Category	Journal Rank in Category	Quartile in Category
RSC Advances	3.840	CHEMISTRY, MULTIDISCIPLIN.	157	33	Q1
Physical Chemistry Chemical Physics	4.493	CHEMISTRY, PHYSICAL	139	32	Q1
Journal of Materials Chemistry A	7.443	CHEMISTRY, PHYSICAL	139	18	Q1
		ENERGY & FUELS	88	5	Q1
		MATERIALS SCI., MULTIDISCIPLIN.	259	20	Q1
Electrochimica Acta	4.504	ELECTROCHEM.	28	4	Q1





# Rational design of high performance lithium iron phosphate positive electrodes with conducting polymer for lithium-ion batteries

(Diseño racional de electrodos positivos de alto rendimiento de fosfato de litio y hierro con polímero conductor para baterías de ión litio)

Trabajo presentado para aspirar al grado de

Doctor en Química por:



Daniel Cíntora Juárez, MSc.

Dirigido por



Dr. José L. Tirado Coello



Dr. Carlos Pérez Vicente



Dr. Shahzada Ahmad



## Agradecimientos

Extiendo mi agradecimiento a las diversas personas e instituciones que me han apoyado durante la realización de este proyecto.

A mis directores de tesis, los doctores José Luis Tirado Coello, Carlos Pérez Vicente y Shahzada Ahmad, les doy las gracias por su confianza, por sus enseñanzas, por su paciencia y por toda su ayuda a lo largo de esta empresa. Sus experiencias, sus conocimientos y nuestras discusiones han aportado mucho a mi formación y me han brindado una visión más amplia acerca de la investigación científica.

Deseo expresar mi gratitud a Abengoa Reseach y a su director, el Dr. Manuel Doblare Castellano, por la ayuda recibida a través del convenio con la Universidad de Córdoba.

Agradezco a la Dra. Samrana Kazim por sus comentarios y sus sugerencias durante nuestro trabajo experimental y nuestras sesiones de discusión.

Al personal del Departamento de Química Inorgánica e Ingeniería Química y a los coordinadores del programa de doctorado “Materiales y Energía”, les doy las gracias por la oportunidad y por el apoyo brindado para realizar mi trabajo.

Le agradezco al personal del Servicio Central de Apoyo a la Investigación (SCAI) de la Universidad de Córdoba la ayuda para llevar a cabo los análisis SEM y XPS.

A los compañeros vecinos de la sección de Química Inorgánica, y a los estudiantes visitantes extranjeros, les doy las gracias por los buenos momentos vividos en el espacio de trabajo y fuera de este.

Muchas gracias a mis compañeros y a mis amigos del laboratorio FQM288-QEMI: Dr. Pedro Lavela Cabello, Dr. Ricardo Alcántara Román, Dr. Gregorio Ortíz Jiménez, Dra. María José Aragón Algarra, Dra. Candela Vidál-Abarca Garrido, Dr. Francisco Nacimiento Cobos, Dra. María del Carmen López Luna, Dr. José Ramón González Jiménez, Dra. María del Carmen Zafra Jiménez; los becarios Marta Cabello Bermúdez y Rafael Klee Morán; y a la técnico M<sup>a</sup> Carmen Mohedano Campos. Ha sido un gran gusto compartir experiencias y experimentos con vosotros durante estos años.

Mia dolcissima Maria, grazie per il tuo affetto, per il tuo aiuto e per stare vicina a me in tutti queste "primavere". Sia à Córdoba oppure in Italia, nel cuore, nella mente e anche attraverso Skype. In qualsiasi posto e in qualunque tempo io ti voglio bene!

Gracias desde el corazón a mis viejos: José y Adelina, a mis hermanos: Mónica y Humberto, y a mis sobrinos: Sofía y Hugo. A cada uno lo considero un gran ejemplo de vida con pasión, dedicación y alegría. Con vuestro cariño y apoyo, cada uno me ha ayudado desde siempre y en todo lugar a tirar pa'lante.

Dedicated to my family for their love and support,  
specially to my niece Sofía and to my nephew Hugo,  
who are powered by highly energetic "kids' batteries",  
and always have the power  
to instantly charge my spirit with their smiles!!!!

Es deseable que los avances en cierto campo se difundan  
y contribuyan al entendimiento y a la solución de problemas  
en otros campos...

**Migración:**

- Un tipo de transporte de carga que se relaciona a los iones y a la existencia de un gradiente de potencial en la solución. (Traducido de: *Electrochemical dictionary*, ISBN 978-3-540-74597-6)
- Desplazamiento geográfico de individuos o grupos, generalmente por causas económicas o sociales. (Diccionario de la lengua española, 23ª edición)



## Table of contents

<b>Summary</b>	<b>1</b>
<b>Resumen</b>	<b>6</b>
<b>Chapter 1: <u>Introduction</u></b>	<b>13</b>
<b>1.1 Electrochemical energy storage in batteries</b>	<b>15</b>
1.1.1 Primary batteries	18
1.1.2 Rechargeable batteries	20
<b>1.2 Lithium metal and Li-ion batteries</b>	<b>21</b>
1.2.1 Anode materials for Li-ion batteries	25
1.2.2 Cathode materials for Li-ion batteries	27
1.2.2-a Layered oxides: $\text{LiMO}_2$ ( $M$ : Mn, Co, Ni)	27
1.2.2-b Spinel-type compounds: $\text{LiM}_2\text{O}_4$ ( $M$ : Mn, Co, Ni)	29
1.2.2-c Phospho-olivines: $\text{LiMPO}_4$ ( $M$ : Fe, Mn, Co, Ni)	29
<b>1.3 Background on <math>\text{LiFePO}_4</math></b>	<b>31</b>
1.3.1 Crystalline structure and voltage of $\text{LiFePO}_4$	31
1.3.2 Electronic and ionic conductivity of $\text{LiFePO}_4$	33
1.3.3 Lithium extraction/insertion mechanisms of $\text{LiFePO}_4$	36
1.3.4 Synthesis of $\text{LiFePO}_4$	38
1.3.5 Improving the conductivity of $\text{LiFePO}_4$ and $\text{LiFePO}_4$ -based electrodes	40
1.3.5-a Carbon-coating	41
1.3.5-b Particle size reduction and morphology	43
1.3.5-c Conducting inorganic additives and coatings	43
1.3.5-d Coatings and films of intrinsically conducting polymers	45



<b>1.4 Overview of intrinsically conducting polymers</b>	<b>50</b>
1.4.1 Synthesis of ICPs	50
1.4.1-a Chemical polymerization	52
1.4.1-b Electrochemical polymerization	53
1.4.2 Doping and charge transport	54
1.4.3 General characteristics of PEDOT and PProDOT	56
<b>References</b>	<b>58</b>

**Chapter 2: Hypotheses, objectives and approaches** **69**

**Chapter 3: Improving the cycling performance of LiFePO<sub>4</sub> cathode material by poly(3,4-ethylenedioxythiophene) coating** **73**

1. Abstract & Introduction	75
2. Results and discussion	76
2.1 Characterization of LFP and LFP/C	76
2.2 Electrochemical properties	77
2.2.1 Initial charge–discharge performance	77
2.2.2 Slow vs. moderate rate performance	80
2.2.3 Charge–discharge polarization and cathode impedance	82
2.2.4 Extended cycling	84
3. Conclusions	86
4. Experimental section	87
References	89
Electronic supporting information (ESI)	91

**Chapter 4: Electrochemical in battery polymerization of poly(alkylenedioxythiophene) over lithium iron phosphate for high-performance cathodes** **93**

1. Abstract and Introduction	95
2. Results and discussion	97
2.1. In battery polymerization process	97
2.2. Mössbauer analysis	101
2.3. Battery cycling	103
2.4. EIS analysis	106
3. Conclusions	108
4. Experimental section	108
Notes and references	110
Electronic Supplementary Information (ESI)	111

**Chapter 5: Judicious design of lithium iron phosphate electrodes using poly(3,4-ethylenedioxythiophene) for high performance battery** **115**

1. Abstract & Introduction	117
2. Experimental section	119
3. Results and discussion	120
4. Conclusions	138
Notes and references	138
Electronic supplementary information (ESI)	141

**Chapter 6: Final conclusions** **145**  
**Conclusiones finales** **151**

<b>Appendix I:</b> <u>Comparison of the performance of LiFePO<sub>4</sub>-based composite electrodes with conducting polymer</u>	<b>159</b>
<b>Appendix II:</b> <u>Other scientific contributions related to the topic of the thesis</u>	<b>161</b>
- Solicitud de Patente: <u>Batería de iones alcalinos y método para producir la misma</u>	162
- Article: <u>LiFePO<sub>4</sub> particle conductive composite strategies for improving cathode rate capability</u>	163
- Article: <u>Effect of the degree of porosity on the performance of poly(vinylidene fluoride-trifluoroethylene)/poly(ethylene oxide) blend membranes for lithium-ion battery separators</u>	164
- Article: <u>Influence of Solvent Evaporation Rate in the Preparation of Carbon-Coated Lithium Iron Phosphate Cathode Films on Battery Performance</u>	165
- Article: <u>Truly quasi-solid-state lithium cells utilizing carbonate free polymer electrolytes on engineered LiFePO<sub>4</sub></u>	166
<b>Appendix III:</b> <u>Characterization techniques</u>	<b>167</b>
1. Galvanostatic battery cycling	168
2. Electrochemical impedance spectroscopy	171
3. X-ray photoelectron spectroscopy	174
4. Scanning electron microscopy	177
4. Mössbauer spectroscopy	180
References	184
<b>Appendix IV:</b> <u>Conference abstracts and posters</u>	<b>185</b>
<b>Appendix V:</b> <u>Author's biodata</u>	<b>193</b>





## Summary

Lithium iron phosphate ( $\text{LiFePO}_4$ ) is considered as a next-generation active material for lithium ion batteries. This material offers better thermal stability and higher power density than lithium cobalt oxide ( $\text{LiCoO}_2$ ). Currently, most of the advantages and limitations of  $\text{LiFePO}_4$  as a cathode material have been identified, and its performance has been progressively improved by optimizing the synthesis methods, in order to control the purity and to obtain carbon-coated nanoparticles. Nevertheless, a review on the recent progress on  $\text{LiFePO}_4$ -based electrodes shows that there is still opportunity for improving the composition and preparation methods at the electrode level, which is necessary in order to maximize the capacity at high charge/discharge rates.

For addressing the performance issues at the electrode level, this thesis is focused on the improvement of the conductivity of  $\text{LiFePO}_4$ -based electrodes in order to achieve better charge transport throughout the different electrode interphases and to ultimately improve the rate capability. In order to promote a more effective charge transport, the general strategy followed in this thesis consisted in the preparation of composite electrodes with intrinsically conducting polymers of the type poly(3,4-alkylenedioxythiophene). This type of polymers can be applied to form conductive coatings and networks that improve the connection between  $\text{LiFePO}_4$  particles and their contact to the current collector.

Diverse electrochemical polymerization, blending and coating methods were devised and applied to obtain  $\text{LiFePO}_4$ -based electrodes that incorporate a coating or a network of conducting polymer. The different methods proposed were published in peer-reviewed articles that are included in this thesis as individual chapters.

Two innovative electrochemical polymerization methods were devised for preparing composite electrodes of  $\text{LiFePO}_4$  with conducting polymer. The first approach for the electrochemical preparation of the composite electrodes (Chapter 3) consisted in the formation of a coating by potentiostatic electropolymerization of 3,4-ethylenedioxythiophene (EDOT) over a pre-formed working electrode, based either on  $\text{LiFePO}_4$  (uncoated) or  $\text{LiFePO}_4/\text{C}$  (carbon-coated). The potentiostatic electropolymerization of EDOT was carried out in an acetonitrile medium with tetraethylammonium tetrafluoroborate. The experimental conditions of the potentiostatic

electropolymerization enabled forming a PEDOT conducting polymer coating over the active material particles, resulting in mechanically stable electrodes of better electrochemical performance than the electrode based on  $\text{LiFePO}_4$  without conducting polymer. This improvement was attributed to the lower electrical resistance of the composite electrode with conducting polymer, as estimated by means of electrochemical impedance spectroscopy and manifested as a low charge/discharge polarization. The PEDOT-coating over  $\text{LiFePO}_4$  offered the possibility of obtaining an electrochemical performance at 1C and 2C superior to that of the electrode with carbon-coated  $\text{LiFePO}_4$ , and comparable to that observed for the  $\text{LiFePO}_4$  electrode with carbon-coating and PEDOT-coating. Thus, the possibility of replacing the classical carbon-coating by PEDOT-coating was demonstrated.

The second approach for preparing composite electrodes by electrochemical polymerization consisted in the galvanostatic oxidation of EDOT or 3,4-propylenedioxythiophene (ProDOT) monomers over a  $\text{LiFePO}_4$ -based electrode during the initial charging cycles in a test battery (Chapter 4). This novel approach was designated as *in battery* because the polymerization is carried out inside the battery. The *in battery* method is based on the oxidative polymerization of monomers over de-lithiated  $\text{LiFePO}_4$  ( $\text{Li}_{1-x}\text{FePO}_4$ ,  $0 < x < 1$ ), which is formed during the battery charging. In this way, there is no need of using any additional oxidizing compound to carry out the polymerization inside the battery. By the end of the battery charging, the conducting polymer coating covers the delithiated  $\text{LiFePO}_4$  and the surface of the electrode. The  $\text{Fe}^{2+}$  to  $\text{Fe}^{3+}$  oxidation in  $\text{Li}_{1-x}\text{FePO}_4$  was monitored by Mössbauer spectroscopy, which revealed that this oxidation process is more efficient upon the formation of the conducting polymer coating. Upon discharge of the battery, the reduction of  $\text{Fe}^{3+}$  to  $\text{Fe}^{2+}$  and the lithium reinsertion are facilitated by the conducting polymer coating.

The *in battery* electrochemical polymerization can be carried out either in one or in two charging steps. Both variations of the *in battery* method produced cathodes with higher initial capacity, superior charge/discharge rate performance, as well as a more extended cycleability than the uncoated  $\text{LiFePO}_4$ -based electrode. The superior electrochemical performance of the composite electrodes with conducting polymer was attributed to the lower resistance of the electrode due to the improvement of the

connectivity between the active material particles, promoted by the conducting polymer coating. Due to the usefulness, novelty and simplicity of the one- and the two-steps *in battery* electropolymerization methods, a patent application was filed (see Appendix II-1).

Regarding the preparation of composite electrodes with  $\text{LiFePO}_4$  and conducting polymer by blending, this procedure was implemented for PEDOT obtained from two different sources: i) PEDOT synthesized by electrochemical polymerization, and ii) PEDOT:PSS (PSS: polystyrene sulfonate), which is commercially available and is produced by chemical polymerization.

PEDOT synthesized electrochemically was prepared by a potentiostatic polymerization method, previously reported, over a platinum electrode in an  $\text{H}_2\text{O}/\text{CH}_2\text{Cl}_2$  medium with tetraethylammonium tetrafluoroborate. These conditions allowed obtaining a porous polymer film of PEDOT. Blending  $\text{LiFePO}_4$  or  $\text{LiFePO}_4/\text{C}$  with electrochemically synthesized PEDOT resulted in an easy and effective way for preparing stable and active composite electrodes, without the need of using extra conducting or agglomerating additives. Although this type of composite electrodes showed a better charge/discharge performance, as compared to previously reported composites with electrochemically synthesized PEDOT, the potentiostatic method to synthesize the polymer has a low yield.

The blending method using PEDOT:PSS (Chapter 5) consisted in incorporating the conducting polymer as an additive for  $\text{LiFePO}_4$ -based electrodes. PEDOT:PSS was incorporated to the composite electrode by blending the polymer in different proportions with a mixture of  $\text{LiFePO}_4$ , carbon black and polyvinylidene fluoride (PVDF) binder. It was found that the presence of 1% w/w of PEDOT:PSS within the bulk of the electrode resulted in a two-fold increase of the capacity and in an increase of the discharge plateau voltage in ca. 0.5 V at 5C, as compared to the electrode without conducting polymer at the same charge/discharge rate.

In order to further increase the conductivity of PEDOT:PSS, a minute amount of ethylene glycol or dimethyl sulfoxide secondary dopants was dissolved in the polymer dispersion. The initial discharge profiles of the electrodes with doped PEDOT:PSS



showed that only ethylene glycol had a small effect on the charge/discharge voltage, whereas dimethyl sulfoxide had no effect. The Mössbauer spectroscopy analysis showed that the oxidation of  $\text{Fe}^{2+}$  to  $\text{Fe}^{3+}$  upon battery discharge at a rate of C/10 is up to 10 % more efficient in the electrode that contains PEDOT:PSS doped with ethylene glycol, as compared to the conventional  $\text{LiFePO}_4$  electrode. This effect was attributed to a higher proportion of the PEDOT phase (electronic conductor) relative to the PSS phase (ionic conductor), as determined by quantitative analysis of XPS spectra.

Additionally, approximated resistance values of the electrodes in charged and in discharged states were obtained from the fitting of impedance spectra. These analyses provided evidence on the more effective electrochemical reaction of the active material promoted by the presence of 1% w/w of PEDOT:PSS mixed conductor, both in undoped state and when treated with ethylene glycol. These electrodes provide almost 50% of the theoretical capacity of  $\text{LiFePO}_4$  in only 6 minutes with a low charge/discharge polarization and showed excellent capacity retention at 2C during 50 charge/discharge cycles.

PEDOT:PSS was also tested as a conductive coating for the aluminium current collector of  $\text{LiFePO}_4$ -based electrodes. This polymer coating was realized by drop casting PEDOT:PSS over the current collector. Conductivity enhancement by treatment with ethylene glycol resulted in a high capacity with relatively low charge/discharge polarization at high charge/discharge rates. The correlation between the initial impedance, the direct current load resistance and the capacity at moderate and high rates of the electrodes containing PEDOT:PSS, showed that the interphase between the electrode layer and the current collector has the highest impact on the performance in  $\text{LiFePO}_4$ -based electrodes.

We elucidated that the use of ethylene glycol-doped PEDOT:PSS coating over the current collector is the best strategy among all the procedures described in this thesis for improving the performance of  $\text{LiFePO}_4$  composite electrodes with conducting polymer.

In general, the strategies developed and used for producing composite electrodes with  $\text{LiFePO}_4$  and conducting polymer by *in battery* methods and using PEDOT:PSS, as

presented in this thesis, are simple and could be implemented with slight modifications to the current methods for producing  $\text{LiFePO}_4$ -based electrodes.

## Resumen

El fosfato de litio y hierro ( $\text{LiFePO}_4$ ) es considerado como un material activo de nueva generación para baterías de iones litio. Este material ofrece mejor estabilidad térmica y mayor densidad de potencia comparado con el óxido de cobalto y litio ( $\text{LiCoO}_2$ ). Actualmente, la mayoría de las ventajas y limitaciones del  $\text{LiFePO}_4$  han sido identificadas y su desempeño se ha ido mejorando progresivamente mediante la optimización de los métodos de síntesis, buscando controlar la pureza y la obtención de nanopartículas cubiertas de carbón. A pesar de lo anterior, una revisión de los avances recientes sobre electrodos basados en  $\text{LiFePO}_4$  muestra que aún es posible mejorar la composición y los métodos de preparación a nivel del electrodo, lo cual es necesario para maximizar la capacidad a tasas altas de carga/descarga.

Para abordar la problemática del funcionamiento a nivel del electrodo, esta tesis se enfoca en la mejora de la conductividad de electrodos basados en  $\text{LiFePO}_4$  para lograr un mejor transporte de carga a través de las diferentes interfaces del electrodo, y así aumentar el desempeño en carga/descarga. Para promover un transporte de carga más efectivo, la estrategia general que se siguió en esta tesis consistió en la preparación de electrodos compuestos con polímeros conductores del tipo poli(3,4-alquilendioxitiofeno). Con este tipo de polímeros conductores se pueden formar recubrimientos y redes conductoras que mejoran la conexión entre partículas de  $\text{LiFePO}_4$  y el contacto de éstas con el colector de corriente.

Diversos métodos de polimerización electroquímica, mezclado y recubrimiento, fueron desarrollados y empleados para preparar electrodos basados en  $\text{LiFePO}_4$  que incorporan un recubrimiento o una red de polímero conductor. Los diferentes métodos propuestos fueron publicados en artículos arbitrados que se incluyen en esta tesis como capítulos individuales.

Dos métodos novedosos de polimerización electroquímica se desarrollaron para preparar electrodos compuestos de  $\text{LiFePO}_4$  con polímero conductor. La primera aproximación para preparar electrodos compuestos por vía electroquímica (Capítulo 3) consistió en la formación de un recubrimiento mediante electropolimerización potencioestática de 3,4-etilendioxitiofeno (EDOT) sobre un electrodo basado en  $\text{LiFePO}_4$  (sin cubrir) o en  $\text{LiFePO}_4/\text{C}$  (cubierto de carbón).

La polimerización del monómero EDOT se llevó a cabo a potencial fijo en un medio de acetonitrilo con tetrafluoroborato de tetraetilamonio y empleando electrodos  $\text{LiFePO}_4$  o  $\text{LiFePO}_4/\text{C}$  preformados. Las condiciones experimentales de la electro-polimerización potencioestática permitieron la formación de un polímero conductor sobre las partículas de material activo, lo que resultó en electrodos mecánicamente estables y de mejor desempeño electroquímico que el electrodo  $\text{LiFePO}_4$  sin recubrimiento de polímero conductor. Dicha mejora se atribuyó a la menor resistencia eléctrica a causa de la presencia del polímero conductor, como se determinó mediante espectroscopía de impedancia electroquímica, y que se manifiesta en una menor polarización de carga/descarga. El recubrimiento de PEDOT sobre  $\text{LiFePO}_4$  ofreció la posibilidad de obtener un desempeño electroquímico a 1C y 2C superior al desempeño del  $\text{LiFePO}_4$  con recubrimiento de carbón y comparable a lo observado para el electrodo  $\text{LiFePO}_4$  con recubrimiento de carbón y PEDOT. Por tanto, se demostró la posibilidad de reemplazar el recubrimiento de carbón por un recubrimiento de PEDOT.

La segunda aproximación para preparar electrodos mediante polimerización electroquímica, consistió en la oxidación galvanostática de monómeros EDOT o monómeros 3,4-propilendioxitiofeno (ProDOT) sobre un electrodo basado en  $\text{LiFePO}_4$  durante los ciclos iniciales de carga en una batería de prueba (Capítulo 4). Este método novedoso fue designado como *in battery*, debido a que la polimerización se lleva a cabo dentro de la batería. El método *in battery* se basa en la polimerización oxidativa de los monómeros sobre  $\text{LiFePO}_4$  delitiado ( $\text{Li}_{1-x}\text{FePO}_4$ ,  $0 < x < 1$ ), el cual se forma durante la carga de la batería. De esta forma, no es necesario añadir ningún compuesto oxidante adicional para efectuar la polimerización dentro de la batería. Al término de la carga de la batería, el polímero conductor cubre al  $\text{LiFePO}_4$  oxidado y a la superficie del electrodo. La oxidación de  $\text{Fe}^{2+}$  a  $\text{Fe}^{3+}$  en  $\text{Li}_{1-x}\text{FePO}_4$  se siguió mediante espectroscopia Mössbauer, la cual reveló que este proceso de oxidación es más eficiente al formarse el recubrimiento de polímero conductor. Al descargar la batería, el recubrimiento de polímero conductor facilita la reducción de  $\text{Fe}^{3+}$  a  $\text{Fe}^{2+}$  y la reinsertión de litio.

La polimerización electroquímica *in battery* se puede efectuar ya sea en uno o en dos pasos de carga. Ambas variaciones del método *in battery* producen cátodos con capacidad inicial más alta, mejor funcionamiento a tasa de carga/descarga, además de

mayor fiabilidad al ciclar comparado con el electrodo basado en  $\text{LiFePO}_4$  sin recubrimiento. El desempeño electroquímico superior de los electrodos compuestos con polímero conductor fue atribuido a la menor resistencia debido a la mejora de la conectividad entre las partículas de material activo, promovida por el recubrimiento de polímero conductor. Debido a la utilidad, novedad y simplicidad del método de electropolimerización *in battery* en uno o en dos pasos, se solicitó una patente (véase Appendix II-1)

Con respecto a la preparación de electrodos compuestos con  $\text{LiFePO}_4$  y polímero conductor mediante mezclado, este procedimiento se aplicó para PEDOT obtenido de dos fuentes distintas: i) PEDOT sintetizado mediante polimerización electroquímica, y ii) PEDOT:PSS (PSS: poliestireno sulfonato), el cual es un producto comercial y se produce mediante polimerización química.

El PEDOT sintetizado por vía electroquímica se preparó mediante un método de polimerización potencioestático, reportado previamente, sobre un electrodo de platino en un medio de  $\text{H}_2\text{O}/\text{CH}_2\text{Cl}_2$  con tetrafluoroborato de tetraetilamonio. Estas condiciones permitieron obtener una película porosa de PEDOT. La mezcla de  $\text{LiFePO}_4$  o  $\text{LiFePO}_4/\text{C}$  con PEDOT sintetizado por vía electroquímica resultó en una manera sencilla y efectiva para preparar electrodos compuestos estables y activos, sin necesidad de emplear aditivos conductores o aglomerantes extra. A pesar de que este tipo de electrodos compuestos mostró un mejor funcionamiento en carga/descarga, comparado con electrodos que contienen PEDOT sintetizado por vía electroquímica reportados previamente, este método para sintetizar el polímero tiene un bajo rendimiento.

El método de mezclado empleando PEDOT:PSS (Capítulo 5) consistió en la incorporación del polímero conductor como un aditivo para electrodos basados en  $\text{LiFePO}_4$ . El PEDOT:PSS fue incorporado al electrodo compuesto combinándolo en diferentes proporciones con una mezcla de  $\text{LiFePO}_4$ , negro de carbono y aglomerante fluoruro de polivinilideno (PVDF). Se encontró que la presencia de 1% w/w de PEDOT:PSS en el seno del electrodo duplicó la capacidad y aumentó el voltaje de la meseta de descarga en unos 0.5 V, comparado con el electrodo sin polímero conductor a la misma tasa de carga/descarga.

En un intento por incrementar la conductividad del PEDOT:PSS, se disolvieron pequeñas cantidades de etilenglicol o dimetilsulfóxido en la dispersión de polímero. Los perfiles iniciales de descarga de los electrodos con PEDOT:PSS dopado mostraron que solo el etilenglicol tiene un pequeño efecto en el voltaje de descarga, mientras que el dimetilsulfóxido no tiene efecto. El análisis mediante espectroscopia Mössbauer permitió verificar que la oxidación de  $\text{Fe}^{2+}$  a  $\text{Fe}^{3+}$  durante la carga de la batería a C/10 es más eficiente en electrodos que contienen PEDOT:PSS dopado con etilenglicol, en comparación con el electrodo convencional de  $\text{LiFePO}_4$ . Este efecto se atribuyó a una mayor proporción de la fase PEDOT (conductor electrónico) con respecto a la fase PSS (conductor iónico), como se determinó mediante el análisis cuantitativo de espectros XPS.

Adicionalmente, los valores aproximados de la resistencia de los electrodos con PEDOT:PSS se determinaron a partir del ajuste de espectros de impedancia. Estos análisis aportaron evidencia de la influencia positiva sobre la reacción electroquímica del material activo, promovida por la presencia de 1% w/w de conductor mixto PEDOT:PSS, tanto sin dopar como dopado con etilenglicol. Estos electrodos proporcionan casi el 50% de la capacidad teórica del  $\text{LiFePO}_4$  en solo 6 minutos con una menor polarización de carga/descarga, además de que mostraron una excelente retención de la capacidad a 2C durante 50 ciclos de carga/descarga.

El PEDOT:PSS también se probó como recubrimiento conductor para el colector de corriente de electrodos basados en  $\text{LiFePO}_4$ . Este recubrimiento de polímero se realizó mediante el depósito de gotas de PEDOT:PSS sobre el colector de corriente. El aumento de la conductividad mediante tratamiento con etilenglicol resultó en una alta capacidad con polarización relativamente baja a tasas altas de carga/descarga. La correlación entre la impedancia inicial, la resistencia de corriente directa y los valores de capacidad a tasas de descarga moderadas y altas de los electrodos que contiene PEDOT:PSS, indicó que la interfaz entre la capa del electrodo y el colector de corriente tiene el mayor impacto en el desempeño de electrodos basados en  $\text{LiFePO}_4$ .

El empleo de PEDOT:PSS dopado con etilenglicol es la mejor estrategia de entre todos los procedimientos descritos en esta tesis para mejorar el desempeño de electrodos compuestos con  $\text{LiFePO}_4$  y polímero conductor.

En general, las estrategias presentadas en esta tesis para producir electrodos compuestos de  $\text{LiFePO}_4$  con polímero conductor mediante el método *in battery* y empleando el PEDOT:PSS, son sencillas y se podrían implementar con ligeras modificaciones a los métodos actuales para producir electrodos basados en  $\text{LiFePO}_4$ .







# Chapter 1

## 1. Introduction

The progress of our society is linked to the way in which energy is harnessed and transformed. In the past, in order to subsist, our ancestors made practical use of the resources available in their communities. As mankind learnt how to apply and transform materials for building rudimentary tools and machines, the exploitation of natural resources became more effective. Agriculture offered the possibility of growing new varieties of food in surplus amounts, which allowed meeting the nourishing requirements of larger populations. The use of animals, water or wind streams, reduced the dependence on the human power required to grow and process crops. In these favourable circumstances the activities and roles of individuals diversified and the quality of life improved substantially.

In the 18<sup>th</sup> century the steam engine and the iron mass production powered and guided some countries towards the industrial revolution. Starting from wood and coal, soon began the hunt for new energetic resources in order to keep on running the industrial production. Electricity came into scene in the 19<sup>th</sup> century with the invention of the voltaic pile and the widespread distribution of electricity from steam-powered generators. The invention of the electric motor and the development of storage batteries pushed forward the popularity of the electric vehicles. However, cheaper and more reliable internal combustion engine cars running on oil-derived fuels became dominant in the emerging transportation sector.

Currently, after almost 250 years, our energy system is still based mostly on fossil fuels. In 2012 almost 82% of the total primary energy was supplied by oil, coal and natural gas.[1] This situation has raised global concerns and debate about the harmful effects of the anthropogenic combustion products released to the global ecosystem. As

our energy requirements continue to grow in amount and complexity, humanity is obliged to consider more abundant, less polluting and fair priced (economically and socially) energy sources. The so-called renewables are very appealing for they constitute a group of energy sources that are presumably inexhaustible or that can be replenished before severe depletion. The major renewable energy sources come from sunlight, water reservoirs, biomass, wind or geothermal activity. Although the share of renewables in 2012 reached approximately 3.5 % of the global, primary energy supply,[1] in recent years Costa Rica or the Spanish island *El Hierro* have demonstrated that some territories are able to meet sustainably all their energy demand from renewable sources.[2a-b]

Nevertheless, sunlight, wind or water streams provide energy intermittently, with daily and seasonal fluctuations. Thus, the integration of the energy from renewable sources into the electrical energy network creates the challenge of maintaining the balance of the production and demand cycles. In order to tackle that challenge, energy storage systems could aid by storing the surplus energy from renewable sources. The stored energy can then be transformed into electricity in order to match the demand with a lower participation of the generation from fossil fuels. Energy storage technologies can be classified depending on the form of the stored energy.[3] This classification is represented in Table 1.

*Table 1. Major energy storage technologies. Adapted from ref. [3].*

<b>Mechanical</b>	<b>Electrical</b>	<b>Electrochemical</b>	<b>Chemical</b>	<b>Thermal</b>
<b>Pumped hydro</b>				
<b>Compressed air</b>	<b>Capacitors</b>	<b>Rechargeable batteries</b>	<b>Fuels</b>	<b>Sensible/latent heat</b>
<b>Flywheel</b>				

Among all these technologies, pumped hydro is currently the most viable for electrical power generation, provided there are convenient locations for installing the infrastructure. Although most of the mechanical-based or thermal-based technologies

are realizable, the indirect energy transformation into electricity presents inherent efficiency disadvantages.

On the contrary, electrical and electrochemical energy storage technologies are more attractive systems due to the higher efficiency of the direct release of stored charge and the transformation of chemical energy into electricity, respectively.

Compared to capacitors, batteries have proven technical and economic viability as energy storage systems for a wider range of applications. Over the years, rechargeable batteries have been used for load levelling and backup in the industrial sector. In recent years, the advances in battery technology have enabled the proliferation of portable consumer electronics that entertain us, allow us to communicate and to work without losing pace with our nomadic lifestyle. Nowadays, rechargeable batteries of high energy and power density are intensively pursued for use in commercial hybrid and battery vehicles. This way of transportation could reduce the local urban air pollution in the near future. Additionally, battery systems coupled to solar panels are available for emergency back-up or even for grid independence in residential applications, which could lead towards a decentralized energy production and distribution.

Batteries have a great potential to become a leading technology for sustainable energy storage. In order to fulfil this endeavour, future research efforts should address the optimization of the existent battery technologies and the development of new materials that provide high energy and power density for a broad range of applications. The next sections introduce the working principles of batteries and presents an overview of the advances that have led to the development of today's most popular battery technology; the Li-ion battery.

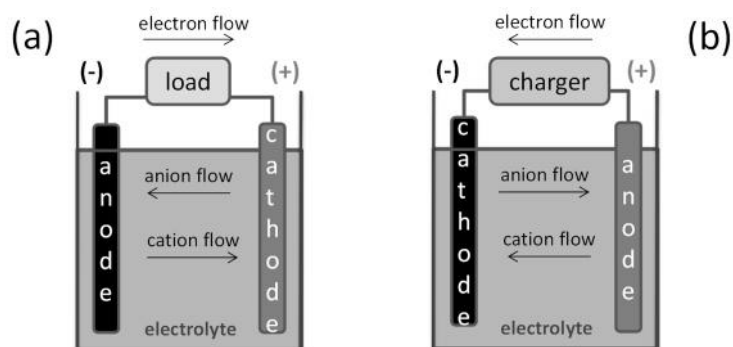
## **1.1 Electrochemical energy storage in batteries**

Batteries are devices that store energy in chemical compounds that are able to provide electrical energy by means of redox reactions. The basic design of today's batteries has not changed much since the first battery described by Alessandro Volta in 1800. The elementary unit of a battery is an individual cell that houses two electrodes containing different redox active materials. Ionic contact between the electrodes is ensured by an electrolyte, while electronic contact is prevented by a separator. The two electrodes of a cell are distinguished by assigning them a positive or negative polarity,

depending on the magnitude of the potential of each electrode versus the other. Fig. 1 represents the basic components and operation of a cell. According to the International Electrochemical Commission, the term battery can be used for referring to an individual cell. This practice is very common and in this thesis the term battery will be used for both a single cell and an arrangement of cells, unless otherwise stated.

A battery undergoes discharge when its two electrodes are connected to the terminals of an external load, for example a wire, an electric motor, etc. In discharge, a spontaneous oxidation reaction takes place at the negative electrode of the battery, while a spontaneous reduction occurs at the positive electrode. Electrons released by the oxidation reaction are collected at the negative electrode and the electrical energy is used by the external load to do work.

Within the battery, the ions from the electrolyte migrate to the electrodes in order to maintain the electroneutrality. Recharging the battery consists in applying an external electric current or voltage in order to reactivate the redox state of the electrode materials by forcing a reduction at the negative electrode and oxidation at the positive electrode.



*Figure 1. Basic components of batteries and operation mode in a) discharge and b) charge for a rechargeable battery*

According to the IUPAC convention for an electrochemical cell, the oxidation takes place at the anode, while the reduction takes place at the cathode. In a battery this situation holds for the spontaneous discharge reaction, therefore it is common to call the negative electrode anode, and the positive electrode cathode. This convention is followed in this document unless stated otherwise. Batteries designed for a single full

discharge are classified as primary, whereas those designed for repetitive discharge-recharge cycles are classified as secondary or rechargeable.

Batteries are characterized by parameters related to the nature and the amount of the materials that compose the system. Three of the main battery parameters are: Voltage, Capacity, and Energy. The voltage of a battery is related to the free energy of the cell reaction according to Eq. 1:

$$\Delta G = -n \times F \times \Delta V \quad (1)$$

where  $\Delta G$  is the change in free energy,  $n$  is the amount of electrons transferred,  $F$  is the Faraday constant and  $\Delta V$  is the potential difference between the two terminals of the battery. The equilibrium value of  $\Delta V$  can be calculated according to Eq. 2 from the equilibrium potentials of the positive electrode ( $E_{(+)\text{electrode}}$ ) and the negative electrode ( $E_{(-)\text{electrode}}$ ).

$$\Delta V = E_{(+)\text{electrode}} - E_{(-)\text{electrode}} \quad (2)$$

The capacity  $Q$  of a battery corresponds to the amount of charge involved in the redox reactions at the electrodes and depends on the amount of active materials. For a given active material its theoretical specific capacity ( $Q_{\text{theo}}$ ), usually expressed in  $\text{Ah g}^{-1}$ , can be calculated by applying Eq. 3:

$$Q_{\text{theo}} = n F / M_w \quad (3)$$

where  $M_w$  corresponds to the molecular weight of the active material. For a battery discharged at constant current  $I$ , during a discharge time  $Ut$ , the experimental discharge capacity  $Q_{\text{exp}}$ , without considering side-reactions, is given by Eq. 4.

$$Q_{\text{exp}} = I \times \Delta t \quad (4)$$

The most remarkable feature of a battery is its ability to interconvert chemical and electrical energy. If the energy interconversion is carried out at constant pressure and temperature, then the energy conservation requires that  $\Delta G = W_{\text{elec}}$ ; being  $W_{\text{elec}}$  the theoretical, electric energy available from the battery. This energy is related to the theoretical voltage and to the theoretical specific capacity of the battery by Eq. 5:

$$W_{\text{elec}} = -Q_{\text{theo}} \times \Delta V \quad (5)$$

where the negative sign indicates that energy is transferred out of the battery. According to the parameters described above, the strategies to follow in order to realize a high performance battery are:

- 1) Maximize the voltage by using a strong reducing substance for the negative electrode and strong oxidizing substance for the positive electrode
- 2) Increase the capacity of the electrodes by increasing the amount of electrons transferred in the redox reactions
- 3) Minimize the weight of the active materials, additives and all the other battery components
- 4) Minimize the internal resistance of the battery

At the cell level the performance is influenced by the ability of the electrode materials and the electrolyte to exchange and transport charges. At the battery level, the performance depends on how several cells are connected (in series or in parallel) and managed.

### **1.1.1 Primary batteries**

Throughout the years, primary batteries have provided reliable energy for a wide variety of stationary and portable applications like toys, medical-aid devices, consumer electronics, military equipment and many other appliances. Primary batteries are easy to use and replace, they are affordable, can be adapted to fit the application, and generally they can be stored inactive for long time without significant performance loss. Table 2 presents a list of the major primary batteries developed and commercialized since the 1950's.

Since the first battery proposed by Volta, zinc has been the most used anode material for aqueous primary batteries because of its practical electrochemical performance, its abundance and its low cost. Improvements in the battery design and the combination of zinc anodes with diverse cathode materials and electrolytes has led to the development of commercially successful batteries, such as the alkaline or the silver oxide batteries.

Table 2. Major primary batteries developed and/or commercialized since the 1950's. Adapted from ref. [4a, p 7.9].

Battery type	Global reaction	Voltage (V)	Specific Capacity (Ah/kg)	Energy Density (Wh/kg)
<b>Alkaline</b>	$\text{Zn} + \text{MnO}_2 \rightarrow \text{ZnO} + \text{Mn}_2\text{O}_3$	1.50	224	336
<b>Zn/Ag<sub>2</sub>O</b>	$\text{Zn} + \text{Ag}_2\text{O} + \text{H}_2\text{O} \rightarrow \text{Zn(OH)}_2 + 2\text{Ag}$	1.60	180	288
<b>Zinc/air</b>	$\text{Zn} + 1/2\text{O}_2 \rightarrow \text{ZnO}$	1.65	820	1353
<b>Li/(CF)<sub>n</sub></b>	$n\text{Li} + (\text{CF})_n \rightarrow n\text{LiF} + n\text{C}$	3.10	706	2189
<b>Li/MnO<sub>2</sub></b>	$\text{Li} + \text{MnO}_2 \rightarrow \text{LiMnO}_2$	3.50	286	1001

Although higher capacity can be achieved with lighter and more reactive anodes like magnesium or aluminium, these anodes suffer from parasitic reactions, which have limited their application to reserve-type or metal/air batteries. Primary, metal/air batteries are very attractive because they can provide very high energy density due to the absence of a contained cathode material, however only zinc/air batteries of moderate performance have been realized so far.

Lithium metal primary batteries take advantage of the strong reducing character and the low weight of lithium, which translates into high specific energy and power densities. Due to the high reactivity of lithium with water, lithium batteries require non-aqueous solvents. These solvents tend to passivate the anode surface and protect it against corrosion, which provides stability. Early concepts of lithium metal batteries considered positive electrodes of transition element halides like  $\text{CuX}_2$  or  $\text{NiX}_2$  (X: F, Cl). However, these compounds suffer from stability and dissolution problems. More stable cathodes for lithium metal primary batteries consist of halogenated compounds such as carbon fluoride [(CF)<sub>n</sub>], I<sub>2</sub>/poly-2-vinylpyridine complex,  $\text{SOCl}_2$  or  $\text{SO}_2\text{Cl}_2$ ; oxides:  $\text{Ag}_2\text{CrO}_4$ ,  $\text{V}_2\text{O}_5$ ,  $\text{CuO}$ ,  $\text{Ag}_2\text{V}_4\text{O}_{11}$ ,  $\text{MnO}_2$  or  $\text{SO}_2$ ; or sulphides:  $\text{FeS}$  and  $\text{FeS}_2$ . [4b]

To date, the alkaline  $\text{MnO}_2$  battery is the most commercially successful among the primary batteries. Considerable advances in the materials and design of primary batteries have led to an increase in the power density and to improvements in shelf life and safety, particularly for lithium metal batteries that provide higher energy density



than the most advanced rechargeable batteries available in the market. However, the energy density of primary batteries has apparently reached its limit due to the lack of novel, higher capacity active materials. Although primary batteries have become an essential commodity in life, the faster development of rechargeable batteries in the last years could provide more appealing batteries in terms of energy output and efficiency.

### **1.1.2 Rechargeable batteries**

Unlike primary batteries, rechargeable batteries can be safely restored several times to an active and useful state. This remarkable characteristic translates into a longer useful life and the possibility of using rechargeable batteries as accumulators that can store and deliver energy when other energy source is not available or is insufficient to meet the demand. Table 3 lists some of the major secondary batteries developed and/or commercialized since the nineteenth century.

The first rechargeable battery was the lead-acid battery invented by G. Planté in 1859. In its early years, Planté's battery was recharged by primary batteries and was used in telegraphy and for powering vehicles' lights. The development of the dynamo and several design modifications and improvements of the lead-acid battery enabled the proliferation of internal combustion engine vehicles where the battery was, and is still used, for starting, lighting and ignition (SLI) purposes. The largest drawback of the lead-acid battery for portable applications is its heavy weight, which limits its energy density. In spite of that disadvantage, lead-acid batteries are widely used for powering small electric service vehicles and for backup systems.

In order to achieve higher specific energy than the lead-acid battery, different rechargeable batteries with alkaline electrolytes and nickel-based cathodes were developed between 1899 and 1970. The basic difference among these nickel alkaline batteries arises from the use of diverse anode materials like iron, zinc, cadmium or metal hydrides (MH). The nickel-cadmium (Ni-Cd) battery offered advantages over its nickel-iron and nickel-zinc counterparts, and it was commercially successful. However, the long-term negative effects of cadmium on human health raised concerns about the production, use and disposal of Ni-Cd batteries. Besides, a major performance limitation

of Ni-Cd batteries is the so-called memory effect, which limits the charging voltage and capacity if the battery was not fully discharged previously.

Table 3. Major commercial secondary batteries. Adapted from ref. [4a, p 22.12].

Battery type	Global reaction	Voltage (V)	Specific Capacity (Ah/kg)	Energy Density (Wh/kg)
Lead-acid	$\text{Pb} + \text{PbO}_2 + \text{H}_2\text{SO}_4 \rightarrow 2\text{PbSO}_4 + 2\text{H}_2\text{O}$	2.1	120	252
Ni-Cd	$\text{Cd} + \text{NiOOH} + 2\text{H}_2\text{O} \rightarrow \text{Ni}(\text{OH})_2 + \text{Cd}(\text{OH})_2$	1.35	181	244
Ni-MH	$\text{MH} + \text{NiOOH} \rightarrow \text{M} + \text{Ni}(\text{OH})_2$	1.35	178	240
Li-ion	$\text{Li}_x\text{C}_6 + \text{Li}_{1-x}\text{CoO}_2 \rightarrow \text{LiCoO}_2 + \text{C}_6$	3.7	158	585

A successor of the Ni-Cd battery is the nickel-metal hydride battery (Ni-MH), in which a metal hydride with adsorbed hydrogen constitutes the anode. Ni-MH batteries provide higher energy density and present less memory effect than the Ni-Cd batteries. Such advantages have caused the gradual replacement of nickel-cadmium by nickel-metal hydride batteries in most popular low drain applications. Nowadays large Ni-MH battery systems provide the critical energy density, cycle life and safety required for hybrid electric vehicles (HEV), as shown in Fig. 2. In the next years, the success of the electric vehicle (EV) will be strongly influenced by the availability of higher performance rechargeable batteries based on light materials. Lithium-based rechargeable batteries are one of the strongest candidates to enable electric transportation.

## 1.2 Lithium metal and lithium-ion batteries

For more than forty years, lithium metal has been considered as an ideal candidate for the anode of high performance rechargeable batteries. For this endeavour, early attempts consisted in achieving reversibility for the reaction of lithium primary batteries such as  $\text{Li}/(\text{CF})_n$  or  $\text{Li}/\text{MnO}_2$ , the latter being successful and initially commercialized by

Sanyo in solar rechargeable calculators. Although some systems working at nearly 500° C with molten lithium anode and sulphur cathode resulted unviable, these systems set the basis for the development of the more successful sodium/sulphur battery.

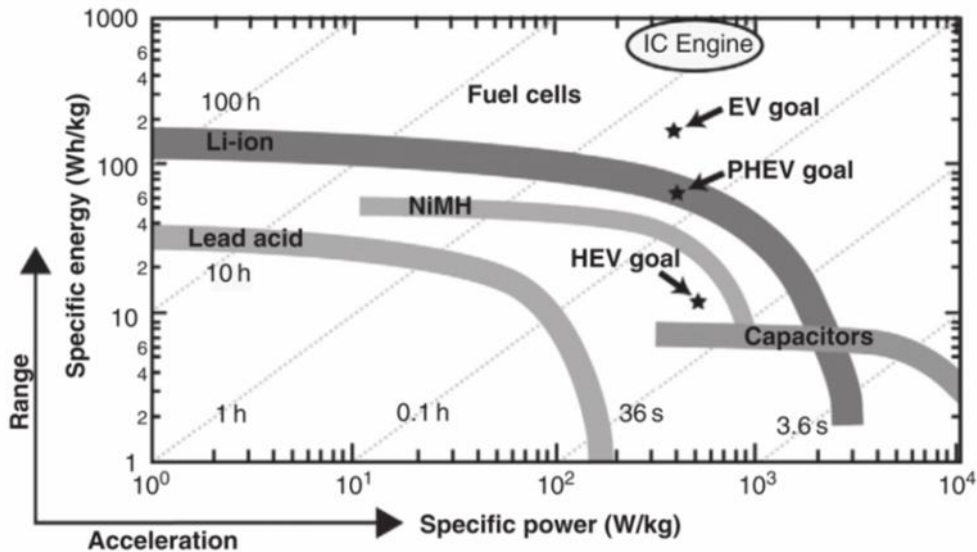


Figure 2. Relative performance of different energy storage systems for electric vehicle applications. Taken from ref. [5].

By 1970, there was evidence of the electrochemical incorporation of guest ions within the structure of host materials; a process later referred to as electrochemical intercalation.[6] Further research on the intercalation of lithium into layered dichalcogenides led to the development of lithium metal anode batteries with TiS<sub>2</sub> and MoS<sub>2</sub> cathodes manufactured by Exxon and MoliEnergy, respectively. However, the potential of these systems is lower than 2.5 V (vs. Li<sup>+</sup>/Li) and their repeated cycling leads to irregular deposition of lithium. This later fact results not only in the total failure of the battery due to short-circuiting of both electrodes, but also in a potential fire risk.

Alloys with aluminium, silicon, zinc, and other elements were proposed as a way to avoid the irregular deposition of lithium. Nevertheless, upon reaction with lithium, the crystal lattice of the lithium-element alloy suffers large volume changes that cause great stress, and result in cracking and crumbling of the alloy particles; this situation leads to capacity failure after several charge-discharge cycles.[7]

Considering structural similarities to layered dichalcogenides, Goodenough's group identified  $\text{LiCoO}_2$  as a higher potential cathode for the electrochemical insertion/extraction of lithium.[8] Regarding the safety problems associated to the use of lithium metal, graphite and synthetic coke were proposed as anode materials due to their ability to insert/extract lithium reversibly.[9a-b] The combination of a  $\text{LiCoO}_2$  cathode with a coke anode led to the development of the first lithium-ion (Li-ion) battery introduced to the market by Sony in 1991.[10] Today's Li-ion battery technology is constituted by a family of anode and cathode materials that can be combined to realize a battery for a given application.

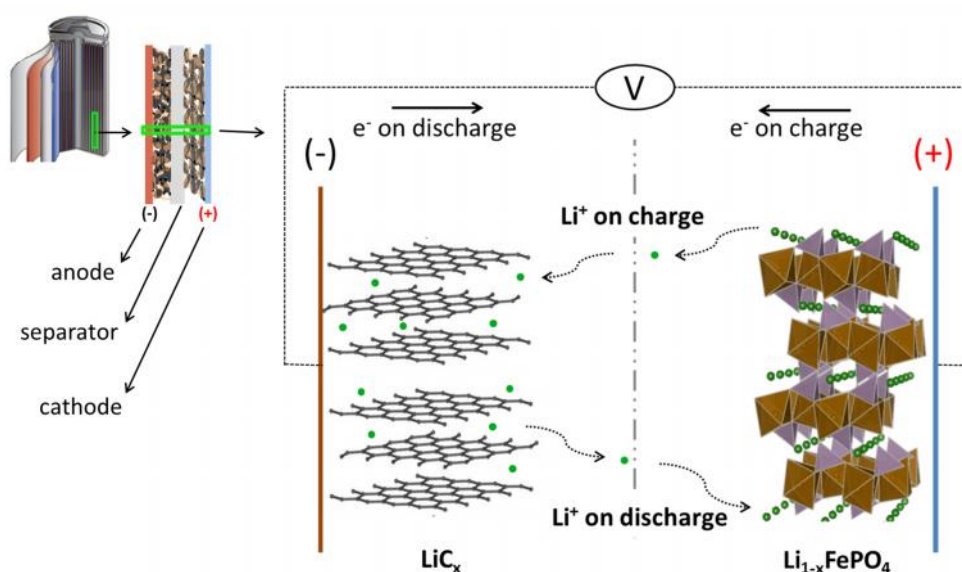


Figure 3. Representation of the multi-scale components and working principle of a lithium ion battery.

Fig. 3 shows a diagram of the working principle of a Li-ion battery. The cathode is a composite electrode with a transition metal oxide ( $\text{LiCoO}_2$ ,  $\text{LiMn}_2\text{O}_4$ , etc.) or a phosphate ( $\text{LiFePO}_4$ ) as active material mixed with conducting and agglomerating additives, all deposited over an aluminium current collector. Graphite or other carbon-based active materials mixed with additives and deposited over a copper current collector form the composite electrode used as the anode in commercial Li-ion batteries.

Both composite electrodes are separated by a polymeric, plastic membrane typically made of polypropylene or polyvinylidene fluoride (PVDF).[11] This plastic membrane is permeable to the electrolyte, which typically consists of a lithium salt (i.e.  $\text{LiPF}_6$ ) dissolved in mixtures of alkyl carbonates of low molecular weight containing soluble additives.

Li-ion batteries are usually sold in charged state and most suppliers recommend fully charging these batteries before their use, in order to recover the capacity lost due to self-discharge. During the charging process, lithium is extracted from the positive electrode's active material as this is oxidized. Simultaneously, lithium is inserted into the negative electrode's active material as this undergoes a reduction reaction, thus allowing the energy storage. In discharge, the electrode reactions and the lithium flow are reversed, thus allowing the energy release.

The performance and safety criteria for developing or selecting electrode materials for Li-ion batteries are:

- 1) The materials have to be as light as possible and able to exchange reversibly large amount of lithium ions in order to provide high specific capacity
- 2) In order to provide high energy density, the reaction with lithium must occur at a high potential for a cathode material. For an anode material, the reaction must occur at a low (positive) potential
- 3) The intrinsic/extrinsic electronic and ionic conductivity of the active materials must be high in order to allow fast charge exchange.
- 4) The stability and compatibility of the materials in presence of the electrolyte and the internal components of the battery has to be retained in charged, in discharged state or during operation
- 5) Upon successive charge/discharge cycles, the structural changes of the active materials must be minimal in order to achieve energy efficiency and prolonged cycle life
- 6) The materials have to be cost effective and environmentally friendly

The following sections present an overview of a series of insertion compounds that have been identified as viable or that are currently used as anode or cathode materials. For a detailed description of electrolytes for Li-ion batteries see refs. [12a-b].

### 1.2.1 Anode materials for Li-ion batteries

Anode materials for Li-ion batteries can be classified depending on their electrochemical reaction with lithium as: insertion/extraction; alloy/de-alloy; or conversion materials (Fig. 4). The following overview focuses on carbonaceous insertion/extraction materials. Recent reviews cover the advances on another attractive insertion material: lithium titanium oxide (LTO),[13a] as well as the development of alloy/de-alloy and conversion materials that are considered for the next generation of Li-ion batteries.[13b-d]

It has been demonstrated that several carbonaceous materials can undergo practical, reversible insertion/extraction of lithium at low potentials vs.  $\text{Li}^+/\text{Li}$ . Such carbons, usually classified as soft (graphitic) or hard (non-graphitic), intercalate lithium between graphene layers to an extent that depends on their morphology, crystallinity and ordering.[14] For instance, turbostratic, disordered coke is able to intercalate low amounts of  $\text{Li}^+$ , and thus form  $\text{Li}_x\text{C}_6$  ( $0 < x < 0.5$ ). Graphite also forms  $\text{Li}_x\text{C}_6$ , and its ordered layered structure allows the intercalation of higher amount of  $\text{Li}^+$  ( $0 < x < 1$ ), which translates into a maximal specific capacity of  $372 \text{ mAh g}^{-1}$ . [15]

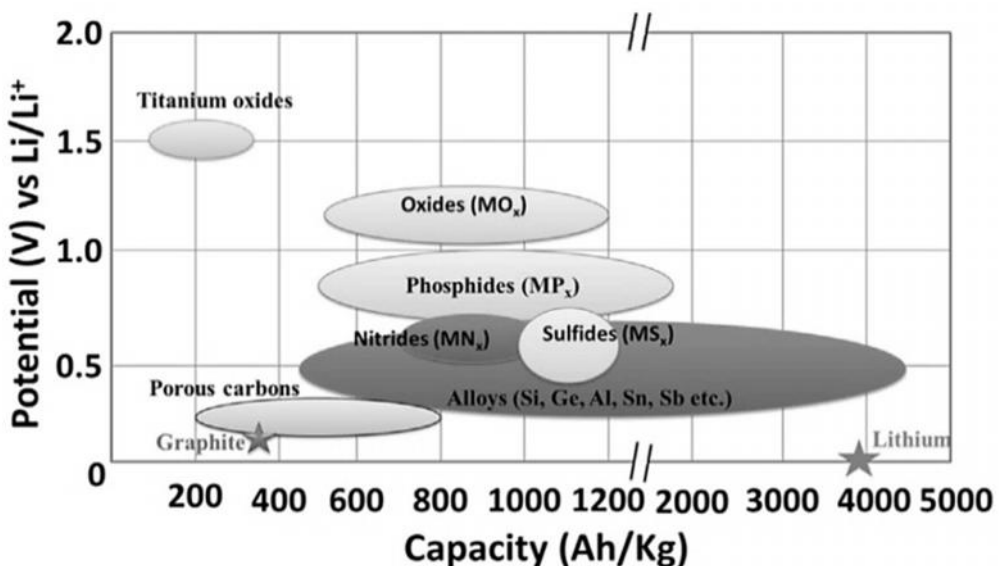


Figure 4. Potential and specific capacity of diverse types of anode materials for lithium-based batteries. Taken from ref. [13c].

Commercially available types of graphite for Li-ion batteries include: Mesocarbon Microbeads (MCMB), vapour grown carbon fibres (VGCF), Massive Artificial Graphite (MAG), among others.[14] Despite the availability, low cost and acceptable performance of graphitic carbons, these materials present undesirable features such as an unpractical volumetric capacity for large-format batteries, and a high initial irreversibility due to the formation of a passivating solid electrolyte interphase over the carbon material caused by the decomposition of the electrolyte.

Hard carbons offer a higher specific capacity ( $400 - 600 \text{ mAh g}^{-1}$ ), which arises from the random alignment of graphene sheets that provide sites for lithium accommodation. Strategies such as surface modification and formation of protective coatings have been applied in order to overcome the irreversible capacity and low tap density of hard, porous carbons.[16a-b] Carbon nanotubes (CNTs) and graphene constitute another group of ordered carbons that have been applied to Li-ion batteries. These versatile materials can be used as active materials, as support for active metal or oxide particles or as conductive additives in composite electrodes. High capacity has been reported for single wall carbon nanotubes ( $1116 \text{ mAh g}^{-1}$ ) based on an average  $\text{LiC}_2$  stoichiometry.[13c]

## 1.2.2 Cathode materials for Li-ion batteries

A vast diversity of active compounds has been considered for the cathode of Li-ion batteries. Inorganic compounds with transition elements are among the most attractive cathode materials, as they have crystalline structures that enable reversible lithium insertion/extraction at practical voltage values vs.  $\text{Li}^+/\text{Li}$ . This section provides an overview on three types of cathode materials: layered oxides, spinel-type compounds and phospho-olivines; all of which are currently used in commercial Li-ion batteries.

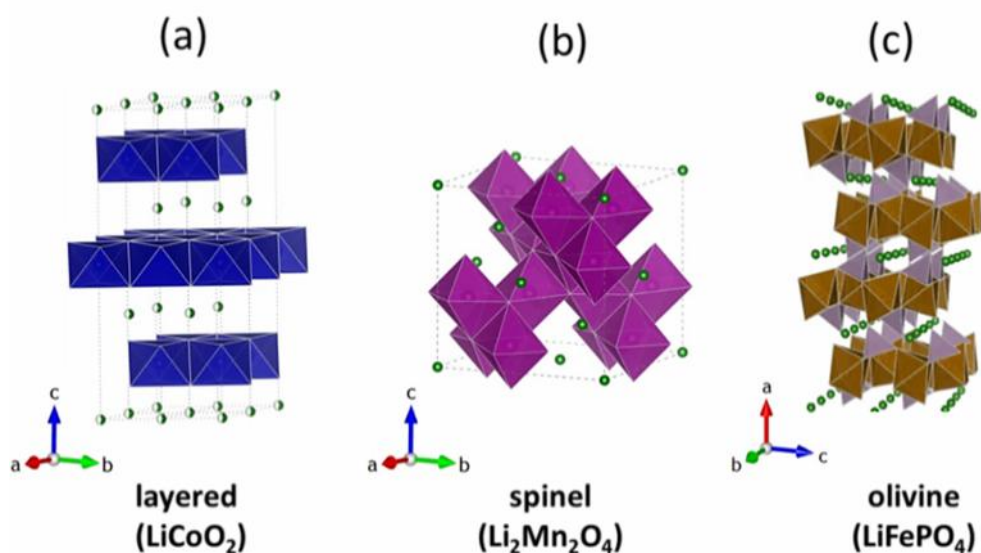


Figure 5. Polyhedral representation of the structure of three types of insertion materials. Lithium is depicted as green spheres.

### 1.2.2-a Layered oxides: $\text{LiMO}_2$ (M: Mn, Co, Ni)

The success of  $\text{LiCoO}_2$  as a cathode material in commercial batteries prompted the research on the family of layered oxides  $\text{LiMO}_2$  (M: Mn, Co, Ni).  $\text{LiCoO}_2$  is isostructural to rhombohedral  $\alpha\text{-NaFeO}_2$  (R-3m space group) with the oxygen atoms in a cubic close packed arrangement. In this ordering, two-dimensional paths exist along the  $ab$  direction, which allows for diffusion of lithium ions, as shown in Fig. 5a. Rearrangement



of the oxygen lattice into a hexagonal close packing takes place if the fraction  $x$  of extracted lithium in  $\text{Li}_{1-x}\text{CoO}_2$  is higher than 0.5. This irreversible change in the crystal structure can be prevented by limiting the charge potential. However, this action limits the practical capacity to ca.  $135 \text{ mAh g}^{-1}$ . [17] Furthermore,  $\text{Co}^{4+}$  from delithiated  $\text{Li}_{1-x}\text{CoO}_2$  can oxidize the organic solvents of the battery electrolyte, especially upon heating. This situation can lead to the ignition of the battery, a risk that renders  $\text{LiCoO}_2$  unattractive for large format batteries.

Although more appealing in terms of cheaper production costs,  $\text{LiNiO}_2$  presents similar structural and thermal instabilities as  $\text{LiCoO}_2$ .  $\text{LiNiO}_2$  is isostructural to  $\text{LiCoO}_2$ , however the two-dimensional paths in  $\text{LiNiO}_2$  usually are partially blocked by excess nickel atoms that limit the Li-ion diffusion rate. The instabilities of  $\text{LiNiO}_2$  can be overcome by replacing a fraction of nickel by cobalt and aluminium. Cobalt mitigates the blocking of the two-dimensional paths, [18] while aluminium prevents the full delithiation and oxidation of  $\text{LiNiO}_2$ . [19] These strategies have led to the development of the mixed oxide  $\text{LiNi}_{0.8}\text{Co}_{0.15}\text{Al}_{0.05}\text{O}_2$ , which is now used in the battery packs that power some models of Tesla electric cars.

$\text{LiMnO}_2$  (LMO) is also an interesting alternative to  $\text{LiCoO}_2$  cathode material in terms of safety, performance and cost. LMO has a stable orthorhombic structure ( $o$ -LMO), although it can also be obtained with a metastable monoclinic structure ( $m$ -LMO) through lithium exchange from  $\text{NaMnO}_2$ . [20] Both  $o$ -LMO and  $m$ -LMO have the cation ordering of layered  $\alpha$ - $\text{NaFeO}_2$  but upon lithium insertion/extraction they tend to transform into  $\text{LiMn}_2\text{O}_4$  with spinel structure (Fig. 5b), that has lower capacity and voltage. Stabilization of oxides containing manganese with the  $\alpha$ - $\text{NaFeO}_2$  structure has been achieved by partial substitution of Mn by Co and Ni. These mixed oxides have a general formula  $\text{Li}[\text{Ni}_x\text{Mn}_y\text{Co}_z]\text{O}_2$ , where nickel is the predominant redox active element in the  $2^+$  and  $4^+$  oxidation states. The optimal composition with the best compromise between thermal stability and performance has been found for  $\text{LiNi}_{0.33}\text{Mn}_{0.33}\text{Co}_{0.33}\text{O}_2$ . [21] In this compound manganese exists as  $\text{Mn}^{4+}$  and provides stability to the lattice, while  $\text{Co}^{3+}$  plays an active role at the later stages of lithium removal, apart from enhancing the conductivity and stabilizing the layered structure of the mixed oxide.

### 1.2.2-b Spinel-type compounds: $\text{LiM}_2\text{O}_4$ (M: Mn, Co, Ni)

$\text{LiMn}_2\text{O}_4$  is one of most representative spinel-type compounds used in Li-ion batteries. It has a cubic structure where lithium ions occupy 8a tetrahedral sites, Mn ions occupy 16c octahedral sites, while oxygen ions occupy the 32e positions forming a cubic close packed lattice. In this arrangement,  $\text{MnO}_6$  octahedra share edges and form a three-dimensional cubic array that can tolerate isotropic expansion and shrinkage upon lithium extraction/insertion.[22] This three-dimensional arrangement (Fig. 5b) enables fast and reversible lithium diffusion required for high rate applications. The full electrochemical insertion/extraction of  $\text{Li}^+$  takes place at two stages, the first at ca. 4.0 V and the second at ca. 3.0 V. This second stage is usually considered unpractical because it entails a detrimental structure transformation.

The theoretical, specific capacity of  $\text{LiMn}_2\text{O}_4$  is  $148 \text{ mAh g}^{-1}$  but in practice it can reach ca. 85% of this value when cycled between 3.5 V and 4.3 V. Capacity fading of  $\text{LiMn}_2\text{O}_4$  has been attributed mainly to Mn dissolution and destabilization of the spinel structure. It has been shown that the dissolution of Mn is triggered by the presence of hydrogen fluoride in the battery electrolyte, which has been avoided by using fluoride-ion getters and fluoride-free salts such as lithium bis(oxalato)borate.[23] Regarding the stabilization of the spinel structure, partial substitution of manganese by nickel in  $\text{LiNi}_{0.5}\text{Mn}_{1.5}\text{O}_2$  has been effective not only to limit the Jahn-Teller distortion of  $\text{Mn}^{3+}$  that causes the transition from cubic to tetragonal structure, but also to increase the operational voltage to ca. 4.7 V.

### 1.2.2-c Phospho-olivines: $\text{LiMPO}_4$ (M: Fe, Mn, Co, Ni)

Lithium transition-metal phosphates  $\text{LiMPO}_4$  (M: Fe, Mn, Co, Ni) with olivine-type structure constitute a group of polyanionic compounds that were proposed by Goodenough's group as safer alternatives to cathode materials based on lithium transition-metal oxides for lithium-ion batteries.[24] In particular, lithium iron phosphate ( $\text{LiFePO}_4$ ) has been the focus of intense research for almost two decades by virtue of its appealing electrochemical characteristics, its convenient thermal stability, its competitive cost and presumable low toxicity.

The four members of the  $\text{LiMPO}_4$  family have similar capacity values. Therefore, the differences in energy density arise from their different operational voltages (Table 4 and Fig. 6a). The trend in the operational voltage:  $\text{Fe} < \text{Mn} < \text{Co} < \text{Ni}$ , is correlated to the  $d$ -electron configurations of each of the  $\text{M}^{2+}/\text{M}^{3+}$  redox couples, and the crystal field splitting in octahedral configuration as represented in Fig. 6b.[25a-b]

Table 4. Characteristics of synthetic phospho-olivines relevant to battery applications.

Phosphate	Voltage (V vs. $\text{Li}^+/\text{Li}$ )	Specific Capacity (mAh/g)	Specific Energy (Wh/kg)
$\text{LiFePO}_4$	~ 3.4	~ 170	~ 578
$\text{LiMnPO}_4$	~ 4.1	~ 171	~ 701
$\text{LiCoPO}_4$	~ 4.8	~ 167	~ 800
$\text{LiNiPO}_4$	~ 5.1	~ 167	~ 851

With an operational voltage of ~3.4 V,  $\text{LiFePO}_4$  provides the lowest energy density, which is the main drawback of this material.  $\text{LiMnPO}_4$  operates ~0.7 V above the voltage of  $\text{LiFePO}_4$ , hence, the former has the potential to compete with common 4 V cathode materials based on transition metal oxides. Unfortunately,  $\text{LiMnPO}_4$  has an intrinsic conductivity of approximately five orders of magnitude lower than that of  $\text{LiFePO}_4$  (as measured at ~500 K), which translates into a limited rate capability.[26] Solid solutions of the type  $\text{LiMn}_{1-y}\text{Fe}_y\text{PO}_4$  ( $0 < y < 1$ ) were initially proposed by Goodenough's group, and later developed as an strategy for operating at 4.1 V and at nearly 3.5 V; without significant detriment to the specific capacity at moderate rates.[27a-b]

Although  $\text{LiCoPO}_4$  and  $\text{LiNiPO}_4$  could offer high theoretical energy density, these materials operate at voltage values close to the stability limit of conventional carbonate-based electrolytes, which leads to deterioration and safety issues. Therefore, the development of high operating voltage  $\text{LiCoPO}_4$  and  $\text{LiNiPO}_4$  materials is strongly linked to the development of more stable electrolytes.[28a-b]

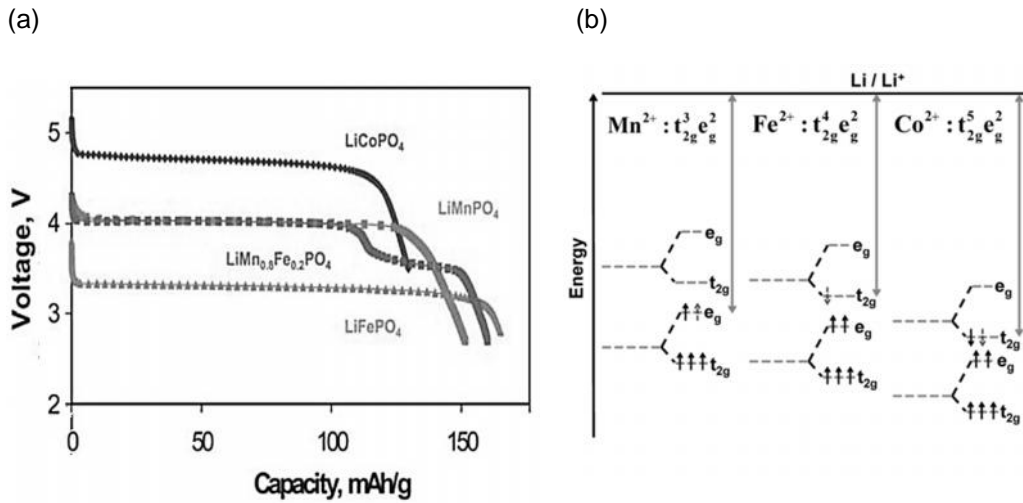


Figure 6. (a) Discharge profiles of LiMPO<sub>4</sub> phospho-olivines.[29] (b) Crystal field splitting diagrams and relative energies of the M<sup>2+</sup> cations in octahedral coordination.[25b]

To date, among the LiMPO<sub>4</sub> phospho-olivines, only LiFePO<sub>4</sub> provides the satisfactory performance and the vital safety requirements for stationary/portable commercial applications such as: power tools, electric bikes/motorcycles, systems for electric vehicle conversion, or even commercial electric cars or grid power storage. The following sections describe relevant properties of LiFePO<sub>4</sub> and the mechanisms of charge transport and phase transformation of this material that account for its attractive electrochemical performance. A summary of the two types of industrial synthesis and the strategies developed in order to maximize the performance of LiFePO<sub>4</sub> is presented.

### 1.3 Background on LiFePO<sub>4</sub>

#### 1.3.1 Crystalline structure and voltage of LiFePO<sub>4</sub>

LiFePO<sub>4</sub>, also known as triphylite, has the orthorhombic, olivine-type crystal structure (Pnmb space group) with typical lattice parameters  $a$ : 10.332 Å,  $b$ : 6.01 Å,  $c$ : 4.692 Å, and a volume of 291.4 Å<sup>3</sup>. [30] The atomic arrangement of LiFePO<sub>4</sub> can be considered as a distorted hexagonal packing of oxygen atoms, with lithium and iron occupying one-half of the octahedral sites, while phosphorous occupies one-eighth of the

tetrahedral sites. Each  $\text{FeO}_6$  octahedra is linked through common corners to other four  $\text{FeO}_6$  octahedra in the  $bc$  plane. Along the  $b$ -axis,  $\text{LiO}_6$  octahedra are connected to each other by one edge forming a lithium diffusion path (Fig. 7). One  $\text{FeO}_6$  octahedron has common edges with two  $\text{LiO}_6$  octahedra.  $\text{PO}_4$  tetrahedra share one edge with a  $\text{FeO}_6$  octahedron and two edges with  $\text{LiO}_6$  octahedra. The de-lithiated phase,  $\text{FePO}_4$  (heterosite), preserves the same framework, although with different lattice parameters, which causes a reduction of the cell volume at approximately 6.8 %.

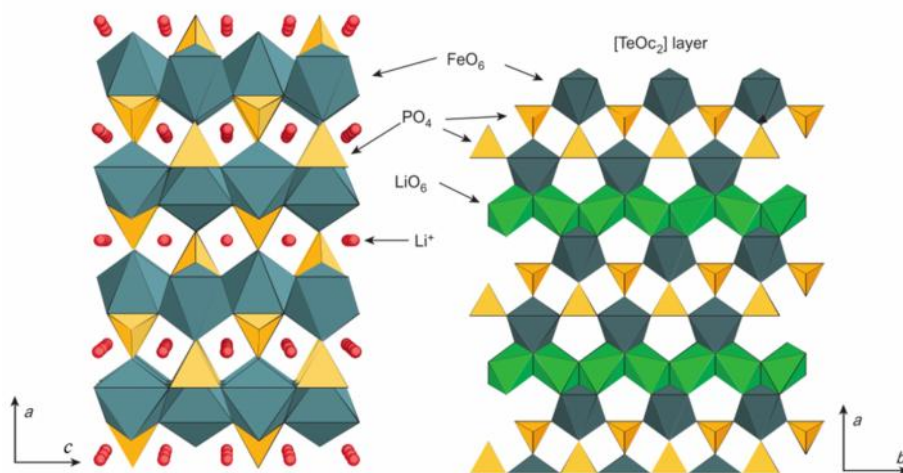


Figure 7. Representations of the atomic arrangement in  $\text{LiFePO}_4$ . Projections along  $[010]$  (left) and along  $[001]$  (right). Adapted from ref. [31].

Prior to its pioneering work on  $\text{LiFePO}_4$ , the group of Goodenough studied the compositional modifications of a series of transition-metal polyanionic compounds with the NASICON-type crystal structure.[32] These compounds have a general formula  $\text{A}_x\text{MM}'(\text{XO}_4)_3$ , where A is a mobile cation; M and M' are the same or different transition metal element; and X is a metallic or non-metallic element. In this structure  $\text{MO}_6$  and  $\text{M}'\text{O}_6$  octahedra share all corners with  $\text{XO}_4$  tetrahedra, forming an open structure that enables reversible insertion/extraction of mobile ions. For a series of iron-based NASICON-type compounds the substitution of X in the  $\text{XO}_4$  anionic framework offers the possibility of tuning the redox potential of the  $\text{Fe}^{2+}/\text{Fe}^{3+}$  pair relative to  $\text{Li}/\text{Li}^+$ . The iron-based NASICON-type compounds operate at convenient voltages vs.  $\text{Li}^+/\text{Li}$ :

$\text{Li}_3\text{Fe}_2(\text{PO}_4)_3$  (2.8 V),  $\text{Fe}_2(\text{MoO}_4)_3$  or  $\text{Fe}_2(\text{WO}_4)_3$  (3.0 V),  $\text{Fe}_2(\text{SO}_4)_3$  (3.6 V). The differences in the operating voltage among these compounds arise from the capacity of the  $\text{XO}_4$  anions to alter the covalent character of the Fe-O bonds through the inductive effect. The strength of the inductive effect on the Fe-O bonds depends on the electronegativity of the X atom in the Fe-O-X linkage. For instance, sulphate, as compared to a phosphate, decreases the covalent character of the Fe-O bond to a higher degree. This causes the antibonding states to rise in energy to a lower extent, resulting in a higher voltage versus  $\text{Li}^+/\text{Li}$ . [25b]

The higher redox potential of  $\text{Fe}^{2+}/\text{Fe}^{3+}$  in  $\text{LiFePO}_4$  (~3.45 V) with olivine structure, compared to the potential of  $\text{Li}_3\text{Fe}_2(\text{PO}_4)_3$  (~2.8 V) with NASICON-type structure, has been related to their different polyhedral connectivity. For  $\text{LiFePO}_4$ , sharing one edge between one  $\text{FeO}_6$  octahedron and one  $\text{PO}_4$  tetrahedron (Fig. 8) brings the two cations closer than they are in the NASICON structure, where  $\text{FeO}_6$  and  $\text{PO}_4$  share corners. This situation means that for  $\text{LiFePO}_4$  the stronger cation-cation repulsion reduces the spatial electric potential within the crystal lattice (Madelung potential) and lowers the  $\text{Fe}^{2+}/\text{Fe}^{3+}$  redox energy, thus increasing the voltage with respect to  $\text{Li}^+/\text{Li}$ . [25b].

### 1.3.2 Electronic and ionic conductivity of $\text{LiFePO}_4$

In their seminal paper, Goodenough's group reported that the electrochemical activity of  $\text{LiFePO}_4$  at room temperature was limited to ~0.6 mol of lithium inserted/extracted at low discharge current. This limited performance was originally attributed by the authors to a sluggish lithium transport across an extending  $\text{Li}_x\text{FePO}_4/\text{Li}_{1-x}\text{FePO}_4$  ( $0 < x < 1$ ) interphase. [24] Ravet *et al.* were the first to show that the performance of both natural and synthetic  $\text{LiFePO}_4$  was greatly improved by covering the particles of the active material with a carbon-coating prepared from different carbon precursors. [33a-b] This conducting-coating strategy set a breakthrough that led to the exploration of diverse methods for reducing the intrinsic resistivity of  $\text{LiFePO}_4$  and the bulk resistance of  $\text{LiFePO}_4$ -based electrodes. Furthermore, such a breakthrough motivated the search for a detailed description of the electronic and ionic conduction processes that are responsible for the advantages and limitations that condition the rate capability of this material.

### 1.3.2-a Electronic conductivity

The process of electronic conduction in  $\text{LiFePO}_4$  has been consensually described as a thermally-activated hopping mechanism of small polaron holes between  $\text{Fe}^{3+}$  sites and neighbouring  $\text{Fe}^{2+}$  sites.[34] Those polarons originate from lithium vacancies and therefore the amount of polarons is set by the amount of lithium, and/or by the presence of impurities and defects. The electronic conductivity is determined by the concentration of polarons as charge carriers, and by the activation energy required to exchange  $\text{Fe}^{3+}$  ions to adjacent  $\text{Fe}^{2+}$  ions upon polaron hopping.[35] The reported values of the activation energy for the polaron hopping in bare  $\text{LiFePO}_4$  range from 0.156 eV to 0.63 eV, while the values of the electronic conductivity, determined either by DC or AC techniques, range from  $10^{-7}$  to  $10^{-9}$   $\text{S cm}^{-1}$  for the lithiated phase, [26, 36] and  $10^{-10}$  to  $10^{-11}$   $\text{S cm}^{-1}$  for the delithiated phase.[37] The uncertainty among these reported values may be associated not only to different experimental set-ups or to the use of different techniques, but also to the difficulties in measuring exclusively the intrinsic electronic conductivity of  $\text{LiFePO}_4$  without interference from its ionic conductivity, or from electrode scale contributions.[35]

### 1.3.2-b Ionic conductivity

Regarding the conduction process of lithium in  $\text{LiFePO}_4$ , Morgan *et al.* determined through first-principles techniques that the migration of lithium has the lowest activation barrier (0.27 eV) for the pathway along the [010] direction.[38] According to the authors, Fe siting on Li sites can limit the mobility of lithium. Using atomistic modelling techniques, Islam *et al.* confirmed the preferred diffusion of lithium along the [010] direction, and also suggested a curved trajectory between adjacent Li sites.[39]. Nishimura *et al.* provided the experimental confirmation of the curved, one-dimensional trajectory for lithium motion by analysing high-temperature powder neutron diffraction data.[40]

### 1.3.2-c Electronic conductivity vs. ionic conductivity in $\text{LiFePO}_4$

The rate limitations for charge transport in  $\text{LiFePO}_4$  have been commonly attributed to a low intrinsic electronic conductivity of this material. This paradigm has been

objected by the following reports concerning the effects of the particle size and the lithium ion transport on the conductivity of the phosphate:

- i) Amin *et al.* reported that the ionic conductivity of  $\text{LiFePO}_4$  single crystals is  $\sim 4$  orders of magnitude less than the respective electronic conductivities along the  $a$ ,  $b$  and  $c$  axes.[41a-b]
- ii) Delacourt *et al.* have reported a notable electrochemical performance for  $\text{LiFePO}_4$  without carbon-coating, when the particle size is lower than a threshold value of  $\sim 150$  nm.[42] Gaberscek *et al.* have also reported that the particle size has a more important effect on the conductivity and on the electrochemical performance, as compared to the effect of the carbon-coating.[43]
- iii) As initially suggested by Morgan *et al.*,[38] and later discussed by Malik *et al.*,[35] and by Yang *et al.*[44] based on theoretical calculations, defects and impurities can hinder the mobility of lithium, especially in the [010] direction, and cause significant poor rate performance.

During charge/discharge operation, the electroneutrality principle requires that the transfer or transport of electrons (or polarons) and lithium ions take place simultaneously within a particle or between neighbouring particles. Using DFT methods, Maxisch *et al.*[45] calculated that the binding energy of the  $\text{Li}^+$ /polaron couple is approximately 0.5 eV. This value is comparable to the values calculated for the polaron migration barrier (0.4 to 0.65 eV),[26, 46] which in turn are comparable to the theoretical values for the lithium migration energy (0.55 eV).[39]

Based reports mentioned above, the question of whether the electronic conductivity or the ionic conductivity determines the rate performance of  $\text{LiFePO}_4$  remains unsolved. Nevertheless, the evidence highlights the necessity of optimizing both mechanisms by modifying intrinsic properties of  $\text{LiFePO}_4$  or by using additives of mixed conductor character, in order to minimize the resistivity at the electrode level.



### 1.3.3 Lithium extraction/insertion mechanisms of $\text{LiFePO}_4$

The mechanism by which  $\text{Li}_x\text{FePO}_4$  ( $0 < x < 1$ ) transforms upon electrochemical lithium extraction/insertion has been the focus of intense research since 1997, and several models have been considered to account for some intriguing observations, such as the prevalence of either a solid-solution or two-phases. This section presents some of the models proposed throughout the years in order to gain understanding on the process responsible for the peculiar performance of  $\text{LiFePO}_4$ .

Padhi *et al.* suggested that the poor performance of  $\text{LiFePO}_4$  at high current is associated to a limited diffusion of lithium across a  $\text{LiFePO}_4/\text{FePO}_4$  interface (Fig. 8a). Upon lithium insertion/extraction, the two-phase boundary would extend to a critical area that could not sustain the rate of lithium transport that is necessary to meet the imposed current.[25] Two similar models proposed by Andersson *et al.*, the radial model and the mosaic model (Fig. 8b), consider the core-shell configuration put forward by Padhi *et al.*, as well as the presence of inactive phases within particles that remain isolated due to poor ionic diffusion or low electronic conductivity; which may accounts for the irreversible capacity after the first cycle.[47]

Srinivasan *et al.* developed a mathematical model for the two phase transformation via a shrinking core, where a shell of one phase covers a core of the second phase upon extraction/insertion of lithium.[48] Similarly to the above mentioned core-shell models, the shrinking core model takes into account the limitations of the diffusion of lithium through the shell, but considering the effects of charge transport through the different interphases within the matrix of the porous electrode and the current collector; a situation that could partially explain why  $\text{LiFePO}_4$  performs better when it is coated by carbon.

The three models described above are intuitive as they assume the coexistence of two-phases within the particles, as well as isotropic lithium diffusion. More descriptive models of the phase transformation mechanism of  $\text{LiFePO}_4$  consider the well known anisotropic diffusion of  $\text{Li}^+$ , [38-40] as well as the coherence strain between the lithiated and the delithiated phases.[51] For instance, experimental evidence on the directionality of the  $\text{Li}_x\text{FePO}_4/\text{Li}_{1-x}\text{PO}_4$  phase transformation was provided by Chen *et al.* and Laffont

*et al.*, by using high resolution electron microscopy[52] and electron energy loss spectroscopy,[53] respectively. Both studies concluded that the preferential diffusion of lithium parallel to the *b*-axis guides the formation of the  $\text{Li}_x\text{FePO}_4/\text{Li}_{1-x}\text{FePO}_4$  interface along the same direction. These observations support the good electrochemical performance commonly observed for  $\text{LiFePO}_4$  with platelet morphologies having short crystal size along the *b*-axis.[54]

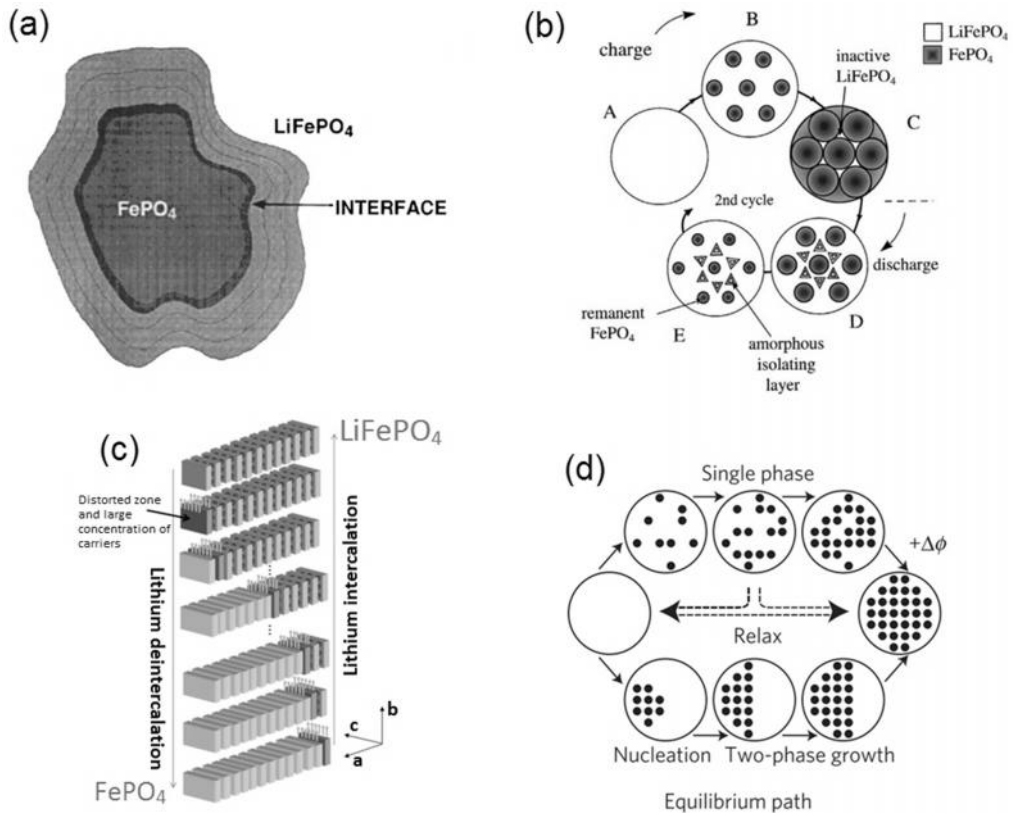


Figure 8. Phase transformations models for  $\text{LiFePO}_4$ : a) by Padhi *et al.*,[25] b) "Mosaic" by Andersson *et al.*,[47] c) "Domino-cascade" by Delmas *et al.*,[49] and d) "Single-phase transformation" by Malik *et al.*,[50] The figures were adapted from their respective sources.

Delmas *et al.* proposed the domino cascade model (Fig. 8c) to explain the coexistence of individual particles composed either of  $\text{LiFePO}_4$  or  $\text{FePO}_4$ , as detected by XRD and electron microscopy.[49] The authors suggest that the nucleation process is the rate determining step and that the growth of a phase at the expense of the other,

by the extraction/insertion reaction, creates a distorted interphase. This interphase has an enhanced lithium and electron conductivity that favours the progressive, full phase transformation at a given particle, by a process driven by the minimization of the stress originated by the lattice mismatch between the  $\text{Li}_x\text{FePO}_4$  and  $\text{Li}_{1-x}\text{PO}_4$  phases.[55]

Single-phase models have also been developed considering not only the existence of a solid solution of  $\text{Li}_x\text{FePO}_4$  ( $0 < x < 1$ ) above  $300^\circ\text{C}$ , but also the possibility of extending the single-phase region by reducing the particle size below a critical value of  $\sim 45\text{ nm}$ . [56a-b] A single phase model proposed by Malik *et al.* (Fig. 8d) considers that an activation overpotential of  $\sim 30\text{ mV}$  is required to access a non-equilibrium solid-solution state.[50] This value is close to the experimental value of  $20\text{ mV}$  determined at a rate of  $C/1000$ , as reported by Dreyer *et al.*[57] Once the single phase starts to form within  $\text{LiFePO}_4$  crystallites, the insertion/reaction can follow a nucleation-growth mechanism until the reaction is completed, or proceed through a relaxation pathway towards the two-phase growth within crystallites. Whether the transformation of  $\text{LiFePO}_4$  involves one or two phases strong dependency on the particle size, the integrity of the crystalline structure, the reaction rate, and the conditions (equilibrium or non-equilibrium) at which the measurements are carried out, among other parameters.[58]

### 1.3.4 Synthesis of $\text{LiFePO}_4$

$\text{LiFePO}_4$  exists in nature as the mixed iron/manganese phosphate  $\text{Li}[\text{FeMn}]\text{PO}_4$ , known as triphylin, which was firstly described by von Fuchs in 1834.[59] Although Ravet *et al.* showed that some natural, impure ores of  $\text{LiFePO}_4$  can undergo electrochemical extraction/insertion of lithium,[33a] it is well known that the presence of unwanted impurities or structural defects have detrimental impact on the performance of this material.[58] Therefore, only synthetic  $\text{LiFePO}_4$  is considered for practical applications. Several methods have been adapted and developed for the synthesis of  $\text{LiFePO}_4$ , not only aiming to obtain a high performance material and to gain understanding on fundamental properties, but also to produce  $\text{LiFePO}_4$  at industrial scale at a competitive cost. The following sections present an overview on two of the main methods that have been applied for the preparation of  $\text{LiFePO}_4$  at industrial scale: a) high temperature solid-state synthesis and b) mild temperature hydrothermal

synthesis. Further details on other synthesis methods can be found in comprehensive reviews from the perspective of academic and industrial players.[60a-d]

### **1.3.4-a High temperature solid-state synthesis**

Two different approaches are common for the high temperature synthesis of  $\text{LiFePO}_4$ : i) solid state reaction of appropriate lithium and phosphate precursors with ferrous compounds; ii) solid state, carbothermal reduction of ferric compounds and reaction with lithium and phosphate precursors.[61] For any of these two approaches, elemental carbon or carbon-containing compounds are commonly used for providing reducing power, for preventing oxidation of the ferrous precursors, or for reducing ferric precursors. Additionally, carbon forms a coating over  $\text{LiFePO}_4$  that not only enhances the electronic conductivity, but also limits the growth of  $\text{LiFePO}_4$  particles.[62]

Common precursors for the solid state synthesis or carbothermal synthesis of  $\text{LiFePO}_4$  include: lithium hydroxide or carbonate, Fe(II) oxalate or acetate, Fe(III) oxide or phosphate, and ammonium phosphate. Both methods consist in heating the precursors in two steps under inert ( $\text{Ar}$ ,  $\text{N}_2$ ) or reducing ( $\text{Ar}/\text{H}_2$ ) atmosphere. After a thorough mixing of the precursors, the first heating step is carried out at temperature values between 200-400°C, in order to decompose the precursors. The product of the first heating step is then re-mixed and/or pelletized, and heated between 600-1000° C.[63a-b] Critical parameters for obtaining pure, active  $\text{LiFePO}_4$  include: the stoichiometric proportions of the precursors, the reaction atmosphere, the carbon source, the heating temperature and the heating time. The main disadvantages of the high temperature methods include the high energy consumption required for the several heating and mixing steps, the difficulties for obtaining nano-sized primary particles, preventing agglomeration, and avoiding the presence of impurities such as  $\text{Li}_3\text{PO}_4$ ,  $\text{Li}_3\text{Fe}_2(\text{PO}_4)_3$ ,  $\text{Fe}_2\text{O}_3$  or iron phosphides.

### **1.3.4-b Mild temperature hydrothermal synthesis**

Mild temperature methods for synthesizing  $\text{LiFePO}_4$  take advantage of the solubility of the precursors in water or in other solvents under different temperature, pH and pressure conditions. In general, these methods require an initial, mild temperature exchange reaction of the starting precursors, which can lead to precipitating  $\text{LiFePO}_4$  directly or by forming intermediate phases. This is achieved by co-precipitation

reactions, sol-gel methods, hydrothermal/solvothermal or ionothermal reactions.[60c] In most of the cases, it is necessary an additional high temperature heating of the mild temperature product in presence of a carbonaceous compound, in order to form crystalline, active  $\text{LiFePO}_4$ .

Currently, one of the most successful mild temperature methods for synthesizing  $\text{LiFePO}_4$  is the autogenous hydrothermal method, which was pioneered by Whittingham's group. Common precursors for the hydrothermal synthesis are:  $\text{FeSO}_4 \cdot 7\text{H}_2\text{O}$ ,  $\text{LiOH}$  and  $\text{H}_3\text{PO}_4$ , which react in aqueous solution inside an autoclave at temperatures ranging from 100-250° C with autogenous pressure. Yang *et al.* demonstrated that the reaction at 120° C favours the amount of Fe on Li sites, which blocks the diffusion of lithium and causes the poor performance of samples prepared below ~180° C.[64] This type of disorder is readily removed by heat treatment above 700° C. On the other hand, the problem of iron oxidation in aqueous solution has been addressed by adding reductants such as sucrose, ascorbic acid or citric acid. One of the most appealing advantages of the hydrothermal/solvothermal methods is the possibility of tuning the particle size and morphology by using of surfactants such as Cetyl Trimethyl Ammonium Bromide or Polysorbate.[65]

### 1.3.5 Improving the conductivity of $\text{LiFePO}_4$ and $\text{LiFePO}_4$ -based electrodes

The low intrinsic conductivity of  $\text{LiFePO}_4$  has been considered as the limiting factor for achieving efficient lithiation/delithiation at fast charge/discharge rates. After the work of Ravet *et al.* on the beneficial effects of carbon-coating,[33a] most efforts have been directed towards increasing the electronic conductivity of  $\text{LiFePO}_4$ . In this regard, Chung *et al.* published a report claiming that "controlled cation non-stoichiometry combined with solid-solution doping by metals supervalent to  $\text{Li}^+$  increases the electronic conductivity of  $\text{LiFePO}_4$  by a factor of  $\sim 10^8$ ".[66] However, some authors have criticized this affirmation by pointing out that the abrupt increase in electric conductivity could be either due to the formation of a carbon-coating over  $\text{LiFePO}_4$  particles by decomposition of the used carbon-containing precursors, or due to the reduction of the aliovalent ions to a metallic, conducting phase. Currently, there is still debate on whether aliovalent

ions can be incorporated or not in the olivine structure by doping, either on Fe or Li sites.[67a-c]

Another controversial report was published by Kang *et al.* regarding the formation of ionically conductive coatings over  $\text{LiFePO}_4$  nano-particles and the possibility to achieve ultrafast charge/discharge rates of up to  $\sim 400\text{C}$  ( $\sim 9$  seconds).[68] The authors claimed that such an ultrafast rate was enabled by the presence of an intentionally produced, poorly crystallized coating, probably composed of  $\text{Li}_3\text{PO}_4$  and  $\text{Li}_4\text{P}_2\text{O}_7$ , which promotes rapid lithium transport to the surface of  $\text{LiFePO}_4$  nanoparticles. Zaghbi *et al.* put forward a challenging critic to that report, suggesting that  $\text{Li}_4\text{P}_2\text{O}_7$  occurs as an impurity that forms nanoparticles that stick to the surface of  $\text{LiFePO}_4$ , and thus the reported rate performance could be mostly due to the conducting carbon-coating over the active material nanoparticles.[69] As pointed out later by Ceder & Kang, the composition and origin of the phases, other than  $\text{LiFePO}_4$ , obtained by reacting off-stoichiometric proportions of precursors is uncertain.[70]

Fig. 9 presents a classification of the different approaches that have been proposed in order to improve the electronic and/or ionic conductivity of  $\text{LiFePO}_4$  and  $\text{LiFePO}_4$ -based electrodes at different scales. Some of the proved and most common approaches are discussed below, with an emphasis on the use of intrinsically conducting polymers.

### 1.3.5-a Carbon-coating

The most common approach adopted for increasing the electronic conductivity of  $\text{LiFePO}_4$ -based electrodes has been the formation of carbon coatings over the active material particles. Such coatings are formed over  $\text{LiFePO}_4$  either by carbonization of precursors or by high energy milling with carbon powders. Carbonization can be carried out during the synthesis of  $\text{LiFePO}_4$  or on ready prepared  $\text{LiFePO}_4$  at temperatures ranging from  $500\text{-}700^\circ\text{C}$  by decomposition of carbon-containing precursors such as: organic salts (acetates, oxalates, carbonates, citrates, etc.), sugars (sucrose, glucose, lactose), surfactants, or polymers.[71a-d]

The quality of the carbon-coating is determined by the following factors: thickness (preferably lower than  $5\text{ nm}$ ); degree of graphitization (high  $\text{sp}^2/\text{sp}^3$  ratio); the amount of carbon (preferably less than  $5\% \text{ wt.}$ ); the porosity and homogeneity.[72] Apart from raising the conductivity of  $\text{LiFePO}_4$  by  $\sim 7$  orders of magnitude, carbon-coating can

restrict the particle overgrowth by avoiding inter-particle coalescence, and also induce the recrystallization of the particle's surface layer.[73] All of these effects led ultimately to an improvement of the electrochemical performance that does not originate from an increase of the intrinsic conductivity of  $\text{LiFePO}_4$ , but from the effective connectivity between the particles and their wiring throughout the electrode and to the current collector. The main disadvantage of applying a carbon coating over  $\text{LiFePO}_4$  is the decrease of the tap density, which can limit the practical cell volumetric energy.[74] Furthermore, the carbonization of organics is a high energy consuming process that generates contaminants. Therefore, alternative, less energy-consuming methods could reduce the environmental footprint of the conventional fabrication of carbon-coated  $\text{LiFePO}_4$ .

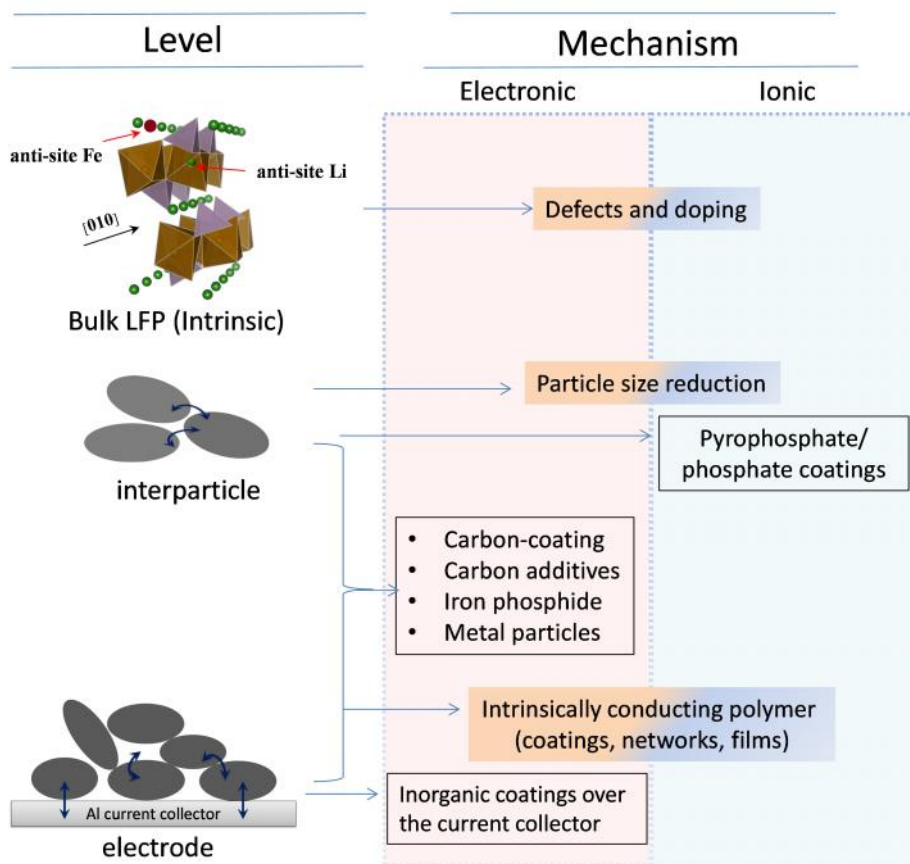


Figure 9. Different approaches for enhancing the conductivity mechanism (electronic or ionic) at different levels for  $\text{LiFePO}_4$  and  $\text{LiFePO}_4$ -based electrodes.

### 1.3.5-b Particle size reduction and morphology

The reduction of the particle size of  $\text{LiFePO}_4$  has been experimentally proven as an effective way for improving the rate performance. This improvement is associated to a decrease of the electrode's resistance, which in turn is attributed to the short distance for lithium and/or electron diffusion/migration in nanoparticles.  $\text{LiFePO}_4$  nano-particles ranging from ~300 to ~5 nm can be produced by low-temperature methods such as hydrothermal,[75] polyol,[76] co-precipitation,[77a-b] or mechanochemical activation.[78] Although the combination of carbon-coating and nano-particles typically results in a synergistic effect for  $\text{LiFePO}_4$ , [79a-b] according to the reports of Delacourt *et al.*, [42] and Gaberscek *et al.*, [43] the role of particle size is more important than that of carbon-coating for  $\text{LiFePO}_4$  particles smaller than ~150 nm.

Together with the particle size, the morphology of the particles plays an important role in enabling fast charge/discharge rates of  $\text{LiFePO}_4$ , as it has been observed for particles that grow in different shapes.[80a-c] Such observations were supported by the theoretical study of Fisher and Islam, who calculated the equilibrium surface energy and the non-equilibrium surface attachment associated to low-index planes of  $\text{LiFePO}_4$  crystals.[81] These authors provided an explanation for the charge/discharge rate improvement in terms of the prevalence of the lowest energy (201) and (010) surfaces in the equilibrium and in the non-equilibrium particle morphology. The latter surface provides the most facile pathway for lithium ion conduction,[81] provided no anti-site defects are present along the lithium migration channels.

### 1.3.5-c Conducting inorganic additives and coatings

#### i) Carbons

Carbons are widely used as conductive additives to reduce the resistance of  $\text{LiFePO}_4$ -based electrodes and other positive or negative electrodes for Li-ion batteries. Carbon materials that have been used for creating electron-conducting networks in  $\text{LiFePO}_4$ -based electrodes are of diverse type and form, these include carbon black or graphite particles,[82a-b] carbon fibres,[83a-b] as well as other advanced carbons such as nanotubes or graphene, which have been reviewed recently.[84a-b]



The type and the optimal amount of carbon conducting additive used in  $\text{LiFePO}_4$ -based electrodes is determined by the shape and size distributions of the active material particles, which determine the percolation threshold for electron conduction by point-to-point contact or by tunnelling effect. The morphological characteristics of carbon additives not only influence the electronic conductivity, but also the ionic conductivity as the electrolyte availability and the ionic transport rate are affected by the porosity and tortuosity of the electrode.[85]

Typically, carbons are attached to the active particles by polymeric binders such as PVDF. Despite being used in small amounts (usually less than 10%), most carbons can absorb the binder and thus influence the electrode's manufacturing process and the mechanical properties of the composite electrodes.[86] Currently, carbon black, graphite or carbon fibres are the most used conducting additives for  $\text{LiFePO}_4$ -based electrodes in commercial batteries. Apart from being cost effective, these additives provide the best compromise between electronic conductivity and low electrolyte or binder absorption, which results in optimal electrode performance due to effective electrolyte wettability and mechanical stability.[87]

## ii) Iron phosphides

Herle *et al.* reported on the attempt to carry out the synthesis of  $\text{LiFePO}_4$  doped by Zr,[67] as previously reported by Chung *et al.*,[66] concluding that the conductivity enhancement of  $\text{LiFePO}_4$ -based electrodes was due to the presence of "a percolating nano-network of metal-rich phosphides". According to Herle *et al.*, such conducting phases are formed upon carbothermal reaction of the precursor above  $800^\circ\text{C}$ , independently of the presence or absence of Zr dopant. Under such conditions, carbon-containing iron salt precursor forms  $\text{LiFePO}_4$  with  $\text{Fe}_2\text{P}$  and/or iron phosphocarbide ( $\text{Fe}_{75}\text{P}_{15}\text{C}_{10}$ ) at grain boundaries, whereas  $\text{FeP}$  has been detected at the bulk by SEM/EDX. Further evidence on the presence of  $\text{Fe}_2\text{P}$  and  $\text{FeP}$  phases was presented by Rho *et al.*, based on Mössbauer and XPS spectroscopies.[88a-b]

### iii) Metal particles

The presence of dispersed metal particles of copper or silver formed during the synthesis of  $\text{LiFePO}_4$  has been reported to improve the rate performance.[89a-b] Although these metal-added composites provide better charge/discharge characteristics than metal-free composites, issues such as the corrosion/passivation of metal particles and their higher cost as compared to other conducting additives, such as carbons, renders the use of metal particles unattractive for mass production.

### iv) Coatings over the current collector

The resistance of the interface between the current collector and the layer containing the active material requires special attention as it contributes to the ohmic drop and can limit the rate capability,[90] even if an optimized  $\text{LiFePO}_4$  is used. Besides, this interphase has to ensure the electrical contact in order to enable high material utilization and reversibility. Furthermore, when corrosive electrolytes are used (e.g. LiTFSI-based), the anodic oxidation of aluminium above  $\sim 3.7$  V can compromise the electrode's integrity and limit the cycle life.[91] Considering these issues, protective coatings based on carbons have been applied over the aluminium current collector.

Carbon-coated aluminium has been prepared by diverse methods such as i) casting of slurries containing a binder and dispersed carbon particles;[92a] ii) dry impregnation of carbon and a binder over aluminium by pressing;[92b] or iii) high temperature reduction of methane over aluminium.[92c] In general, the improvement in rate capability and cycle life of  $\text{LiFePO}_4$ -based electrodes with protected aluminium current collector has been attributed to a better adhesion and mechanical integrity of the composite layer or to the removal of the native, insulating  $\text{Al}_2\text{O}_3$  layer.

#### 1.3.5-d Coatings and films of intrinsically conducting polymers

Intrinsically conducting polymers (ICPs) resemble inorganic insertion compounds as the former undergo electrochemical oxidation/reduction reactions and can insert or extract ions in order to maintain electroneutrality (see section 1.4 for an overview on ICPs). Their ability to conduct electrons and ions, together with their stability in common lithium battery electrolytes, enable the use of ICPs as active materials for lithium-based batteries[93a-d] or as functional additives in composite materials with  $\text{LiMnO}_2$ .[94]

$\text{LiMn}_2\text{O}_4$ , [95a-b]  $\text{LiV}_2\text{O}_5$  [96a-b],  $\text{LiCoO}_2$ , [97a-b] among other active materials that have been recently reviewed. [98a-b]

$\text{LiFePO}_4$  and C- $\text{LiFePO}_4$  have also been combined with common ICPs such as polyaniline, [99a-f] polypyrrole, [100a-f] and polythiophene, [101] taking advantage of the favourable redox states of these conducting polymers at the operational voltage of  $\text{LiFePO}_4$ . Although their mechanical properties are not as good as those of common polymeric binders, ICPs improve the connectivity between the active material particles and provide conducting pathways that extend to the current collector, thus enabling higher material utilization and homogeneous current distribution. Additionally, ICPs have been applied for corrosion inhibition and protection of the aluminium current collector in lithium batteries. [99g] Thus, ICPs could offer several advantages over previously reported carbon-coatings, either when applied over the  $\text{LiFePO}_4$  particles or over the aluminium current collector of  $\text{LiFePO}_4$ -based electrodes. These advantages include: i) the formation of compact, functional polymeric coatings and layers that can be prepared chemically, electrochemically or by mechanical deposition methods; ii) contribution to the electrode capacity; [100d] iii) enabling the lithium insertion/extraction reaction fronts from the current collector towards the electrode/separator interface; [102] or iv) overcharge/overdischarge protection by virtue of the polymer's voltage-dependent conductivity. [103a-b]

Poly(3,4-ethylenedioxythiophene) [PEDOT] is one of the most studied ICPs for  $\text{LiFePO}_4$ /ICP composites due to its high conductivity in the doped state. Besides, PEDOT is commercially available as a complex with polystyrene sulfonate (PEDOT:PSS), which facilitates the formation and processing of composites.

Different methods have been applied for synthesizing PEDOT and for combining it with  $\text{LiFePO}_4$ . In general, oxidative chemical polymerization and electropolymerization are the most common ways to synthesize ICPs, as detailed in section 1.4.1. Regarding the formation of the  $\text{LiFePO}_4$ /PEDOT composites, two general approaches are usually applied: 1) blending  $\text{LiFePO}_4$  and ready synthesized PEDOT; [104a-h] and 2) chemical or electrochemical polymerization of EDOT monomers in presence of  $\text{LiFePO}_4$ . [104i-j]

Table 5 lists a selection of reports on the preparation of  $\text{LiFePO}_4$ -based electrodes with different conducting polymers published in the last years, with an emphasis on the use of PEDOT.

*Table 5. Characteristics of some LiFePO<sub>4</sub>-based composite electrodes with different conducting polymer obtained by chemical, electrochemical or by blending methods. The values of specific capacity and energy are referred to the weight of the electrode without current collector. PANI≡Polyaniline, PPy≡Polypyrrole, PTH≡Polythiophene.*

Polymer	Preparation chem≡chemical echem≡electrochemical	Polymerization			Composition (% w)				Performance “C-rate/(Q <sub>total</sub> *E <sub>50%DOD</sub> )” Q <sub>total</sub> ≡total disch. capacity E <sub>50%DOD</sub> ≡potential at 50 % DOD	Capacity (Ah/kg)	Energy density @50% DOD (Wh/kg)	Ref.
		Oxidant or electrode	Source of counter ion	Solvent	LFP	ICP	C	Binder				
Reference preparation without conducting polymer												
PANI	Chem	(NH <sub>4</sub> ) <sub>2</sub> S <sub>2</sub> O <sub>8</sub>	p-TSNa	H <sub>2</sub> O	70	5	20	5	1C(127*3.26), 2C(116*3.14), 5C(91*2.84), 10C(47*2.46) [interpolated]	104 95 74 39	169 149 106 48	83b
PPy	Chem	(NH <sub>4</sub> ) <sub>2</sub> S <sub>2</sub> O <sub>8</sub>	p-TSNa	H <sub>2</sub> O	70	5	20	5	1C(133*3.36), 2C(125*3.34), 5C(110*3.1), 10C(81*3.02)	93 88 77 57	156 146 119 86	99a
PPy	echem (potential steps)	Steel mesh	LiClO <sub>4</sub>	CH <sub>3</sub> CN	80	20	-	-	1C(112*n/a)	90	n/a	100d
PPy	echem (cyclic voltammetry)	Steel mesh	LiClO <sub>4</sub>	CH <sub>3</sub> CN	80	20	-	-	1C(101*n/a)	81	n/a	100d
PTH	Chem	FeCl <sub>3</sub>	FeCl <sub>3</sub>	CHCl <sub>3</sub>	64.5	10.5	5	20	1C(106*n/a)	68	n/a	101
PEDOT	Chem	(NH <sub>4</sub> ) <sub>2</sub> S <sub>2</sub> O <sub>8</sub>	p-TSA	H <sub>2</sub> O- metanol	73.5	1.5	20	5	1C(154*3.24), 2C(144*3.11), 5C(121*2.8)	113 106 89	183 165 125	104a
PEDOT	Chem	FeCl <sub>3</sub>	p-TSA	H <sub>2</sub> O	90	10	-	-	1C(153*3.36), 2C(146*n/a), 5C(131*n/a)	138 118	231 n/a	104e
PEDOT	Chem	Li <sub>3</sub> *FePO <sub>4</sub>	LITFSI	H <sub>2</sub> O	84.5	8	-	7.5	1C(152*3.27), 2C(146*3.23), 5C(135*3.1), 10C(123*2.89)	128 123 114 104	210 199 177 150	104i
PEDOT	echem (potentiostatic)	Pt wire	TEABF <sub>4</sub>	H <sub>2</sub> O- CH <sub>2</sub> Cl <sub>2</sub>	33.5	76.5	-	-	1C(51*3.04), 5C(32*2.67)	51 32	78 43	104j
PEDOT	Commercial (Chem)	n/a	PSS	H <sub>2</sub> O	92	8	-	-	C/5(117*3.4), 1C(107*n/a)	107	n/a	104g
PEDOT	Commercial (Chem)	n/a	PSS	H <sub>2</sub> O	92	8	-	-	1C(142*3.21), 2C(132*3.1), 5C(126*2.8)	131 121 116	210 188 162	104h

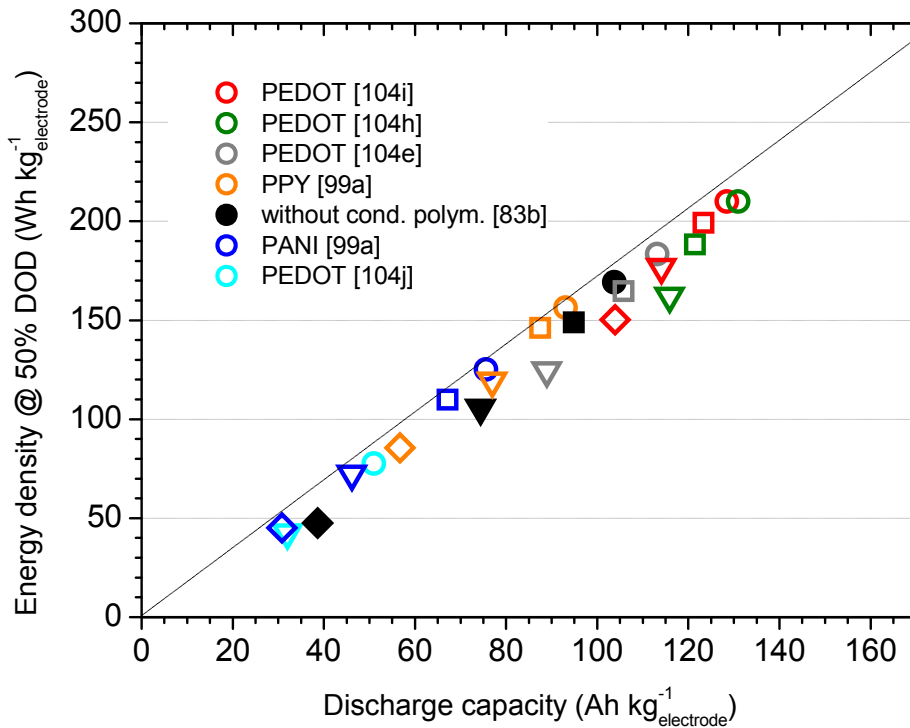


Figure 10. Plot of the gravimetric capacity and energy density of a series of  $\text{LiFePO}_4$ -based composites listed in Table 5. Both capacity and energy are referred to the weight of the electrode without considering the current collector. Circles: data @ 1C, squares: data @ 2C, triangles: data @ 5C, diamonds: data @ 10C. The dotted line indicates the theoretical limit assuming a constant voltage of 3.42 V for an electrode composed of only  $\text{LiFePO}_4$ . DOD  $\equiv$  Depth of discharge, PPY  $\equiv$  Polypyrrole, PANI  $\equiv$  Polyaniline.

Fig. 10 presents a graphical comparison of the gravimetric capacity and the gravimetric energy density at a depth of discharge (DOD) of 50% at 1C, 2C, 5C and 10C discharge rates for a selection of composites listed in Table 5. The reader may consult Appendix III (Galvanostatic cycling) for a description on how to estimate the values at 50 % DOD. The benchmark performance considered here is set by an electrode prepared with commercial C- $\text{LiFePO}_4$  by a standard procedure and without conducting polymer.[83b] One must keep in mind that the performance of  $\text{LiFePO}_4$ -based electrodes is affected by factors such as the quality of the active material, the presence of carbon-coating, the electrode composition, the preparation steps, as well as the

cycling conditions. Due to the marked different experimental conditions listed in Table 5, the comparison presented in Fig. 10 has to be considered only as indicative of the effect of the different conducting polymers on the performance of the electrodes. Having considered the previous statements, the electrodes containing chemically synthesized PEDOT may be considered superior in terms of rate performance than the electrode without conducting polymer or the electrodes containing chemically synthesized polyaniline (PANI) or polypyrrole (PPy).

To date, only a few reports deal with  $\text{LiFePO}_4$ -based composites with conducting polymers formed by electropolymerization. The reviewed reports on such electrochemically prepared composites containing PPY or PEDOT present very poor rate performance, most probably due to the bad incorporation of active material to the polymer during electropolymerization. Therefore, there is an opportunity to develop new strategies to carry out the electrochemical polymerization of monomers, EDOT in particular, in presence of the active material or directly over the electrodes. Preferably, such electrochemical strategies for preparing  $\text{LiFePO}_4$ /ICP composites have to be simple, without causing major modifications to the of state-of-the-art methods for producing  $\text{LiFePO}_4$ -based electrodes.

## 1.4 Overview of intrinsically conducting polymers

Intrinsically conducting polymers (ICPs) are organic, polymeric materials which show conductivity values in the range of semiconductors to metals ( $\sim 10^{-8}$  to  $\sim 10^3$  S cm<sup>-1</sup>), depending on the oxidation and doping level of the polymer.[105] The designation “intrinsically” is used for specifying that the conductivity is inherent to the polymer and not due to an added conducting component, as it is the case for blends of polymers and carbons or metallic particles. The first studies concerning ICPs date back to the works done in the 19<sup>th</sup> century by Runge, Lightfoot, Letheby, among others, on the reactivity and the electropolymerization of aniline.[106a-c] During the second half of the 20<sup>th</sup> century, fundamental studies on polypyrrole, poly(sulfurnitride), and mainly on the doping of polyacetylene, promoted the consolidation of the field of conducting polymers led by the 2000 Chemistry Nobel Prize recipients A. J. Heeger, A. G. MacDiarmid and H. Shirakawa.

The combination of metallic conductivity and plasticity has prompted the commercial use of ICPs. Nowadays, these materials are available for electronic or photographic applications that require conducting, thin protective films to prevent corrosion or static dust contamination. Other technological applications of ICPs include sensors, electromagnetic shielding, electrochromic windows, LEDs or devices for energy storage and conversion, among other applications that have been summarized and discussed in recent reviews.[93d, 107a-b]

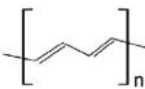
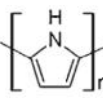
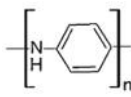
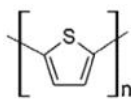
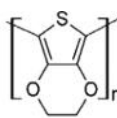
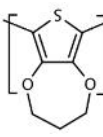
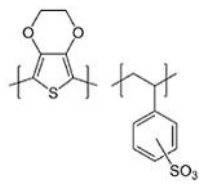
### 1.4.1 Synthesis of ICPs

Intrinsically conducting polymers have alternating single and double C-C bonds forming a  $\pi$ -conjugated system by the overlapping of carbon  $p_z$  orbitals. In some conjugated polymers with heteroatoms, such as polyaniline, the heteroatom is also involved in the conjugated system. Table 6 presents a list of conducting polymers and reported values for their bandgap, conductivity and redox potential. These properties are affected by several factors that involve the  $\pi$ -conjugation and bond length, the effect of substituents, as well as inter-chain and intra-chain interactions.

Conjugated polymers are synthesized by chemical, electrochemical or by photochemical polymerization methods. Each of these methods allows obtaining the final polymer in different forms, either as an insoluble powder, as a film coating an

electrode, or even as a stable dispersion. The chemical and the electrochemical synthesis of ICPs are briefly described in the following sections.

*Table 6. Reported values for selected properties of a series of intrinsically conducting polymers. Most of the values were taken from refs. [93b and 98a].*

Polymer	Repeating unit	Band gap (ev)	Conductivity ( $S\text{ cm}^{-1}$ )	Oxidation-reduction potential in $\text{LiPF}_6$ -based electrolyte (V vs. $\text{Li}^+/\text{Li}$ )
Polyacetylene		1.4 – 1.5	200 – 1000	3.8 [93d]
Polypyrrole		3.1	40 – 200	4.0 – 3.0
Polyaniline		3.2	1 – 100	4.0 – 3.0
Polythiophene		2.0	10 – 100	4.0 – 3.1
PEDOT		1.4 – 2.5	1 – 1000	4.06 – 2.38 [This work Ch. 4]
PProDOT		1.8 [108a]	$\leq 350$ [108b]	4.18– 2.52 [This work Ch. 4]
PEDOT:PSS		2.2 [108c]	$10^{-3}$ – 1000 [108b]	3.8 – 2.63



### 1.4.1-a Chemical polymerization

Conventional polymer synthesis routes have been adapted for the chemical synthesis of conducting polymers, as it is the case of the polymerization of polyacetylene using the Ziegler-Natta catalyst. Polycondensation reactions of halogenated alkylthiophene derivatives, either through Grignard reactions, in presence of a nickel catalyst  $\text{NiCl}_2[3\text{-bis}(\text{diphenylphosphino})\text{propane}]$  or by self-oxidation, can be applied for synthesizing poly-alkylthiophenes of controlled regioselectivity.[109] One of the most common ways to synthesize ICPs is by oxidative polymerization in alcohols or in aprotic polar solvents (e.g. n-butanol or acetonitrile), using Fe(III) salts (e.g. chloride, nitrate and tosylate), peroxydisulfates ( $(\text{NH}_4)_2\text{S}_2\text{O}_8$ ,  $\text{Na}_2\text{S}_2\text{O}_8$ ), organic peroxides, etc.[108b] Fig. 11 presents reaction schemes for the chemical synthesis of PEDOT[FeCl<sub>4</sub>] and PEDOT:PSS.

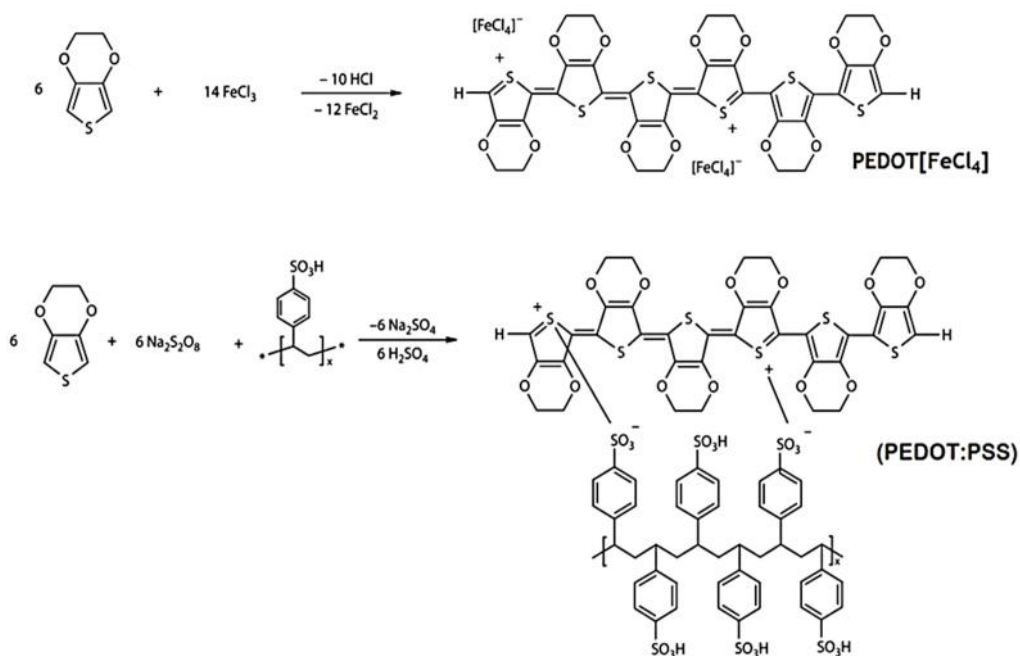


Figure 11. Reaction schemes for the chemical synthesis of PEDOT[FeCl<sub>4</sub>] and PEDOT:PSS. Adapted from ref. [108b].

The oxidative, chemical polymerization of monomers has been described by a radical cation coupling mechanism, as presented in Fig. 12 for the polymerization of thiophene.[109] The transformation steps involve:

- (1) the oxidation of the monomer by electron transfer to an oxidant
- (2) coupling between radical cations at the 2- or 5-position
- (3) stabilization of a dimer by loss of two protons
- (4) oxidation of the dimer
- (5) further coupling and proton loss until reaction completion to produce the polymer in neutral or in doped state

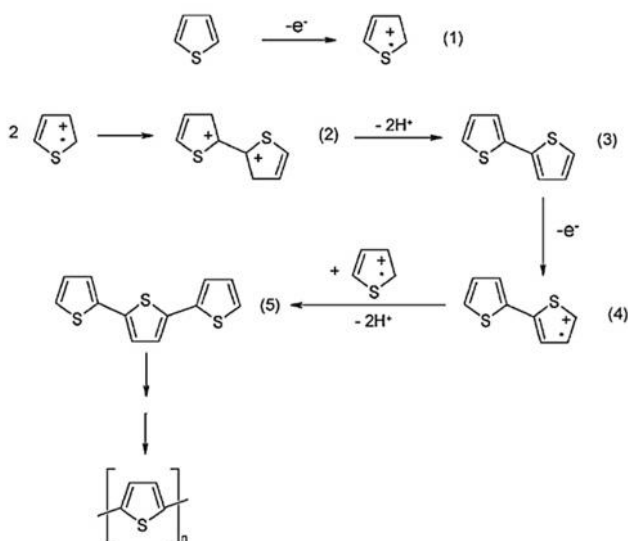


Figure 12. Illustration of the mechanism for the chemical, oxidative polymerization of thiophene. Adapted from ref. [109].

#### 1.4.1-b Electrochemical polymerization

The oxidative polymerization of monomers for obtaining ICPs can also be promoted electrochemically inside a two or three-electrode cell by oxidation (less commonly by reduction) of monomers over an electrode. By electropolymerization, the polymer grows as a conducting film or as a deposit directly over the working electrode. In an electropolymerization experiment, the composition of the solution (solvent, electrolyte,

impurities, etc.), the composition and shape of the working electrode affect the properties of the final polymer. Furthermore, the way to impose the potential or the current, either at fixed values or in steps, allows tuning some properties of the deposited polymer, such as the morphology or the conductivity.

Similarly to the chemical synthesis of ICPs, the electropolymerization is described as an electrophilic substitution proceeding via radical cation intermediates. The first step involves the electrochemical activation of the monomer by formation of a radical cation at the surface of the electrode. The reaction mechanism continues as described before for the chemical polymerization (Fig. 12); through steps (2) to (5). Oligomers can go into solution or deposit onto the electrode to form nucleation sites that continue to react with monomers, thus forming so-called polymer islands. Coalescence of these islands triggers the two-dimensional growth of a primer, usually compact polymer layer over the electrode. In an advanced stage, one-dimensional growth and branching of polymer chains create a less compact structure. As the polymer deposit grows thicker, the rate of polymerization reaction is slowed down due to resistive and transport limitations.[110]

Tuning the potential not only allows controlling the activation of monomers and the reactivity of intermediate oligomers, but it also influences the oxidation state of the formed polymer and prevents the electrolyte decomposition. The potentiodynamic cycling is usually more effective than the potentiostatic mode as the former causes a partial reduction of the oligomers, which promotes the polymerization reaction. The control of the current provides a way to set the extent of the polymerization by affecting the growth mechanism and the structure of the polymer.[111] Usually, the polymerization of monomers is irreversible, although the polymer can undergo oxidation or reduction linked to insertion/release of ions by process referred to as doping.

#### 1.4.2 Doping and charge transport

The pristine, neutral form of  $\pi$ -conjugated polymers has low conductivity as such a system has no partially filled bands, but a completely filled  $\pi$ -band (valence band) and an empty  $\pi^*$ -band (conduction band) separated by an energy gap, as illustrated in Fig. 13a. In order to enable electronic conductivity, free charge carriers have to be available. This is achieved either by oxidation, or by reduction, both of which result in the presence of electronic and counterbalancing ionic charge carriers in the bulk of the conducting polymer. Upon oxidation or reduction of the polymer, unpaired electrons

occupy new energy levels within the energy gap, closer to the valence band or closer to the conduction band, respectively (Fig. 13b). By oxidation, the generated radical cation is equivalent to a positive charge polaron delocalized in the polymer backbone within several repeating units. Further oxidation withdraws more electrons from the valence band causing the merging the localized polaronic levels into a continuous polaronic band (Fig. 13c).

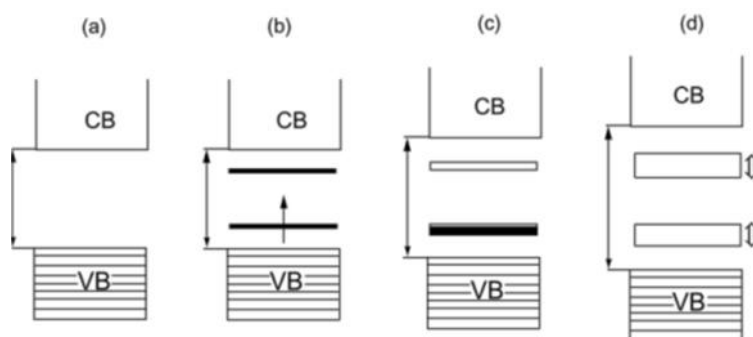


Figure 13. Band diagrams of a non-degenerate  $\pi$ -conjugated polymer related to different doping levels. (a) Undoped (neutral state); (b) Slightly doped polymer with localized polaronic levels; (c) Moderately doped polymer with polaronic bands; (d) Heavily doped polymer with bipolaronic bands. Taken from ref. [105].

Overoxidation results in the spin recombination of polaronic charge carriers forming spinless, double charged bipolarons (dications) that expand their own bands in the gap at the expense of the polaronic and valence bands (Fig. 13d).

Doping of an ICP can take place as the polymer is synthesized (chemically or electrochemically) or can be carried out for ready synthesized polymers. The incorporation of anions from the oxidizing compound is the most common way of doping, although the polymer can incorporate other ions or solvent molecules present in solution. When the polymer is subjected to oxidation/reduction cycles, ions are released or inserted depending on the oxidation state of the polymer and the size of the ions. For instance, during reduction, large anions such as poly(4-styrene sulfonate) remain trapped within the polymer and instead, the polymer inserts cations in order to attain electroneutrality. Therefore, in addition to the electronic transport by polarons or bipolarons, the ionic transport also influences the kinetics of the oxidation/reduction reactions of ICPs.

### 1.4.3 General characteristics of PEDOT and PProDOT

Poly(alkylenedioxythiophenes) constitute a family of oxygen-substituted polythiophenes that were developed in order to improve the stability of this type of polymer against air and/or moisture, as well as to simplify its processing. Despite the low solubility of most conducting polymers in common solvents, polythiophene is more attractive for practical applications than other conducting polymers that are more conducting but present lower stability (e.g. polycetylene), or that are highly toxic (e.g. polyaniline). Substitution in the 3- and 4-position of polythiophene has proven to be effective for eliminating the undesired - coupling reactions during polymerization and, in the case of alkoxy-substituted polythiophenes, it has resulted in an increase of the conductivity by stabilization of the bipolaronic state.[108b]

A technological breakthrough on the conductivity and stability of 3,4-substituted thiophenes was achieved by synthesizing bicyclic systems. In particular, poly(3,4-ethylenedioxythiophene) [PEDOT] can reach a high conductivity ( $400\text{-}600\text{ S cm}^{-1}$ ) in the doped state, depending on the counterion and the polymerization method.[112] For instance, when PEDOT is polymerized in presence of polystyrenesulfonic acid, the complex PEDOT:PSS is formed (see Fig. 11). This complex not only can be dispersed in water and form stable deposits, but also can reach conductivity values of up to  $1000\text{ S cm}^{-1}$  or higher when treated with oxygenated conductivity enhancement agents such as ethylene glycol, dimethyl sulfoxide, *N*-methylpyrrolidone, among other solvents.

Poly(3,4-propylenedioxythiophene) [PProDOT] shares some of the characteristics of PEDOT, although the former can reach only half the conductivity values of PEDOT and it cannot form the PProDOT:PSS complex. Nevertheless, PProDOT can be functionalized in the 2-position of the propylene bridge, thus offering the possibility to synthesize soluble derivatives depending on the length of the substituent chain.

PEDOT and PProDOT share a similar voltammetric response. Fig. 14 presents voltammograms that show the characteristic redox behaviour of EDOT monomers and PEDOT reported vs. the Ag/AgCl electrode, and referred to the  $\text{Li}^+/\text{Li}$  redox pair. The peak at  $\sim 4.2\text{ V}$  (vs.  $\text{Li}^+/\text{Li}$ ) is attributed to the irreversible oxidation of EDOT in the initial forward scan. In the backward scan, the two peaks at  $\sim 2.9$  and  $\sim 2.5\text{ V}$  (vs.  $\text{Li}^+/\text{Li}$ ) evidence the reduction of the polymer grown over the electrode. Upon repeated scans,

the switching between the oxidized and the reduced states takes place in the range of  $\sim 3.0$  V to  $\sim 2.3$  V (vs.  $\text{Li}^+/\text{Li}$ ). Further polymerization of EDOT causes the current to increase, whereas the oxidation potential shifts towards lower values as the reactivity of the oligomers is higher when the conjugation length increases. The oxidation potential of ProDOT is slightly higher (70-120 mV) than that of PEDOT. This is related to the decrease of the  $\pi$ -overlap along the conjugated backbone caused by the extra methylene group, which causes an increase in the bandgap. Nevertheless, PProDOT is characterized by a faster switching redox behaviour between the neutral and the p-doped states.[112]

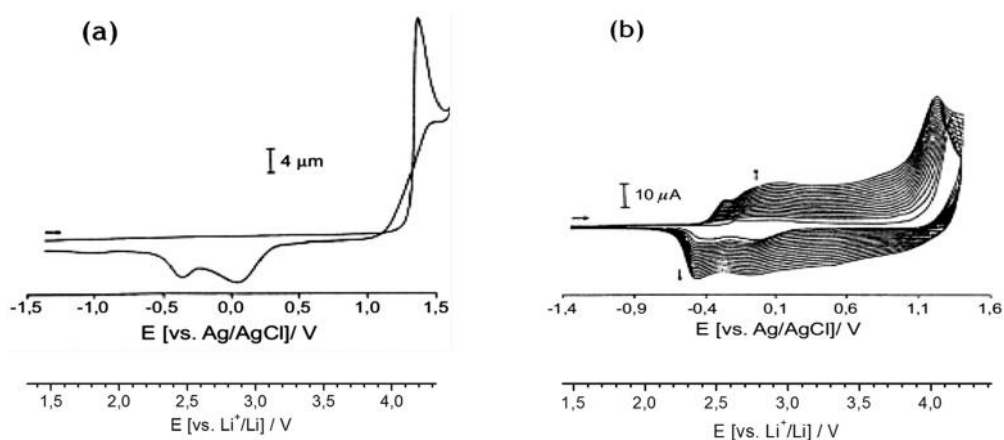


Figure 14. Cyclic voltammetry profiles for (a) EDOT (17 mM) and (b) PEDOT (17 mM EDOT). Both tests were carried out in a supporting electrolyte of tetrabutyl ammonium hexafluorophosphate (0.1 M) in propylene carbonate, at a scan rate of  $100 \text{ mV s}^{-1}$ . The blue scale was added for referring to the potential of the  $\text{Li}^+/\text{Li}$  redox pair. Figures adapted from ref. [108a].

Considering the information exposed in this section and in section 1.3.5-d, the interest in using PEDOT or PProDOT in composite electrodes with  $\text{LiFePO}_4$  stems from the mixed conductor character of these polymers and from the compatibility between the switching potentials of the polymers and the redox potential of  $\text{LiFePO}_4$ . In this way, the polymer molecules may not only provide ionic/electronic communication to  $\text{LiFePO}_4$ , but also assist in the oxidation/reduction process of the active material.

## References

- 2014 Key World Energy STATISTICS, International Energy Agency (OECD/IEA), p 6, 2014.
- (a) <http://www.ecsblog.org/costa-rica-goes-100-green/> (Accessed 19 January 2016)  
(b) [http://www.endesa.com/es/sostenibilidad/PoliticaSostenibilidad/CompromisoTecnologia/El\\_Hierro](http://www.endesa.com/es/sostenibilidad/PoliticaSostenibilidad/CompromisoTecnologia/El_Hierro) (Accessed 19 January 2016).
- X. Luo, J. Wang, M. Dooner and J. Clarke, Overview of current development in electrical energy storage technologies and the application potential in power system operation, *Appl. Energy*. 137 (2015) 511–536.
- (a) D. Linden, Primary Batteries-Introduction. In: D. Linden and T. B. Reddy (Eds.), *Handbook of Batteries*, third edition, The McGraw-Hill Companies Inc; USA, 2001.  
(b) T. Sarakonsri and R. Vasant Kumar, Primary Batteries. In: K. E. Aifantis, S. A Hackney, R Vasant Kumar (eds.), *High Energy Density Lithium Batteries*, p 46, WILEY-VCH Verlag GmbH & Co. KGaA; Weinheim, Germany, 2010.
- A. Arora, N. K. Medora, T. Livernois and J. Swart. Safety of Lithium-Ion Batteries for Hybrid Electric Vehicle. In: G. Pistoia (ed.), *Electric and Hybrid Vehicles, Power Sources, Models, Sustainability, Infrastructure and the Market*, p 465, Elsevier B.V.; Great Britain, 2010.
- M.S. Whittingham, Intercalation chemistry and energy storage, *J. Solid State Chem.* 29 (1979) 303–310.
- Z. Ogumi and H. Wang, Carbon Anode Materials. In: M. Yoshio, R. J. Brodd and A. Kozawa (Eds.), *Lithium-Ion Batteries*, p 49, Springer Science+Business Media; New York, USA, 2009.
- K. Mizushima, P. C. Jones, P. J. Wiseman, J. B. Goodenough, A New Cathode Material for Batteries of High Energy Density, *Mater. Res. Bull.* 15 (1980) 783–789.
- (a) R. Kanno, Y. Takeda, T. Ichikawa, K. Nakanishi, O. Yamamoto, Carbon as negative electrodes in lithium secondary cells, *J. Power Sources*. 26 (1989) 535–543.  
(b) M. Mohri, N. Yanagisawa, Y Tajima, H. Tanaka, T. Mitate, S. Nakajima, M. Yoshida, Y. Yoshimoto, T. Suzuki and H. Wada, Rechargeable lithium battery based on pyrolytic carbon as a negative electrode, *J. Power Sources*, 26 (1989) 545–551.
- Nagura, T. and Tozawa, K., Lithium ion rechargeable battery, *Prog. Batteries & Solar Cells*, 9 (1999), 209–217.
- A. Gören, C. M. Costa, M. N. Tamaño Machiavello, D. Cíntora-Juárez, J. Nunes-Pereira, J. L. Tirado, M.M. Silva, J. L. Gomez Ribelles, S. Lanceros-Méndez, Effect of the degree of porosity on the performance of poly(vinylidene fluoride-trifluoroethylene)/poly(ethylene oxide) blend membranes for lithium-ion battery separators, *Solid State Ionics*, 280 (2015) 1–9.
- (a) K. Xu, Electrolytes and Interphases in Li-Ion Batteries and Beyond, *Chem. Rev.*, 2014, 114 (23), 11503–11618. (b) K. Xu, Nonaqueous liquid electrolytes for lithium-based rechargeable batteries, *Chem. Rev.* 104 (2004) 4303–4417.
- (a) T.-F. Yi, S.-Y. Yang, Y. Xie, Recent advances of  $\text{Li}_4\text{Ti}_5\text{O}_{12}$  as a promising next generation anode material for high power lithium-ion batteries, *J. Mater. Chem. A*, 3(2015) 5750–5777. (b) N. Nitta, F. Wu, J.T. Lee, G. Yushin, Li-ion battery materials: present and future, *Mater. Today*, 18 (2014) 252–264. (c) S. Goriparti, E. Miele, F. De Angelis, E. Di Fabrizio, R. Proietti Zaccaria, C. Capiglia, Review on recent progress of nanostructured anode materials for Li-ion batteries, *J. Power Sources*. 257 (2014) 421–443. (d) J. Chen, Recent Progress in Advanced Materials for Lithium Ion Batteries, *Materials (Basel)*, 6 (2013) 156–183.

14. M. Winter, K.-C. Moeller and J. O. Besenhard, Carbonaceous and Graphitic Anodes. In: G.-A. Nazri and G. Pistoia (Eds.), *Lithium Battery Science and Technology*, pp. 144-194, New York, Springer Science+Business Media; New York, USA, 2009.
15. K. E. Aifantis, Next-Generation Anodes for Secondary Li-Ion Batteries. In: K. E. Aifantis, S. A. Hackney and R. V. Kumar (Eds.), *High Energy Density Lithium Batteries Materials Engineering, Applications*, p 129, WILEY-VCH Verlag GmbH & Co. KGaA; Weinheim, Germany, 2010.
16. **(a)** H. Fujimoto, K. Tokumitsu, A. Mabuchi, N. Chinnasamy, T. Kasuh, The anode performance of the hard carbon for the lithium ion battery derived from the oxygen-containing aromatic precursors, *J. Power Sources*, 195 (2010) 7452-7456.  
**(b)** J. Wang, H.L. Xin, D. Wang, Recent Progress on Mesoporous Carbon Materials for Advanced Energy Conversion and Storage, *Part. Part. Syst. Charact.* 31 (2014) 515–539.
17. M. S. Whittingham, Lithium Batteries and Cathode Materials, *Chem. Rev.* 104 (2004) 4271–4302.
18. G. Prado, L. Fournès, C. Delmas, On The  $\text{Li}_x\text{Ni}_{0.70}\text{Fe}_{0.15}\text{Co}_{0.15}\text{O}_2$  System: An X-Ray Diffraction and Mössbauer Study, *J. Solid State Chem.* 159 (2001) 103–112.
19. S.-T. Myung, S. Komaba, N. Hirotsaki, K. Hosoya, N. Kumagai, Improvement of structural integrity and battery performance of  $\text{LiNi}_{0.5}\text{Mn}_{0.5}\text{O}_2$  by Al and Ti doping, *J. Power Sources*, 146 (2005) 645–649.
20. A. R. Armstrong, P. G. Bruce, Synthesis of layered  $\text{LiMnO}_2$  as an electrode for rechargeable lithium batteries, *Nature*, 381 (1996) 499–500.
21. H. J. Noh, S. Youn, C.S. Yoon, Y.K. Sun, Comparison of the structural and electrochemical properties of layered  $\text{Li}[\text{Ni}_x\text{Co}_y\text{Mn}_z]\text{O}_2$  ( $x = 1/3, 0.5, 0.6, 0.7, 0.8$  and  $0.85$ ) cathode material for lithium-ion batteries, *J. Power Sources*, 233 (2013) 121–130.
22. M. M. Thackeray, Manganese oxides for lithium batteries, *Prog. Solid State Chem.*, 25 (1997) 1–71.
23. Zhicong Shi, Hansan Liu and Jiujun Zhang, Inorganic Cathode Materials for Lithium Ion Batteries. In: G. R. Dahlin and K. E. Strom (Eds.), *Lithium Batteries: Research, Technology and Applications*, Nova Science Publishers Inc; New York, USA, 2010.
24. A. K. Padhi, K. S. Nanjundaswamy and J. B. Goodenough, Phospho-olivines as Positive-Electrode Materials for Rechargeable Lithium Batteries, *J. Electrochem. Soc.*, 4 (1997), 1188–1194.
25. **(a)** Z. Chen, C. Zhang, Z. Zhang, J. Li, Correlation of intercalation potential with d-electron configurations for cathode compounds of lithium-ion batteries, *Phys. Chem. Chem. Phys.*, 16 (2014) 13255–13261. **(b)** A. Gutierrez, N. A. Benedek, A. Manthiram, Crystal-chemical guide for understanding redox energy variations of  $\text{M}^{2+/3+}$  couples in polyanion cathodes for lithium-ion batteries, *Chem. Mater.*, 25 (2013) 4010–4016.
26. C. Delacourt, L. Laffont, R. Bouchet, C. Wurm, J.-B. Leriche, M. Morcrette, J.-M. Tarascon and C. Masquelier, Toward Understanding of Electrical Limitations (Electronic, Ionic) in  $\text{LiMPO}_4$  (M=Fe, Mn) Electrode Materials, *J. Electrochem. Soc.* 152 (2005), A913–A921.
27. **(a)** S. K. Martha, J. Grinblat, O. Haik, E. Zinigrad, T. Drezen, J. H. Miners, I. Exnar, A. Kay, B. Markovsky and D. Aurbach,  $\text{LiMnPO}_4$  as an Advanced Cathode Material for Rechargeable Lithium Batteries, *J. Electrochem. Soc.* 156(7) (2009) A541-A552. **(b)** V. Aravindan, J. Gnanaraj, Y.-S. Lee and S. Madhavi,  $\text{LiMnPO}_4$  – A next generation cathode material for lithium-ion batteries, *J. Mater. Chem. A*, 1(2013), 3518–3539.



28. **(a)** W. Xu, X. Chen, F. Ding, J. Xiao, D. Wang, A. Pan, J. Zheng, X. S. Li, A. B. Padmaperuma, J.-G. Zhang, Reinvestigation on the state-of-the-art nonaqueous carbonate electrolytes for 5 V Li-ion battery applications, *J. Power Sources*, 213 (2012) 304–316. **(b)** C.M. Julien, A. Mauger, Review of 5-V electrodes for Li-ion batteries: Status and trends, *Ionics*, 19 (2013), 951–988.
29. V. Etacheri, R. Marom, R. Elazari, G. Salitra, D. Aurbach, Challenges in the development of advanced Li-ion batteries: A review, *Energy Environ. Sci.*, 4 (2011), 3243–3262.
30. V. A. Strelstov, E. L. Belokoneva, V. G. Tsirelson, N. K. Hansen, Multipole analysis of the electron density in triphylite,  $\text{LiFePO}_4$ , using X-ray diffraction data, *Acta Crystallogr. Sect. B*. 49 (1993), 147–153.
31. J. M. Tarascon, M. Armand, Issues and challenges facing rechargeable lithium batteries, *Nature*, 414 (2001) 359–367.
32. A. K. Padhi, K. S. Nanjundaswamy, C. Masquelier and J. B. Goodenough, Mapping of Transition Metal Redox Energies in Phosphates with NASICON Structure by Lithium Intercalation, *J. Electrochem. Soc.*, 144 (1997), 2581–2586.
33. **(a)** N. Ravet, Y. Chouinard, J.F.F. Magnan, S. Besner, M. Gauthier, M. Armand, Electroactivity of natural and synthetic triphylite, *J. Power Sources*, 97–98 (2001) 503–507. **(b)** U.S. Patent No. 7,601,318 B2 (issued Oct. 13, 2009).
34. K. Zaghib, A. Mauger, C. M. Julien, Overview of olivines in lithium batteries for green transportation and energy storage, *J. Solid State Electrochem.*, 16 (2012), 835–845.
35. R. Malik, A. Abdellahi, G. Ceder, A Critical Review of the Li Insertion Mechanisms in  $\text{LiFePO}_4$  Electrodes, *J. Electrochem. Soc.*, 160 (2013), A3179–A3197.
36. K. A. Seid, J.-C. Badot, O. Dubrunfaut, S. Levasseur, D. Guyomard, B. Lestriez, Multiscale electronic transport mechanism and true conductivities in amorphous carbon– $\text{LiFePO}_4$  nanocomposites, *J. Mater. Chem.*, 22 (2012), 2641–2649.
37. C. Zhu, K. Weichert, J. Maier, Electronic conductivity and defect chemistry of heterosite  $\text{FePO}_4$ , *Adv. Funct. Mater.*, 21 (2011), 1917–1921.
38. D. Morgan, A. Van der Ven, G. Ceder, Li Conductivity in  $\text{Li}_x\text{MPO}_4$  (M = Mn, Fe, Co, Ni) Olivine Materials, *Electrochem. Solid-State Lett.*, 7 (2004), A30–A32.
39. M.S. Islam, D. J. Driscoll, C. A. J. Fisher, P.R. Slater, Atomic-scale investigation of defects, dopants, and lithium transport in the  $\text{LiFePO}_4$  olivine-type battery material, *Chem. Mater.*, 17 (2005), 5085–5092.
40. S. Nishimura, G. Kobayashi, K. Ohoyama, R. Kanno, M. Yashima, A. Yamada, Experimental visualization of lithium diffusion in  $\text{Li}_x\text{FePO}_4$ , *Nat. Mater.*, 7 (2008), 707–711.
41. **(a)** R. Amin, J. Maier, P. Balaya, D. P. Chen, C. T. Lin, Ionic and electronic transport in single crystalline  $\text{LiFePO}_4$  grown by optical floating zone technique, *Solid State Ionics*, 179 (2008), 1683–1687 **(b)** R. Amin, P. Balaya, and J. Maier, Anisotropy of Electronic and Ionic Transport in  $\text{LiFePO}_4$  Single Crystals, *Electrochem. Solid-State Lett.*, 10(1) (2007), A13–A16.
42. C. Delacourt, P. Poizot, S. Levasseur, C. Masquelier, Size Effects on Carbon-Free  $\text{LiFePO}_4$  Powders, *Electrochem. Solid-State Lett.*, 9 (2006), A352–355.
43. M. Gaberscek, R. Dominko and J. Jamnik, Is small particle size more important than carbon coating? An example study on  $\text{LiFePO}_4$  cathodes, *Electrochem. Commun.* 9 (2007), 2778–2783.
44. J. Yang and J. S. Tse, Li Ion Diffusion Mechanisms in  $\text{LiFePO}_4$ : An ab Initio Molecular Dynamics Study, *J. Phys. Chem. A*. 115 (2011), 13045–13049.

45. T. Maxisch, F. Zhou, and G. Ceder, Elastic properties of olivine  $\text{Li}_x\text{FePO}_4$  from first principles, *Phys. Rev. B.*, 73 (2006), 174112(1-4).
46. K. Zaghbi, A. Mauger, J. B. Goodenough, F. Gendron and C. M. Julien, Electronic, Optical, and Magnetic Properties of  $\text{LiFePO}_4$ : Small Magnetic Polaron Effects, *Chem. Mater.*, 19 (2007), 3740–3747.
47. A. S. Andersson and J. O. Thomas, The source of first-cycle capacity loss in  $\text{LiFePO}_4$ , *J. Power Sources*, 97-98 (2001), 498–502.
48. V. Srinivasan, J. Newman, Discharge Model for the Lithium Iron-Phosphate Electrode, *J. Electrochem. Soc.*, 151 (2004), A1517–A1529.
49. C. Delmas, M. Maccario, L. Croguennec, F. Le Cras, F. Weill, Lithium deintercalation in  $\text{LiFePO}_4$  nanoparticles via a domino-cascade model, *Nat. Mater.*, 7 (2008), 665–671.
50. R. Malik, F. Zhou and G. Ceder, Kinetics of non-equilibrium lithium incorporation in  $\text{LiFePO}_4$ , *Nat. Mater.*, 10 (2011), 587–590.
51. A. Van der Ven, K. Garikipati, S. Kim and M. Wagemaker, The Role of Coherency Strains on Phase Stability in  $\text{Li}_x\text{FePO}_4$ : Needle Crystallites Minimize Coherency Strain and overpotential, *J. Electrochem. Soc.*, 156 (2009), A949–A957.
52. G. Chen, X. Song and T. Richardson, Electron Microscopy Study of the  $\text{LiFePO}_4$  to  $\text{FePO}_4$  Phase Transition, *J. Electrochem. Solid-State Lett.*, 9(6) (2006), A295–A298.
53. L. Laffont, C. Delacourt, P. Gibot, M.Y. Wu, P. Kooyman, C. Masquelier and J-M. Tarascon, Study of the  $\text{LiFePO}_4/\text{FePO}_4$  Two-Phase System by High-Resolution Electron Energy Loss Spectroscopy, *Chem. Mater.*, 18 (2006), 5520–5529.
54. Z. Lu, H. Chen, R. Robert, B.Y.X. Zhu, J. Deng, L. Wu, C. Y. Chung, C. P. Grey, Citric Acid- and Ammonium-Mediated Morphological Transformations of Olivine  $\text{LiFePO}_4$  Particles. *Chem. Mater.* 23 (2011) 2848–2859.
55. P.P. Prohini, Modeling the Voltage Profile for  $\text{LiFePO}_4$ , *J. Electrochem. Soc.*, 152 (2005) A1925–A1929.
56. **(a)** C. Delacourt, J. Rodríguez-Carvajal, B. Schmitt, J.-M. Tarascon, C. Masquelier, Crystal chemistry of the olivine-type  $\text{Li}_x\text{FePO}_4$  system ( $0 \leq x \leq 1$ ) between 25 and 370 °C, *Solid State Sci.*, 7 (2005), 1506–1516. **(b)** J. L. Dodd, R. Yazami and B. Fultz, Phase Diagram of  $\text{Li}_x\text{FePO}_4$ , *Electrochem. Solid-State Lett.*, 9 (2006), A151–A155.
57. W. Dreyer, J. Jamnik, C. Guhlke, R. Huth, J. Moskon, M. Gaberscek, The thermodynamic origin of hysteresis in insertion batteries, *Nat. Mater.*, 9 (2010) 448–453.
58. M. S. Whittingham, Lithium Batteries and Cathode Materials, *Chem. Rev.*, 104 (2004), 4271–4302.
59. J. N. von Fuchs, Über ein neues mineral (triphylin), *J. für Praktische Chem.*, 3 (1834), 98–104.
60. **(a)** H.-K. Song, K. T. Lee, M. G. Kim, L. F. Nazar and J. Cho, Recent Progress in Nanostructured Cathode Materials for Lithium Secondary Batteries, *Adv. Funct. Mater.*, 20 (2010), 3818–3834. **(b)** C. M. Julien, A. Mauger and K. Zaghbi, Surface effects on electrochemical properties of nano-sized  $\text{LiFePO}_4$ , *J. Mater. Chem.*, 21 (2011), 9955–9968. **(c)** Y. Zhang, Q. Huo, P. Du, L. Wang, A. Zhang, Y. Song, Y. Lv, G. Li., Advances in new cathode material  $\text{LiFePO}_4$  for lithium-ion batteries, *Synth. Met.*, 162 (2012), 1315–1326. **(d)** J. Chen, A review of nanostructured lithium ion battery materials via low temperature synthesis, *Recent Pat. Nanotechnol.*, 7 (2013), 2–12.
61. M. S. Whittingham, Ultimate Limits to Intercalation Reactions for Lithium Batteries, *Chem. Rev.*, 114 (2014), 11683–11720.

62. J. Wang and X. Sun, Understanding and recent development of carbon coating on LiFePO<sub>4</sub> cathode materials for lithium-ion batteries, *Energy Environ. Sci.*, 5 (2012), 5163–5185.
63. (a) H. Huang, Y. M. Saidi, Synthesis of metal phosphates, Canadian Patent No. CA 2557238 C, issued Oct. 9, 2012. (b) C. Laurent, M. Gauthier, D. Lavoie, C. Michot, N. Ravet, Process for preparing electroactive insertion compounds and electrode materials obtained therefrom, Canadian Patent No. CA 2790784, issued Dec. 15, 2015.
64. S. Yang, P.Y. Zavalij, M.S. Whittingham, Hydrothermal synthesis of lithium iron phosphate cathodes, *Electrochem. Commun.*, 3 (2001) 505–508.
65. S. Bodoardo, C. Gerbaldi, G. Meligrana, A. Tuel, S. Enzo, N. Penazzi, Optimisation of some parameters for the preparation of nanostructured LiFePO<sub>4</sub>/C cathode, *Ionics (Kiel)*, 15 (2008), 19–26.
66. S.-Y. Chung, J.T. Bloking and Y.-M. Chiang, Electronically conductive phospho-olivines as lithium storage electrodes, *Nat. Mater.*, 1 (2002), 123–128.
67. (a) P. S. Herle, B. Ellis, N. Coombs and L. F. Nazar, Nano-network electronic conduction in iron and nickel olivine phosphates, *Nat. Mater.*, 3 (2004), 147–152. (b) M. S. Islam, D. J. Driscoll, C. A. J. Fisher and P. R. Slater, Atomic-scale investigation of defects, dopants, and lithium transport in the LiFePO<sub>4</sub> olivine-type battery material, *Chem. Mater.*, 17 (2005), 5085–5092. (c) K. Zaghib, A. Mauger, J. B. Goodenough, F. Gendron and C. M. Julien, Electronic, Optical, and Magnetic Properties of LiFePO<sub>4</sub> : Small Magnetic Polaron Effects, *Chem. Mater.*, 19 (2007), 3740–3747.
68. B. Kang, G. Ceder, Battery materials for ultrafast charging and discharging, *Nature*. 458 (2009), 190–193.
69. K. Zaghib, J. B. Goodenough, A. Mauger and C. Julien, Unsupported claims of ultrafast charging of LiFePO<sub>4</sub> Li-ion batteries, *J. Power Sources*, 194 (2009), 1021–1023.
70. G. Ceder and B. Kang, Response to “unsupported claims of ultrafast charging of Li-ion batteries, *J. Power Sources*, 194 (2009), 1024–1028.
71. (a) J. Wang and X. Sun, Understanding and recent development of carbon coating on LiFePO<sub>4</sub> cathode materials for lithium-ion batteries, *Energy Environ. Sci.*, 5 (2012), 5163–5185. (b) E. Avci, E., M. Mazman, D. Uzun, E. Bicer and T. Sener, High performance LiFePO<sub>4</sub>/CN cathode material promoted by polyaniline as carbon-nitrogen precursor, *J. Power Sources*, 240 (2013), 328–337. (c) Z. Shao, J. Xia, X. Liu and G. Li, Preparation and performance study of LiFePO<sub>4</sub> and xLiFePO<sub>4</sub>-yLi<sub>3</sub>V<sub>2</sub>(PO<sub>4</sub>)<sub>3</sub>. *Res. Chem. Intermed.*, 2 (2015), 2263–2275. (d) J. Wang, Z. Shao and H. Ru, Influence of carbon sources on LiFePO<sub>4</sub>/C composites synthesized by the high-temperature high-energy ball milling method, *Ceram. Int.*, 40 (2014), 6979–6985.
72. M. Maccario, L. Croguennec, F. Weill, F. Le Cras and C. Delmas, C-containing LiFePO<sub>4</sub> materials - Part II: Electrochemical characterization, *Solid State Ionics*, 179 (2008) 2383–2389.
73. H. Li and H. Zhou, Enhancing the performances of Li-ion batteries by carbon-coating: present and future, *Chem. Commun.*, 48 (2012), 1201–1217.
74. Z. Chen and J. R. Dahn, Reducing Carbon in LiFePO<sub>4</sub>/C Composite Electrodes to Maximize Specific Energy, Volumetric Energy, and Tap Density, *J. Electrochem. Soc.*, 149 (2002) A1184–A1189.
75. K. Dokko, S. Koizumi, H. Nakano and K. Kanamura, Particle morphology, crystal orientation, and electrochemical reactivity of LiFePO<sub>4</sub> synthesized by the hydrothermal method at 443 K, *J. Mater. Chem.*, 17 (2007) 4803–4810.

76. D.-H. Kim and J. Kim, Synthesis of LiFePO<sub>4</sub> Nanoparticles in Polyol Medium and Their Electrochemical Properties, *Electrochem. Solid-State Lett.*, 9 (2006) A439–A442.
77. **(a)** A. Singhal, G. Skandan, G. Amatucci, F. Badway, N. Ye, A. Manthiram, H. Ye and J.J. Xu, Nanostructured electrodes for next generation rechargeable electrochemical devices, *J. Power Sources*, 129 (2004) 38–44. **(b)** C. Delacourt, P. Poizot, S. Levasseur, C. Masquelier, Size Effects on Carbon-Free LiFePO<sub>4</sub> Powders, *Electrochem. Solid-State Lett.*, 9 (2006) A352–A355.
78. S. Franger, C. Benoit, C. Bourbon and F. Le Cras, Chemistry and electrochemistry of composite LiFePO<sub>4</sub> materials for secondary lithium batteries, *J. Phys. Chem. Solids*, 67 (2006) 1338–1342.
79. **(a)** H. Huang, S.-C Yin and L. F. Nazar, Approaching Theoretical Capacity of LiFePO<sub>4</sub> at Room Temperature at High Rates, *Electrochem. Solid-State Lett.*, 4 (2001), A170–A172. **(b)** C. M. Julien, A. Mauger and K. Zaghib, Surface effects on electrochemical properties of nano-sized LiFePO<sub>4</sub>, *J. Mater. Chem.*, 21 (2011), 9955–9968.
80. **(a)** N. Recham, L. Dupont, M. Courty, K. Djellab, D. Larcher, M. Armand and J. M. Tarascon, Ionothermal synthesis of tailor-made LiFePO<sub>4</sub> powders for li-ion battery applications, *Chem. Mater.*, 21 (2009) 1096–1107. **(b)** Z. Lu, C. Hailong, R. Robert, B. Y. X. Zhu, J. Deng, L. Wu, C. Y. Chung and C. P. Grey, Citric Acid- and Ammonium-Mediated Morphological Transformations of Olivine LiFePO<sub>4</sub> Particles, *Chem. Mater.*, 23 (2011), 2848–2859. **(c)** J. Lim, S.-W. Kang, J. Moon, S. Kim, H. Park, J.P. Baboo and J. Kim, Low-temperature synthesis of LiFePO<sub>4</sub> nanocrystals by solvothermal route, *Nanoscale Res. Lett.*, 7 (2012), 1–7.
81. M. S. Islam, D. J. Driscoll, c. A. J. Fisher, and P. R. Slater, Atomic-scale investigation of defects, dopants, and lithium transport in the LiFePO<sub>4</sub> olivine-type battery material, *Chem. Mater.*, 17 (2005), 5085–5092.
82. **(a)** K. Zaghib, J. Shim, A. Guerfi, P. Charest and K. A. Striebel, Effect of Carbon Source as Additives in LiFePO<sub>4</sub> as Positive Electrode for Lithium-Ion Batteries, *Electrochem. Solid-State Lett.*, 8 (2005), A207–A210. **(b)** I. V Thorat, T. Joshi, K. Zaghib, J. N. Harb and D. R. Wheeler, Understanding Rate-Limiting Mechanisms in LiFePO<sub>4</sub> Cathodes for Li-Ion Batteries, *J. Electrochem. Soc.*, 158 (2011) A1185–A1193.
83. **(a)** T. Azib, S. Ammar, S. Nowak, S. Lau-Truing, H. Groult, K. Zaghib, A. Mauger and C. M. Julien, Crystallinity of nano C-LiFePO<sub>4</sub> prepared by the polyol process, *J. Power Sources*, 217 (2012) 220–228. **(b)** A. Guerfi, N. Ravet, P. Charest, M. Dontigny, M. Petitclerc, M. Gauthier and K. Zaghib, Temperature Effects on LiFePO<sub>4</sub> Cathode Performance, *ECS Trans.*, 3 (2007) 3–17.
84. **(a)** J. Wang and X. Sun, Olivine LiFePO<sub>4</sub>: the remaining challenges for future energy storage, *Energy Environ. Sci.* 8 (2015) 1–29. **(b)** W. Shen, Y. Wang, J. Yan, H. Wu and S. Guo, Enhanced electrochemical performance of lithium iron(II) phosphate modified cooperatively via chemically reduced graphene oxide and polyaniline, *Electrochim. Acta.*, 173 (2015) 310–315.
85. C. Fongy, A.-C. Gaillot, S. Jouanneau, D. Guyomard and B. Lestriez, Ionic vs. Electronic Power Limitations and Analysis of the Fraction of Wired Grains in LiFePO<sub>4</sub> Composite Electrodes, *J. Electrochem. Soc.*, 157 (2010) A885–891.
86. M. E. Spahr, Carbon-Conductive Additives for Lithium-Ion Batteries. In: *Lithium-Ion Batteries Science and Technologies*, M. Yoshio, R. J. Brodd and A. Kozawa (eds.), New York, NY: Springer Science+Business Media, 2009, p 119.

87. K. Zaghib, C. Sotowa, P. Charest, M. Takeuchi, A. Guerfi, Composite electrode material, United States Patent US8652361 B2, issued Feb. 18, 2014.
88. **(a)** Y.-H. Rho, L.F. Nazar, L. Perry, D. Ryan, Surface Chemistry of LiFePO<sub>4</sub> Studied by Mössbauer and X-Ray Photoelectron Spectroscopy and Its Effect on Electrochemical Properties, *J. Electrochem. Soc.*, 154 (2007) A283–A289. **(b)** B. Ellis, P. Subramanya Herle, Y.H. Rho, L.F. Nazar, R. Dunlap, L.K. Perry, D. H. Ryan, Nanostructured materials for lithium-ion batteries: surface conductivity vs. bulk ion/electron transport, *Faraday Discuss.*, 134 (2007) 119–141
89. **(a)** F. Croce, A. D' Epifanio, J. Hassoun, A. Deptula, T. Olczac, B. Scrosati, A Novel Concept for the Synthesis of an Improved LiFePO<sub>4</sub> Lithium Battery Cathode, *Electrochem. Solid-State Lett.*, 5 (2002) A47–A50. **(b)** C. H. Mi, Y. X. Cao, X. G. Zhang, X. B. Zhao, H. L. Li, Synthesis and characterization of LiFePO<sub>4</sub>/(Ag+C) composite cathodes with nano-carbon webs, *Powder Technol.*, 181 (2008) 301–306.
90. V. Srinivasan, J. Newman, Discharge Model for the Lithium Iron-Phosphate Electrode, *J. Electrochem. Soc.*, 151 (2004), A1517–A1529.
91. F. Li, Y. Gong, G. Jia, Q. Wang, Z. Peng, W. Fan, B. Bai, A novel dual-salts of LiTFSI and LiODFB in LiFePO<sub>4</sub>-based batteries for suppressing aluminum corrosion and improving cycling stability, *J. Power Sources*, 295 (2015), 47–54.
92. **(a)** K. Striebel, J. Shim, A. Sierra, H. Yang, X. Song, R. Kostecki, C. McCarthy, The development of low cost LiFePO<sub>4</sub>-based high power lithium-ion batteries, *J. Power Sources*, 146 (2005), 33–38. **(b)** R. Divigalpitiya, M. I. Bukett, Electrode including current collector with nano-scale coating and method of making the same, US Patent US8178241 B2, issued 15 May 2012. **(c)** H.C. Wu, H.C. Wu, E. Lee, N.L. Wu, High-temperature carbon-coated aluminum current collector for enhanced power performance of LiFePO<sub>4</sub> electrode of Li-ion batteries, *Electrochem. Commun.*, 12 (2010), 488–49.
93. **(a)** N. Furukawa and K. Nishio, Lithium batteries with polymer electrodes. In: *Applications of electroactive polymers*, B. Scrosati (ed.), Springer Science & Business Media, 1993. **(b)** P. Novák, K. Müller, K. S. V. Santhanam and O. Haas, *Chem. Rev.*, 97 (1997), 207–282. **(c)** Z. Song and H. Zhou, *Energy Environ. Sci.*, 6 (2013), 2280–2301. **(d)** R. Gracia, D. Mecerreyes, Polymers with redox properties: materials for batteries, biosensors and more, *Polym. Chem.*, 4 (2013) 2206–2214. **(d)** Z. Song and H. Zhou, Towards sustainable and versatile energy storage device - An overview of organic electrode materials. *Energy Environ. Sci.*, 6 (2013), 2280–2301.
94. H. Yoneyama, A. Kishimoto, S. Kuwabata, Charge-discharge properties of polypyrrole films containing manganese dioxide particles, *J. Chem. Soc. Chem. Commun.*, (1991) 986–987.
95. **(a)** A. D. Pasquier, F. Orsini, A.S. Gozdz, J.-M. Tarascon, Electrochemical behaviour of LiMn<sub>2</sub>O<sub>4</sub>-PPy composite cathodes in the 4-V region, *J. Power Sources*, 81-82 (1999) 607–611. **(b)** S. Kuwabata, S. Masui, H. Tomiyori, H. Yoneyama, Charge-discharge properties of chemically prepared composites of V<sub>2</sub>O<sub>5</sub> and polypyrrole as positive electrode materials in rechargeable Li batteries, *Electrochim. Acta.*, 46 (2000) 91–97.
96. **(a)** A.V. Murugan, C.-W. Kwon, G. Campet, B.. Kale, T. Maddanimath, K. Vijayamohanam, Electrochemical lithium insertion into a poly(3,4-ethylenedioxythiophene)PEDOT/V<sub>2</sub>O<sub>5</sub> nanocomposite, *J. Power Sources*, 105 (2002) 1–5. **(b)** H. M. Song, D. Y. Yoo, S. K. Hong, J. S. Kim, W. I. Cho, S. I. Mho, Electrochemical impedance analysis of V<sub>2</sub>O<sub>5</sub> and PEDOT composite film cathodes, *Electroanalysis*, 23 (2011) 2094–2102.

97. **(a)** C. Chang, L. Her, J. Hong, W. Ho, S. Liu, Poly(3-methylthiophene) as a Conductive Additive on LiCoO<sub>2</sub> Composite Cathode in Lithium-Ion Battery, *J. New Mater. Electrochem. Syst.* 54 (2008) 49–54. **(b)** J. M. Kim, H. S. Park, J. H. Park, T. H. Kim, H. K. Song, S. Y. Lee, Conducting polymer-skinned electroactive materials of lithium-ion batteries: Ready for monocomponent electrodes without additional binders and conductive agents, *ACS Appl. Mater. Interfaces*, 6 (2014) 12789–12797.
98. **(a)** P. Sengodu, A. Deshmukh, Conducting Polymers and their Inorganic Composites for Advanced Li-ion Batteries: A Review, *RSC Adv.*, 5 (2015) 42109 – 42130. **(b)** W. Loevenich, L. Komsiyiska, E.-M. Hammer and D. Ledwoch, Use of conductive polymers in battery electrodes, Patent Application WO2013EP03533, filed Nov 22, 2013.
99. **(a)** Y.-H. Huang, J. B. Goodenough, High-Rate LiFePO<sub>4</sub> Lithium Rechargeable Battery Promoted by Electrochemically Active Polymers, *Chem. Mater.*, 20 (2008), 7237–7241. **(b)** G. Lei, X. Yi, L. Wang, Z. Li, J. Zhou, An investigation of the electrochemical performance of polyaniline coated LiFePO<sub>4</sub> materials, *Polym. Adv. Technol.*, 20 (2009), 576–580. **(c)** W.M. Chen, L. Qie, L.X. Yuan, S.A. Xia, X.L. Hu, W.X. Zhang, Y. H. Huang, Insight into the improvement of rate capability and cyclability in LiFePO<sub>4</sub>/polyaniline composite cathode, *Electrochim. Acta.*, 56 (2011), 2689–2695. **(d)** W.-M. Chen, Y.-H. Huang, L.-X. Yuan, Self-assembly LiFePO<sub>4</sub>/polyaniline composite cathode materials with inorganic acids as dopants for lithium-ion batteries, *J. Electroanal. Chem.*, 660 (2011) 108–113. **(e)** O. Y. Posudievsky, O. A. Kozarenko, V. S. Dyadyun, V. G. Koshechko, V. D. Pokhodenko, Advanced electrochemical performance of hybrid nanocomposites based on LiFePO<sub>4</sub> and lithium salt doped polyaniline, *J. Solid State Electrochem.*, 19 (2015) 2733–2740. **(f)** W. Shen, Y. Wang, J. Yan, H. Wu, S. Guo, Enhanced Electrochemical Performance of Lithium Iron(II) Phosphate Modified Cooperatively via Chemically Reduced Graphene Oxide and Polyaniline, *Electrochim. Acta.*, 173 (2015) 310–315. **(g)** S. J. Richard Prabakar, M. Pyo, Corrosion protection of aluminum in LiPF<sub>6</sub> by poly(3,4-ethylenedioxythiophene) nanosphere-coated multiwalled carbon nanotube, *Corros. Sci.*, 57 (2012) 42–48.
100. **(a)** G. X. Wang, L. Yang, Y. Chen, J. Z. Wang, S. Bewlay, H. K. Liu, An investigation of polypyrrole-LiFePO<sub>4</sub> composite cathode materials for lithium-ion batteries, *Electrochim. Acta.*, 50 (2005) 4649–4654. **(b)** Y.-H. Huang, K.-S. Park, J.B. Goodenough, Improving Lithium Batteries by Tethering Carbon-Coated LiFePO<sub>4</sub> to Polypyrrole, *J. Electrochem. Soc.*, 153 (2006) A2282–A2286. **(c)** Y.H. Huang, J.B. Goodenough, High-rate LiFePO<sub>4</sub> lithium rechargeable battery promoted by electrochemically active polymers, *Chem. Mater.*, 20 (2008) 7237–7241. **(d)** I. Boyano, J.A. Blazquez, I. de Meatza, M. Bengoechea, O. Miguel, H. Grande, Y. Huang, J. B. Goodenough, Preparation of C-LiFePO<sub>4</sub>/polypyrrole lithium rechargeable cathode by consecutive potential steps electrodeposition, *J. Power Sources.*, 195 (2010) 5351–5359. **(e)** A. Fedorková, R. Oriňáková, A. Oriňák, I. Talian, A. Heile, H.-D. Wiemhöfer, D. KAnyansky, H. F. Arlinghaus, PPy doped PEG conducting polymer films synthesized on LiFePO<sub>4</sub> particles, *J. Power Sources*, 195 (2010), 3907–3912. **(f)** H. C. Dinh, S. il Mho, I. H. Yeo, Electrochemical analysis of conductive polymer-coated LiFePO<sub>4</sub> nanocrystalline cathodes with controlled morphology, *Electroanalysis*, 23 (2011), 2079–2086.
101. Y. Bai, P. Qiu, Z. Wen, S. Han, Improvement of electrochemical performances of LiFePO<sub>4</sub> cathode materials by coating of polythiophene, *J. Alloys Compd.*, 508 (2010), 1–4.

102. S.-L. Wu, A. E. Javier, D. Devaux, N.P. Balsara, V. Srinivasan, Discharge Characteristics of Lithium Battery Electrodes with a Semiconducting Polymer Studied by Continuum Modeling and Experiment, *J. Electrochem. Soc.*, 161 (2014), A1836–A1843.
103. **(a)** S.-J. Choi, S.-M. Park, Electrochemistry of Conductive Polymers 42. Mixed Polymer Films as an Overcharge Inhibitor for Lithium-Ion Batteries, *J. Electrochem. Soc.*, 155 (2008) A783–A787. **(b)** S.N. Patel, A.E. Javier, N.P. Balsara, Electrochemically oxidized electronic and ionic conducting nanostructured block copolymers for lithium battery electrodes, *ACS Nano.*, 7 (2013) 6056–6068.
104. **(a)** A. Vadivel Murugan, T. Muraliganth, A. Manthiram, Rapid microwave-solvothermal synthesis of phospho-olivine nanorods and their coating with a mixed conducting polymer for lithium ion batteries, *Electrochem. Commun.*, 10 (2008), 903–906. **(b)** D. Rangappa, K. Sone, M. Ichihara, T. Kudo, I. Honma, Rapid one-pot synthesis of  $\text{LiMPO}_4$  ( $M = \text{Fe}, \text{Mn}$ ) colloidal nanocrystals by supercritical ethanol process. *Chem. Commun.*, (Cambridge, United Kingdom) 46 (2010), 7548–7550. **(c)** J. Y. Shi, C.-W. Yi & K. Kim, An investigation of  $\text{LiFePO}_4$ /poly(3,4-ethylenedioxythiophene) composite cathode materials for lithium-ion batteries. *Bull. Korean Chem. Soc.*, 31 (2010), 2698–2700. **(d)** H.-C. Dinh, I.-H. Yeo, W. Il Cho, S. Mho, Characteristics of conducting polymer-coated nanosized  $\text{LiFePO}_4$  cathode in the  $\text{Li}^+$  batteries. *ECS Trans.*, 28 (2010), 167–175. **(e)** H.-C. Dinh, S. Mho, I.-H. Yeo, Electrochemical Analysis of Conductive Polymer-Coated  $\text{LiFePO}_4$  Nanocrystalline Cathodes with Controlled Morphology. *Electroanalysis*, 23 (2011), 2079–2086. **(f)** H.-C. Dinh, H. Lim, K.D. Park, I.-H. Yeo, Y. Kang, S. Mho, Long-term cycle stability at a high current for nanocrystalline  $\text{LiFePO}_4$  coated with a conductive polymer, *Adv. Nat. Sci. Nanosci. Nanotechnol.*, 4 (2013), 1–5. **(g)** P.R. Das, L. Komsijska, O. Ostera, G. Wittstock, PEDOT:PSS as a Functional Binder for Cathodes in Lithium Ion Batteries. *J. Electrochem. Soc.*, 162 (2015), A674–A678. **(h)** S.N. Eliseeva, O.V. Levin, E.G. Tolstopjatova, E.V. Alekseeva, R.V. Apraksin, V.V. Kondratiev, New functional conducting poly-3,4-ethylenedioxythiophene:polystyrene sulfonate/carboxymethylcellulose binder for improvement of capacity of  $\text{LiFePO}_4$ -based cathode materials, *Mater. Lett.*, 161 (2015), 117–119. **(i)** D. Lepage, C. Michot, G.-X. Liang, M. Gauthier, S. B. Schougaard, A Soft Chemistry Approach to Coating of  $\text{LiFePO}_4$  with a Conducting Polymer. *Angew. Chemie, Int. Ed.*, 50 (2011), 6884–6887. **(j)** N.D. Trinh, M. Saulnier, D. Lepage, S.B. Schougaard, Conductive polymer film supporting  $\text{LiFePO}_4$  as composite cathode for lithium ion batteries, *J. Power Sources.*, 221 (2013) 284–289.
105. M. Levi and D. Aurbach, Electrochemistry of electronically conducting polymers. In: V. V. Kharton (ed.), *Handbook of Solid State Electrochemistry Fundamentals, Methodologies, Applications, Volume 1*, Weinheim: WILEY-VCH Verlag GmbH & Co. KGaA, 2008, pp. 372.
106. **(a)** H. Letheby, *J Chem Soc*, XV (1862), 161–163. **(b)** F. F. Runge, Poggendorfs, *Ann. Phys. u. Chemie*, 31 (1834), 513–524. **(c)** J. Lightfoot, Improvement in dyeing and printing a black color on fabrics with aniline compounds, United States Patent US38,589 A, issued May 19, 1863.
107. **(a)** R. Holze and Y. P. Wu, Intrinsically conducting polymers in electrochemical energy technology: Trends and progress. *Electrochim. Acta*, 122 (2014), 93–107. **(b)** M. E. Abdelhamid, A. P. O’Mullane, G. A. Snook, Storing energy in plastics: A review on conducting polymers & their role in electrochemical energy storage, *RSC Adv.*, 5 (2015) 11611–11626.

108. **(a)** M. Dietrich, J. Heinze, G. Heywang, F. Jonas, Electrochemical and spectroscopic characterization of polyalkylenedioxythiophenes, *J. Electroanal. Chem.*, 369 (1994) 87-92. **(b)** A. Elschner, S. Kirchmeyer, W. Lövenich, U. Merker, K. Reuter, PEDOT Principles and Applications of an Intrinsically conducting Polymer, Boca Raton, FL: CRC Press Taylor & Francis Group, 2011. **(c)** P. Tehrani, A. Kanciurowska, X. Crispin, N.D. Robinson, M. Fahlman, M. Berggren, The effect of pH on the electrochemical over-oxidation in PEDOT:PSS films, *Solid State Ionics*, 177 (2007), 3521–3527.
109. W. Plieth, Intrinsically Conducting Polymers. In: *Electrochemistry for Materials Science*, Hungary: Elsevier, 2008, p. 326.
110. W. H. Smyrl and M. Lien, Electrical and electrochemical properties of electronically conducting polymers. In: B. Scrossati (ed.), *Applications of Electroactive Polymers*, Springer Science & Business Media, 1993.
111. J. Heinze, B. A. Frontana-Urbe, S. Ludwigs, Electrochemistry of conducting polymers-persistent models and new concepts, *Chem. Rev.*, 110 (2010), 4724–4771.
112. L. Groenendaal, G. Zotti, P.-H. Aubert, S.M. Waybright, J.R. Reynolds, Electrochemistry of Poly(3,4-alkylenedioxythiophene) Derivatives, *Adv. Mater.*, 15 (2003) 855–879.





## Chapter 2

### Hypotheses, objectives and approaches

In the previous chapter, the characteristics of  $\text{LiFePO}_4$  were detailed, together with the limitations and advantages that determine the performance of this active material. The review of the recent strategies applied for improving the electrochemical performance of  $\text{LiFePO}_4$ -based electrodes shows that there is still opportunity for improving the charge transport between particles, throughout the electrode and at the interphase with the current collector. Furthermore, the use of conducting polymers as additives for  $\text{LiFePO}_4$ -based electrodes was identified as a promising strategy in order to improve both the ionic and the electronic conductivity. Considering these aspects, the hypotheses of this work are the following:

- H1) Conducting polymers of the poly(alkylenedioxythiophene) family can form active and stable composites with  $\text{LiFePO}_4$  or with  $\text{LiFePO}_4$ -based electrodes when these composites are prepared by electrochemical polymerization of monomers or by mechanical processing methods using ready available polymers.
- H2) The use of poly(alkylenedioxythiophene) conducting polymers as additives for  $\text{LiFePO}_4$ -based electrodes will have a positive influence on the charge transport and on the electrochemical performance of the active material, provided coatings or networks of conducting polymer can be formed at or extended to the different interphases of the electrode where ionic or electronic transport are limiting.

Based on the hypotheses, the main objective of the work consists in developing and applying electrochemical polymerization, blending and coating methods to produce composite electrodes of  $\text{LiFePO}_4$  with poly(alkylenedioxythiophene) [PXDOT] in order to increase the charge transport and the electrochemical performance of  $\text{LiFePO}_4$ -based electrodes.

The following approaches were investigated in order to combine  $\text{LiFePO}_4$  and the conducting polymer into a composite electrode by electropolymerization, blending or coating methods. A reference is included to the chapter in this document where each approach is developed.

#### A1) Electropolymerization of monomers over $\text{LiFePO}_4$ -based electrodes

- a. Potentiostatic electropolymerization of EDOT over a  $\text{LiFePO}_4$ -based electrode in acetonitrile medium with tetraethyl ammonium tetrafluoroborate salt. (Chapter 3 )
- b. Galvanostatic electropolymerization of EDOT or ProDOT monomers over a delithiated  $\text{Li}_{1-x}\text{FePO}_4$  electrode inside a test battery upon charging in one step or in two steps. (Chapter 4)

#### A2) Blending $\text{LiFePO}_4$ with PEDOT obtained by electropolymerization

- a. Electropolymerization of EDOT at a platinum electrode in acetonitrile/water medium with tetraethyl ammonium tetrafluoroborate salt. Blending of the obtained PEDOT with  $\text{LiFePO}_4$  to form a composite electrode. (Chapter 3)

#### A3) Use of commercial PEDOT:PSS as an additive for $\text{LiFePO}_4$ in combination with other conducting and agglomerating additives

- a. Blending PEDOT:PSS with  $\text{LiFePO}_4$ , carbon black and polyvinylidene fluoride in different proportions to form a composite electrode. (Chapter 5)

- b. Similar to A3a, but using PEDOT:PSS treated with ethylene glycol and dimethylsulfoxide as conductivity enhancement agents. (Chapter 5)

#### A4) Coating the aluminium current collector with PEDOT:PSS

- a. Drop-casting PEDOT:PSS over the aluminium current collector and formation of a  $\text{LiFePO}_4$ -based electrode. (Chapter 5)
- b. Similar to A4a, but using PEDOT:PSS treated with ethylene glycol or dimethylsulfoxide as conductivity enhancement agents. (Chapter 5)

The following techniques were applied for characterizing the different composite materials and electrodes:

- Scanning electron microscopy in order to visualize the morphology of the particles and the texture of the electrodes.
- Galvanostatic cycling of test batteries in order to evaluate the charge/discharge performance of the electrodes.
- Electrochemical impedance spectroscopy in order to estimate the resistance of the electrodes.
- Mössbauer spectroscopy and X-ray photoelectron spectroscopy in order to follow the bulk and surface variation of the oxidation state of iron at different states of charge.



# Chapter 3

## Improving the cycling performance of $\text{LiFePO}_4$ cathode material by poly(3,4-ethylenedioxythiophene) coating

D. Cíntora-Juárez<sup>a</sup>, C. Pérez-Vicente<sup>a</sup>, S. Ahmad<sup>b</sup> and J. L. Tirado<sup>a</sup>, *RSC Adv.*, 2014, **4**, 26108-26114.

<sup>a</sup>Laboratorio de Química Inorgánica, Campus de Rabanales, Universidad de Córdoba, 14071, Spain

<sup>b</sup>Abengoa Research, C/ Energía Solar nº 1, Campus Palmas Altas, 41014, Spain, E-mail: shahzada.ahmad@research.abengoa.com

Received: 4th April 2014

Accepted: 3rd June 2014

RSC Advances



PAPER

Improving the cycling performance of  $\text{LiFePO}_4$  cathode material by poly(3,4-ethylenedioxythiophene) coating†

Cite this: *RSC Adv.*, 2014, **4**, 26108

D. Cíntora-Juárez,<sup>a</sup> C. Pérez-Vicente,<sup>a</sup> Shahzada Ahmad<sup>\*b</sup> and J. L. Tirado<sup>\*a</sup>



## Abstract

LiFePO<sub>4</sub> composite cathode materials with PEDOT [poly(3,4-ethylenedioxythiophene)] were prepared by electropolymerization or by blending methods. The cycling performance of these composites in lithium test cells were then evaluated and compared with bare and carbon-coated LiFePO<sub>4</sub>. The electrodes were further fine-tuned by optimizing the materials and different preparative methods adopted. It was found that the LiFePO<sub>4</sub>/PEDOT composite obtained by direct electropolymerization over the cathode shows better cycling performance in terms of capacity (110 mAh/g<sub>LFP</sub> at 2C) and capacity retention (125 mAh/g<sub>LFP</sub> after 50 cycles at C/2). We attribute the improved performance to an enhanced conductivity, as evidenced by the initial impedance of the cathodes and low charge–discharge polarization during cycling.

## 1. Introduction

Lithium-ion batteries incorporating LiFePO<sub>4</sub> or other LiMPO<sub>4</sub> (*M*: Mn, Co, Ni) olivine-related compounds are attractive in terms of safety, energy and power density, general performance and cost.<sup>1–3</sup> However, these compounds possess low electronic conductivity and poor ionic diffusivity, which ultimately result in poor cycling performance for Li-ion batteries.<sup>4</sup>

Strategies to improve the electronic conductivity of the active material include coating with carbon or conducting polymers,<sup>5–7</sup> the control of the particle size and morphology, blending with metallic additives, ionic doping or substitution in the crystalline lattice, among other approaches that have been adopted.<sup>8,9</sup> To overcome the current bottleneck in these materials the electronic and ionic wiring of the active material is one of the strategies which can be applied to increase the rate performance and mechanical stability of the electrode. For this, electron-conducting additives and polymeric binders are usually incorporated to the formulation. In the past, various kinds of carbon black and fluorinated polymers have been used as common additives; however, such materials do not contribute to the electrode capacity and thus reduce the energy and power density of the battery.<sup>10</sup>

In this scenario the incorporation of conducting polymers to the electrode formulation is an attractive option, as it can act in two folds. First, as electron conducting additive



and as binder, and secondly, to provide enhanced electrochemical performance, apart from improving the mechanical properties of the electrodes, and protecting the battery electrolyte from decomposition by the formation of protective layers.<sup>11,12</sup> The role of polypyrrole, polyaniline and poly(3,4-ethyl-enedioxythiophene) [PEDOT] on the performance of  $\text{LiFePO}_4$  in lithium batteries has been investigated during recent years.<sup>2,6,7,11,13</sup>

Composite electrode materials with PEDOT are especially attractive in terms of high electronic conductivity, contribution to the electrode capacity and the ability to improve Li-ion transport.<sup>12a</sup>

PEDOT has low band gap, chemical stability and can withstand cycling for practical applications, and was also shown to be efficient cathode in dye sensitized solar cells for the reduction of redox electrolyte.<sup>12b,c</sup>

Various methods have been proposed to prepare  $\text{LiFePO}_4$ /conducting polymer composites, including blending with a chemically synthesized polymer,<sup>14–16</sup> chemical polymerization in the presence of  $\text{LiFePO}_4$  or  $\text{Li}_{1-x}\text{FePO}_4$ ,<sup>13</sup> potentiostatic or potentiodynamic electropolymerization of monomers to form a deposit in the presence of  $\text{LiFePO}_4$ ,<sup>6,7</sup> among other approaches. It is well known that a different synthetic procedure leads to different stoichiometry and microstructure that largely influence the physico-chemical properties of the material. In order to further improve the cycling performance of  $\text{LiFePO}_4$ , synthetic approach was fine tuned to incorporate PEDOT into  $\text{LiFePO}_4$  by electropolymerization or by mechanical blending. The results presented here are obtained from moderate-performance  $\text{LiFePO}_4$ , which allows evaluating more clearly the response of the composites. To understand the performance of different preparative methods adopted, a comparative study of PEDOT-coated  $\text{LiFePO}_4$  (LFP) has been carried out which was hereto unreported. This is paramount to choose the right chemistry, to yield higher performance materials.

## 2. Results and discussion

### 2.1 Characterization of LFP and LFP/C

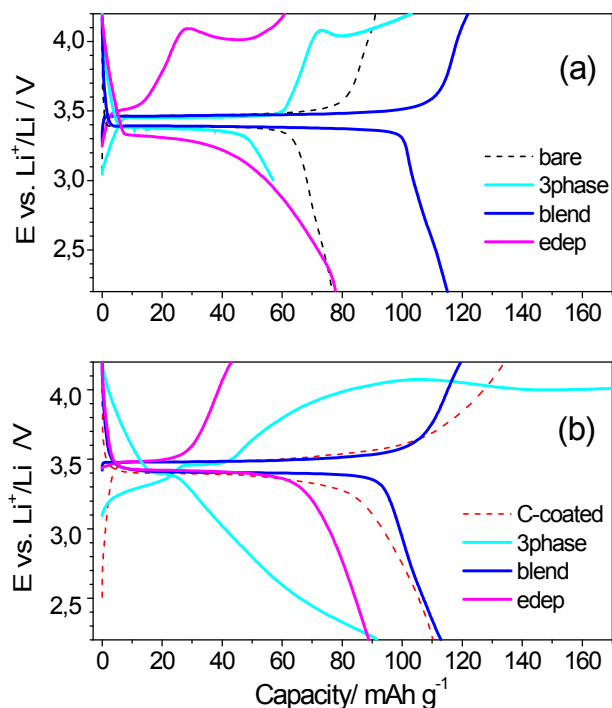
X-ray powder diffraction (XRD) patterns were obtained from a Siemens D5000 diffractometer using Cu K radiation in the  $2\theta$  range from 15 to  $80^\circ$  in steps of  $0.04^\circ$  at 20 s per step. The XRD patterns of LFP and LFP/C pristine materials (ESI†) showed the characteristic reflections for the orthorhombic structure of  $\text{LiFePO}_4$  (JCPDS 40-1499),

except for very weak signals in the  $2\theta$  interval from  $22.3$  to  $34.3^\circ$ , attributed to  $\text{Li}_3\text{PO}_4$  (JCPDS 15-0760). These reflections are almost undetectable in the pattern of the carbon-coated sample. The refinement of the lattice parameters for LFP with space group  $\text{Pnmb}$  provided the values  $a = 6.004(1) \text{ \AA}$ ,  $b = 10.322(4) \text{ \AA}$ ,  $c = 4.691(1) \text{ \AA}$ , which is in accordance with previous reports.<sup>17,18</sup> However, refined unit cell parameters for LFP/C showed no significant difference.

## 2.2 Electrochemical properties

### 2.2.1 Initial charge–discharge performance

Fig. 1 compares the initial charge-discharge profiles at  $C/10$  for the LFP and LFP/C samples and their composites with PEDOT. The LFP and LFP/C samples show the typical profiles with a potential plateau at ca.  $3.4\text{--}3.5 \text{ V}$ , characteristic of the two phase transformation of  $\text{LiFePO}_4$  into isostructural  $\text{FePO}_4$  upon lithium extraction/re-insertion. The charge capacity for the bare sample reaches  $91 \text{ mAh g}^{-1}$  and in discharge the cell delivers a reversible capacity of only  $77 \text{ mAh g}^{-1}$ . In this article the reported capacities are referred to the total weight of the composite electrode, including LFP active material and additives.



**Fig. 1** Initial charge/discharge profiles at  $C/10$  for (a) LFP-PEDOT composites and (b) LFP/C-PEDOT composites.

For benchmark purposes, common loadings of active material range from 70–85% w, which would correspond to capacity values of ca.  $130 \text{ mAh g}^{-1}$ . The carbon-coated sample shows higher capacity than the bare sample, reaching  $134 \text{ mAh g}^{-1}$  in charge and  $110 \text{ mAh g}^{-1}$  in discharge. In spite of the improvement in the discharge capacity observed for the carbon-coated sample, this composite illustrates irreversible capacity, while also contains electrochemically inactive carbon black (CB) and polymeric binder (polyvinylidene fluoride [PVDF]) additives. Recently, Trinh et al.<sup>6</sup> adapted a dynamic three phase interline electropolymerization to produce cathode films that incorporate PEDOT and LFP without the need of carbon black and PVDF additives, thus improving the power and energy densities. We have adopted the three phase (3phase) method to prepare LFP/C–PEDOT composites and extended it for preparing LFP–PEDOT composites, designated, respectively, as LFP/C–3phase and LFP–3phase.

Fig. 1a displays the initial charge and discharge profiles for the LFP–3phase composite. The charge and discharge profiles present the characteristic voltage plateaus for LFP at nearly 3.45–3.37 V. In charge, a particular feature for this sample is the abrupt change of slope at ca. 4.0 V, in the region where de-lithiation of active  $\text{LiFePO}_4$  has taken place. To further investigate the abnormal profile above 4.0 V, we performed a linear voltammetry test for the EDOT monomer in the battery conditions over a platinum electrode. The voltammetry test (ESI†) revealed an oxidation onset potential at nearly 4.0 V, and a current peak at 4.13 V (vs.  $\text{Li}^+/\text{Li}$ ), in agreement with previous reports.<sup>12</sup> Therefore, we attribute the 4.0 V signal in the charge profile of the LFP–3phase composite to the oxidation of unreacted EDOT monomers or oligomeric species trapped within the LFP–3phase composite during its preparation. In discharge, the potential profile for the LFP–3phase composite is similar to that of the LFP sample and the discharge capacity reaches ca.  $53 \text{ mAh g}^{-1}$ , a value that is close compared to the reported<sup>6</sup> (ca.  $45 \text{ mAh g}^{-1}$ ). Fig. 1b shows the charge-discharge profiles for the LFP/C–3phase composite. The charge profile for this sample presents a smooth increase in potential from the open circuit potential to the characteristic plateau at ca. 3.45 V. The potential then continues to rise up to a capacity of  $216 \text{ mAh g}^{-1}$  (off-scale) at the cut-off potential. In discharge, the LFP/C–3phase composite shows a short plateau at ca. 3.4 V, with further potential decrease until reaching the cut-off potential and a total

discharge capacity of ca. 91 mAh g<sup>-1</sup>. The poor discharge capacity in the 3.4 V plateau region for the LFP–3phase, and particularly for the LFP/C–3phase samples, reflects the difficulties for incorporating active LFP into the composite. Contrary to the report,<sup>6</sup> we have found that the composite was fragile and required additional reprocessing to form an electrode. Considering these obstacles, the sample LFP/C–3phase was not chosen to study further. To control better the amount of PEDOT in the composite and improving its electrochemical performance, EDOT was electropolymerized using the 3phase method,<sup>6,19</sup> and then blended with LFP or LFP/C active materials.

**Table 1.** Characteristics of the different composite cathodes

Sample	Preparation details	LFP content (%)	PEDOT content (%)	LFP:PEDOT weight ratio	Additives CB + PVDF (8:7 wt) content (%)
LFP	LFP cathode with CB and PVDF additives.	85	0	100:0	15
LFP-3phase	Three phase electropolymerization of EDOT in presence of LFP.	70	30	70:30	0
LFP-blend	LFP blended with PEDOT obtained by three phase electropolymerization.	80	20	80:20	0
LFP-edep	Electrodeposition of PEDOT over preformed LFP cathode.	66	19	78:22	15
LFP/C	LFP/C cathode with CB and PVDF additives.	85 (2 % wt. C)	0	100:0	15
LFP/C-3phase	Three phase electropolymerization of EDOT in presence of LFP/C.	50 (2 % wt. C)	50	50:50	0
LFP/C-blend	LFP/C blended with PEDOT obtained by three phase electropolymerization.	83 (2 % wt. C)	17	83:17	0
LFP/C-edep	Electrodeposition of PEDOT over preformed LFP/C cathode.	82 (2 % wt. C)	3	97:3	15

Fig. 1 shows the charge-discharge profiles for the LFP–blend and the LFP/C–blend samples. The charge-discharge profiles for the LFP–blend sample (Fig. 1a) show flat potential plateaus at ca. 3.47–3.38 V. The charge capacity for this sample reaches ca. 122 mAh g<sup>-1</sup>, without any profile abnormality near 4.0 V, which was observed for the LFP–3phase composite. These findings suggest an enhanced stability of the polymer

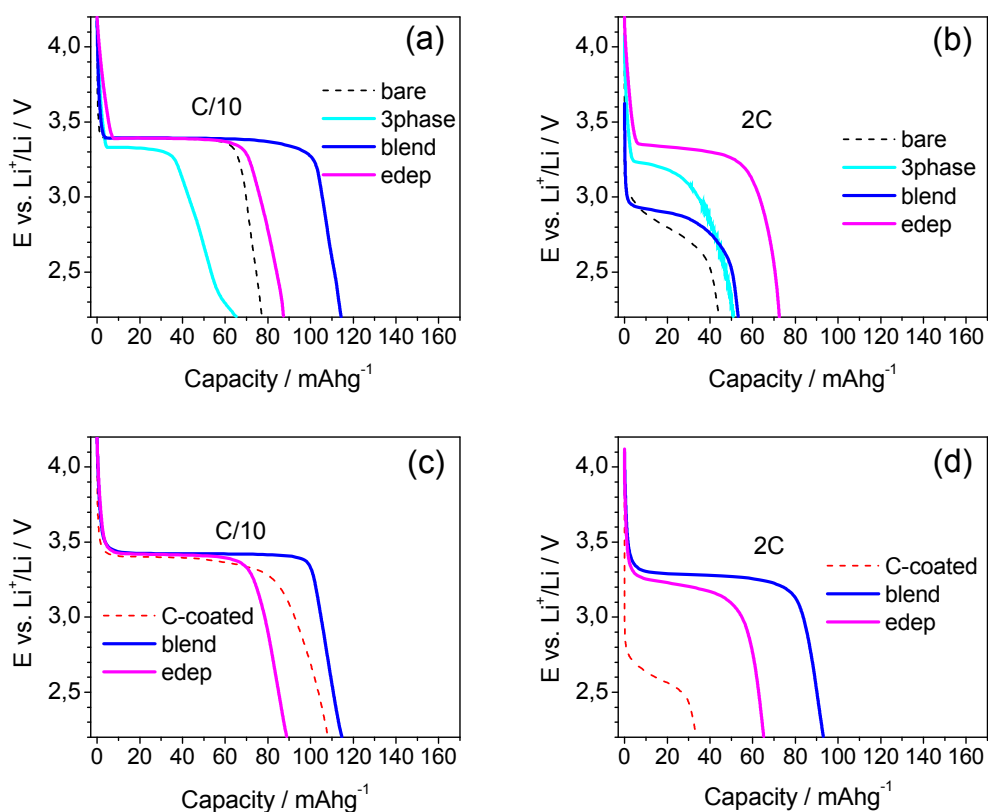
against further oxidation, in the absence of LFP during the electropolymerization using three-phase method. In discharge, the LFP–blend sample delivers a total capacity of  $115 \text{ mAh g}^{-1}$ , which is close to the benchmark capacity of  $130 \text{ mAh g}^{-1}$ . These results indicate a notable improvement in performance compared to those obtained for LFP–3phase, and show the importance of incorporating PEDOT with higher degree of polymerization to the active LFP material. In Fig. 1b, the charge-discharge profiles of LFP/C–blend present the plateau at ca. 3.48–3.40 V and capacities of 119 and 113  $\text{mAh g}^{-1}$  in charge and discharge, respectively, which are very close to the capacity values obtained for the LFP–blend composite.

Charge-discharge profiles of the samples obtained by direct electrodeposition (edep) of PEDOT on cathodes are shown in Fig. 1. In charge, the LFP–edep composite (Fig. 1a) show a short plateau at 3.5 V, followed by an increase in potential and an abrupt change of slope at c.a. 4.0 V, yielding charge capacity at the cut-off potential close to  $61 \text{ mAh g}^{-1}$ . The charge profiles for the LFP–edep and the LFP–3phase samples are similar, showing that the electropolymerization of EDOT monomers over LFP cathode was incomplete and produced redox active oligomeric species. The LFP–edep composite has the lowest discharge potential and a capacity of ca.  $78 \text{ mAh g}^{-1}$ . While the LFP/C–edep sample (Fig. 1b) indicates that the charge profile lacks the potential abnormality observed for the LFP–edep composite. This was in accordance to our understanding, as the extent of electrodeposition will be higher over more conducting surface (carbon-coated LFP particles). The fact that the discharge capacity for both LFP–edep and LFP/C–edep samples was higher than their corresponding charge capacity, indicates simultaneous delithiation of LFP and oxidation of EDOT monomers during the preparation of the composites by the electrodeposition method.

### 2.2.2 Slow vs. moderate rate performance

Fig. 2 shows average discharge curves at C/10 and 2C for the standard LFP and LFP/C, and their different composites with PEDOT. Comparison between slow and moderate rate indicates that both standard LFP and LFP/C samples show capacity loss and potential drop with the increase in rate. The performance of the LFP–3phase composite is inferior among all the samples at C/10 (Fig. 2a). However, at higher rate (Fig. 2b) it retains 80% of its capacity at C/10 and is free from large potential drop found for the LFP and LFP/C. The performance of the LFP–blend composite also deteriorates

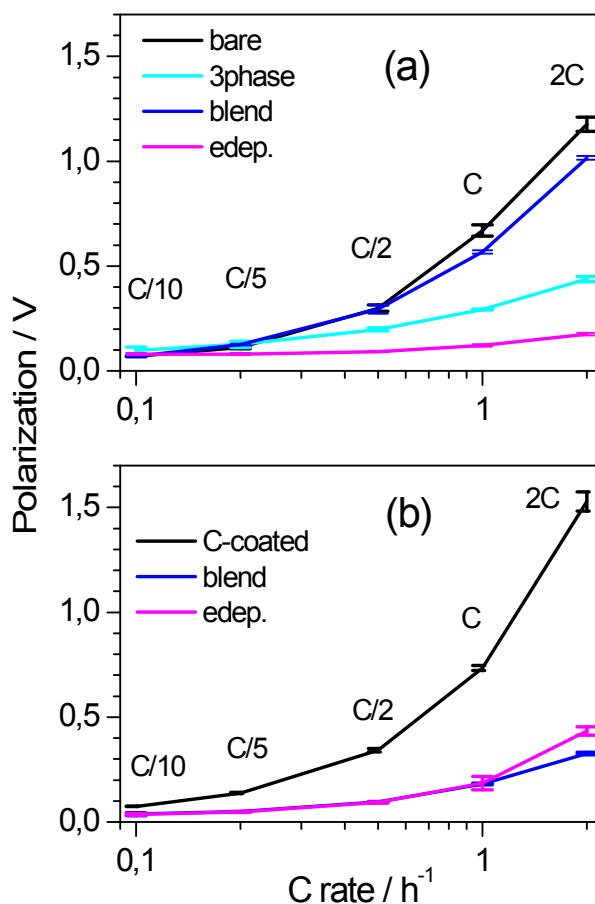
considerably at 2C, losing more than 50% of its low rate capacity and suffering considerable drop in potential. The lower performance of the LFP–blend at 2C (Fig. 2b) contrasts with the better performance of the LFP/C–blend at similar rate (Fig. 2d). Earlier it was found that carbon materials are compatible with conducting polymers and give synergistic results in electroactive composites.<sup>22</sup> We believe that the chemical affinity of TEABF<sub>4</sub>-doped PEDOT and the carbon coating of LFP/C particles favours the anchoring of PEDOT. Therefore, a more extended conducting polymer matrix is expected to form when both the inorganic and organic materials are blended. Improved performance, compared to parent LFP, was also observed for the cathode materials prepared by the electrodeposition method, especially at 2C. Thus, the LFP–edep sample shows a reversible capacity of ca. 87 mAh g<sup>-1</sup> and 72 mAh g<sup>-1</sup> at C/10 and 2C, respectively, with a voltage drop of less than 100 mV.



**Fig. 2** Discharge curves at C/10 and 2C for (a-b) LFP–PEDOT composites and (c-d) LFP/C–PEDOT composites.

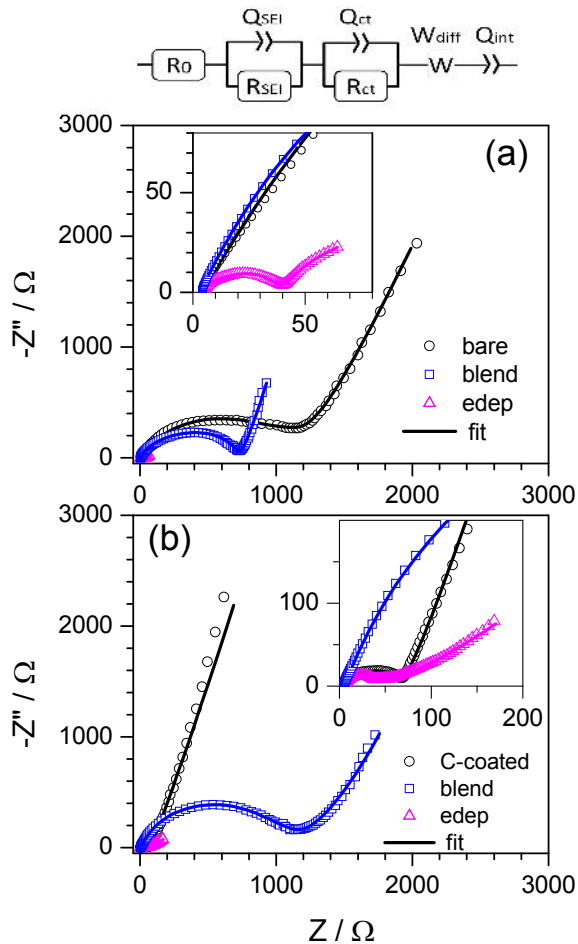
### 2.2.3 Charge–discharge polarization and cathode impedance

Fig. 3 shows polarization graphs for the standard samples and PEDOT composites. As expected, composites with polymer show lower charge-discharge polarization than the standard samples. Particularly, the composite prepared by electrodeposition over the LFP cathode shows the lowest polarization, which reflects its increased conductivity and reactivity for extraction-reinsertion of lithium ions in the active material. Comparison against the polarization of LFP/C–edep composite (Fig. 3b) suggests that carbon coating is not necessary for the LFP–edep composite. Electrochemical impedance spectroscopy (EIS) was employed to investigate the effect of PEDOT on the conducting properties of the composite cathodes.



**Fig. 3** Charge-discharge polarization plots for (a) LFP–PEDOT and (b) LFP/C–PEDOT composites.

In the past, EIS studies on LFP cathode materials were reported, and the spectra can be fitted by using an equivalent electrical circuit consisting of a high and a medium-to-low frequency semicircles (R-Q elements), the former corresponding to the lithium ion migration resistance in the SEI and the later to the charge transfer resistance. Semi-infinite diffusion and differential intercalation capacity are usually fitted by a series capacitance and a Warburg element in the low frequency region. Besides, the equivalent circuit includes an inductor and a resistor to account for the cables inductance and the contact resistances in the cell. Fig. 4a presents the experimental and fitted spectra by using the above mentioned equivalent circuit. The resistance values obtained from the fitting procedure are listed in Table 2.



**Fig. 4.** AC impedance spectra of pristine composites. a) LFP–PEDOT and b) LFP/C–PEDOT.



**Table 2.** Data of the fitting of the EIS spectra shown in Fig. 4.  $R_{\text{Total}} = R_o + R_{\text{SEI}} + R_{\text{ct}}$ 

Material	$R_o$ ( $\Omega$ )	$R_{\text{SEI}}$ ( $\Omega$ )	$R_{\text{ct}}$ ( $\Omega$ )	$R_{\text{Total}}$ ( $\Omega$ )
LFP	4.1	781	258	1043
LFP-blend	3.1	626	102	731
LFP-edep	4.7	33	8	46
LFP/C	3.9	52.5	12	68
LFP/C-blend	4.7	889	242	1136
LFP/C-edep	5.0	25	16	46

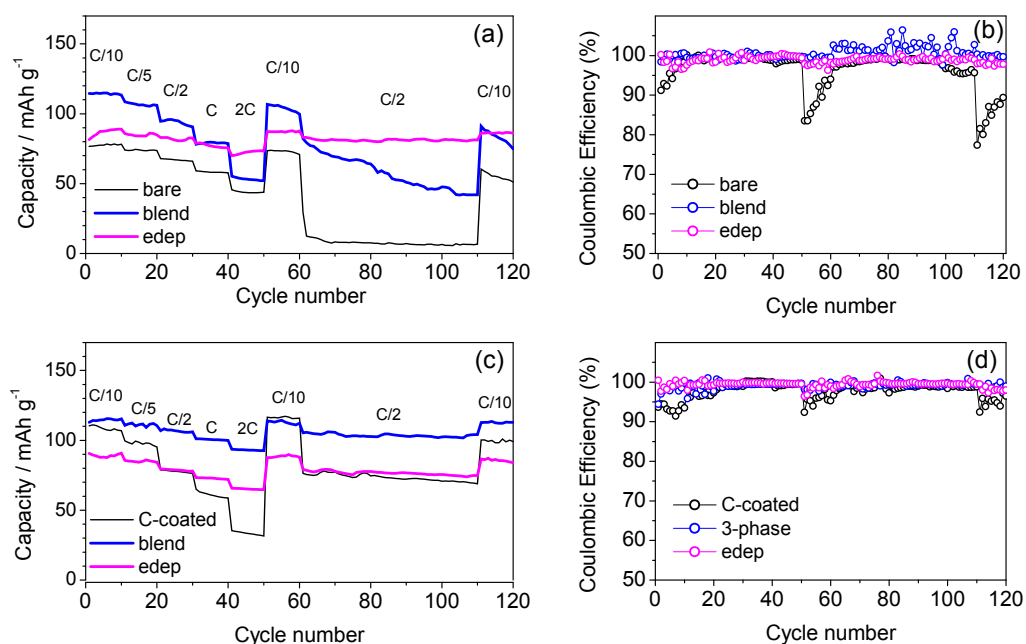
It is evident from Fig. 4 that the charge transfer resistance values for the LFP–PEDOT composites are lower than for the parent LFP. In particular, the lowest resistance values were found for the LFP–edep composite, which translates into a lower polarization and a higher cycling performance. The lowest impedance value was found for the composite prepared by electrodeposition, which suggests that the polymerization over LFP active material particles favours the growth of a highly conducting polymer that improves the electrical wiring between LFP particles. The impedance data of the C-coated samples show the improvement in the total conductivity for the sample prepared by electrodeposition. However, the sample prepared by blending C-coated LFP and PEDOT give the high value of impedance. This observation can be explained in terms of formation of poorly conducting PEDOT that requires activation in order to reach an ideal polymerization degree and doping. The higher resistance for blend samples can also be related to the textural properties of the composites (Fig. 6). For PEDOT-bearing samples, the information provided by SEM showed that the particles are visible after PEDOT addition. However, for blend samples the surface is more abrupt, which is indicative of a less uniform distribution of the polymer.

#### 2.2.4 Extended cycling

Fig. 5 presents the cycling performance of the standard samples and the different LFP–PEDOT and LFP/C–PEDOT composites. During the first 50 cycles, the capacity of all samples decreases progressively as rate increases. After 50 cycles, all the samples, except for the LFP–3phase and LFP–blend (Fig. 5a), recover at least 90% of their initial

capacity at C/10 rate. The best performance, in terms of capacity values and capacity retention at C/2 during the first 50 cycles, was found for the LFP–edep sample. After 110 cycles at variable rates, only the LFP–edep sample recovers ca. 99% of its initial capacity at C/10, which confirms its remarkable cycling performance. The enhanced cycleability obtained for the LFP–edep cathode materials suggests that the PEDOT obtained by this method is more chemically and mechanically stable (tethered) over LFP in the battery environment.

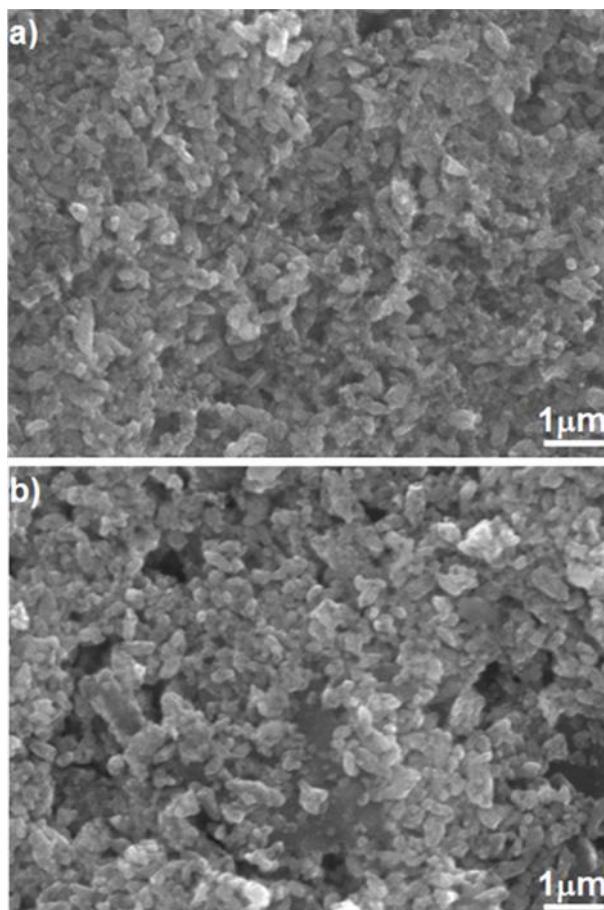
Fig. 5b presents the cycling performance of two LFP/C–PEDOT composites. During the initial cycles at low rates (C/10–C/5), only the LFP/C–blend composite outperforms the LFP/C sample. At moderate rates (C/2–2C), both LFP/C–blend and LFP/C–edep composites outperform the LFP and the LFP/C samples.



**Fig. 5** Cycleability at different rates for (a–b) LFP–PEDOT and (c–d) LFP/C–PEDOT composites.

After 50 cycles, both LFP/C–PEDOT composites recover almost 99% of its initial capacity at C/10, and show good capacity retention at C/2, and after 110 cycles both LFP/C–PEDOT samples recover more than 95% of the initial capacity. Comparing the performance of the composites prepared by the blending method, the carbon coating in

the LFP/C active material could provide a good substrate that favours the formation of a more extended conducting polymer matrix. In electrodeposition, the higher electrodeposition time for the LFP–edep composite allows better wetting of the LFP active material by EDOT monomers, promoting a more quantitative PEDOT electrodeposition.



**Fig. 6** Scanning Electron Micrographs of composites (a) electrodeposition and (b) blend based on  $\text{LiFePO}_4$ .

### 3. Conclusions

A comparative study of LFP–PEDOT and LFP/C–PEDOT composites prepared by different methods such as electropolymerization and blending methods were carried

out. The  $\text{LiFePO}_4/\text{PEDOT}$  composite obtained by direct electrodeposition over the cathode showed the best cycling performance, with a reversible capacity of ca.  $110 \text{ mAh g}_{\text{LFP}}^{-1}$  at 2C, notable capacity retention at C/2 ( $125 \text{ mAh g}_{\text{LFP}}^{-1}$  after 50 cycles), and low charge–discharge polarization. The improved performance is ascribed to an enhanced overall conductivity of the electrode (active material plus additives) emerging from the conductive nature of polymer. PEDOT alone can well improve the performance of phosphate materials and thus the combination of carbon and PEDOT coating is not necessary to improve the performance of the phosphate.

## 4. Experimental section

### 4.1 Electrode preparation and materials

$\text{LiFePO}_4$  and carbon-coated  $\text{LiFePO}_4$  (LFP/C) active materials were obtained as described elsewhere.<sup>4</sup> LFP and LFP/C electrodes were prepared by mixing the active material with carbon black (CB) and PVDF additives (85 : 8 : 7 wt%) in N-methyl pyrrolidone to form slurry. The slurry was ultrasonicated, deposited over an aluminium disk ( $0.64 \text{ cm}^2$ ) and dried at  $80^\circ \text{ C}$  under vacuum for 12 h. The average amount of active material ranges from 3–5  $\text{mg cm}^{-2}$ . 3,4-ethylenedioxythiophene (EDOT) and tetraethylammonium tetrafluoroborate (TEABF<sub>4</sub>) were obtained from Aldrich, and were used without any further treatment. The preparative methods used to obtain the composites with PEDOT and LFP or LFP/C active materials are described below.

### 4.2 Materials synthesis

Three phase electropolymerization (3phase) consisted in the potentiostatic electropolymerization of PEDOT in the presence of LFP or LFP/C through interphasial electropolymerization.<sup>6</sup> The three-phase reaction medium contained TEABF<sub>4</sub> (0.1 M) dissolved in water, EDOT (0.1 M) dissolved in dichloromethane and the active material spread over the aqueous/organic phase boundary. The experiment was carried out in a three-electrode cell with platinum wire as working electrode situated across the interphase, a carbon rod as counter electrode and an Ag/AgCl (3 M KCl, AgCl sat.) reference electrode, both electrodes immersed in the aqueous phase. The electropolymerization of EDOT monomer took place over platinum at the aqueous/organic interphase when a potential difference of 1.3 V was applied. The obtained composite film was grinded, washed with deionized water followed by

acetonitrile, and dried for 12 h under vacuum at  $60^\circ\text{C}$ . The dry product was dispersed in NMP and deposited on an aluminium current collector. Finally it was dried for 12 h under vacuum at  $80^\circ\text{C}$ . Composites prepared by this method with LFP or LFP/C will be referred as LFP-3phase and LFP/C-3phase, respectively. The blending method consisted of mixing PEDOT, prepared by 3phase electropolymerization, and the active material (without CB and PVDF additives) in N-methyl pyrrolidone to form slurry. The slurry was ultrasonicated, deposited over an aluminium disk and dried at  $80\text{--}100^\circ\text{C}$  under vacuum for 12 h. Composites prepared by this method will be henceforth referred to as LFP-blend or LFP/C-blend. Electrodeposition of PEDOT was performed on LFP and LFP/C cathodes as the substrate. The electrodeposition was carried out using the cathode as working electrode in a three electrode cell with an aluminium disk as counter electrode and Ag/AgCl (3 M KCl, AgCl sat.) as reference electrode. The reaction medium consisted of a 0.1 M EDOT, 0.1 M TEABF<sub>4</sub> solution in acetonitrile. The electropolymerization over the LFP and LFP/C electrodes was performed potentiostatically at 1.3 V (Ag/AgCl) during 30 and 3 min, respectively. After electropolymerization, the composite electrode was washed with acetonitrile and dried at  $80^\circ\text{C}$  under vacuum for 12 h. The samples prepared with LFP and LFP/C will be henceforth referred to as LFP-edep and LFP/C-edep, respectively. Table 1 summarizes the characteristics of the different LFP-PEDOT and LFP/C-PEDOT composites.

### 4.3 Battery testing

Batteries were assembled in two-electrode Swagelok-type cells, using the cathode as working electrode, 1 M  $\text{LiPF}_6$  (EC : DEC, 1 : 1 volume ratio) electrolyte (SelectiLyte LP40, Merk), with Whatman glass-paper as separator and 1.5 mm thick lithium metal foil as reference/counter electrode. The cells were assembled in a glove box under controlled argon atmosphere ( $\text{H}_2\text{O}$ ,  $\text{O} < 1$  ppm). Galvanostatic cycling at different C-rates ( $\text{C} = 1 \text{ Li h}^{-1} \text{ mol}^{-1}$ ) was carried out at room temperature using a Biologic MPG station. The cut-off potential for charge and discharge were set at 4.2 and 2.2 V (vs.  $\text{Li}^+/\text{Li}$ ), respectively. The reported capacities refer to the total weight of the composite electrode, including LFP active material and additives. Extended cycling was performed in order to evaluate the rate capability, the capacity recovery and the capacity retention of the different samples. Rate capability was assessed by repeated and progressive

cycling at rates of: C/10, C/5, C/2, C and 2C (10 cycles each). Afterwards, a first evaluation of the capacity recovery at C/10 (10 cycles) was carried out. The capacity retention was evaluated at C/2 for 50 cycles. At the end of the capacity retention test, a second capacity recovery test was carried out by cycling at C/10 for 10 cycles. Electrochemical impedance spectra were recorded for the cathode materials in an Autolab PGSTAT12 station. Measurements were done in three-electrode Swagelok cells housing LFP-based composites as working electrode, lithium metal counter electrode and a perpendicularly aligned lithium reference electrode. The applied ac voltage was 10 mV and the frequency was varied in the range from 1 MHz to 10 mHz.

## References

- (1) A. K. Padhi, K.S. Nanjundaswamy and J.B. Goodenough, *J. Electrochem. Soc.*, 1997, 144 (4), 1188.
- (2) L. X. Yuan, Z. H. Wang, W. X. Zhang, X. L. Hu, J. T. Chen, Y. H. Huang and J. B. Goodenough, *Energy Environ Sci.*, 2011, 4, 269.
- (3) K. Zaghib, A. Mauger and C. M. Julien, *J. Solid State Electrochem.*, 2012, 16, 835.
- (4) C. Delacourt, L. Laffont, R. Bouchet, C. Wurm, J.-B. Leriche, M. Morcrette, J.-M. Tarascon and C. Masquelier, *J. Electrochem. Soc.*, 2005, 152(5), A913.
- (5) M. M. Doeff, J. D. Wilcox, R. Kostecky and G. Lau, *J. Power Sources*, 2006, 163, 180.
- (6) N. D. Trinh, M. Saulnier, D. Lepage and S.B. Schougaard, *J. Power Sources*, 2013, 221, 284.
- (7) I. Boyano, J. A. Blazquez, I. Meatza, M. Bengoechea, O. Miguel, H. Grande, Y. Huang and J. B. Goodenough, *J. Power Sources*, 2010, 195, 5351.
- (8) S.-Y. Chung, J. T. Bloking and Y.-M. Chiang, *Nat. Mater.*, 2002, 1, 123.
- (9) B. Kang and G. Ceder, *Nature*, 2009, 458, 190.
- (10) Y.-H. Chen, C.-W. Wang, X. Zhang and A. M. Sastry, *J. Power Sources*, 2010, 195, 2851.
- (11) A. V. Murugan, T. Muraliganth and A. Manthiram, *Electrochem. Commun.*, 2008, 10, 903.
- (12) (a) K. Abe, Y. Ushio, H. Yoshitake and M. Yoshio, *J. Power Sources*, 2006, 153, 328; (b) S. Ahmad, T. Carstens, R. Berger, H.-J. Butt, F. Endres, *Nanoscale*, 2011,

- 3, 251; (c) S.Ahmad, J.-H.Yum, Z. Xianxi, M. Grätzel, H.-J.Butt and M. K. Nazeeruddin, *J. Mater.Chem.*, 2010, 20, 1654.
- (13) D. Lepage, C. Michot, G. Liang, M. Gauthier and S. B. Schougaard, *Angew. Chem. Int. Ed.*, 2011, 50, 6884.
- (14) M. G. Han and S. P. Armes, *Langmuir*, 2003, 19, 4523.
- (15) H.-C. Dinh, I.-H. Yeo, W. I. Cho and S. Mho, *Trans. Electrochem. Soc.*, 2010, 28, 167.
- (16) J. Y. Shi, C-W. Yi and K. Kim, *Bull. Korean Chem. Soc.*, 2010, 31(9), 2698.
- (17) G. Rousse, J. Rodriguez-Carvajal, S. Patoux and C. Masquelier, *Chem. Mater.* 2003, 15, 4082.
- (18) C. Delacourt, J. Rodríguez-Carvajal, B. Schmitt, J.-M. Tarascon and Christian Masquelier, *Solid State Science*, 2005, 7, 1506.
- (19) H. Zhu, L. Gao, M. Li, H. Yin and D. Wang, *Electrochem. Commun.*, 2011, 13, 1479.
- (20) B. León, C. Pérez Vicente, J. L. Tirado, Ph. Biensan and C. Tessier, *J. Electrochem. Soc.* 2008, 155, A211.
- (21) J. P. Schmidt, T. C. Chrobak, M. Ender, D. Klotz, E. I-Tiffée, *J. Power Sources*, 2011, 196, 5342.
- (22) Y. Huang, K. Park and J. B. Goodenough, *J. Electrochem. Soc.*, 2006, 153(12), A2282.

## Electronic supporting Information (ESI)

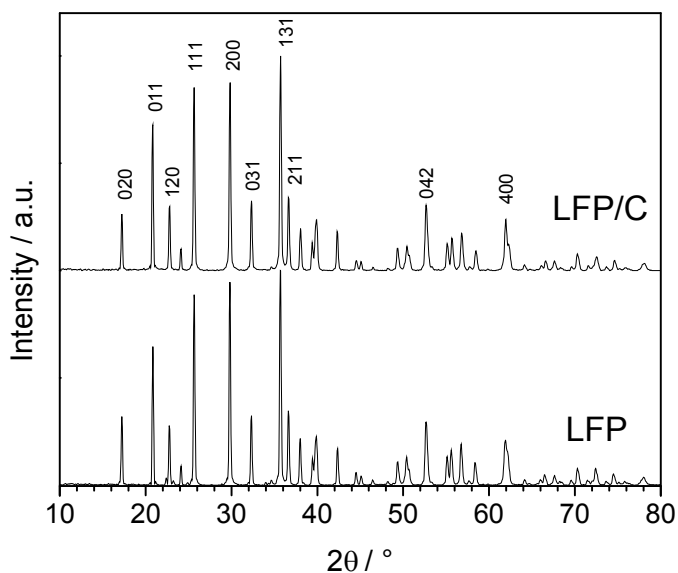


Fig. S1: XRD patterns of LFP and LFP/C active materials.

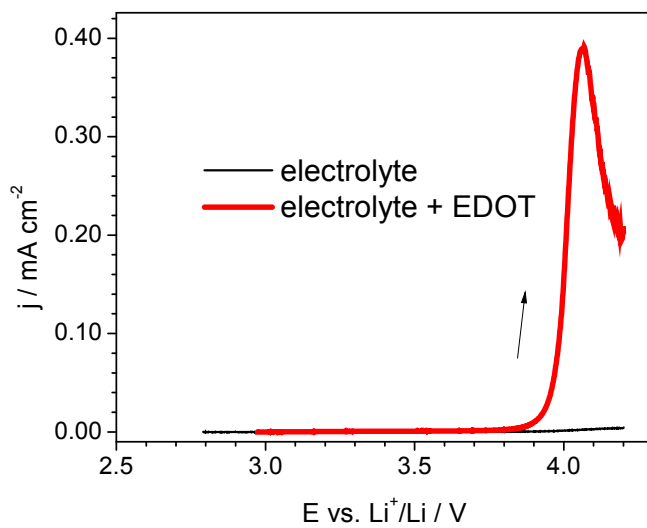


Fig. S2: Linear voltammetry plot of 0.01 M EDOT in the LiPF<sub>6</sub>-based battery electrolyte.





## Chapter 4

### Electrochemical in battery polymerization of poly(alkylenedioxythiophene) over lithium iron phosphate for high performance cathodes

D. Cíntora-Juárez<sup>a</sup>, C. Pérez-Vicente<sup>a</sup>, S. Ahmad<sup>b</sup> and J. L. Tirado<sup>a</sup>, *Phys. Chem. Chem. Phys.*, 2014, **16**, 20724–20730.

<sup>a</sup>Laboratorio de Química Inorgánica, Campus de Rabanales, Universidad de Córdoba, 14071, Spain

<sup>b</sup>Abengoa Research, C/ Energía Solar nº 1, Campus Palmas Altas, 41014, Spain, E-mail: shahzada.ahmad@research.abengoa.com

Submitted: 25th June 2014,

Accepted: 12th August 2014



The image shows the cover of a paper in the journal PCCP (Physical Chemistry Chemical Physics). The cover features the journal logo in the top left, the Royal Society of Chemistry logo in the top right, and a dark blue horizontal bar with the word 'PAPER' in white. Below this bar, the title of the paper is displayed in bold black text, followed by the authors' names. A CrossMark logo is present in the bottom left corner.

**PCCP**

ROYAL SOCIETY OF CHEMISTRY

**PAPER**

**Electrochemical in battery polymerization of poly(alkylenedioxythiophene) over lithium iron phosphate for high-performance cathodes†**

Daniel Cíntora-Juárez,<sup>a</sup> Carlos Pérez-Vicente,<sup>a</sup> Shahzada Ahmad<sup>\*b</sup> and José Luis Tirado<sup>a</sup>

Cite this: *Phys. Chem. Chem. Phys.*, 2014, **16**, 20724



## Abstract

Molecular wiring concept was induced in  $\text{LiFePO}_4$  cathodes by in battery polymerization methods. This was performed by the addition of alkylthiophene monomers over the  $\text{LiFePO}_4$ -based cathode during the first charging step in lithium test cells. The driving force for the in battery polymerization of the monomers was supplied by the oxidizing current and by the physical contact of monomers with delithiated  $\text{Li}_{1-x}\text{FePO}_4$  formed during the charging of the battery. The resulted molecularly engineered cathodes give higher initial capacity, superior rate capability and improved cycleability compared to the pristine  $\text{LiFePO}_4$  compound. Further, to observe changes in the oxidation state of iron, Mössbauer spectroscopy was employed and the results were correlated with impedance spectroscopy, which reveal a significant increase in conductivity during charging. The presented methods allow simple, yet effective routes to manufacture efficient cathode materials at room temperature, without the need of additional oxidizing compounds to carry out the polymerization process, and to rival high temperature based carbon coatings.

## 1. Introduction

Electricity generation through energy conversion is a discontinuous process and requires energy storage at cost effective rate. In this scenario, electrochemical systems play a crucial role as they have proven to be highly efficient for storing and converting energy, and major technological solutions are considered to be in the use of batteries and supercapacitors. Currently, lithium-ion batteries are seen as one of the most mature technologies available for powering portable electronic devices and have found niches in electric vehicles and stationary applications. Materials used in electric vehicle batteries should provide fast charging/discharging rates, high energy density and cycle life, be safe and producible at low cost. The key component in lithium ion batteries is the cathode and it imposes performance and costs limitations to the widespread implementation of this technology.<sup>1,2</sup>

After the seminal work of Padhi *et al.* on olivine structured lithium transition metal phosphates ( $\text{LiMPO}_4$ ) as cathode materials, significant efforts were made, in particular for  $\text{LiFePO}_4$  (LFP), due to its attractive features of being cost

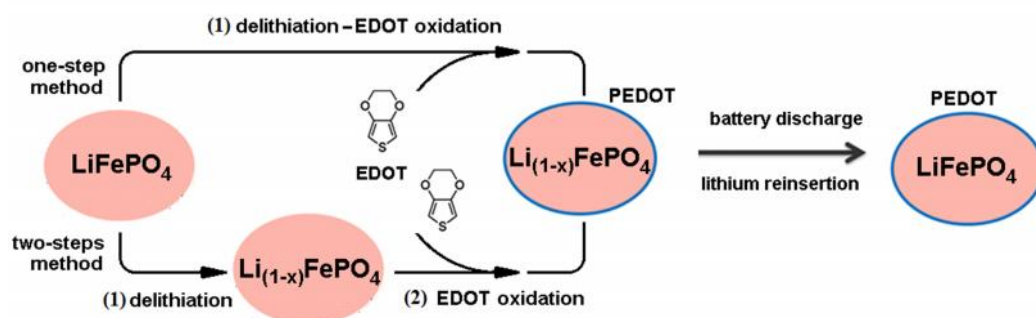
effective, environmentally friendly, electrochemically and thermally stable.<sup>3</sup> However, LFP and related cathode materials suffer from disadvantages, such as low ionic and/or electronic conductivities, which makes the task for the lithiation/delithiation processes uneasy, while making electron transfer to active sites cumbersome.<sup>4</sup> In this direction, different approaches have been explored to increase the conductivity of  $\text{LiFePO}_4$ , for example: blending with metal particles, aliovalent ion doping and reducing the particle size down to the nanoscale.<sup>5-8</sup>

To date, the most common approach adopted to increase conductivity of  $\text{LiFePO}_4$  is the formation of homogeneous carbon-coatings over the active material particles, which can be achieved by calcination of sugars or surfactants at 500-700° C.<sup>9-11a-c</sup> However, apart from the high energy consumption, the decomposition of the organics generates contaminants that pose severe environmental hazards. Thus, the electrochemical and mechanical performance of electrodes can be further improved by using carbon or polymer as additives to form conducting networks.<sup>12</sup> On the contrary, these electrochemically inactive additives entail a decrease of the practical energy/power density, as the additives do not contribute to the electrode capacity.

Earlier, it was shown that conducting polymers like polypyrroles and polythiophenes can enhance the performance of  $\text{LiFePO}_4$  and other cathode active materials.<sup>13</sup> In particular, poly(3,4-ethylenedioxythiophene) [PEDOT] has drawn special attention due to its high electronic conductivity in the doped state, contribution to the electrode discharge capacity and the ability to improve Li-ion transport due to its highly nanoporous structure, which provides deep accessibility to ions into the inner matrix of the polymer layer.<sup>14</sup>

Therefore, different methods have been used to make  $\text{LiFePO}_4$ /polymer, including blending with chemically synthesized conducting polymer<sup>15-17</sup> chemical polymerization in presence of  $\text{LiFePO}_4$  or  $\text{Li}_{1-x}\text{FePO}_4$ ,<sup>18</sup> or by electropolymerization over substrates containing  $\text{LiFePO}_4$ .<sup>19,20</sup> For such  $\text{LiFePO}_4$ /polymer, it is expected that, upon charging, conjugated polymer delivers the charge to the LFP particles by intermolecular hopping, leading to reversible  $\text{Li}^+$  extraction, while the process can be reversed on discharge. Additionally, the redox polymer can also act as binder, which offers the possibility to reduce further the use of electrode additives and produce higher energy density

batteries. Within this context, we applied the molecular-wiring concept to improve the conduction in the insulating LFP material by in battery electro-polymerization of thiophene-based monomers directly over LFP-based electrodes under battery operation conditions (scheme1), and eliminating the need of any external chemical oxidant. The use of a set of electrochemical and spectroscopic techniques allowed us to confirm the effective electronic communication between the redox polymer and LFP, as the resulting composite electrodes show higher initial capacity, superior rate capability and improved cycleability than the pristine LFP material.



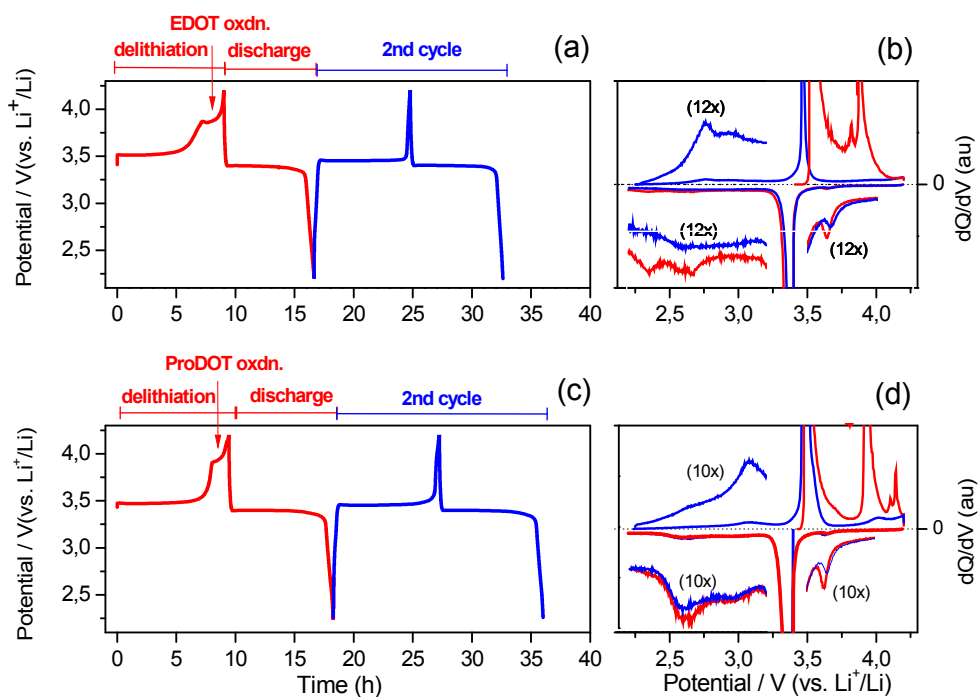
**Scheme 1.** Illustrating the one and the two step polymerization methods adopted for inducing the molecular wiring approach.

## 2. Results and discussion

### 2.1. In battery polymerization process

Figure 1 presents the plot of the two first charge/discharge cycles for the one-step in battery formation of LFP/PEDOT and LFP/poly(3,4-propylenedioxythiophene) [PProDOT]. In both systems, the initial part of the profile shows a first stage involving the oxidation of  $\text{Fe}^{2+}$  to  $\text{Fe}^{3+}$ , linked to the de-lithiation of LFP, with the characteristic charge plateau at ca. 3.5 V. As the galvanostatic charging proceeds, the oxidative polymerization of EDOT and ProDOT monomers appears as a pseudo plateau above 3.8 V. Compared to EDOT, the higher oxidation potential of ProDOT relates to the influence of the extra methylene group on the conjugated ring, which decreases the  $\pi$ -overlap along the backbone, leading to an increase of the bandgap.<sup>21</sup> In the first

discharge, the profile for both LFP/PEDOT and LFP/PProDOT shows the characteristic plateau at ca. 3.4 V, attributed to the  $\text{Fe}^{3+}$  to  $\text{Fe}^{2+}$  reduction and reinsertion of lithium ions. Independently of the monomer, the discharge capacities are higher than the charge capacities measured near 3.8 V before the beginning of the polymerization. This observation suggests that de-lithiation of LFP takes place simultaneously with the formation of PEDOT and PProDOT during the first charging step up to 4.2 V. This will be discussed in detail with our  $^{57}\text{Fe}$  Mössbauer results in next section.



**Figure 1.** Initial charge/discharge and differential capacity plots for the one-step in battery formation of composites from a-b) EDOT and c-d) ProDOT.

For both monomers, the second cycle presents flatter charge/discharge plateaus having lower polarization and increased capacity, thus pointing towards the better active material utilization and revealing the positive effect of PEDOT or PProDOT on the conductivity of the fabricated cathodes. At the end of the second charge, the oxidation of both monomers is almost complete, as evidenced by the

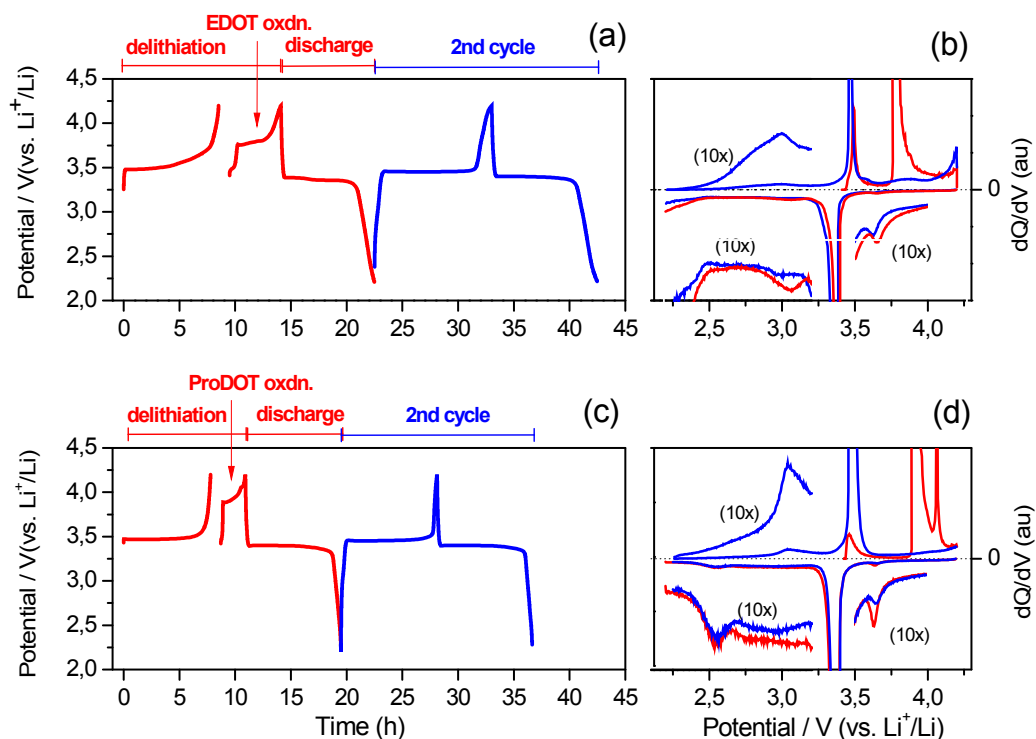
remnant trace above 3.8 V and by the lower intensity of the respective polymer oxidation peaks in the differential capacity plots (Figure 1b and 1d). For subsequent charge/discharge cycles, the pseudo plateau near 3.8 V vanishes, indicating the end of the oxidative polymerization.

The voltammogram for EDOT and ProDOT monomers (Figure S1) dissolved in the  $\text{LiPF}_6$ -based electrolyte, shows the signals ascribed to the initial oxidation of monomers, followed by undoping and reduction of deposited polymer.<sup>22</sup> It is evident (Figure 1b and 1d) that the redox processes of the polymer occur over the LFP electrode in the range from ca. 4.0 to 2.5 V, which lies within the potential window used to cycle LFP (4.2 - 2.2 V). These signals arising from the polymer are minute. Therefore, the contribution from PEDOT and PProDOT to the total discharge capacity in successive cycles is negligible as compared to the capacity from LFP active material.

Figure 2 presents the first and second charge/discharge cycles for batteries with monomers polymerized over de-lithiated LFP via the two-steps method. The observed profiles are in accordance to those for the one-step method (Figure 1), except for the first charging/delithiation step, which was carried out in the absence of a polymerizable monomer. After the first charging step, the cell was open and the monomer was added to the cathode. In a second step, the re-assembled battery was charged to induce the electropolymerization of the monomers over de-lithiated LFP. As shown in Figure 2, for the second charge step, there is a minimal initial contribution coming from  $\text{Fe}^{2+}$  to  $\text{Fe}^{3+}$  oxidation near 3.5 V indicating that the  $\text{Fe}^{2+}$  to  $\text{Fe}^{3+}$  oxidation was almost completed at the end of the first charge step. Due to the rise in potential ( $>3.8$  V), polymerization of EDOT or ProDOT monomers takes place and continues up to the cut-off voltage at 4.2 V. The lower polarization in the second cycle observed for this two-step method suggests an improvement in the conductivity of the resulting LFP-Polymer cathode.

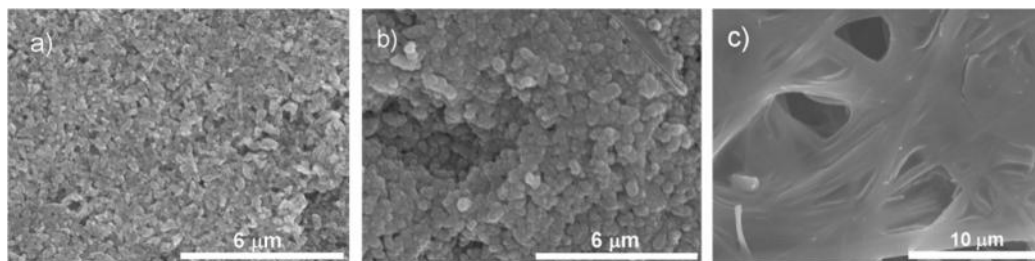
Figure 2b and 2d show the inverse derivative of the capacity as a function of potential. Additional to the main signals coming from LFP (3.4 and 3.5 V on charge and discharge, respectively), the other oxidation and reduction signals can be attributed to the redox processes of PEDOT and PProDOT previously described for the one-step method.





**Figure 2.** Initial charge/discharge and differential capacity plots for the two-steps in battery formation of composites from a-b) EDOT and c-d) ProDOT.

Figure 3 presents scanning electron microscopy images of the surface of the LFP-based cathode including binder and conductive additives as a function of the charge potential. Figure 3a shows irregular individual particles of pristine LFP. At 3.7 V, the partially delithiated cathodes with EDOT or ProDOT monomers displayed no variation with respect to the pristine LFP cathode. Contrary to this, the surface of the electrode at 4.2 V shown in Fig. 3b, illustrates the characteristic globular structure of PEDOT grown in close contact with the LFP particles, yielding a material with enhanced mechanical and conductive communication between the active particles. These features were also observed in case of LFP-PProDOT. The polymers prepared electrochemically in the absence of LFP (Fig. 3c) show a completely different texture,<sup>14c,d</sup> which emphasizes the role of LFP in the formation of the polymer by the in battery method.



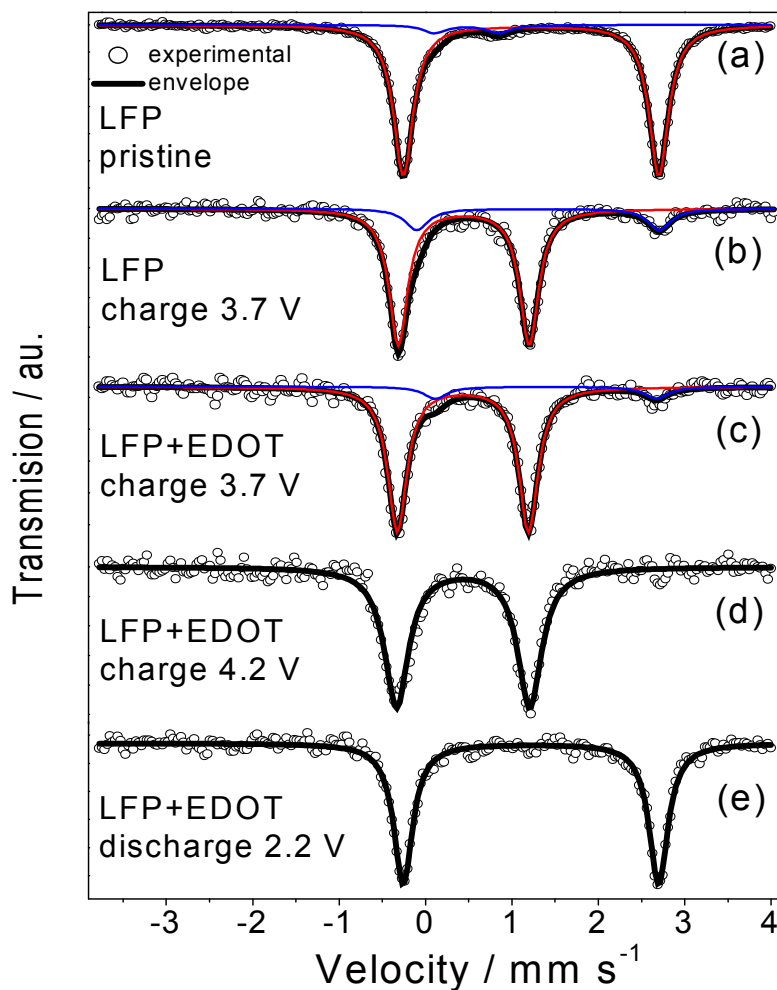
**Figure 3.** SEM pictures of the cathode surface as a function of charge potential. a) pristine LFP, b) LFP + EDOT charged at 4.2 V and c) PEDOT.

## 2.2. Mössbauer analysis

In order to elucidate the delithiation process of LFP in the presence of EDOT and ProDOT monomers, Mössbauer spectra were recorded at different depth of charge/discharge corresponding to different stages of the in battery polymerization process. Figure 4 shows the experimental and calculated  $^{57}\text{Fe}$  Mössbauer spectra of the LFP active material, both in absence and in presence of EDOT monomers at different charge/discharge potentials. Table S1 provides the hyperfine parameters obtained from the fitting of the spectra. The spectrum of pristine LFP shows a main doublet with isomer shift (IS) value of 1.22 mm/s and a quadrupolar splitting (QS) of 2.96 mm/s. These values are characteristic of  $\text{Fe}^{2+}$  ions in high spin configuration, distorted octahedral coordination, as found in LFP. Additionally, a second doublet of lower intensity with IS = 0.48 mm/s and QS = 0.79 is ascribable to  $\text{Fe}^{3+}$ . The hyperfine parameters allow assigning this signal to FeP impurities.<sup>23</sup> This signal has been previously described in the literature, and is commonly found in samples prepared under carbothermal reducing conditions.<sup>24</sup> In our sample, this impurity accounts for ca. 5-7 % of the total iron content. It has been firmly demonstrated that iron phosphide impurities for less than 10 % decrease the capacity of the  $\text{LiFePO}_4$  but enhance the utilization efficiency at high discharge rate, due to the high electron conductivity FeP.<sup>25,26</sup>

Pristine LFP was charged galvanostatically at 3.7 V. At this potential the main signal consists of a doublet with IS = 0.44 mm/s and QS = 1.51 mm/s. These values are consistent with  $\text{Fe}^{3+}$  phosphate in high spin configuration, distorted

octahedral coordination. Additionally, the contribution of the signal previously assigned to  $\text{Fe}^{2+}$  strongly decreases. These observations provide evidence of the progressive oxidation of  $\text{Fe}^{2+}$  to  $\text{Fe}^{3+}$  linked to the extraction of  $\text{Li}^+$  to form  $\text{FePO}_4$ . At this potential, ca. 16 % of the total iron remain unoxidized, corresponding to a fraction  $x = 0.84$  of lithium extracted from LFP.



**Figure 4.** Mössbauer spectra at different potentials for a-b) LFP and c-e) LFP with EDOT.

The Mössbauer analysis for the LFP sample in presence of PEDOT and charged at 3.7 V shows that the amount of unoxidized  $\text{Fe}^{2+}$  decreases to ca. 9 %.

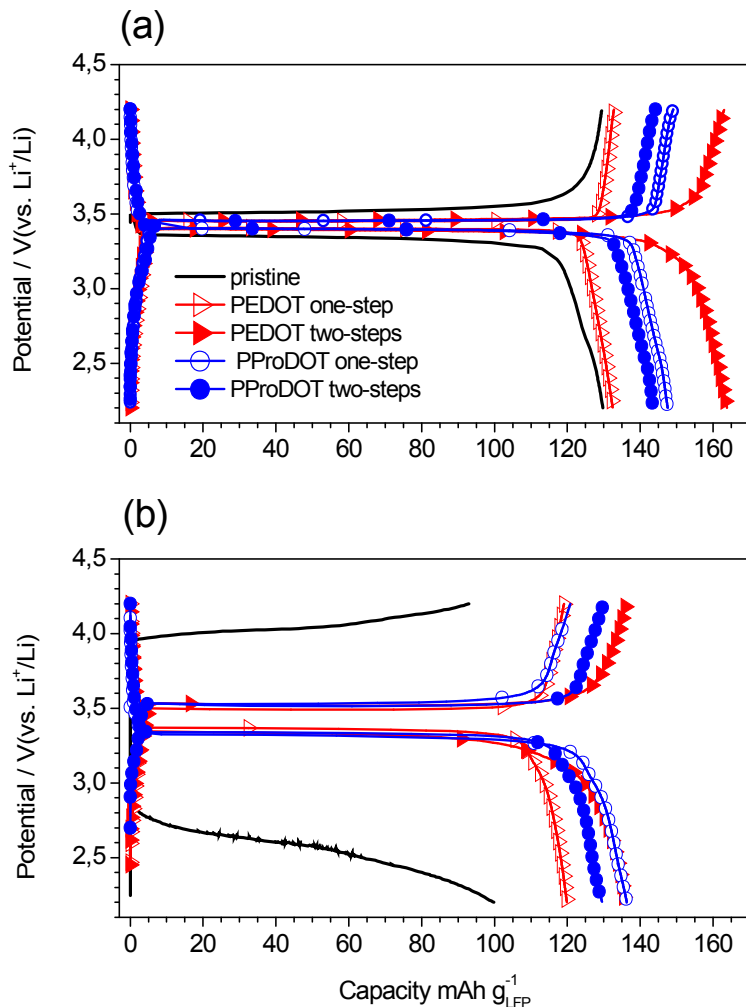
This indicates that the use of the monomer in the battery results in a higher efficiency for the lithium extraction, compared to the LFP without monomer/polymer. We speculate that the observed improvement is related to an enhanced conductivity of the materials, which is in agreement with our impedance analysis. After charging to 4.2 V, the Mössbauer spectrum of the LFP/PEDOT composite showed only one doublet ascribable to  $\text{Fe}^{3+}$ , indicating the full delithiation and transformation of  $\text{LiFePO}_4$  into  $\text{FePO}_4$ . The further discharge of the battery down to 2.2 V results in the full reduction of  $\text{Fe}^{3+}$  into  $\text{Fe}^{2+}$  and reinsertion of  $\text{Li}^+$ , as evidenced by the signal in the Mössbauer spectrum ascribable to  $\text{Fe}^{2+}$ , similar to that observed for the pristine LFP.

### 2.3. Battery cycling

The charge/discharge profiles, at C/10 and 1C rates, for LFP and the composites with PEDOT and PProDOT are shown in Figure 5. In the following discussion, the presented data correspond to the average results from 10 cycles at each rate.

The profiles for all the samples present the characteristic charge/discharge plateaus centred near 3.4 V. At C/10, pristine LFP shows the lowest performance with a discharge capacity of ca.  $130 \text{ mAh g}^{-1}$ , which represents 76 % of the theoretical value for LFP ( $Q_{\text{theo}}$  ca.  $170 \text{ mAh g}^{-1}$ ). Higher capacities were found for the cathode with PEDOT or PProDOT, confirming an improvement arising from incorporation of the polymers. For PEDOT based cathode, the capacity value obtained via one-step method was  $132 \text{ mAh g}^{-1}$ , whereas the two-step method gave an unprecedented, higher capacity of  $165 \text{ mAh g}^{-1}$  (25% increase), very close to the theoretical value. On the contrary, the inverse situation was observed for PProDOT, as the capacity value obtained via the one-step method ( $148 \text{ mAh g}^{-1}$ ) is slightly higher than the value measured for the composite obtained by the two-step method ( $144 \text{ mAh g}^{-1}$ ). This indicates that the different properties of the monomers —structure and redox potentials— influence the formation of the composites under similar preparation conditions. Although the performance at 1C rate is lower than at C/10, all the samples with PEDOT and PProDOT display

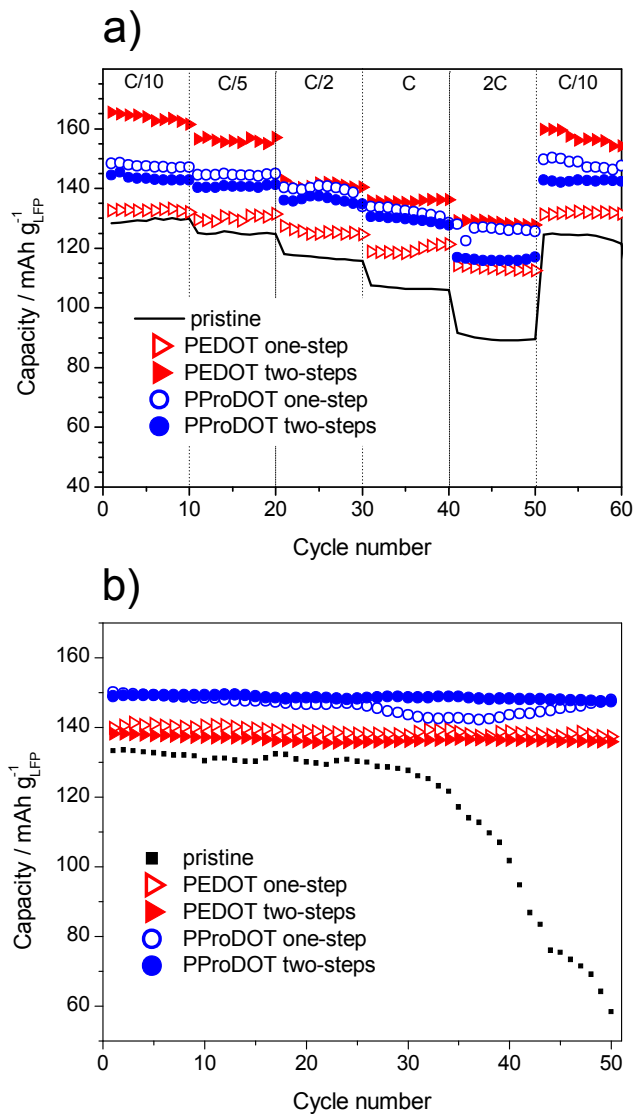
enhanced capacity and notably lower charge/discharge polarization, when compared to pristine LFP.



**Figure 5.** Charge/discharge plots for the different composites at a) C/10 rate and b) 1C rate.

Figure 6a presents the discharge capacity as a function of the cycle number at different rates for all the composites. All the samples with polymer outperform the pristine LFP in terms of capacity at increasing rates. Apart from this, the incorporation of PEDOT and PProDOT polymers allows the recovery of more than 95% of the initial capacity at C/10 after 60 cycles.

Figure 6b presents the results for the evaluation of the capacity retention at C/2 for 50 cycles. Prior to the capacity retention test, all the samples were subjected to three charge/discharge cycles at C/10 in order to form the LFP/polymer interphase and to activate LFP. It is evident that pristine LFP not only shows lower initial capacity, but also marked capacity fade of nearly 60% after 30 cycles. On the contrary, the capacity fading of our engineered LFP/polymer cathodes was less than 4% of the initial capacity at C/2 rate, giving rise to longer and more practical cycle life.

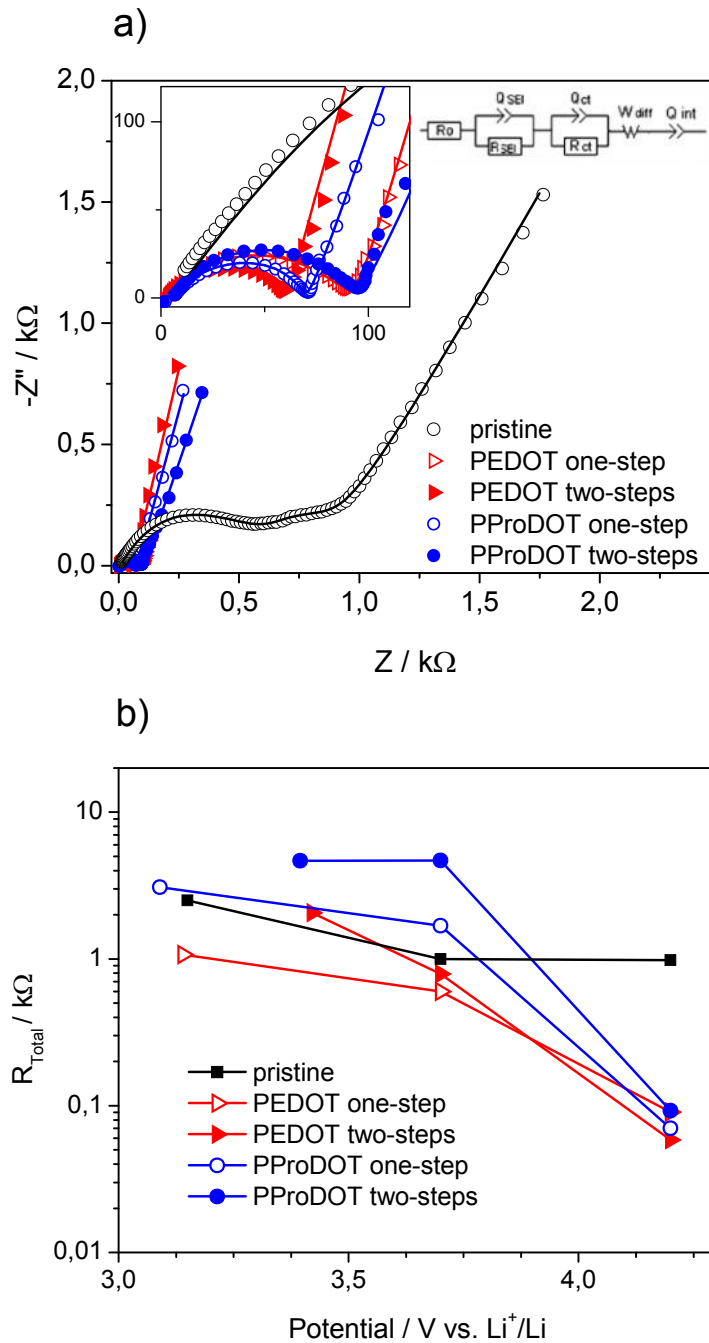


**Figure 6.** a) Cycleability for the different samples at different rates. b) Capacity retention tests at C/2 rate.

The best electrochemical results were obtained for PEDOT based sample by the two-step preparation. This behaviour has a two-fold origin. First, the conductivity of PEDOT is significantly higher as compared with ProDOT,<sup>21</sup> which is in accordance with our EIS data. On the other hand, a first activation for the polymerization process was achieved by adding the monomer to a previously charged electrode, which constitutes the basis of the two-step procedure.

#### 2.4. EIS analysis

We explored the variation of the total resistance of the cathode as a function of the charge and discharge potential by means of impedance spectroscopy. Fig. 7a compares the spectra at a particular potential of 4.2 V at which polymerization has occurred. We fitted the experimental spectra to an equivalent electrical circuit described previously for LFP-based electrodes.<sup>27</sup> The circuit consists of a high and a medium-to-low frequency semicircles, the former corresponding to the lithium ion migration resistance in the solid electrolyte interface (SEI), while the later to the charge transfer resistance. Semi-infinite diffusion and differential intercalation capacity are usually fitted by a series of constant phase elements and a Warburg element in the low frequency region. Besides, the equivalent circuit includes an inductor and a resistor to account for the cables inductance and the contact resistances in the cell (inset Figure 7a). It is worth to mention that during battery charging the total resistance progressively drops as the monomers oxidizes over the cathode (Fig. 7b). Charging the battery until 4.2 V can lead to p-doped, highly conducting forms of PEDOT and PProDOT that favour the discharge performance of LFP.



**Figure 7.** a) Impedance spectra of the composites at for the first charge/discharge cycle at 4.2 V. b) Variation of the total resistance of the cell for the first charge/discharge cycle.

$$R_{Total} = R_o + R_{SEI} + R_{ct}$$



### 3. Conclusions

A simple and cost effective method is proposed to improve the performance of LFP electrodes, by using in battery polymerization of alkylthiophenes (ProDOT, preferably EDOT) in one- or two-steps. The procedures differ in the addition of the monomer, prior or after in battery electrochemical delithiation of the phosphate cathode. The latter is particularly attractive as it allows capacities close to the theoretical limit, low polarization, low cycling losses, excellent rate performance, and improved capacity retentions after 50 cycles.  $^{57}\text{Fe}$  Mössbauer spectroscopy reveals that the oxidation of  $\text{Fe}^{2+}$  to  $\text{Fe}^{3+}$  takes place during the polymerization-doping step. The enhanced electronic conduction in the materials, particularly when using the two-step procedure is the main origin of the improved performance.

### 4. Experimental section

$\text{LiFePO}_4$  was synthesized as described elsewhere<sup>24</sup>. The battery electrolyte consisted of conventional 1 M  $\text{LiPF}_6$  dissolved in ethylenecarbonate:diethylcarbonate (EC:DEC, 1:1 volume ratio). 3,4-ethylenedioxythiophene monomer (EDOT) and 3,4-propylenedioxythiophene (ProDOT) monomer were purchased from Aldrich and used as such. Electrodes were prepared by mixing the LFP active material with carbon black and polyvinylidene fluoride (85:8:7wt.) in *N*-methyl pyrrolidone. The mixture was sonicated and the obtained ink was deposited over an aluminum disk ( $0.64 \text{ cm}^2$ ) and dried at  $80^\circ\text{C}$  under vacuum for 12 h. The average amount of LFP in the electrodes was estimated to  $5 \text{ mg cm}^{-2}$ .

LFP test batteries without monomers were assembled in two-electrode Swagelok-type cells using the cathode as working electrode, Whatman glass-paper separator soaked with electrolyte, and 1.5 mm thick lithium metal foil as reference/counter electrode. All the cells were assembled inside a glove box under controlled argon atmosphere.

Galvanostatic cycling at different C-rates ( $C = 1 \text{ Li h}^{-1} \text{ mol}^{-1}$ ) was carried out at room temperature using a Biologic VMP or MPG station. The cut-off potential for charge and discharge were set at 4.2 and 2.2 V (vs.  $\text{Li}^+/\text{Li}$ ), respectively.

The modified cathodes of LFP with conducting polymer were prepared inside test batteries by polymerization of EDOT and ProDOT monomers, using two different methods. The first method consisted in assembling the battery with a pristine LFP cathode covered by a solution of monomer (0.02 M in battery electrolyte) and applying a single charging step to the battery, in order to perform the cathode delithiation and the polymerization of the monomers in one step. The composites prepared by the single charging step are referred as “one-step”. The second in battery method consisted in charging a test battery with a pristine cathode at C/10, in order to de-lithiate LFP. Afterwards, the battery housing the delithiated cathode was opened inside the glove box and monomers were added over the cathode surface. Polymerization of the monomers was carried out by applying a second galvanostatic charge at C/10. LFP/polymer cathodes prepared by the two charging steps are referred to as “two-steps”. The amount of added monomer was 3.6 wt. % of the total electrode mass. To estimate the contribution of the resulting conductive polymer to the total discharge capacity of the composite electrodes, the electroactivity (reversible doping) of the polymer was determined by measuring the capacity associated to the peak at 3.75-3.60 V during cell discharge, and referred to the capacity of LFP. The result was less than 1 %, and thus it was not considered further.

Cyclic voltammetry of the battery electrolyte, EDOT and ProDOT monomers was performed in a three-electrode cell at room temperature at a scanning rate of 1 mV/s from 2.2 - 4.2 V. Platinum wire was used as working electrode fitted between two glass fiber separator wetted with the electrolyte and solution of monomers. Two lithium disks acted as reference and counter electrodes.

Electrochemical impedance spectra of the cathode materials were made with the help of Biologic SP-150. The measurements were carried out in three-electrode Swagelok cells with the LFP-based composite as working electrode, lithium metal counter electrode and lithium reference electrode. The applied sinus amplitude was fixed at 5 mV and the frequency was scanned from 1 MHz to 1 mHz.

$^{57}\text{Fe}$  Mössbauer spectra were recorded at room temperature with an EG&G spectrometer at constant acceleration and transmission mode. The gamma radiation source was  $^{57}\text{Co}$  (Rh matrix). The velocity scale was calibrated from the sextet lines recorded for high-purity iron foil. The spectra were fitted to Lorentzian profiles by a least

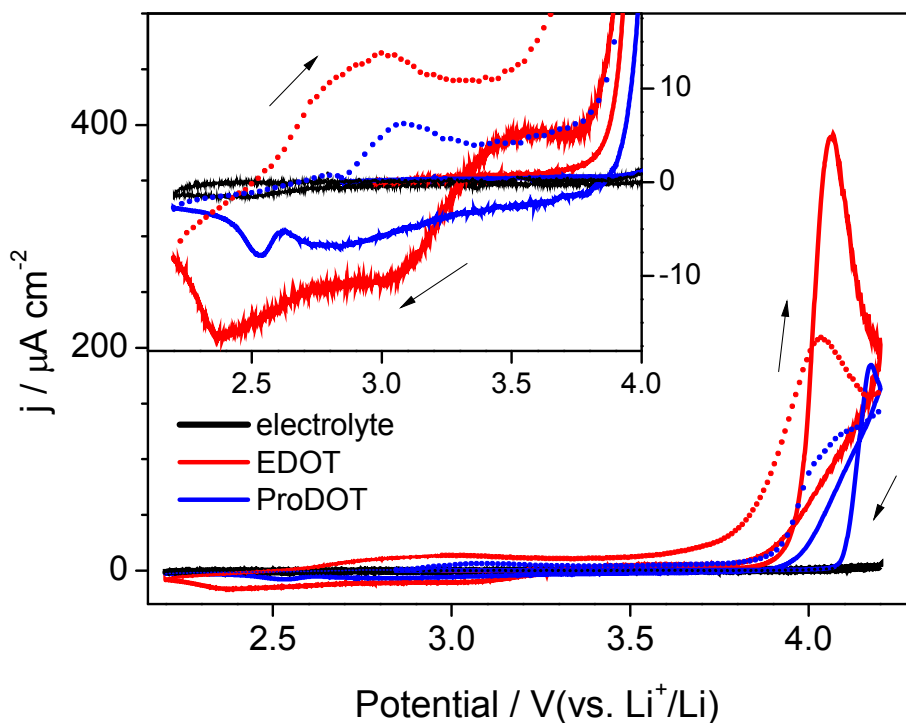
square method using WinISO software. Scanning electron microscopy (SEM) images were obtained in a JEOL JSM63000 microscope.

### Notes and references

1. M. Winter, J. O. Besenhard, M. E. Spahrand P. Novák, *Adv. Mater.* 1998, **10**, 725.
2. J. W. Fergus, *J. Power Sources* 2010, **19**, 939.
3. A.K. Padhi, K.S. Nanjundaswamy and J.B. Goodenough, *J. Electrochem. Soc.* 1997, **144** (4), 1188.
4. C. Delacourt, L. Laffont, R. Bouchet, C. Wurm, J.-B.Leriché, M. Morcrette, J.-M.Tarascon and C. Masquelier, *J. Electrochem.Soc.* 2005, **152**(5), A913.
5. F. Corce, A. D'Epifanio, J. Assounn, A. Deptula, T. Olczac, B. Scrosati, *Electrochem. Solid State Lett.* 2002, **5**, A47.
6. B. Kang and G. Ceder, *Nature* 2009, **458**, 190.
7. A. Yamada, S. Chung and K. Hinokuma, *J. Electrochem. Soc.* 2001, **148**, A224.
8. Zaghib, A. Mauger and C. M. Julien, *J. Solid State Electrochem.* 2012, **16**, 835.
9. N. Ravet, Y. Chouinard, J.F. Magnan, S. Besner, M. Gauthier, M. Armand, *J. Power Sources* 2001, **97**, 503.
10. N. Ravet, J.B. Goodenough, S. Besner, M. Simoneau, P. Hovington, M. Armand. In: Proceedings of the 196th ECS Meeting, Honolulu, October 1999.
11. (a) M. M. Doeff, J. D. Wilcox, R. Kosteci and G. Lau, *J. Power Sources* 2006, **163**, 180; (b) G. Meligrana, C. Gerbaldi, A. Tuel, S. Bodoardo, N. Penazzi, *J. Power Sources* 2006, **160**, 516; (c) S. Bodoardo, C. Gerbaldi, G. Meligrana, A. Tuel, S. Enzo, N. Penazzi, *Ionics* 2009, **15**, 19.
12. Y. -H. Chen, C.-W. Wang, X. Zhang and A. M. Sastry, *J. Power Sources* 2010, **195**, 2851.
13. A. V. Murugan, T. Muraliganth and A. Manthiram, *Electrochem.Comm.* 2008, **10**, 903.
14. G. Inzelt, *Chem. Biochem. Eng.* 2007, **21**(1), 1; b) J.-H.Yum, E. Baranoff, F. Kessler, T. Moehl, S. Ahmad, T. Bessho, A. Marchioro, E.Ghadiri, J.-E. Moser, C. Yi, M. K. Nazeeruddin, M. Grätzel, *Nature Commun.* 2012, **3**, 631; c) S. Ahmad, J.-H. Yum, Z. Xianxi, M. Grätzel, H.-J.Butt and M. K. Nazeeruddin, *J. Mater. Chem.*, 2010, **20**, 1654; d) S. Ahmad, J.-H. Yum, H.-J.Butt, M. K. Nazeeruddin and M. Grätzel, *Chem. Phys Chem.* 2010, **11**, 2814.
15. M. G. Han and S. P. Armes, *Langmuir* 2003, **19**, 4523.
16. H. -C. Dinh, I. -H. Yeo, W. I. Cho and S. Mho, *Trans. J. Electrochem. Soc.* 2010, **28**, 167.
17. J. Y. Shi, C-W. Yi and K. Kim, *Bull. Korean Chem. Soc.* 2010, 31(9), 2698.
18. D. Lepage, C. Michot, G. Liang, M. Gauthier and S. B. Schougaard, *Angew. Chem. Int. Ed.* 2011, **50**, 6884.
19. N. D. Trinh, M. Saulnier, D. Lepage and S.B. Schougaard, *J. Power Sources* 2013, **221**, 284.
20. I. Boyano, J. A. Blazquez, I. Meatza, M. Bengoechea, O. Miguel, H. Grande, Y. Huang and J. B. Goodenough, *J. Power Sources* 2010, **195**, 5351.

21. L. Groenendaal, G. Zotti, P.-H. Aubert, S. M. Waybright, and J. R. Reynolds, *Adv. Mater.* 2003, **15**, 855.
22. A.R. Hillman, S.J. Daisley, and S. Bruckenstein, *Electrochim. Acta* 2008, **53**, 3763.
23. Y. Lin, H. Pan, M. Gao, and Y. Liu, *J. Electrochem. Soc.* 2007, **154**, A1124.
24. B. León, C. Pérez Vicente, J. L. Tirado, Ph. Biensan and C. Tessier, *J. Electrochem. Soc.* 2008, **155**, A211.
25. P. S. Herle, B. Ellis, N. Coombs and L. F. Nazar, *Nature Materials* 2004, **3**, 147.
26. Y. Lin, M. X. Gao, D. Zhu, Y. F. Liu and H. G. Pan, *J. Power Sources*, 2008, **184**, 444.
27. J. P. Schmidt, T. C. Chrobak, M. Ender, D. Klotz, E. I-Tiffée, *J. Power Sources* 2011, **196**, 5342.

### Electronic Supplementary Information (ESI)



**Figure S1.** Cyclic voltammogram for the blank electrolyte and the EDOT and ProDOT in electrolyte solution (20 mM). The second forward scan is depicted with dotted lines.

**Table S1.** Results from the fitting of the experimental Mössbauer spectra showed in Figure 4

Sample	Monomer	Assignment	IS	QS	LW	Contribution
			[mm/s]	[mm/s]	[mm/s]	[%]
Pristine LFP	No	Fe <sup>2+</sup>	1.220(1)	2.96(1)	0.275(2)	94(1)
		FeP	0.47(2)	0.74(2)	0.31(3)	6(1)
Charged at 3.7 V	No	Fe <sup>2+</sup>	1.30(2)	2.81(3)	0.33(4)	16(4)
		Fe <sup>3+</sup>	0.442(2)	1.514(6)	0.264(5)	84(4)
Charged at 3.7 V	EDOT	Fe <sup>2+</sup>	1.39(3)	2.56(4)	0.32(7)	9(6)
		Fe <sup>3+</sup>	0.432(2)	1.518(6)	0.268(5)	91(6)
Charged at 4.2 V	EDOT	Fe <sup>3+</sup>	0.435(3)	1.542(5)	0.337(9)	100
Discharged at 2.2 V	EDOT	Fe <sup>2+</sup>	1.220(2)	2.96(1)	0.266(6)	100

*\*IS = Isomer Shift, QS = Quadrupole Splitting and LW = Line Width.*





## Chapter 5

### Judicious design of lithium iron phosphate electrodes using poly(3,4-ethylenedioxythiophene) for high performance batteries

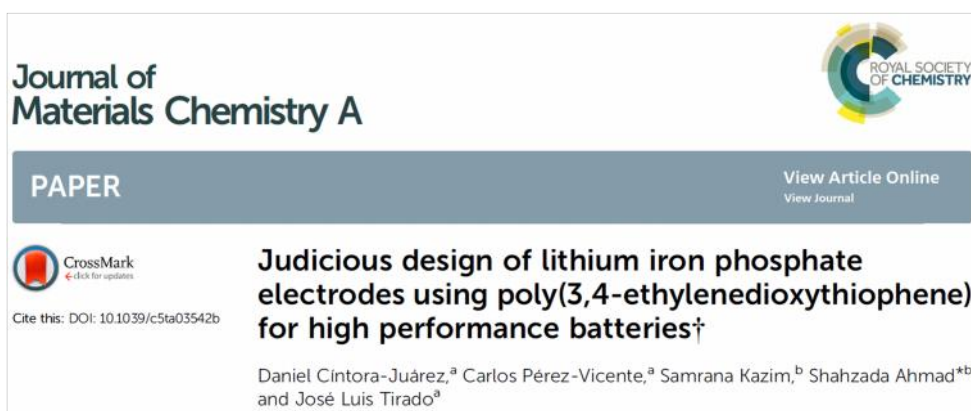
D. Cíntora-Juárez<sup>a</sup>, C. Pérez-Vicente<sup>a</sup>, S. Kazim<sup>b</sup>, S. Ahmad<sup>b</sup> and J. L. Tirado<sup>a</sup>,  
*J. Mater. Chem. A*, 3 (2015), 14254–14262.

<sup>a</sup>Laboratorio de Química Inorgánica, Campus de Rabanales, Universidad de Córdoba, 14071, Spain

<sup>b</sup>Abengoa Research, C/ Energía Solar nº 1, Campus Palmas Altas, 41014, Spain

Received: 14th May 2015


Accepted: 29th May 2015



**Journal of Materials Chemistry A**

**PAPER**


[View Article Online](#)  
[View Journal](#)

 CrossMark  
Click for updates

Cite this: DOI: 10.1039/c5ta03542b

**Judicious design of lithium iron phosphate electrodes using poly(3,4-ethylenedioxythiophene) for high performance batteries†**

Daniel Cíntora-Juárez,<sup>a</sup> Carlos Pérez-Vicente,<sup>a</sup> Samrana Kazim,<sup>b</sup> Shahzada Ahmad<sup>\*b</sup> and José Luis Tirado<sup>a</sup>







## Abstract

LiFePO<sub>4</sub> electrodes were built in different architectures using a poly(3,4-ethylenedioxythiophene)-polystyrene sulfonate (PEDOT:PSS) mixed conductor as an additive. Conductivity enhancement of PEDOT:PSS was achieved by the addition of ethylene glycol and dimethyl sulfoxide solvents. The amounts of conducting polymer and solvent additives strongly influence the discharge capacity and potential of LiFePO<sub>4</sub> electrodes at high rates. The initial impedance and the direct current resistance were correlated with the discharge performance at high rates. The optimized amount of PEDOT:PSS added within the bulk resulted in a lower value of impedance, lower load resistance and higher capacity as compared to the standard preparation. Furthermore <sup>57</sup>Fe Mössbauer spectroscopy and X-ray photoelectron spectroscopy were employed to probe the bulk transformation of the LiFePO<sub>4</sub> active material and the surface changes of the composite electrodes with the conducting polymer upon lithiation. The electrode with PEDOT:PSS coated on the aluminium current collector and doped with ethylene glycol showed highly competitive performance (132 mAh g<sup>-1</sup> at 5C and 145 mAh g<sup>-1</sup> at 2C for 50 cycles).

## 1. Introduction

Lithium ion batteries are the current choice for powering consumer electronic devices, and are considered for use in electric vehicles and stationary back-up for renewable energy sources. Electric vehicles and power gadgets require batteries able to sustain high charge/discharge currents safely and provide high energy density and long cycle life. In the present Li-ion batteries, the positive electrode (cathode) imposes performance and cost requirements that limit the implementation of a sustainable market for electric cars. The pioneering work of Padhi *et al.*<sup>1</sup> on lithium transition metal phosphates (LiMPO<sub>4</sub>, M: Fe, Mn, Co, Ni) as positive electrode materials set the cornerstone for the development and commercialization of lithium iron phosphate (LiFePO<sub>4</sub>), a new-generation material that offers safety and performance advantages over typical LiCoO<sub>2</sub>. Besides, LiFePO<sub>4</sub> (LFP) is considered as environmentally friendly and can be produced at competitive cost by different synthetic routes.<sup>2,3</sup> In spite of their outstanding features, the low intrinsic conductivity of lithium transition metal phosphates, ranging from 10<sup>-7</sup> to 10<sup>-11</sup> S cm<sup>-1</sup> for LFP,<sup>4,5</sup> was considered as the limiting factor to achieve fast lithiation/delithiation in these materials. However, it was later

demonstrated that structural and compositional modifications of the surface and the bulk of  $\text{LiFePO}_4$  can turn it into a material with high rate capability. For instance, the ionic diffusivity of LFP has been improved by reducing the diffusion paths along the less impeded [010] direction in nano-particles<sup>6</sup> or by coating the surface of LFP with glassy lithium pyrophosphate.<sup>7</sup>

For the enhancement of electronic conductivity of LFP, the currently adopted strategy consists of carbon-coating over the active material particles through ball milling with inorganic carbon or by calcination of organic carbonaceous compounds.<sup>8,9</sup> In order to ensure the electronic connection between particles and to the current collector, composite electrodes are formed using carbon additives in combination with polymeric binders like polyvinylidene fluoride (PVDF). Conducting polymers are known for their excellent electronic properties and mechanical stability. These polymers can be utilized for the design of composite electrodes in order to increase the conductivity without penalizing the electrochemical performance.<sup>10,11</sup> In particular for  $\text{LiFePO}_4$ , composites with polyaniline,<sup>12,13</sup> polypyrrole<sup>14,15</sup> and polythiophene<sup>16,17</sup> derivatives have been prepared by blending LFP with chemically synthesized polymers, by chemical or electrochemical polymerization in the presence of the phosphate.<sup>18–20</sup>

Recently, we reported the improved performance of LFP-conducting polymer composites obtained directly over LFP-based electrodes by electrodeposition in an acetonitrile medium<sup>21</sup> and on the battery electrode by polymerization of alkylendioxythiophene-based monomers under battery operation conditions.<sup>22</sup> In our present approach to further improve the performance of LFP-based electrodes, mixed conductor poly(3,4-ethylenedioxythiophene)-poly(styrene sulfonate) (PEDOT:PSS) has been used as a conducting additive to develop an ionic/electronic conducting network for the interconnection of the LFP particles. PEDOT:PSS is a commercial product and provides conductivity due to the coexistence of the PEDOT electron conducting phase complexed with polystyrene sulfonate (PSS), where the sulfonate group is able to solvate  $\text{Li}^+$  ions.<sup>23</sup> Besides, the conductivity of PEDOT:PSS can be further increased by 2–3 orders of magnitude by the use of additives (so-called secondary doping) with oxygenated compounds like ethylene glycol or dimethyl sulfoxide.<sup>24,25</sup> In order to discern the main contribution of PEDOT:PSS to the conductivity of the LFP-based composite electrodes, we investigated the effects of the conducting polymer when it is coated over the aluminium current collector and/or dispersed within the bulk of the electrode.

## 2. Experimental section

LiFePO<sub>4</sub> (LFP) was synthesized as described elsewhere.<sup>26</sup> Standard LFP electrodes (standard) were prepared by dispersing the active material with carbon black (CB) and polyvinylidene fluoride (PVDF) (85 : 8 : 7 by weight) in N-methyl pyrrolidone. The obtained ink was deposited over an aluminium current collector (0.64 cm<sup>2</sup>) and dried at 80° C under vacuum for 12 h. The average load of LFP in the electrodes was estimated to be 5–6mg cm<sup>-2</sup>. Commercial PEDOT:PSS polymer aqueous dispersion 1.1% w/w (Clevios PH1000, Heraeus) was filtered using Whatman 0.45 mm pore size filters. The conducting polymer was incorporated into the LFP-based electrode in three different ways: (i) over the current collector, (ii) in the bulk, and (iii) both over the current collector and in the bulk. The PEDOT:PSS coating over the current collector was achieved by drop-casting the polymer dispersion (30 μL cm<sup>-2</sup>) and allowing it to dry at 100° C for 24 h under vacuum. Afterwards, the LFP based ink was deposited over PEDOT:PSS-coated aluminium and the electrode was prepared as described above for the standard sample. The second preparation consisted in blending LFP with CB, PVDF and PEDOT:PSS (79:7:7:7 or 84:8:7:1 by weight) to form the electrode in a similar fashion to that of the standard LFP-based electrodes (see above). Finally, both methods were combined in order to form an electrode containing PEDOT:PSS both over the Al current collector and in the bulk. The different samples will be referred to as: collector, bulk, and coll-bulk, respectively, considering where the polymer is present in the electrode. Finally, all the electrodes were pressed at 1.5 ton cm<sup>-2</sup>.

To further enhance the PEDOT:PSS conductivity either 5% v/v ethylene glycol (EG) or dimethyl sulfoxide (DMSO) was used as an additive for the polymer dispersion. Test batteries were assembled in two or three-electrode Swagelok-type cells using the above mentioned LFP-based electrodes, a Whatman glass-paper separator soaked with the electrolyte (1 M LiPF<sub>6</sub> in ethylene carbonate:diethyl carbonate, 1:1 weight ratio) and lithium metal foil as the reference/counter electrode. All the cells were assembled inside a glovebox under a controlled argon atmosphere (H<sub>2</sub>O, O<sub>2</sub> < 1 ppm). Galvanostatic cycling at different C-rates (1 C = 1Li h<sup>-1</sup> mol<sup>-1</sup>) was carried out at room temperature using a Biologic VMP or MPG station. The cut-off potential for charge and discharge was set at 4.2 and 2.2 V (vs. Li<sup>+</sup>/Li), respectively. Electrochemical impedance spectra were recorded in a Biologic SP-150 equipment using a three-electrode Swagelok-type

cell with the LFP-based composite as the working electrode, lithium counter electrode and lithium reference electrode. The applied sinus amplitude was fixed at 10 mV and the frequency was scanned from 1 MHz to 10 mHz. X-ray photoelectron spectroscopy (XPS) studies were performed with a Phoibos 150MCD (SPECS) instrument under vacuum ( $4 \times 10^{-9}$  mbar) at room temperature with an Mg K source. Prior to the analysis, all the samples were maintained overnight inside the chamber under constant vacuum. The samples taken from test batteries were rinsed with propylene carbonate solvent, dried and then carefully transferred into the instrument's chamber, minimizing contact with the external atmosphere. Fitting of the experimental spectra was performed with CasaXPS software, applying Gaussian-Lorentzian symmetric or asymmetric line shapes, and considering the software's library of relative sensitivity factors for the quantitative analysis. The energy scale was referenced to the C 1s level (285 eV) from adventitious carbon.

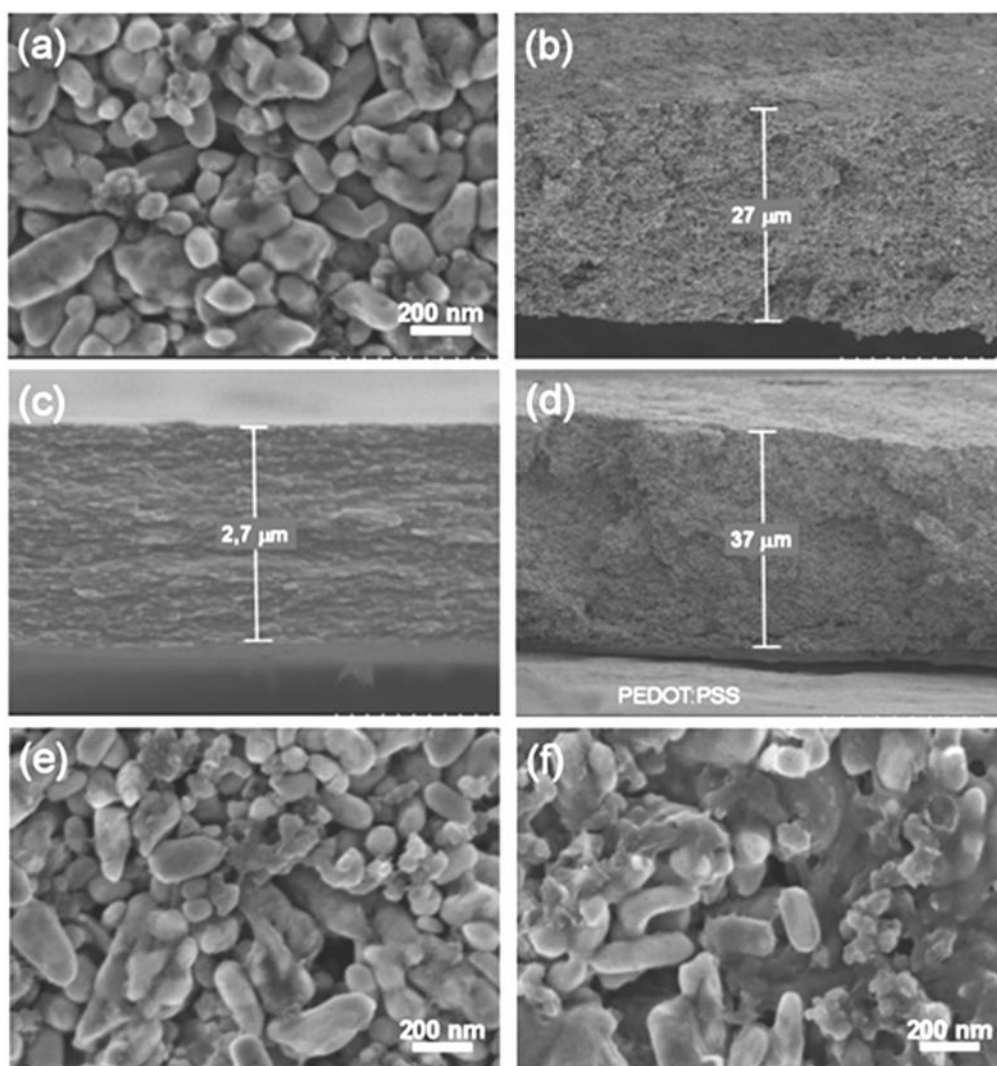
$^{57}\text{Fe}$  Mössbauer spectra were recorded at room temperature using an EG&G spectrometer at constant transmission and acceleration mode. The gamma radiation source was  $^{57}\text{Co}$  (Rh matrix). The sextet lines recorded for high-purity iron foil were used to calibrate the velocity scale. The fitting of the spectra to Lorentzian profiles was carried out by a least squares method using WinISO software. The microstructure was imaged with the use of a Hitachi S5200 field-emission scanning electron microscope (FE-SEM) operating at 5.0 keV.

### 3. Results and discussion

Fig. 1 presents SEM images of the LFP-based standard electrode and different electrode preparations incorporating PEDOT:PSS. The standard electrode was composed of varying shapes of LFP particles (ca. 80–300 nm), homogeneously mixed with CB and PVDF (Fig. 1a). The cross-section view (Fig. 1b) shows that the porosity was preserved though the sample was pressed to improve the contact to the current collector and between particles.

Fig. 1c shows a cross-sectional profile of the PEDOT:PSS deposit used for the collector sample. The PEDOT:PSS film (ca. 3  $\mu\text{m}$ ) forms into a compact lamellar structure rich in the PSS phase as previously described.<sup>27</sup> Fig. 1d displays a close view of the composite formed by the collector method, where the PEDOT:PSS film over the

current collector provides a compatible surface for the active material particles. The texture of the bulk 1% and bulk 7% electrodes can be observed in Fig. 1e and f. The primary particles in the bulk appear embedded in a continuous PEDOT:PSS network, the polymer acted as a glue that provides mechanical and conductive interconnection between LFP active particles. The texture and cross-section profiles of the coll-bulk samples were very similar to the features of the bulk electrodes.



*Fig. 1. SEM images. (a and b) Particles and cross-section of the LFP standard electrode, (c) PEDOT:PSS film formed over the aluminium current collector, (d) collector sample, (e) bulk 1% sample and (f) bulk 7% sample.*

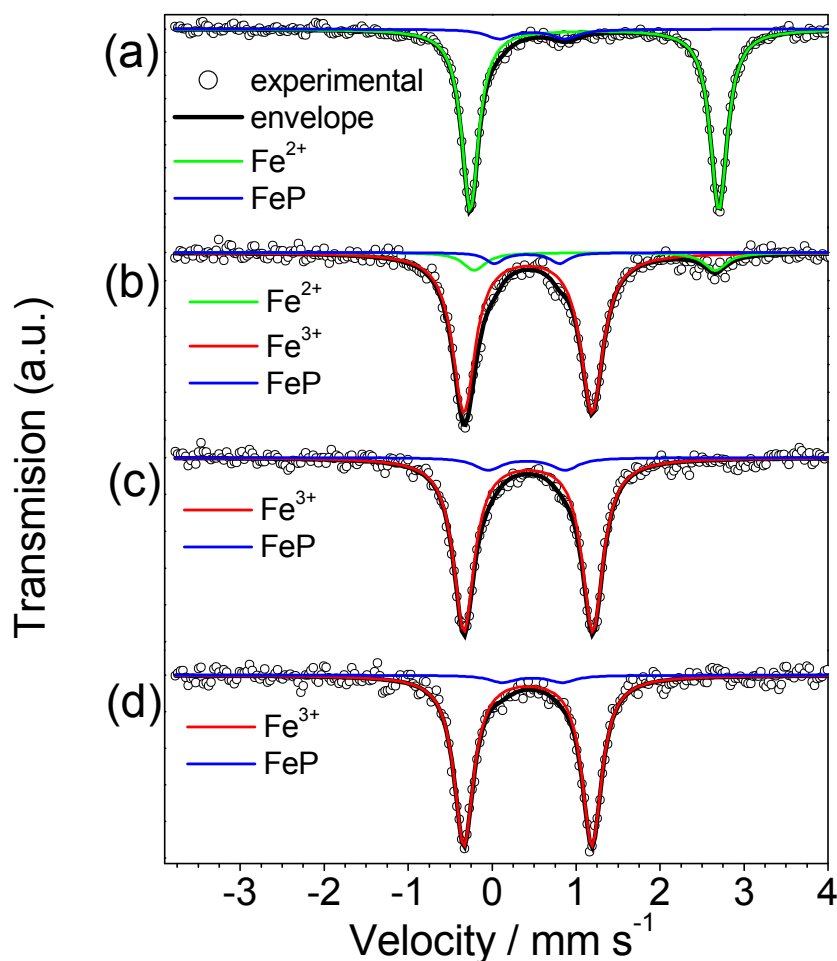


Fig. 2. Mössbauer spectra of (a) pristine LFP-based electrode, and charged electrodes: (b) LFP-based, (c) bulk 1% and (d) EG-bulk 1%.

Mössbauer spectroscopy was used to investigate the oxidation state of iron in the pristine LFP-based electrode (Fig. 2a). The Mössbauer spectrum of this sample features an intense doublet with characteristic hyperfine parameters typical of high spin  $\text{Fe}^{2+}$  ions in distorted octahedral coordination ( $IS = 1.22 \text{ mm s}^{-1}$  and  $QS = 2.96 \text{ mm s}^{-1}$ ) as previously reported.<sup>26,28,29</sup> The fitting was improved by considering the contribution of an additional, less intense doublet ( $IS = 0.48 \text{ mm s}^{-1}$  and  $QS = 0.79 \text{ mm s}^{-1}$ ) ascribable to FeP, which was formed under carbothermal, reducing synthesis conditions<sup>26,30</sup> and constitutes  $\sim 7\%$  of the total iron content in the pristine electrode.

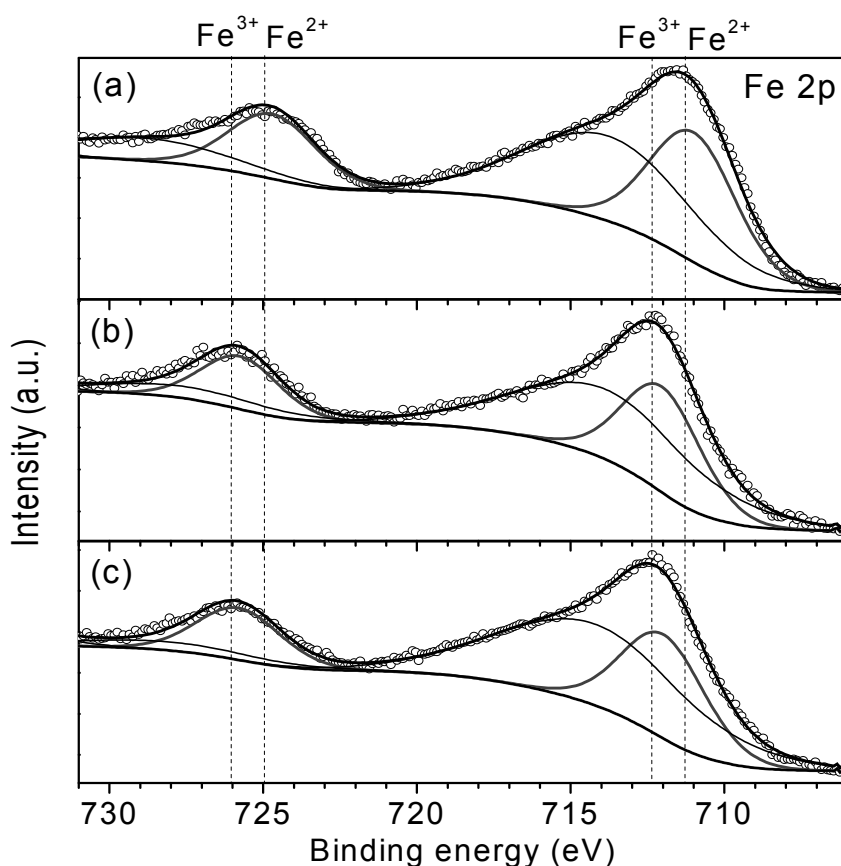


Fig. 3. Fe(2p) XPS spectra of (a) pristine LFP electrode and two charged electrodes with the conducting polymer: (b) bulk 1% and (c) EG-bulk 1%.

In order to complement the sample analysis, XPS was used to characterize the pristine state of the surface of the standard electrode. Fig. 3a presents the XPS signal of the Fe(2p) core levels. By comparing the peak position with the usual location of Fe<sup>3+</sup> and Fe<sup>2+</sup> marked with dashed lines in Fig. 3, it can be concluded that in the pristine sample iron exists as Fe<sup>2+</sup> with 2p<sub>3/2</sub> and 2p<sub>1/2</sub> split levels at binding energy values of ca. 711 and ca. 725 eV, respectively, in accordance with previous reports for LiFePO<sub>4</sub>.<sup>31,32</sup> The broad signals at ca. 714 and ca. 728 eV correspond to satellite signals. The characteristic signals of FeP were un-resolved, which suggests a lower proportion of this impurity on the surface of the electrode. Fig. 4a presents the initial charge at C/10 and the discharge profiles at increasing rates of the LFP standard sample. The characteristic charge/discharge plateaus are centred near the equilibrium potential for



the redox pair  $\text{Fe}^{3+}/\text{Fe}^{2+}$  at 3.43 V, with a charge/discharge polarization of ca. 69 mV. The initial charge capacity of ca. 149  $\text{mAh g}^{-1}$  corresponds to 0.88 mole of lithium extracted from  $\text{LiFePO}_4$ . This value indicates limited active material utilization as confirmed by Mössbauer spectroscopy of the charged sample (Fig. 2b), which shows a considerable contribution of ca. 10% of the total iron assigned to  $\text{Fe}^{2+}$ , according to the hyperfine parameters presented in Table S1.† The reduced charge efficiency is evident upon lithium reinsertion as the discharge capacity of 144  $\text{mAh g}^{-1}$  corresponds to 85% of the theoretical capacity for  $\text{LiFePO}_4$  ( $Q_{\text{theo.}}: 170 \text{ mA h g}^{-1}$ ).

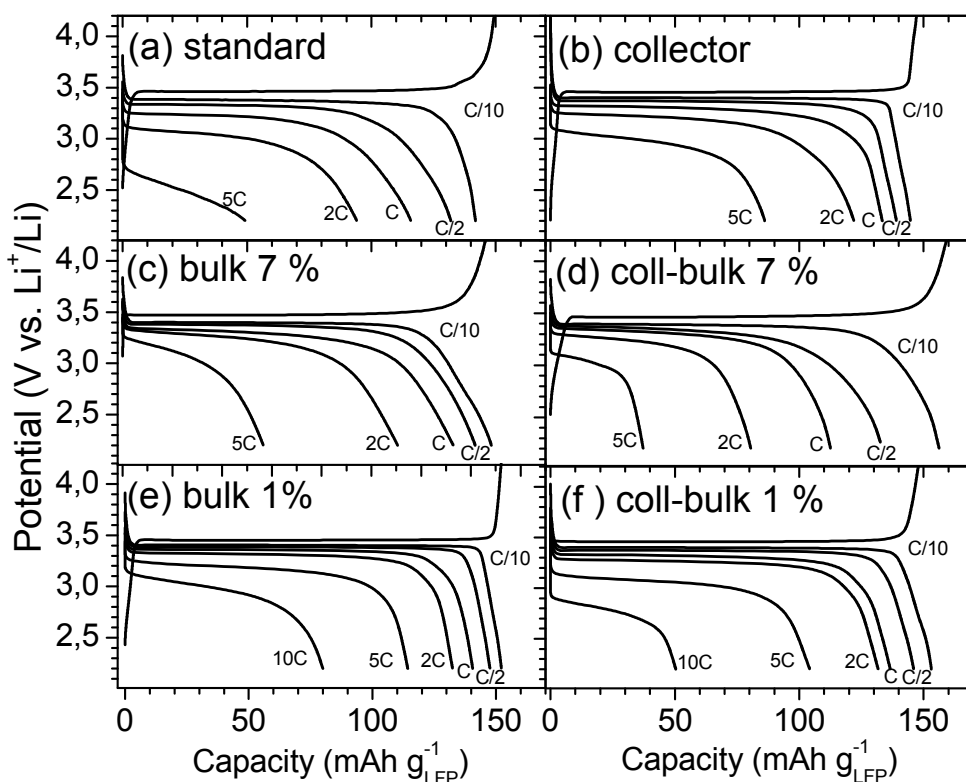


Fig. 4. Initial discharge profiles at increasing rates of the different LFP-based composite electrodes.

Although iron phosphide is known to improve the electronic conductivity of  $\text{LiFePO}_4$  particles,<sup>29,33</sup> its presence is detrimental to the overall electrode capacity. The performance of the LFP electrode at higher currents shows that the capacity decreases

while the polarization increases due to transport limitations, as not all the particles can sustain high rates.<sup>34</sup> Thus, at 5C, the discharge capacity drastically decreases to 50 mAh g<sup>-1</sup> and the discharge potential at half of the total delivered capacity ( $E_{Q_{1/2}}$ ) reaches 2.49 V. This value translates into a poor energy and power density. Aiming to improve the active material utilization, a PEDOT:PSS film was formed over aluminium to act as a conductive interface to promote the electrical contact of LFP particles to the current collector. The initial capacity (145 mAh g<sup>-1</sup>) of this collector sample (Fig. 4b) is the same as that of the standard preparation. However, at 5C, the higher capacity (86 mAh g<sup>-1</sup>) and the higher discharge potential ( $E_{Q_{1/2}}$ : 2.97 V at 5C) indicate an improvement in the energy and power density. The effect of PEDOT:PSS present within the bulk of the electrode was also tested. Fig. 4c shows that for the *bulk 7%* sample, PEDOT:PSS shows a beneficial impact on the discharge voltage ( $E_{Q_{1/2}}$ : 3.05 V at 5C) with no capacity improvement at low and high rates ( $Q_{C/10}$ : 148 mAh g<sup>-1</sup>,  $Q_{5C}$ : 56 mAh g<sup>-1</sup>).

In order to take advantage of the features found for the collector (high capacity) and the bulk (high voltage) preparations, these architectures were simultaneously applied to form a single composite electrode with PEDOT:PSS coated over the aluminium current collector and also blended in the bulk (7% w) of the electrode. The resulting preparation was named *coll-bulk 7%*. For the initial discharge, this preparation (Fig. 4d) provided ca. 92% of  $Q_{\text{theo}}$ . However, at 5 C, the discharge capacity faded to 32 mAh g<sup>-1</sup>, indicating the inefficient use of the active material. Despite the inferior rate capability of this *coll-bulk 7%* sample, its discharge potential ( $E_{Q_{1/2}}$ : 3.01 V) holds near the level found for the collector sample, although its power density is expected to drop as a consequence of the lower proportion of the active material.

As a way to increase the gravimetric energy and power densities of the LFP-based electrodes, the amount of PEDOT:PSS additive in the bulk was reduced to 1% w. In this manner, the *bulk 1%* preparation provided ca. 90% of the theoretical capacity at C/10 in discharge, a value considerably higher than that observed for the standard LFP sample (83%). The improved performance of the *bulk 1%* sample was confirmed at higher rates as the discharge capacity at 5C reaches 114 mAh g<sup>-1</sup> (Fig. 4e) and it was possible to discharge ca. 50% of the theoretical capacity in 6 minutes (10C rate) at  $E_{Q_{1/2}} \sim 2.96$  V. These observations reflect a higher efficiency for the lithium extraction/re-insertion linked to the Fe<sup>2+</sup> to Fe<sup>3+</sup> oxidation when a small amount of PEDOT:PSS is present in

the bulk of the electrode. This was further supported by Mössbauer spectroscopy and XPS results of the charged *bulk 1%* sample. The Mössbauer spectrum (Fig. 2c) shows a symmetric doublet assigned to  $\text{Fe}^{3+}$ , while no  $\text{Fe}^{2+}$  doublet could be resolved. As expected, most of the iron in the charged electrode is ascribable to  $\text{Fe}^{3+}$  and the contribution from the FeP component is similar to that of the pristine LFP electrode (Table S1†). Fig. 3b presents the Fe(2p) XPS spectrum of the charged *bulk 1%* sample. The position of the Fe(2p<sub>3/2</sub>) and Fe(2p<sub>1/2</sub>) bands appear ca. 1.1 eV shifted to a higher binding energy compared to the pristine LFP-based electrode (Table S2†). This shift has been described previously and it is attributed to the  $\text{Fe}^{2+}$  to  $\text{Fe}^{3+}$  oxidation.<sup>31,32</sup>

The characteristic signals of FeP were not resolved neither in the Fe(2p) region nor in the P(2p) region (not shown). Regarding the electrochemical performance of the *coll-bulk 1%* sample (Fig. 4f), it also showed improvement in terms of capacity at 5C (104 mAh g<sup>-1</sup>) with respect to its *col-bulk 7%* analogue and to the standard electrode, although its performance at 10C is inferior to that achieved by the *bulk 1%* preparation. Therefore, 1% w of the conducting polymer in the bulk is pointed out as the optimum strategy to achieve high rate performance with undoped PEDOT:PSS.

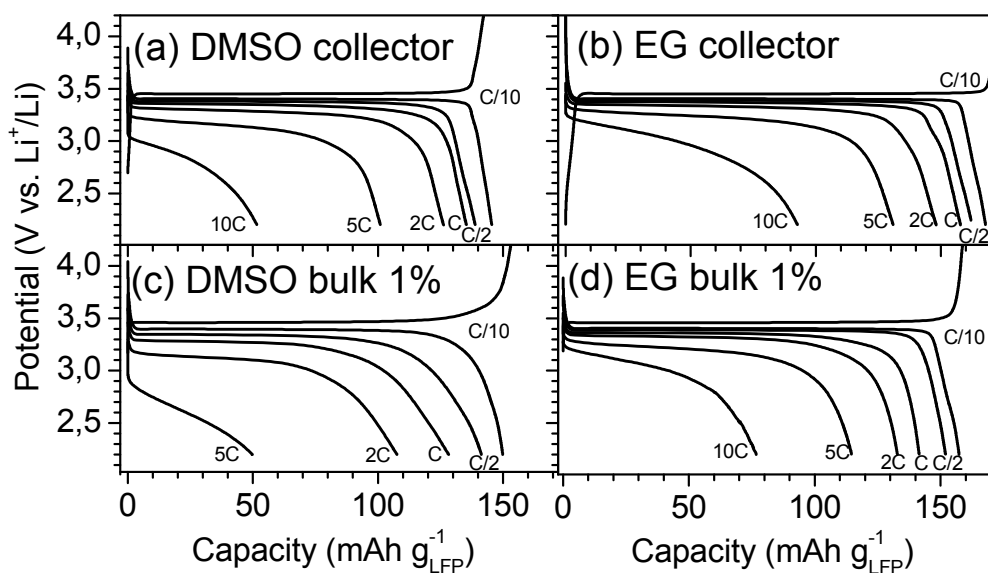


Fig. 5. Initial discharge profiles at increasing rates of the different LFP-based composite electrodes with doped PEDOT:PSS.

Fig. 5 shows the discharge profiles of the LFP-based composites with PEDOT:PSS treated with EG and DMSO conductivity enhancement agents, and tested for the collector and *bulk* 1% preparations. Both additives act as an agent to increase the conductivity of PEDOT:PSS by 2–3 orders of magnitude, reaching values as high as  $1000 \text{ S cm}^{-1}$  for 5% v/v DMSO.<sup>35</sup> Thus, for the collector preparation with DMSO (Fig. 3a), we found substantial improvement for both the capacity ( $101 \text{ mAh g}^{-1}$ ) and the discharge potential ( $E_{Q1/2}$ : 3.1 V) at 5C, as compared to its undoped analogue (Fig. 4b). Ethylene glycol boosted the performance of the collector preparation even further as it discharges higher capacity at 5 C ( $132 \text{ mAh g}^{-1}$ ) and also at 10C ( $93 \text{ mAh g}^{-1}$ ) as shown in Fig. 5b. For the *bulk* 1% preparations, doping with DMSO was ineffective as its discharge characteristics are very similar to those of the standard sample (see Fig. 4a).

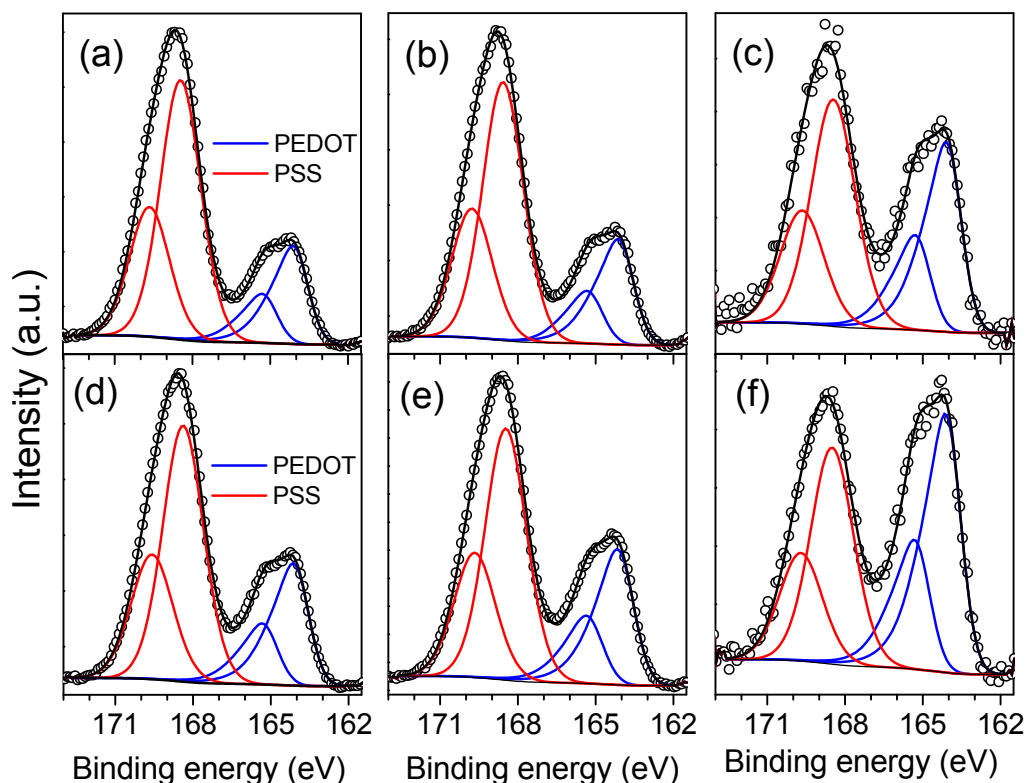


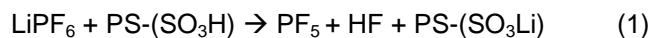
Fig. 6. XPS plots of the S(2p) core level of undoped (a–c) and EG-doped samples (d–f). (a) PEDOT:PSS, (b) PEDOT:PSS @ C/10, (c) bulk 1% @ C/10. (d) EG-PEDOT:PSS, (e) EG-PEDOT:PSS @ C/10, and (f) EG-bulk 1% @ C/10.

Compared to the undoped *bulk 1%* preparation (Fig. 4e), the EG-doped sample showed similar capacity values at high rates, with a substantial improvement in the discharge potential at 10C ( $E_{Q1/2}$ : 3.03 V). Similarly for the undoped *bulk 1%* sample, the Mössbauer spectroscopy and XPS results of the *EG-bulk 1%* sample (Fig. 2d and 3c, respectively) showed no signals ascribable to  $Fe^{2+}$ , indicating that the oxidation of  $Fe^{2+}$  to  $Fe^{3+}$  was complete. As observed for the standard and the *bulk 1%* preparations, FeP was detected using Mössbauer spectroscopy of the charged EG-*bulk 1%* sample (Table S1†). From the results presented above, it is evident that the incorporation of undoped and doped PEDOT:PSS has a beneficial impact on the discharge performance of the composite electrodes at high rates.

Several studies have explained the mechanism of the conductivity enhancement of PEDOT:PSS with secondary dopants in terms of the segregation of the insulating, excess PSS phase.<sup>36,37</sup> Ethylene glycol (EG) and dimethylsulfoxide (DMSO) are among the most common secondary dopants. Also, the modifications of the conformation, the size and morphology of PEDOT:PSS, have been pointed out as reasons for the conductivity improvement of PEDOT:PSS, as supported by atomic force microscopy and XPS.<sup>37–39</sup> In particular, the segregation of the PSS phase has been correlated to the decrease of the PSS/PEDOT ratio, which can be estimated from the intensity ratio of the well resolved S(2p) XPS signals attributed to PSS and PEDOT sulphur atoms of different bonding environments.<sup>39</sup> We applied this approach to estimate the PSS/PEDOT ratios of undoped and EG-doped polymer deposits over the current collector and for the *bulk 1%* preparations in pristine and charged states.

Fig. 6 presents the XPS plots of the S(2p) levels of the different samples. The S(2p) spectra of all the samples with PEDOT:PSS display two peaks, irrespective of the charge state or the presence of the EG secondary dopant. The lower binding energy peak is attributed to the sulphur atoms in PEDOT. Due to the presence of electronegative oxygen atoms in the sulfonate fragments, the characteristic peak of PSS appears at a higher binding energy. The two peaks were deconvoluted into doublets according to the S(2p<sub>3/2</sub>) and S(2p<sub>1/2</sub>) spin-orbit splitting. An asymmetric peak shape was considered for the PEDOT doublet in order to account for the positive charge delocalization over adjacent PEDOT rings.<sup>37</sup> The signals of neutral and ionic polystyrene (PS) sulfonate (PS-SO<sub>3</sub>H and PS-SO<sub>3</sub><sup>-</sup>) are commonly separated by an

energy of ca. 0.4 eV,<sup>39</sup> resulting in a high overlapping that leads to accuracy problems in the signal resolution. Taking this disadvantage under consideration, we used only one component for the refinement of these spectra. The results of the fitting and the quantitative analysis are listed in Table S3.† Fig. 6a–c show the S(2p) XPS spectra of the samples with undoped PEDOT:PSS. A comparison of the XPS signals of the pristine and the charged PEDOT:PSS deposits over aluminium shows that the chemical environment of sulphur is preserved after the initial charge inside a test battery. The variation of the PSS/PEDOT ratio from 3.7 in the pristine state to 3.33 in the charged state indicates a slight decrease of the PSS amount upon charging. This finding suggests a modification of the PEDOT:PSS complex in the presence of the battery electrolyte, where the acidic PSS fragment could react with LiPF<sub>6</sub> according to Eqn. (1). LiPF<sub>6</sub> is known to undergo decomposition reactions in the presence of water and other acidic species.<sup>40,41</sup> If a fraction of PSS were engaged in the reaction represented in Eqn. (1), then PF<sub>6</sub><sup>-</sup> could act as an alternative counterion for positively charged PEDOT. Conductivity values ranging from 100–300 S cm<sup>-1</sup> have been reported for electropolymerized PEDOT films doped with PF<sub>6</sub><sup>-</sup>.<sup>42–44</sup> The microstructures (pores) in such thin films show different morphologies depending on the size of the anion and the cation from the electrolyte used in the polymerization.<sup>45</sup>



For the *bulk* 1% sample the PSS/PEDOT ratio of 1.74 indicates a more pronounced decrease of the PSS phase. This observation could arise from a combination of the PF<sub>6</sub><sup>-</sup> counter ion effect described above, and also to a certain extent from the contact with N-methyl pyrrolidone (NMP) that was used as the solvent for the PVDF binder during the electrode preparation. In the past, the conductivity enhancement of PEDOT:PSS by NMP treatment was reported and reasoned in terms of a decrease of the thickness of the excess, insulating PSS phase.<sup>36,46</sup> The EG-doped samples showed the same tendency in the PSS/PEDOT ratio variation upon charging as observed for undoped samples. However, the use of EG as the secondary dopant causes a more pronounced reduction of the PSS/PEDOT ratio, in agreement with previous observations.<sup>37,47</sup> Thus, the charged *EG-bulk* 1% sample shows the lowest PSS/PEDOT ratio of ~1.19, indicating a notably large decrease of the PSS content. Fig. 7 presents

the charge/discharge polarization of the different samples as a function of the charge/discharge current. Polarization tends to increase with the rate due to the thermodynamics of the de-lithiation/lithiation reaction in LFP, and also due to the transport hindrance through the electrode interfaces.<sup>49</sup> In the absence of PEDOT:PSS, the polarization can be as high as 1.54 V at 5 C, resulting in a poor charge/discharge energy efficiency for the standard sample.

Among the undoped samples (Fig. 7a), the *bulk 1%* architecture has the lowest polarization at 5 C (0.54 V), which is almost three times lower than the value for the LFP standard sample. For the undoped samples, the polarization tends to increase with the amount of PEDOT:PSS. Interestingly, at 5C, the polarization of the *coll-bulk 7%* sample matches the value found for the collector sample. These observations suggest the existence of a threshold where the amount of undoped polymer in the bulk has no beneficial effect at high rates. Regarding the doped samples, the collector and bulk 1% preparations with EG showed the lowest polarization at 5C: 0.42 and 0.37 V, respectively. We verified that DMSO had little effect on the polarization of the *bulk 1%* (0.54 V) and the collector (1.37 V) preparations. Dreyer et al.<sup>48</sup> described the thermodynamical origin of the charge/discharge hysteresis (polarization) in LiFePO<sub>4</sub> at nearly zero current (20 mV @ C/1000), which arises from the inherent multiple-particle equilibria involving Li<sup>+</sup> insertion/extraction. It is expected that these equilibria were affected by the presence of PEDOT:PSS that acts as a mixed ionic and electronic network with enhanced charge transport.

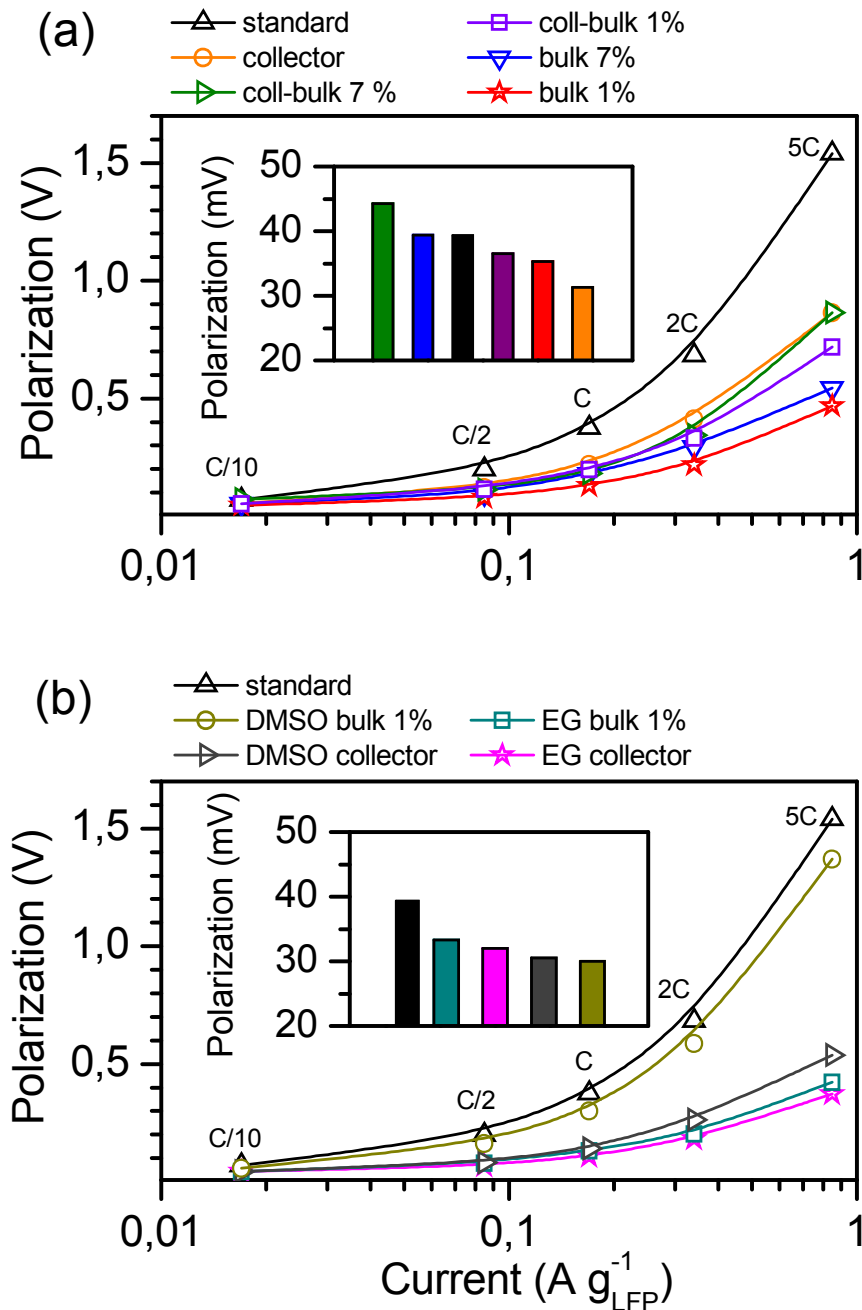


Fig. 7 Charge/discharge polarization plots of the standard and the different LFP-based composite electrodes with (a) undoped PEDOT:PSS and (b) doped PEDOT:PSS with EG or DMSO. Inset: comparison of the zero-current polarization (computed by extrapolation).



We estimated the zero-current polarization for the different samples (insets in Fig. 7) by extrapolation of linear plots of polarization vs. current (not shown). The value determined for the standard LFP sample was 40 mV and differs from the reported value of 20 mV,<sup>48</sup> most probably due to the different characteristics of our sample. To support our estimation, we recorded a charge/discharge cycle for standard  $\text{LiFePO}_4$  at C/200. The experimental value was 48 mV, while at C/10 the polarization was 69 mV. Among the undoped samples (inset Fig. 7a), the collector preparation has the lowest zero current polarization value (31 mV), which contrasts with its high polarization values found at higher currents. For the samples containing PEDOT:PSS in the bulk, low amounts of PEDOT:PSS result in lower zero-current polarization, namely: 35 mV for bulk 1% compared to 40 mV for bulk 7%. Regarding the doped samples, the zero-current polarization values are very similar, ranging from 29 to 33 mV. Thus, we suggest that the presence of a conducting medium between the current collector and the active particles is crucial to promote their electronic connectivity and improve the current distribution and charge collection/delivery efficiencies, especially at high rates.

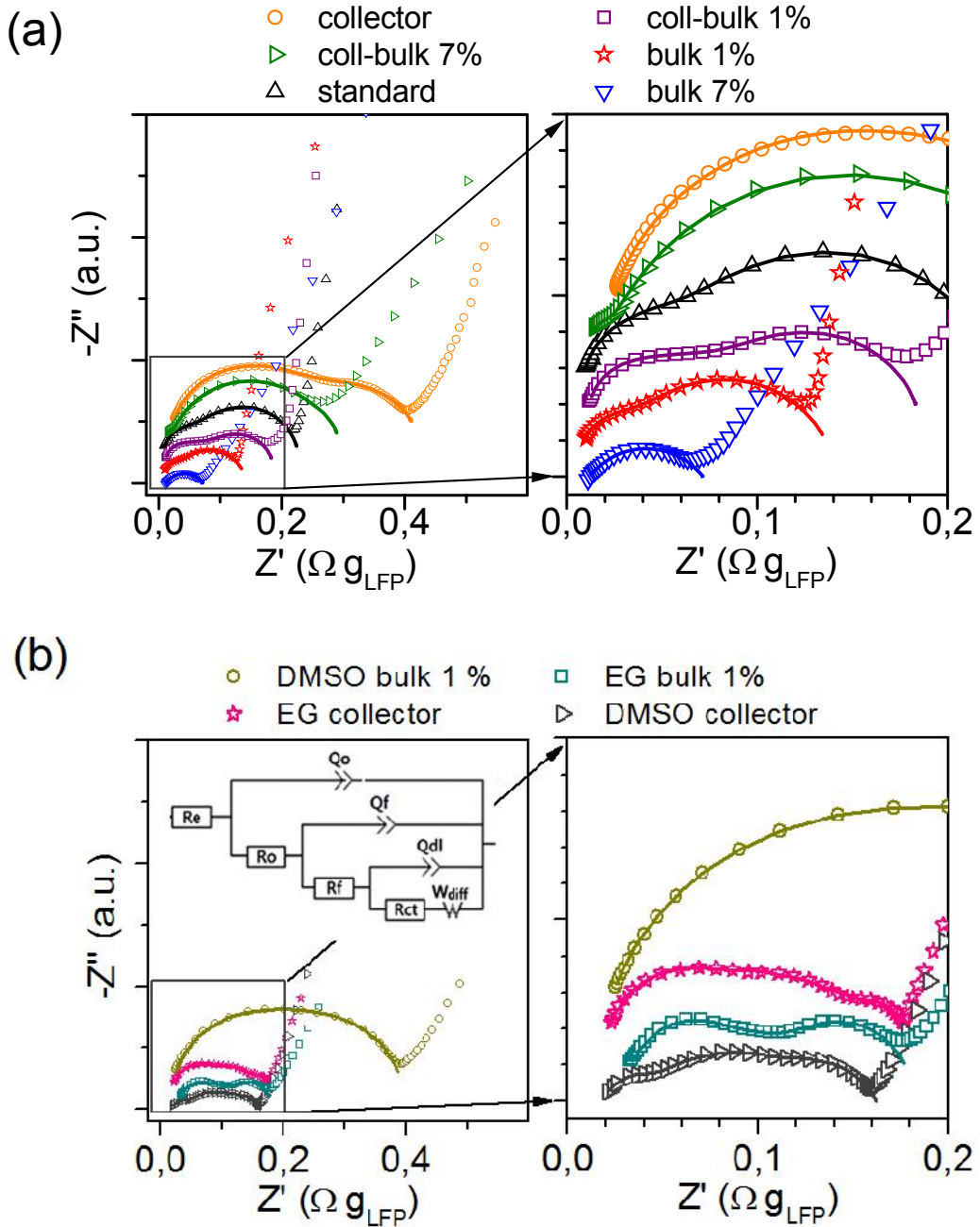


Fig. 8 Impedance spectra of the standard and the different LFP-based composite electrodes with (a) PEDOT:PSS and (b) PEDOT:PSS doped with EG or DMSO. Inset: equivalent circuit used to fit the experimental data (hollow symbols).

Fig. 8 presents the impedance spectra of the different samples after the initial charge at C/10. A previously reported equivalent circuit<sup>49</sup> was used to estimate the high-to-mid frequency resistance. In that equivalent circuit (shown in the inset of Fig. 8),  $R_e$  corresponds to the electrolyte resistance,  $R_0$  and  $Q_0$ , respectively, to the resistance and capacitance of the interface between the current collector and the active material particles (including additives). The sum in series of the charge transfer resistance ( $R_{ct}$ ) and the diffusion impedance ( $Z_w$ ) is added in parallel to the interfacial (double layer) capacitance ( $Q_{dl}$ ) that develops around active particles. The resistance ( $R_f$ ) and capacitance ( $Q_f$ ) of films (e.g. SEI) formed around the active particles are also considered in the model. In order to improve the quality of the fitting, constant phase elements (Q) were used instead of simple capacitors.

In the spectra (Fig. 8a), three features considered in the equivalent circuit can be distinguished at different frequency ranges for undoped samples, namely: two depressed semicircles in the high and mid frequency range and the diffusional tail at lower frequencies. Additionally, for the samples with PEDOT:PSS over the current collector, a small bump is distinguishable at high frequencies. The spectra of EG and DMSO-doped samples (Fig. 8b) have similar features to those of undoped samples, however at high frequency the semi-arc is better resolved in the collector samples with EG and DMSO, which highlights the attribution of this feature to the interface between the conducting polymer-coated current collector and the active material particles. In order to obtain comparative resistance values for the different samples, we considered only the high to mid frequency range ( $1 \text{ MHz} > \omega > 10 \text{ Hz}$ ).

Fig. 9 shows the high-to-mid frequency impedance in charged and discharged states, correlated with capacity values at 1 C, 2 C and 5 C. The comparison of the impedance values in charged and discharged states shows how the electronic conductivity of all the samples is lower in the charged state. For LFP, the lower impedance in the charged state has been related to some rearrangement of particles when  $\text{Li}^+$  ions are extracted from the phosphate.<sup>49</sup> For PEDOT and other conjugated polymers, the lower impedance in charge is related to the higher conductivity in the p-doped oxidized state.<sup>50</sup> The initial impedance values in the charged state reflect the quality of the electronic wiring throughout the electrode achieved during the preparation step. However, it is well known that new interfaces (e.g. SEI) develop as a function of time in open circuit and during the first charging/discharging of the battery.

In order to gain further insight into the performance of the different samples, the direct current resistance ( $R_{dc}$ ) at the voltage plateau was calculated from the slope of the polarization vs. current plot (not shown). Fig. 9a shows that the higher the resistance of the standard LFP electrode, the lower the capacity at moderate and high rates. This observation indicates that solely carbon black particles and PVDF are ineffective to ensure the connectivity of the active material particles, and highlights the importance of the electrode composition and architecture.

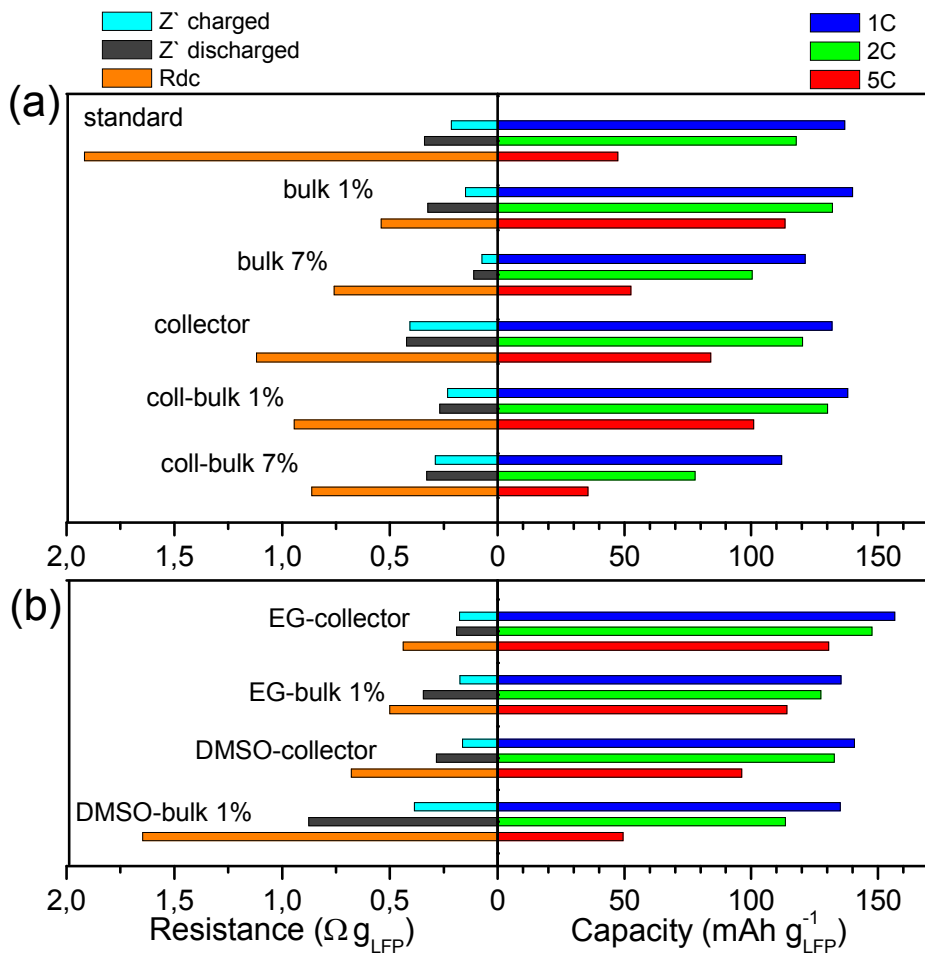


Fig. 9. Discharge capacity and resistances for the standard and the different LFP based composite electrodes with (a) PEDOT:PSS and (b) PEDOT:PSS doped with EG or DMSO.  $Z'$  and  $R_{dc}$  refer to the real part of the impedance and the direct current resistance, respectively.

The particle connectivity is notably improved by using a low amount of PEDOT:PSS mixed conductor in the bulk 1% electrode, resulting in a lower initial impedance and  $R_{dc}$ . The PEDOT:PSS network thus formed promotes the ionic and electronic wiring of the LFP particles, including their contact to the current collector. In this way the capacity increases as the charge is transferred and collected more efficiently throughout the electrode. In the bulk 7% sample, the higher amount of polymer does improve the electronic conductivity of the electrode, as evidenced from its low initial impedance values. However, its lower capacity, compared to bulk 1%, could arise from an increase in the length of the conduction pathways at the PSS phase within the bulk.<sup>27,36,51</sup> This condition limits the initial discharge performance and could affect the stability of the electrode for extended cycling.

The PEDOT:PSS coating on the aluminium current collector tends to increase its impedance due to the thickening of the conduction length and the formation of aluminium oxide by reaction with the polystyrene sulfonic acid.<sup>52</sup> Nevertheless, these drawbacks are compensated by an increase of the effective contact points between the aluminium current collector and the active material as the PEDOT:PSS coating acts as a plastic cushion that can adapt to the shape of LFP particles and accommodate them closely. This architecture results in a higher utilization of LFP and thus a higher capacity than the standard sample. The coll-bulk 1% combines the features of the bulk 1% and collector preparations, although this combination does not result in a synergistic effect.

During the preparation of the coll-bulk 7% and coll-bulk 1%, we noticed that the PEDOT:PSS dispersion present in the cathode slurry tends to dissolve the PEDOT:PSS film deposited on the collector. This was reflected in the higher polarization of these samples in Fig. 7a, and the higher direct current resistance shown in Fig. 9a. For this reason, we discarded the coll-bulk preparations with EG or DMSO dopants. Thus, the improvement in the conduction paths between the LFP particles due to the presence of a three-dimensional, conducting polymer network in the bulk leads to a higher discharge potential (lower charge/discharge polarization), which results in a higher power density of the battery. The better contact between the current collector and the electrode materials through a conducting PEDOT:PSS interface improves the active material utilization. This last characteristic was found for the EG-doped collector sample (Fig. 9b), which yielded the highest capacity values among all the studied samples.

Fig. 10 presents the rate performance of the different samples as a function of the number of cycles. For undoped samples, the best performance at all rates is confirmed for the sample with the lowest amount of polymer, namely bulk 1%. This sample is able to discharge almost 50% of the theoretical capacity at 10 C and delivers a stable capacity of  $133 \text{ mAh g}_{\text{LFP}}^{-1}$  at 2 C for 50 cycles, which outperforms the standard sample.

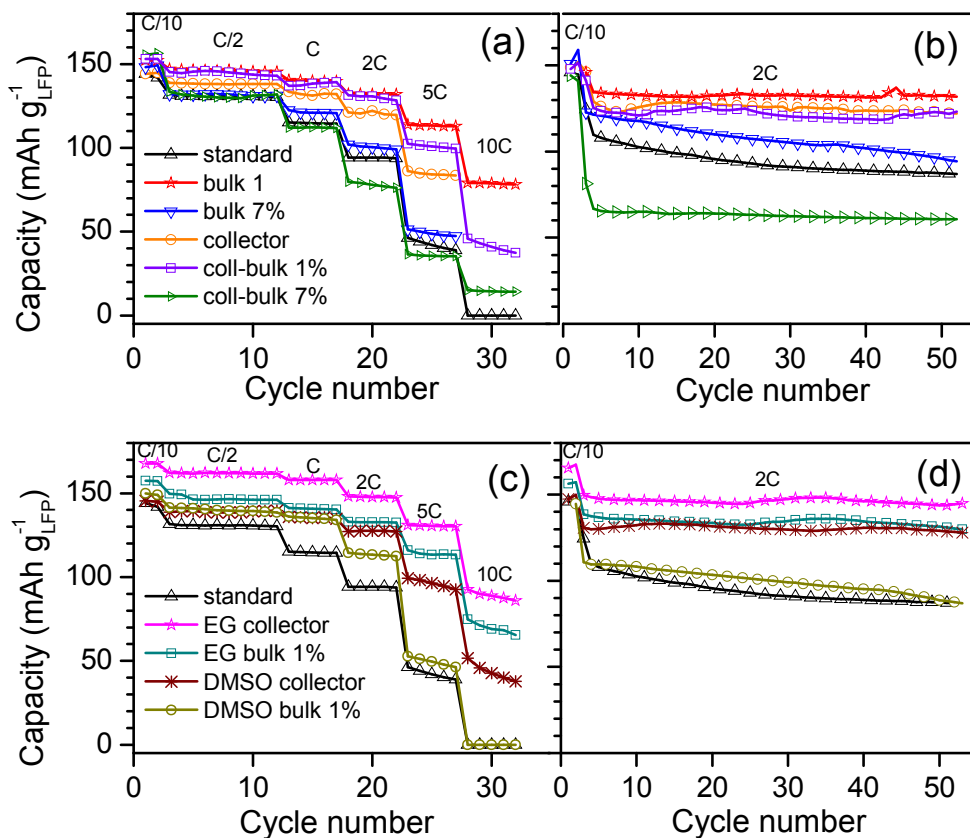


Fig. 10 Cycling performance of the standard and the different LFP-based composite electrodes with PEDOT:PSS. (a and b) Samples with PEDOT:PSS and c and d) samples doped with EG and DMSO.

Further improvement of the discharge properties of LFP was achieved by coating the aluminium current collector with PEDOT:PSS doped with a small amount of ethylene glycol. This simple EG collector preparation has the best rate performance among all

the tested electrode architectures as it can discharge  $90 \text{ mA h g}_{\text{LFP}}^{-1}$  at a high rate of 10 C, and deliver  $145 \text{ mA h g}_{\text{LFP}}^{-1}$  continuously at 2 C during 50 cycles. As previously reported by other authors, EG or DMSO increases the surface proportion of electron-conducting PEDOT in the final polymer film. Therefore, the EG-collector and the DMSO-collector could present a more conducting PEDOT:PSS/Al interface at which the charge collection could be efficient during cycling at high rates. For the undoped collector, the surface proportion of non-conducting PSS is higher, therefore the less conducting PEDOT:PSS/Al interface could limit the charge collection at high rates.

#### 4. Conclusions

LiFePO<sub>4</sub> electrodes were built in different architectures encompassing PEDOT:PSS conducting polymer. The incorporation of PEDOT:PSS additives within the bulk of the electrode was achieved by a simple blending technique and provides a three-dimensional, mixed conducting network that notably improves the performance of LiFePO<sub>4</sub> electrodes. The addition of a small amount of PEDOT:PSS resulted in high capacity values specially at high rates, achieving a reversible capacity of  $114 \text{ mA h g}^{-1}$  at 5 C and  $132 \text{ mA h g}^{-1}$  at 2 C for extended cycling. We found that the use of ethylene glycol as a conductivity enhancement agent for PEDOT:PSS deposited over the aluminium collector is an effective strategy to boost the performance of LiFePO<sub>4</sub> electrodes. The electrodes thus formed show lower load resistance with a discharge plateau above 3.0 V at high rates and deliver  $132 \text{ mA h g}^{-1}$  at 5 C. These features and the excellent capacity retention of  $145 \text{ mA h g}^{-1}$  at 2 C for the measured 50 cycles are attributed to the enhanced conductivity of EG-doped PEDOT:PSS that arises from the segregation of insulating PSS, as evidenced from the XPS analysis. The presented methods are easy to scale-up and could be applied to other electrode active materials for alkali ion batteries.

#### Notes and references

- 1 A. K. Padhi, K. S. Nanjundaswamy and J. B. Goodenough, *J. Electrochem. Soc.*, 1997, **144**(4), 1188.
- 2 C. M. Julien, A. Mauger, K. Zaghib, *J. Mater. Chem.*, 2011, **21** (27), 9950.

- 3 Y. Zhang, Q. Huo, P. Du, L. Wang, A. Zhang, Y. Song, Y. Lv, G. Li, *Synth. Met.*, 2012, **162** (13-14), 1315.
- 4 C. Delacourt, L. Laffont, R. Bouchet, C. Wurm, J.-B. Leriche, M. Morcrette, J.-M. Tarascon, C. Masquelier, *J. Electrochem. Soc.*, 2005, **152** (5), A913.
- 5 C. Zhu, K. Weichert, J. Maier, *Adv. Funct. Mater.*, 2011, **21** (10), 1917.
- 6 H. Huang, S.-C. Yin, L. F. Nazar, *Electrochem. Solid-State Lett.* 2001, **4** (10), A170.
- 7 B. Kang, G. Ceder, *Nature*, 2009, **458** (7235), 190.
- 8 N. Ravet, Y. Chouinard, J. F Magnan, S. Besner, M. Gauthier, M. Armand, *J. Power Sources*, 2001, **97-98**, 503.
- 9 J. Wang, X. Sun, *Energy Environ. Sci.*, 2012, **5**(1), 5163.
- 10 A. D. Pasquier, F. Orsini, A. S. Gozdz, J.-M. Tarascon, *J. Power Sources*, 1999, **81-82**, 607.
- 11 A. V. Murugan, C. W. Kwon, G. Campet, B. Kale, T. Maddanimath, K. Vijayamohanam, *J. Power Sources*, 2002, **105** (1), 1.
- 12 W. M. Chen, Y. H. Huang, L. X. Yuan, *J. Electroanal. Chem.* 2011, **660** (1), 108.
- 13 W. M. Chen, L. Qie, L. X. Yuan, S. A. Xia, X. L. Hu, W. X. Zhang, Y. H. Huang, *Electrochim. Acta.*, 2011, **56** (6), 2689.
- 14 I. Boyano, J. A. Blazquez, I. de Meatza, M. Bengoechea, O. Miguel, H. Grande, Y. Huang, J. B. Goodenough, *J. Power Sources*, 2010, **195**(16), 5351.
- 15 G. X. Wang, L. Yang, Y. Chen, J. Z. Wang, S. Bewlay, H. K. Liu, *Electrochim. Acta*, 2005, **50**, 4649.
- 16 J. Liu, G. Yang, X. Zhang, J. Wang, R. Wang, *J. Power Sources*, 2012, **197**, 253.
- 17 Y. M. Bai, P. Qiu, Z. L. Wen, S. C. Han, *J. Alloys Compd.*, 2010, **508**(1), 1.
- 18 D. Lepage, C. Michot, G. Liang, M. Gauthier, S. B. Schougaard, *Angew. Chemie - Int. Ed.*, 2011, **50**(30), 6884.
- 19 H. C. Dinh, S. il Mho, I. H. Yeo, *Electroanalysis*, 2011, **23**(9), 2079.
- 20 N. D. Trinh, M. Saulnier, D. Lepage, S. B. Schougaard, *J. Power Sources*, 2013, **221**, 284.
- 21 D. Cíntora-Juárez, C. Pérez-Vicente, S. Ahmad, J. L. Tirado, *RSC Adv.*, 2014, **4**(50), 26108.
- 22 D. Cíntora-Juárez, C. Pérez-Vicente, S. Ahmad, J. L. Tirado, *Phys. Chem. Chem. Phys.*, 2014, **16**(38), 20724.
- 23 S. Guhathakurta, K. Min, *Polymer (Guildf)*, 2010, **51**(1), 211.
- 24 J. Ouyang, Q. Xu, C. W. Chu, Y. Yang, G. Li, J. Shinar, *Polymer (Guildf)*, 2004, **45**(25), 8443.
- 25 J. Y. Kim, J. H. Jung, D. E. Lee, J. Joo, *Synth. Met.*, 2002, **126** (2-3), 311.
- 26 B. León, C. Pérez-Vicente, J. L. Tirado, P. Biensan, C. Tessier, *J. Electrochem. Soc.*, 2008, **155**(3), A211.
- 27 A. M. Nardes, M. Kemerink, R. a J. Janssen, J. a M. Bastiaansen, N. M. M. Kiggen, B. M. W. Langeveld, A. J. J. M. Van Breemen and M. M. De Kok, *Adv. Mater.*, 2007, **19**, 1196.
- 28 B. Hannover, A. a M. Prince, M. Jean, R. S. Liu and G. X. Wang, *Hyperfine Interact.*, 2006, **167**, 767.
- 29 Y.-H. Rho, L. F. Nazar, L. Perry and D. Ryan, *J. Electrochem. Soc.*, 2007, **154**, A283.
- 30 A. Andersson, B. Kalska, L. Haggstrom, J. O. Thomas, *Solid State Ionics.*, 2000, **130**(1-2), 41.
- 31 R. Dedryvère, M. Maccario, L. Croguennec, F. Le Cras, C. Delmas and D. Gonbeau, *Chem. Mater.*, 2008, **20**, 7164.
- 32 L. Castro, R. Dedryvère, M. El Khalifi, P. E. Lippens, J. Bréger, C. Tessier and D. Gonbeau, *J. Phys. Chem. C*, 2010, **114**, 17995.



- 33 C. W. Kim, J. S. Park, K. S. Lee, *J. Power Sources*, 2006, **163**(1 SPEC. ISS.), 144.
- 34 R. Malik, A. Abdellahi and G. Ceder, *J. Electrochem. Soc.*, 2013, **160**, A3179.
- 35 A. Elschner, S. Kirchmeyer, W. Lövenich, U. Merker and K. Reuter, PEDOT: Principles and Applications of an Intrinsically Conductive Polymer. CRC Press: Florida, 2010. Chapter 9, p. 122.
- 36 S. K. M. Jönsson, J. Birgersson, X. Crispin, G. Greczynski, W. Osikowicz, a. W. Denier van der Gon, W. R. Salaneck and M. Fahlman, *Synth. Met.*, 2003, **139**, 1.
- 37 X. Crispin, S. Marciniak, W. Osikowicz, G. Zotti, a. W. Denier Van Der Gon, F. Louwet, M. Fahlman, L. Groenendaal, F. De Schryver and W. R. Salaneck, *J. Polym. Sci. Part B Polym. Phys.*, 2003, **41**, 2561.
- 38 X. Crispin, F. L. E. Jakobsson, a Crispin, P. C. M. Grim, P. Andersson, a Volodin, C. van Haesendonck, M. Van der Auweraer, W. R. Salaneck and M. Berggren, *Chem. Mater.*, 2006, **18**, 4354.
- 39 G. Greczynski, T. Kugler and W. R. Salaneck, *Thin Solid Films*, 1999, **354**, 129.
- 40 U. Heider, R. Oesten and M. Jungnitz, *J. Power Sources*, 1999, **81-82**, 119.
- 41 T. Kawamura, S. Okada and J. I. Yamaki, *J. Power Sources*, 2006, **156**, 547.
- 42 A. Aleshin, R. Kiebooms, R. Menon, F. Wudl and A. Heeger, *Phys. Rev. B*, 1997, **56**, 3659.
- 43 A. Aleshin, R. Kiebooms, R. Menon and A. J. Heeger, *Synth. Met.*, 1997, **90**, 61.
- 44 I. Giurgiu, K. Zong, J. R. Reynolds, W. P. Lee, K. R. Breneman, A. V. Saprigin, a. J. Epstein, J. Hwang and D. B. Tanner, *Synth. Met.*, 2001, **119**, 405.
- 45 A. I. Melato, M. H. Mendonça and L. M. Abrantes, *J. Solid State Electrochem.*, 2009, **13**, 417.
- 46 C.-H. Chen, L. Zhou and J. Lv, *J. Appl. Polym. Sci.*, 2012, **125**, 3134.
- 47 J. Ouyang, Q. Xu, C. W. Chu, Y. Yang, G. Li and J. Shinar, *Polymer (Guildf)*, 2004, **45**, 8443.
- 48 W. Dreyer, J. Jamnik, C. Guhlke, R. Huth, J. Moskon and M. Gaberscek, *Nat. Mater.*, 2010, **9**, 448.
- 49 J.-M. Atebamba, J. Moskon, S. Pejovnik and M. Gaberscek, *J. Electrochem. Soc.*, 2010, **157**, A1218.
- 50 J. Heinze, B. A. Frontana-Urbe and S. Ludwigs, *Chem. Rev.*, 2010, **110**, 4724.
- 51 T. Stöcker, A. Köhler and R. Moos, *J. Polym. Sci. Part B Polym. Phys.*, 2012, **50**, 976.
- 52 W. Bantikassegn and O. Inganäs, *Thin Solid Films*, 1997, **293**, 138.

**Electronic supplementary information (ESI)****Table S1.** Fitted hyperfine parameters for pristine and charged electrodes. (IS: Isomer shift, QS: Quadrupolar splitting, LW: Line width)

Sample	Polymer	Assignment	IS (mm/s)	QS (mm/s)	LW (mm/s)	Contribution (%)
LFP pristine	No	$Fe^{2+}$	1.220(1)	2.96(1)	0.245(3)	93(2)
		FeP	0.48(3)	0.79(4)	0.38(6)	7(2)
LFP Charged	No	$Fe^{2+}$	1.22(3)	2.87(4)	0.33(6)	10(4)
		$Fe^{3+}$	0.427(3)	1.526(7)	0.326(7)	85(4)
		FeP	0.42(4)	0.78(5)	0.26(1)	5(4)
bulk 1% Charged	PEDOT:PSS	$Fe^{3+}$	0.431(3)	1.534(7)	0.301(8)	92(1)
		FeP	0.41(6)	0.9(1)	0.4(1)	8(1)
EG-bulk1% Charged	EG-PEDOT:PSS	$Fe^{3+}$	0.426(3)	1.525(7)	0.285(7)	95(7)
		FeP	0.48	0.7(1)	0.4(2)	5(7)

**Table S2.** Fitted binding energy (BE) of the Fe(2p) levels and satellite (Sat) signals for LFP-based electrodes.

Sample	BE 2p <sub>3/2</sub> (eV)	BE 2p <sub>1/2</sub> (eV)	BE Sat 1 (eV)	BE Sat 2 (eV)
standard (pristine)	710.98	724.64	713.73	727.38
bulk 1% (charged)	712.03	725.75	713.80	727.52
EG-bulk 1% (charged)	711.98	725.80	714.20	728.03

**Table S3.** Fitted peak positions for the  $S(2p_{3/2})$  level and calculated PSS / PEDOT ratios with associated standard deviation values. The binding energy (BE) of the corresponding  $S(2p_{1/2})$  signals was fixed 1.2 eV above the corresponding  $S(2p_{3/2})$  signals.

Sample	State	BE $S(2p_{3/2})$ (eV)		PSS/PEDOT ratio
		PEDOT	PSS	
PEDOT:PSS	pristine	164.12	168.46	3.70(2)
PEDOT:PSS	charged C/10	164.14	168.57	3.3(2)
bulk 1%	charged C/10	164.11	168.44	1.74(3)
EG-PEDOT:PSS	pristine	164.14	168.38	2.90(2)
EG-PEDOT:PSS	charged C/10	164.17	168.47	2.43(3)
EG-bulk 1%	charged C/10	164.13	168.50	1.186(3)





# Chapter 6

## Final conclusions<sup>1</sup>

The following three general conclusions are deduced by comparing the hypothesis and objectives to the main results presented in Chapters 3, 4 and 5:

- 1) Composite electrodes based on  $\text{LiFePO}_4$  and poly(alkylenedioxiophene) [PXDOT] were successfully prepared by electropolymerization, by blending or by coating methods. Different variations of these methods were devised and applied for obtaining cathodes that are active for the reversible insertion/extraction of lithium in test batteries. The effectiveness of the prepared electrodes depends on the synthesis conditions of the conducting polymer and on how this is combined with  $\text{LiFePO}_4$  to form the composite electrode.
- 2) The preparation conditions of the composite electrodes with  $\text{LiFePO}_4$  and PXDOT affect their electrical resistance, their morphology and their texture. Besides, the way in which the conducting polymer interacts with  $\text{LiFePO}_4$  particles and with the other components of the electrode influences the charge transport through the different interphases of the electrode.

---

<sup>1</sup> NOTE: In order to enable a performance comparison between the different electrodes, the total discharge capacity at 2C and the corresponding energy density at 50 % DOD (Depth Of Discharge) were determined and are referred to the weight of  $\text{LiFePO}_4$  in the electrode. A graphical comparison of these parameters is presented in Figure 1 (Appendix I). The reader can consult in Figure 2 (Appendix I) the same type of comparison but referred to the weight of the composite electrodes without considering the weight of the current collector.

- 3) The strategies presented in this thesis for preparing and analyzing  $\text{LiFePO}_4/\text{PXDOT}$  composite electrodes highlight the relevance of charge transport through interphases in battery electrodes. In general, these strategies could be implemented with slight modifications to the present methods for preparing  $\text{LiFePO}_4$ -based electrodes. Furthermore, these strategies could be applied to other families of active materials and conducting polymers that present redox compatibility and stability when combined in order to form composite electrodes for alkali-ion batteries.

The conclusions listed below are derived from the individual analysis and from the comparison of the results presented in Chapters 3, 4 and 5. For clarity, the conclusions are classified into two groups according to the general method used for preparing the composite electrodes. The reference to the corresponding chapters is included for each of the conclusions.

### **Electropolymerization methods**

- 4) The potentiostatic electropolymerization (electrodeposition: *edep*) of EDOT monomers in an acetonitrile medium over cathodes based on  $\text{LiFePO}_4$  or  $\text{LiFePO}_4/\text{C}$  produces stable electrodes coated by PEDOT. In these electrodes,  $\text{LiFePO}_4$  undergoes oxidation and lithium extraction reactions during the potentiostatic polymerization of the monomers. Nevertheless, these modifications of  $\text{LiFePO}_4$  do not limit the reversibility of the redox and insertion/extraction reactions of the active material in further charge/discharge cycles.

Chapter 3, sections 2.2.1 and 2.2.4

- 5) During the preparation of the *LFP-edep* electrode, EDOT monomers or oligomers are incorporated to the composite electrode and these species undergo further polymerization during the first charge in a test battery. This situation is not observed for the *LFP/C-edep* composite electrode due to the more efficient polymerization of the monomers and oligomers over the carbon-coated  $\text{LiFePO}_4$  particles.

Chapter 3, section 2.2.1

- 6) The presence of 19 % w/w PEDOT in the *LFP-edep* electrode enables a higher capacity and a higher energy density, as compared to the *LFP/C-edep* electrode. Although the amount of PEDOT in the *LFP/C-edep* electrode is considerably lower (3 % w/w), both electrodes formed by the *edep* method showed a very similar cycling stability, which demonstrates the possibility of obtaining good electrochemical performance for the  $\text{LiFePO}_4$ -based electrode by coating it with PEDOT. A further increase of the capacity and energy density values could be achieved by adjusting the amount of PEDOT and pressing the electrode in order to improve the utilization of the active material.

Chapter 3, sections 2.2.3 and 2.2.4

- 7) The *in battery* electropolymerization of EDOT or ProDOT monomers produces PEDOT or PProDOT coatings over electrochemically de-lithiated  $\text{LiFePO}_4$ -based electrodes upon the first battery charging up to 4.2 V. The reaction of  $\text{Li}_{1-x}\text{FePO}_4$  upon discharge is facilitated by the conducting polymer coating. The polymer coating improves the active material utilization in further charge/discharge cycles due to a better connectivity between the active material particles throughout the electrode, which also confers mechanical stability.

Chapter 4, section 2.1

- 8)  $^{57}\text{Fe}$  Mössbauer spectroscopy analysis indicated that the oxidation of  $\text{LiFePO}_4$  is more efficient for the electrode charged in one step up to 3.7 V in presence of EDOT, as compared to the charging process of the electrode without monomers. This higher efficiency was attributed to the presence of PEDOT, which is formed through oxidation over  $\text{Li}_{1-x}\text{FePO}_4$  and over the conducting substrates (current collector and carbon particles) by effect of the anodic current. PEDOT formed *in battery* not only facilitates the oxidation of the active materials upon charging up to 4.2 V, but also the inverse reaction upon discharge, which results in a high efficiency and stability upon successive charge/discharge cycles.



Chapter 4, section 2.2

9) The electric resistance of all the composite electrodes formed *in battery* decreases progressively as the potential during the initial charge increases. This resistance decrease was evidenced through impedance spectroscopy analysis, which allowed proving that PEDOT or PProDOT are progressively formed over the  $\text{LiFePO}_4$ -based electrode. These polymers attain a conducting state due to the oxidation and doping processes that take place upon charging the battery up to 4.2 V. The composite electrodes formed *in battery* have a total resistance of at least one order of magnitude lower than the standard  $\text{LiFePO}_4$ -based electrode in charged state at 4.2 V. This lower resistance is related to the improvement in the charge/discharge rate capability and the stability observed for the electrodes formed *in battery*.

Chapter 4, sections 2.3 and 2.4

- 10) Due to their simplicity and effectiveness, the galvanostatic *in battery* methods constitute a more attractive strategy for the electropolymerization of monomers over  $\text{LiFePO}_4$ -based electrodes, as compared to the potentiostatic *edep* method, which requires additional reagents and processing steps. In particular, the one step *in battery* method is compatible with existing battery production processes as it requires adding a small amount of EDOT or ProDOT monomers to the battery electrolyte and charging the battery as a conditioning step.

Chapters 3 and 4

### **Blending methods and coating of the current collector**

11) PEDOT obtained by potentiostatic electropolymerization using the *3phase* method can be used as an agglomerating and conducting additive in carbon-free LiFePO<sub>4</sub> electrodes (*LFP-blend*), or in LiFePO<sub>4</sub> electrodes with carbon-coating (*LFP/C-blend*). These composite electrodes with PEDOT are mechanically stable and provide very similar capacity at low discharge rate. At higher charge/discharge rates, the better performance and cycling stability of the *LFP/C-blend* electrode, as compared to *LFP-blend* and *LFP/C* electrodes, is attributed to the compatibility between PEDOT and the carbon-coating, and to their synergistic effect for lowering the electrode resistance.

#### Chapter 3

12) It is possible to incorporate PEDOT:PSS to a mixture of LiFePO<sub>4</sub>, carbon black and PVDF binder by blending. The presence of 7 % w/w of PEDOT:PSS in the bulk of an LiFePO<sub>4</sub>-based electrode has a positive effect on the charge/discharge capacity and potential, although a high amount of conducting polymer lowers the energy density. By reducing the amount of PEDOT:PSS to 1 % w/w, the capacity and energy density values are higher than the values determined for the electrode without conducting polymer. This improvement is related to the higher efficiency of the redox reaction of LiFePO<sub>4</sub> in presence of a small amount of the mixed conductor, as it was determined through <sup>57</sup>Fe Mössbauer spectroscopy.

#### Chapter 5

13) The PEDOT:PSS coating over the aluminum current collector provides a compatible surface for depositing the ink that contains an standard mixture of LiFePO<sub>4</sub> and additives. This conducting polymer coating not only facilitates the formation of the electrode film, but also improves notably the capacity and the energy density, as compared to the electrode formed over the uncoated current collector. The joint use of PEDOT:PSS within the bulk of the electrode (7 or 1 % w/w) and over the current collector does not result in a synergistic effect.

#### Chapter 5

- 14) Doping PEDOT:PSS by ethylene glycol (EG) slightly improves the charge/discharge capacity and potential when the polymer is used within the bulk of the electrode, as compared to the electrode with undoped 1% w/w PEDOT:PSS. On the contrary, doping by dimethylsulfoxide (DMSO) results detrimental to the electrochemical performance. EG- and DMSO-doped PEDOT:PSS coating over the current collector boosts the capacity and lowers the charge/discharge polarization at high charge/discharge rates. The high performance of the  $\text{LiFePO}_4$ -based electrodes containing EG-doped PEDOT:PSS is attributed to a high proportion of the electron conducting PEDOT phase, as evidenced from the quantitative XPS analysis.

Chapter 5

- 15) The correlation between the initial impedance, the direct current load resistance and the capacity at high discharge rate showed that the interphase between the electrode layer and the current collector has the highest impact on the performance of the electrodes that contain PEDOT:PSS. Thus, the application of EG-doped PEDOT:PSS coating over the current collector is pointed out as the best procedure among all the strategies described in this thesis for improving the performance in  $\text{LiFePO}_4$ -based electrodes.

Chapter 5

- 16) The composite electrodes with PEDOT:PSS showed higher discharge capacity and voltage at fast rates than those obtained from electrochemically synthesized PEDOT due to three factors: 1) the higher conductivity of undoped and doped PEDOT:PSS, 2) the difficulties for dispersing the pulverized PEDOT synthesized electrochemically, and 3) the better film-forming properties of PEDOT:PSS.

Chapters 3 and 5

## Conclusiones finales<sup>1</sup>

Las siguientes tres conclusiones generales se deducen al comparar las hipótesis y objetivos (Capítulo 2) con los principales resultados presentados en los Capítulos 3, 4 y 5:

- 1) Se logró la preparación de electrodos compuestos basados en  $\text{LiFePO}_4$  y polímeros conductores poli(alquilendioxitiofeno) [PXDOT] mediante métodos de electropolimerización, mezclado y recubrimiento. Se desarrollaron y se aplicaron variaciones de estos métodos para obtener cátodos que son activos para la inserción/extracción reversible de litio en baterías de prueba. La efectividad de los electrodos preparados depende de las condiciones de síntesis del polímero conductor y de como éste se combina con  $\text{LiFePO}_4$  para formar el electrodo compuesto.
- 2) Las condiciones de preparación de los electrodos compuestos con  $\text{LiFePO}_4$  y PXDOT afectan su resistencia eléctrica, su morfología y textura. Además, la manera en como el polímero conductor interactúa con el material activo y con los demás componentes del electrodo, influye en el transporte de carga a través de las diferentes interfaces del electrodo.

---

<sup>1</sup> *NOTA: Para posibilitar una comparación de las prestaciones de los diferentes electrodos, la capacidad total de descarga a 2C y la correspondiente densidad de energía al 50 % DOD (Depth Of Discharge) se determinaron y se refirieron al peso de  $\text{LiFePO}_4$  en los electrodos. Una comparación gráfica de estos parámetros se presenta en la Figura 1 (Appendix I). El lector puede consultar en la Figura 2 (Appendix I) el mismo tipo de comparación pero referida al peso del electrodo sin considerar el peso del colector de corriente.*

- 3) Las estrategias de preparación y análisis de electrodos compuestos  $\text{LiFePO}_4/\text{PXDOT}$  presentadas en esta tesis destacan la relevancia del transporte de carga a través de interfaces en electrodos para baterías. En general, estas estrategias podrían ser implementadas con ligeras modificaciones a los métodos actuales de preparación de electrodos basados en  $\text{LiFePO}_4$ . Además, estas estrategias podrían aplicarse para otras familias de materiales activos y polímeros conductores que presenten compatibilidad redox y estabilidad al combinarse para formar electrodos compuestos para baterías de iones alcalinos.

Las conclusiones que se listan a continuación se derivan a partir del análisis individual y a partir de la comparación de los resultados presentados en los capítulos 3, 4 y 5. Para mayor claridad, las conclusiones se clasifican en dos grupos según el método general empleado para preparar los electrodos compuestos. La referencia al capítulo correspondiente se incluye para cada una de las conclusiones.

#### **Métodos de electropolimerización**

- 4) La electropolimerización potencioestática (*electrodeposition: edep*) de monómeros EDOT en un medio de acetonitrilo sobre cátodos basados en  $\text{LiFePO}_4$  o  $\text{LiFePO}_4/\text{C}$  produce electrodos estables cubiertos con PEDOT. En estos electrodos las reacciones de oxidación y de extracción de litio del  $\text{LiFePO}_4$  ocurren durante la electropolimerización potencioestática de los monómeros. Sin embargo, estas modificaciones del  $\text{LiFePO}_4$  no limitan la reversibilidad de la reacción redox ni la de inserción/extracción en el material activo en ciclos sucesivos de carga/descarga.

Chapter 3, sections 2.2.1 and 2.2.4

- 5) Durante la preparación del electrodo *LFP-edep* los monómeros u oligómeros de EDOT se incorporan al electrodo compuesto y dichas especies polimerizan durante la primera carga al emplearse en una batería. Esta situación no se observa al emplear el electrodo compuesto *LFP/C-edep*, lo cual se atribuye a

una reacción más eficiente de los monómeros u oligómeros sobre las partículas de  $\text{LiFePO}_4$  cubiertas de carbón.

Chapter 3, section 2.2.1

- 6) La presencia de 19 % w/w de PEDOT en el electrodo *LFP-edep* permite una mayor capacidad y una mayor densidad de energía comparado con el electrodo *LFP/C-edep*. A pesar de que la cantidad de PEDOT en el electrodo *LFP/C-edep* es considerablemente menor (3 % w/w), ambos electrodos formados mediante el método *edep* presentaron una estabilidad muy similar durante el ciclado, lo cual demuestra la posibilidad de obtener buen comportamiento electroquímico para el electrodo basado en  $\text{LiFePO}_4$  al cubrirlo con PEDOT. Se podría lograr un aumento de los valores de capacidad específica y densidad de energía mediante el ajuste de la cantidad de PEDOT y prensando el electrodo para mejorar el uso del material activo.

Chapter 3, sections 2.2.3 and 2.2.4

- 7) La electropolimerización *in battery* de monómeros EDOT o ProDOT produce recubrimientos de PEDOT o PProDOT sobre electrodos basados en  $\text{LiFePO}_4$  al cargar la batería por primer vez hasta 4.2 V. El recubrimiento de polímero conductor facilita la reacción del  $\text{Li}_{1-x}\text{FePO}_4$  durante la descarga de la batería. El recubrimiento de polímero conductor mejora la utilización del material activo en ciclos sucesivos de carga/descarga debido a una mejor conectividad entre las partículas de material activo a través del electrodo, lo cual confiere también estabilidad mecánica.

Chapter 4, section 2.1

- 8) El análisis mediante espectroscopía Mössbauer de  $^{57}\text{Fe}$  indicó que la oxidación de  $\text{LiFePO}_4$  es más eficiente para el electrodo cargado en un paso hasta 3.7 V en presencia de EDOT, comparado con el proceso de carga del electrodo en ausencia de monómeros. Esta mayor eficiencia se atribuyó a la presencia de PEDOT, el cual se forma por oxidación sobre  $\text{Li}_{1-x}\text{FePO}_4$  y sobre los sustratos conductores (colector de corriente o partículas de carbón) por efecto de la corriente anódica. El PEDOT formado *in battery* no solo facilita la oxidación del

material activo al cargar hasta 4.2 V, sino también la reacción inversa al descargar, resultando en una mayor eficiencia y estabilidad en ciclos sucesivos de carga/descarga.

Chapter 4, section 2.1

- 9) La resistencia eléctrica de los electrodos formados *in battery* disminuye progresivamente conforme se incrementa el potencial durante la primera carga de la batería. Esta disminución de la resistencia se hizo evidente mediante análisis de espectroscopía de impedancia, lo que permitió probar que el PEDOT y el PProDOT se forman progresivamente sobre el electrodo basado en  $\text{LiFePO}_4$ . Estos polímeros alcanzan un estado conductor debido al proceso de oxidación y dopado que ocurre al cargar la batería hasta 4.2 V. Los electrodos compuestos preparados *in battery* tienen valores de resistencia de al menos un orden de magnitud menores que el electrodo estándar cargado a 4.2 V. Esta menor resistencia está relacionada con las mejores prestaciones de carga/descarga y la estabilidad observada al ciclar los electrodos formados *in battery*.

Chapter 4, sections 2.3 and 2.4.

- 10) Debido a su sencillez y efectividad, el método galvanostático *in battery* constituye una estrategia más atractiva para la electropolimerización de monómeros sobre electrodos basados en  $\text{LiFePO}_4$  en comparación con el método potencioestático *edep*, el cual requiere reactivos y etapas de preparación adicionales. En particular, el método *in battery* en una etapa es compatible con los procesos actuales de producción de baterías ya que solo se requiere la adición de pequeñas cantidades de monómeros EDOT o ProDOT en el electrolito y cargar la batería a manera de etapa de acondicionamiento.

Chapters 3 and 4.

### **Métodos de mezclado y de recubrimiento del colector de corriente**

11) El PEDOT obtenido por electropolimerización potencioestática empleando el método *3phase* se puede emplear como aditivo aglomerante y conductor en electrodos de  $\text{LiFePO}_4$  sin carbón (*LFP-blend*), o en electrodos de  $\text{LiFePO}_4$  cubierto con carbón (*LFP/C-blend*). Estos electrodos compuestos con PEDOT son mecánicamente estables y proporcionan valores de capacidad muy similar a velocidades de descarga bajas. A velocidades de carga/descarga más altas, el mejor rendimiento y estabilidad al ciclar el electrodo *LFP/C-blend*, comparado con los electrodos *LFP-blend* y *LFP/C*, se atribuye a la compatibilidad entre el PEDOT y el recubrimiento de carbón, y a su efecto sinérgico para disminuir la resistencia del electrodo.

#### Chapter 3.

12) Es posible incorporar PEDOT:PSS a una mezcla de  $\text{LiFePO}_4$ , negro de carbono y aglomerante PVDF mediante mezclado. La presencia de 7 % w/w de PEDOT:PSS en la masa de un electrodo basado en  $\text{LiFePO}_4$  tiene un efecto positivo en la capacidad y en el potencial de carga/descarga, aunque una alta cantidad de polímero conductor disminuye la densidad de energía. Al reducir la cantidad de PEDOT:PSS a un 1 % w/w, los valores de capacidad, potencial y densidad de energía son mayores a los valores determinados para el electrodo sin polímero conductor. Esta mejora se relaciona a la alta eficiencia de la reacción redox del  $\text{LiFePO}_4$  en presencia de una pequeña cantidad de conductor mixto, como se determinó mediante espectroscopia Mössbauer.

#### Chapter 5.

13) El recubrimiento de PEDOT:PSS sobre el colector de corriente de aluminio ofrece una superficie compatible para depositar la tinta que contiene una mezcla estándar de  $\text{LiFePO}_4$  y aditivos. Este recubrimiento no solo mejora la formación de la película del electrodo, también mejora la capacidad y densidad de energía en comparación con el electrodo formado sobre el colector de corriente sin recubrimiento. El uso conjunto de PEDOT:PSS en la masa del



electrodo (7 o 1 % w/w) y sobre el colector de corriente no resulta en un efecto sinérgico.

Chapter 5

- 14) El dopaje de PEDOT:PSS con etilenglicol (EG) mejora ligeramente la capacidad y potencial en carga/descarga cuando el polímero se usa en la masa del electrodo, comparado con lo observado para el electrodo con 1 % w/w de PEDOT:PSS sin dopar. Por el contrario, el dopaje con dimetilsulfóxido (DMSO) resulta perjudicial para el comportamiento electroquímico. El recubrimiento de PEDOT:PSS dopado mediante EG o DMSO, y depositado sobre el colector de corriente incrementa la capacidad del electrodo basado en  $\text{LiFePO}_4$  y disminuye su polarización a tasas altas de carga/descarga. Las buenas prestaciones de los electrodos que contienen PEDOT:PSS dopado mediante EG se atribuyen a la alta proporción de la fase conductora electrónica PEDOT, como se evidenció mediante el análisis XPS cuantitativo.

Chapter 5

- 15) La correlación entre los valores de impedancia inicial, de resistencia de corriente directa y de capacidad a velocidades altas de descarga, mostró que la interface entre la capa de electrodo y el colector de corriente tiene el mayor impacto en el comportamiento electroquímico de los electrodos que contienen PEDOT:PSS. En este sentido, el PEDOT:PSS dopado con EG y empleado como recubrimiento del colector de corriente se destaca como el mejor procedimiento entre todas las estrategias descritas en esta tesis para mejorar el funcionamiento de electrodos basados en  $\text{LiFePO}_4$ .

Chapter 5

- 16) Los electrodos compuestos con PEDOT:PSS presentan mayor voltaje y capacidad en descarga que los electrodos compuestos con PEDOT sintetizado por vía electroquímica debido a tres factores: 1) la mayor conductividad del PEDOT:PSS sin dopar y dopado, 2) las dificultades para dispersar el polvo de PEDOT sintetizado por vía electroquímica, y 3) las mejores propiedades de formación de película del PEDOT:PSS. Chapters 3 and 5.





# Appendix I

## Comparison of the performance of $\text{LiFePO}_4$ -based composite electrodes with conducting polymer

Figure 1. Comparison of capacity and energy density values at 2C rate, referred to the weight of the active material.

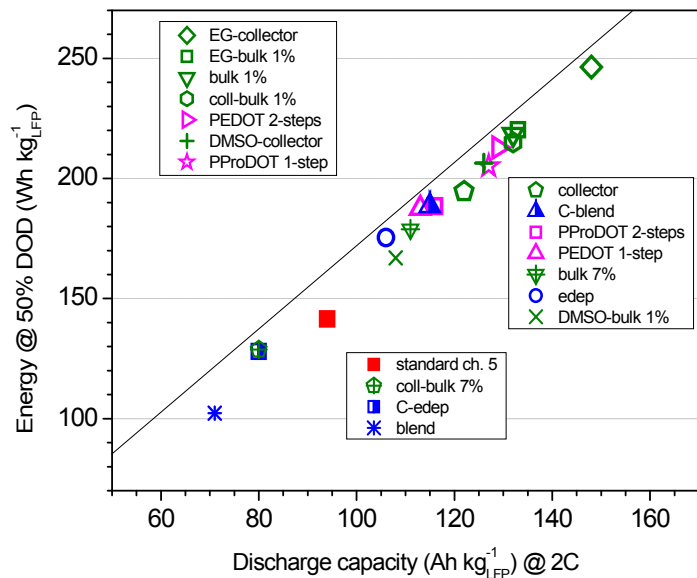
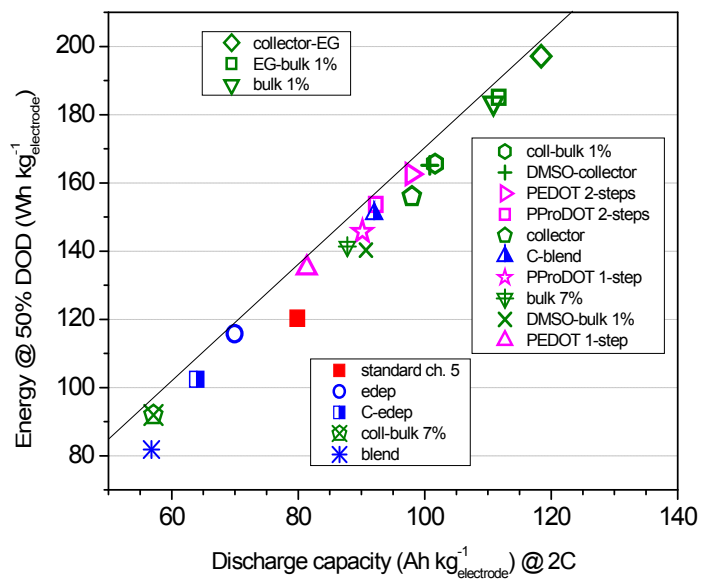


Figure 2. Comparison of capacity and energy density values at 2C rate, referred to the weight of the electrode (active material, additives and conducting polymer) without considering the current collector.






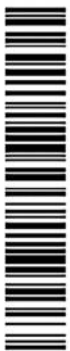
## Appendix II

### Other scientific contributions related to the topic of the thesis

1. Solicitud de Patente: Batería de iones alcalinos y método para producir la misma  
Inventores: CÍNTORA JUAREZ Daniel; AHMAD Shahzada; PÉREZ VICENTE Carlos; TIRADO COELLO José Luis; KAZIM Samrana y DOBLARÉ CASTELLANO Manuel. Solicitud No. 201331793, 5 de diciembre, 2013. International Publication Number: WO 2015/082711 A1. International Publication Date: 11 June 2015.
2. Article: LiFePO<sub>4</sub> particle conductive composite strategies for improving cathode rate capability  
Authors: N. Vicente, M. Haro, D. Cíntora-Juárez, C. Pérez-Vicente, J. L. Tirado, S. Ahmad and G. Garcia-Belmonte. *Electrochim. Acta*, 2015, 163, 323–329.
3. Article: Effect of the degree of porosity on the performance of poly(vinylidene fluoride-trifluoroethylene)/poly(ethylene oxide) blend membranes for lithium-ion battery separators  
Authors: A. Gören, C.M. Costa, M.N. Tamaño Machiavello, D. Cíntora-Juárez, J. Nunes-Pereira, J.L. Tirado, M.M. Silva, J.L. Gomez Ribelles, S. Lancers-Méndez. *Solid State Ionics*, 2015 (280), 1–9.
4. Article: Influence of Solvent Evaporation Rate in the Preparation of Carbon-Coated Lithium Iron Phosphate Cathode Films on Battery Performance LiFePO<sub>4</sub>  
Authors: A. Gören, D. Cíntora-Juárez, P. Martins, S. Ferdov, M.M. Silva, J.L. Tirado, C.M. Costa, S. Lancers-Méndez. *Energy Technol.* Article first published online: 22 DEC 2015. DOI: 10.1002/ente.201500392.
5. Article: Truly quasi-solid-state lithium cells utilizing carbonate free polymer electrolytes on engineered LiFePO<sub>4</sub>  
Authors: Jijeesh R. Nair, Daniel Cíntora-Juárez, Carlos Pérez-Vicente, José L. Tirado, Shahzada Ahmad, Claudio Gerbaldi. To appear in *Electrochim. Acta*, <http://dx.doi.org/doi:10.1016/j.electacta.2016.03.156>

OFICINA ESPAÑOLA DE  
PATENTES Y MARCAS  
ESPAÑA





① Número de publicación: **2 537 588**

② Número de solicitud: 201331793

⑤ Int. Cl.:  
**H01M 6/14** (2006.01)

**A2**

**SOLICITUD DE PATENTE**

⑦ Solicitantes:  
**ABENGOA RESEARCH, S.L. (100.0%)**  
Campus Palmas Altas, Calle Energía Solar, 1  
41018 Sevilla ES


⑧ Inventores:  
**CINTORA JUÁREZ, Daniel;**  
**AHMAD, Shahzad;**  
**PEREZ VICENTE, Carlos;**  
**TIRADO COELLO, José Luis;**  
**KAZIM, Samrana y**  
**DOBLARE CASTELLANO, Manuel**


⑨ Agente/Representante:  
**VALLEJO LÓPEZ, Juan Pedro**

⑩ Título: **Baterías de iones alcalinos y método para producir la misma**

⑪ Resumen:  
La presente invención se refiere a métodos para producir una batería de iones alcalinos y a una batería de iones alcalinos secundaria. De acuerdo con el método de la invención, se monta una batería de iones alcalinos, en donde dicha batería comprende un electrodo que comprende monómeros polimerizables o un cátodo sobre el que pueden añadirse monómeros polimerizables antes de ponerlo en contacto con el electrolito. Cuando se carga la batería, se forma un revestimiento de polímero sobre el cátodo de la batería. En una realización preferida, el cátodo compuesto que comprende el polímero se forma in situ, es decir, en el interior de la batería de iones alcalinos montada. Las baterías alcalinas de la invención tienen unas capacidades más altas; adolecen de menos pérdida de capacidad a tasas de descarga más altas. Además, las baterías de la invención tienen una mayor fiabilidad de batería ya que el desvanecimiento de la capacidad disminuye y el rendimiento de tasa aumenta.

OFICINA ESPAÑOLA DE  
PATENTES Y MARCAS  
ESPAÑA





⑫ Internacional Publication Number  
**WO 2015/082711 A1**

⑬ International Patent Classification:  
**H01M 4/04 (2006.01) H01M 4/38 (2010.01)**  
**H01M 4/156 (2010.01) H01M 4/60 (2006.01)**  
**H01M 4/137 (2010.01) H01M 10/04 (2006.01)**  
**H01M 4/1397 (2010.01) H01M 10/052 (2010.01)**  
**H01M 4/1399 (2010.01) H01M 10/0567 (2010.01)**  
**H01M 4/36 (2006.01) C06G 6/12 (2006.01)**

⑭ International Application Number:  
**PCT/EP2014/076787**

⑮ International Filing Date:  
**5 December 2014 (05.12.2014)**

⑯ Filing Language:  
**English**

⑰ Publication Language:  
**English**

⑱ Priority Date:  
**5 December 2013 (05.12.2013)**

⑲ Applicant:  
**ABENGOA RESEARCH, S.L. [ES/ES]**  
Campus Palmas Altas, Calle Energía Solar nº1, E-41014 Sevilla (ES).

⑳ Inventors:  
**CINTORA JUÁREZ, Daniel; AHI, Ronda de los Tejares, nº 9, 1º-2, E-14001 Córdoba (ES), AHMAD, Shahzad, Calle de Corbea 2, Vivienda 6, E-14012 Sevilla (ES), PEREZ VICENTE, Carlos, Pedroche 5, portal 2, piso 3-1, E-14006 Córdoba (ES), TIRADO COELLO, GW, KM, ML, MR, NI, NS, TD, TU).**

**(10) International Publication Number**  
**WO 2015/082711 A1**

⑳ International Patent Classification:  
**H01M 4/04 (2006.01) H01M 4/38 (2010.01)**  
**H01M 4/156 (2010.01) H01M 4/60 (2006.01)**  
**H01M 4/137 (2010.01) H01M 10/04 (2006.01)**  
**H01M 4/1397 (2010.01) H01M 10/052 (2010.01)**  
**H01M 4/1399 (2010.01) H01M 10/0567 (2010.01)**  
**H01M 4/36 (2006.01) C06G 6/12 (2006.01)**

㉑ Designated States (unless otherwise indicated, for every kind of national protection available): AE, AG, AL, AM, AN, AU, BA, BB, BG, BH, BR, CA, CN, CO, CR, CU, CY, CZ, DE, DK, DM, DO, DZ, EC, EG, ES, FI, GB, GD, GE, GH, GM, GT, HN, HR, HU, IL, IN, IR, IS, JP, KE, KG, KN, KP, KR, KZ, LA, LC, LK, LR, LS, LU, LY, MA, MD, ME, MG, MK, MN, MW, MX, MY, MZ, NA, NG, NI, NO, NZ, OM, PA, PE, PG, PH, PL, PT, QA, RO, RU, RW, SA, SC, SD, SE, SG, SK, SL, SM, ST, SV, SY, TH, TI, TN, TR, TT, TZ, UA, UG, US, UZ, VN, ZA, ZM, ZW.

㉒ Designated States (unless otherwise indicated, for every kind of regional protection available): ARIPO (BW, GH, GM, KE, LR, LS, MW, MZ, NA, RW, SD, SL, SZ, TZ, UG, ZM, ZW), Eurasian (AM, AZ, BY, KG, KZ, RU, TJ, TM), European (AL, AT, BE, BG, CH, CY, CZ, DE, DK, EE, ES, FI, FR, GB, GR, HR, HU, IE, IT, LT, LU, LV, MC, MK, MT, NL, NO, PL, PT, RO, RS, SE, SI, SK, SM, TR), OAPI (BF, BJ, CF, CG, CI, CM, GA, GN, GQ, GW, KM, ML, MR, NI, NS, TD, TU).

㉓ Abstract: The present invention relates to methods for producing an alkali ion battery and to a secondary alkali ion battery. In accordance with the method of the invention, an alkali ion battery is assembled, wherein said battery comprises an electrolyte comprising polymerizable monomers or a cathode on which polymerizable monomers can be added before charging in contact with the electrolyte. When charged, the battery polymer coating is formed on the cathode of the battery. In a preferred embodiment, the composite cathode comprising the polymer is formed in situ, that is, within the assembled alkali ion battery. The alkali batteries of the invention have higher capacities; suffer less capacity loss at faster discharge rates. Furthermore, the batteries of the invention have increased battery reliability in that capacity fading decreases and rate performance increases.

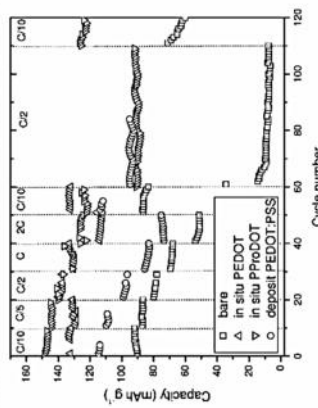


Figure 3



## LiFePO<sub>4</sub> particle conductive composite strategies for improving cathode rate capability



Nuria Vicente<sup>a</sup>, Marta Haro<sup>a</sup>, Daniel Cíntora-Juárez<sup>b</sup>, Carlos Pérez-Vicente<sup>b</sup>, José Luis Tirado<sup>b</sup>, Shahzada Ahmad<sup>c,\*</sup>, Germà Garcia-Belmonte<sup>a,\*</sup>

<sup>a</sup> Photovoltaics and Optoelectronic Devices Group, Departament de Física, Universitat Jaume I, 12071 Castelló, Spain

<sup>b</sup> Laboratorio de Química Inorgánica, Campus de Rabanales, Universidad de Córdoba, 14071, Spain

<sup>c</sup> Abengoa Research, Abengoa, C/Energía Solar n° 1, Campus Palmas Altas, 41014 Seville, Spain

### ARTICLE INFO

#### Article history:

Received 14 January 2015

Received in revised form 17 February 2015

Accepted 17 February 2015

Available online 18 February 2015

#### Keywords:

LiFePO<sub>4</sub> composite  
impedance spectroscopy  
conductive polymer

### ABSTRACT

Lithium iron phosphate (LFP) cathodes are one of the most promising candidates to find application in hybrid electric vehicle energy storage system. For this reason advances in the performance of its theoretical capacity at high charge/discharge rates is under continuous development. Most used strategies to improve power performance are the addition to the LFP particles of an electric conductive carbon or polymer, such as poly(3,4-ethylenedioxythiophene) [PEDOT] doped with polystyrene sulfonate (PSS). The data obtained from impedance analysis provide new insight on the role of these additives that not only improve the charge transfer but also favor the lithiation/delithiation processes in the phosphate matrix. Furthermore, PEDOT is capable to reduce the resistances of charge transfer and lithiation reaction inside the phosphate matrix by one order of magnitude in comparison with those achieved with the carbon coating strategy. In this study, the most effective approach has been the addition of PEDOT by a blending method, resulting in a specific capacity of 130 mA h g<sup>-1</sup> at 2 C.

© 2015 Elsevier Ltd. All rights reserved.

### 1. Introduction

In the last decades, lithium iron phosphate (LiFePO<sub>4</sub>) has been extensively studied, and currently it is regarded as one of the most likely candidate for the large-sized Li-ion batteries for hybrid electric vehicles (HEV) [1]. Other applications include cathode in portable electronic devices, bulk electricity storage at power stations and to provide back-up energy for solar and wind power [2,3]. This electrode has attracted extensive attention due to a high theoretical specific capacity (170 mA h g<sup>-1</sup>), high stability, low cost, high compatibility with environment, and small amount of oxygen generation at the fully charged state. Its main drawback is to attain the full capacity due to its low electronic conductivity which leads to initial capacity loss and poor rate capability.

To gain the full capacity of these materials, the mechanism of charging–discharging of this cathode has been deeply studied [4,5] and explained in terms of charge transfer followed by a phase change, denominated “domino-cascade model” [4]. In the LiFePO<sub>4</sub>

olivine structure, the oxygen atoms adopt a hexagonal closed-packing configuration with Li<sup>+</sup> and Fe<sup>2+</sup> cations located in half of the octahedral sites and P<sup>5+</sup> cations in 1/8 of tetrahedral sites. Then, there exist 1D channels for Li<sup>+</sup> ions exchange. Once the mechanism is understood, several strategies have been investigated to improve both electronic and ionic conductivity to overcome the current bottleneck in these materials. Two of these strategies are the addition to the LFP particles of electric conductive carbon and/or polymers. Carbon improves the electronic conductivity and can contribute to increase the electrode capacity [6–10]. However, perfect surface coatings and desired mixtures are often very difficult to achieve and the power-performance enhancement of these electrode materials is still limited. More recently, the use of conductive polymers such as poly(3,4-ethylenedioxythiophene) (PEDOT) doped with polystyrene sulfonate (PSS) is especially attractive in terms of the improvement of the mechanical flexibility, the option to be coated under mild processing conditions compared to carbon coating, improvement of Li-ion transport, and for its dual role as conductive and binder additive [11–13]. For these reasons, PEDOT like other materials such as ZnO, [14] has increased interest in the energy scientific community with multipurpose features and applications (photovoltaics, photoelectrochemistry besides in energy storage) [15]. In these cathodes,

\* Corresponding author.

E-mail address: [garcia@uji.es](mailto:garcia@uji.es) (G. Garcia-Belmonte).





Contents lists available at ScienceDirect

Solid State Ionics

journal homepage: [www.elsevier.com/locate/ssi](http://www.elsevier.com/locate/ssi)

## Effect of the degree of porosity on the performance of poly(vinylidene fluoride-trifluoroethylene)/poly(ethylene oxide) blend membranes for lithium-ion battery separators



A. Gören<sup>a,b</sup>, C.M. Costa<sup>a,\*</sup>, M.N. Tamaño Machiavello<sup>c</sup>, D. Cíntora-Juárez<sup>d</sup>, J. Nunes-Pereira<sup>a</sup>, J.L. Tirado<sup>d</sup>, M.M. Silva<sup>b</sup>, J.L. Gomez Ribelles<sup>c,e</sup>, S. Lanceros-Méndez<sup>a,\*</sup>

<sup>a</sup> Centro/Departamento de Física, Universidade do Minho, 4710-057 Braga, Portugal

<sup>b</sup> Centro/Departamento de Química, Universidade do Minho, 4710-057 Braga, Portugal

<sup>c</sup> Center for Biomaterials and Tissue Engineering, CIBIT, Universitat Politècnica de València, 46022 Valencia, Spain

<sup>d</sup> Laboratorio de Química Inorgánica, Universidad de Córdoba, Edificio Marie Curie, Campus de Rabanales, 14071 Córdoba, Spain

<sup>e</sup> Networking Research Center on Bioengineering, Biomaterials and Nanomedicine, (CIBER-BBN), Valencia, Spain

### ARTICLE INFO

#### Article history:

Received 17 April 2015

Received in revised form 29 July 2015

Accepted 6 August 2015

Available online 21 August 2015

#### Keywords:

PVDF-TrFE

PEO

Battery separator

Lithium-ion battery application

### ABSTRACT

Porous polymer membranes based on poly(vinylidene fluoride-trifluoroethylene)/poly(ethylene oxide) copolymers, P(VDF-TrFE)/PEO, are prepared through elimination (from partial to total) of PEO, leading to interconnected micropores in the polymer blends.

Electrolyte uptake, thermal and mechanical properties depend on the amount of PEO present in the polymer blend. Further, the degree of crystallinity of PEO and the elastic modulus ( $E'$ ) of the polymer blend decrease with increasing PEO removal.

Electrical properties of the polymer blend membranes are influenced by the porosity and are dominated by diffusion. The temperature dependence of the ionic conductivity follows the Arrhenius behavior. The ionic conductivity is the highest for the membranes with a volume fraction of pores of 44% (i.e., 90% PEO removal), reaching a value of  $0.54 \text{ mS cm}^{-1}$  at room temperature.

Battery performance was determined by assembling Li/C-LiFePO<sub>4</sub> swagelok cells. The polymer blends with 90% PEO removal exhibit rate ( $124 \text{ mAhg}^{-1}$  at C/5 and  $47 \text{ mAhg}^{-1}$  at 2C) and cycling capabilities suitable for lithium ion battery applications.

© 2015 Elsevier B.V. All rights reserved.

### 1. Introduction

Rechargeable Li-ion batteries are the most intensively studied energy storage systems for applications in computers, mobile phones and electric vehicles, among others, due to their outstanding properties: they are lighter and cheaper than other battery types, show high specific energy (100–265 Wh/Kg) and suitable power/weight relation (1800 W/Kg) [1,2].

The main goal of the different investigations is to maximize the energy and power per unit of weight or volume taking into account its safety [3–5].

One essential component in Li-ion batteries is the polymer electrolyte (PE). PE are defined as macromolecular systems (polymer blended or complexes with salts [6]) with high ionic conductivity ( $>10^{-7}$  at  $10^{-1} \text{ S/cm}$ ) [7,8]. Further, polymer electrolytes can be used in multiple applications, including electrochromic devices [9–11], fuel cells [12,13]

and sensors/actuators [14], supercapacitors/ultracapacitors [15], together with Li-ion batteries [4,16].

Solid polymer electrolytes (SPE) [8], gel polymer electrolytes (GPE) [17] and composite polymer electrolytes (CPE) [18] are different types of polymer electrolytes (PEs).

The SPE are the ones with the simplest fabrication. For Li-ion battery applications, different lithium salts are dissolved in a polymeric matrix. CPE are very similar to SPE but differ in the inclusion of different nanofillers (inert oxide ceramic, molecular sieves, metallic, carbonaceous fillers, ferroelectric materials) dispersed in the polymer matrix to improve the mechanical, thermal and electrochemical properties. The GPE are obtained in two steps, first the salts are dissolved in a polar or ionic liquid and then added to a host polymer to provide an adequate mechanical stability [19,20].

For battery applications, the separator/electrolyte is extremely important as it separates both electrodes (anode and cathode), controls the number of ions and allows the movement of the ions between the electrodes during the charge and discharge process of the battery [21].

The main parameters of a separator/electrolyte are permeability, porosity/pore size, electrolyte absorption and retention, low ionic

\* Corresponding authors.

E-mail addresses: [cmcosta@fisica.uminho.pt](mailto:cmcosta@fisica.uminho.pt) (C.M. Costa), [lanceros@fisica.uminho.pt](mailto:lanceros@fisica.uminho.pt) (S. Lanceros-Méndez).

## Influence of Solvent Evaporation Rate in the Preparation of Carbon-Coated Lithium Iron Phosphate Cathode Films on Battery Performance

Attila Gören,<sup>[a, b]</sup> Daniel Cíntora-Juárez,<sup>[c]</sup> Pedro Martins,<sup>[a]</sup> Stanislav Ferdov,<sup>[a]</sup> Maria Manuela Silva,<sup>[b]</sup> José Luís Tirado,<sup>[c]</sup> Carlos M. Costa,<sup>\*,[a, b]</sup> and Senentxu Lanceros-Méndez<sup>[a]</sup>

In this work, the drying step for cathodes based on carbon-coated LiFePO<sub>4</sub> prepared in the temperature range of 60–120 °C has been investigated in detail. The microstructure of the cathode shows a homogeneous distribution of the active material and conductive additive particles independent of the drying temperature. However, the results of impedance spectroscopy and cycling voltammetry are affected by the drying temperature. The solvent evaporation temperature, therefore, affects the polymer binder distribution and its

characteristics, which include the polar phase content of the polymer and its affinity with the other components of the cathode. The discharge capacity value after 50 cycles is 120 and 81 mAh g<sup>-1</sup> for the samples dried at 80 and 60 °C, respectively, which show the best and worst battery performance, respectively. It was concluded that carbon-coated LiFePO<sub>4</sub> cathodes should be prepared at drying temperatures between 80 and 100 °C for optimized performance.

### Introduction

The rechargeable battery market is estimated to reach ~60 billion U.S. dollars in 2015 because of the growth of the automotive and mobile phone sectors and because of the emergence of new fields of application such as radiofrequency identification devices, e-labels, e-packaging, and medical disposables for diagnostics and drug delivery, among others.<sup>[1]</sup> The growth of the rechargeable battery market is mainly based on Li-ion batteries, which have a market share of 75%.<sup>[1]</sup> Commercial Li-ion secondary cells, introduced to the market in 1992, consist mainly of two Li-ion intercalation electrodes (anode and cathode) with a separator/electrolyte for ionic conduction between them.<sup>[2]</sup> In comparison with other battery types, such as Ni–Cd, Li-ion batteries show significant advantages as they are light and cheap, show a high energy density (100–150 Wh kg<sup>-1</sup>), and have a large number of charge/discharge cycles.<sup>[3]</sup>

The cathode is one of the most important components of batteries<sup>[4]</sup> as it determines its capacity. The materials used for cathodes must show the following characteristics: they must be easily reducible (such as, for example, a transition metal), react with Li in a reversible manner, should be a good electronic conductor, preferably a metal, and must be stable, that is, they should not undergo structural changes or degradation during charge and discharge of the battery.<sup>[5]</sup> The most used materials for cathodes are LiCoO<sub>2</sub>,<sup>[6]</sup> Li[Mn, Ni, Co]O<sub>2</sub>,<sup>[7]</sup> lithium metal polyoxyanion Li<sub>3</sub>V<sub>2</sub>PO<sub>4</sub>,<sup>[8]</sup> LiMPO<sub>4</sub>, and LiMSiO<sub>4</sub> (M = Mn, Fe, Co, and their combinations).<sup>[9]</sup>

Lithium iron phosphate (LiFePO<sub>4</sub>),<sup>[10]</sup> which has an olivine-type structure, has attracted much attention because of

its low cost, low density (3.6 g cm<sup>-3</sup>), and high theoretical capacity of 170 mAh g<sup>-1</sup> (2.0–4.0 V).<sup>[11,12]</sup> LiFePO<sub>4</sub> is one of the materials used for electric vehicle (EV) applications.<sup>[13]</sup> The drawbacks of LiFePO<sub>4</sub> are its low electrical conductivity (~10<sup>-9</sup> S cm<sup>-1</sup>)<sup>[14]</sup> and low lithium ion diffusivity (~10<sup>-18</sup> cm<sup>2</sup> s<sup>-1</sup>).<sup>[15]</sup> To overcome the low electronic conductivity and improve the electrochemical performance and thermal stability of LiFePO<sub>4</sub>, the coating of LiFePO<sub>4</sub> nanoparticles with different carbonaceous compounds has been proposed.<sup>[16,17]</sup>

Thus, different methods have been developed to synthesize small-particle-size and high-purity carbon-coated LiFePO<sub>4</sub> (C-LiFePO<sub>4</sub>) to improve the electrochemical performance of the battery by improving the rate performance and capacity. These methods include solid-state synthesis,<sup>[18]</sup> mechanochemical activation,<sup>[19]</sup> microwave heating,<sup>[20]</sup> hydrothermal

[a] A. Gören, Dr. P. Martins, Dr. S. Ferdov, Dr. C. M. Costa, Prof. S. Lanceros-Méndez  
Centre/Department of Physics  
University of Minho  
Campus de Gualtar, 4710-057 Braga (Portugal)  
cmcosta@fisica.uminho.pt

[b] A. Gören, Prof. M. M. Silva, Dr. C. M. Costa  
Centre/Department of Chemistry  
University of Minho  
Campus de Gualtar, 4710-057 Braga (Portugal)

[c] D. Cíntora-Juárez, Prof. J. L. Tirado  
Laboratorio de Química Inorgánica  
Universidad de Córdoba, Edificio Maria Curie  
Campus de Rabanales, 14071 Córdoba (Spain)

## Accepted Manuscript

Title: Truly quasi-solid-state lithium cells utilizing carbonate free polymer electrolytes on engineered LiFePO<sub>4</sub>

Author: Jijeesh R. Nair Daniel Cíntora-Juárez Carlos Pérez-Vicente José L. Tirado Shahzada Ahmad Claudio Gerbaldi



PII: S0013-4686(16)30727-7  
DOI: <http://dx.doi.org/doi:10.1016/j.electacta.2016.03.156>  
Reference: EA 26986

To appear in: *Electrochimica Acta*

Received date: 18-1-2016

Revised date: 23-3-2016

Accepted date: 26-3-2016

Please cite this article as: Jijeesh R.Nair, Daniel Cíntora-Juárez, Carlos Pérez-Vicente, José L.Tirado, Shahzada Ahmad, Claudio Gerbaldi, Truly quasi-solid-state lithium cells utilizing carbonate free polymer electrolytes on engineered LiFePO<sub>4</sub>, *Electrochimica Acta* <http://dx.doi.org/10.1016/j.electacta.2016.03.156>

This is a PDF file of an unedited manuscript that has been accepted for publication. As a service to our customers we are providing this early version of the manuscript. The manuscript will undergo copyediting, typesetting, and review of the resulting proof before it is published in its final form. Please note that during the production process errors may be discovered which could affect the content, and all legal disclaimers that apply to the journal pertain.

# Appendix III

## Characterization techniques

1. Galvanostatic battery cycling	168
2. Electrochemical impedance spectroscopy	171
3. X-ray photoelectron spectroscopy	174
4. Scanning electron microscopy	177
5. Mössbauer spectroscopy	180
References	184

## 1. Galvanostatic battery cycling

Different protocols are available for evaluating the charge/discharge performance of battery electrodes and full batteries. These protocols differ both in the parameters that are controlled or monitored during the experiment (e.g. potential, current, resistance, charge) and in the way to carry out the control (e.g. fixed value, stepped or intermittent variation). Galvanostatic cycling with potential limitation (GCPL) is one of the most popular protocols for testing Li-ion batteries. GCPL consists in setting a constant charging or discharging current between a counter and a working electrode, and monitoring the voltage of the later as a function of time until a specified cut-off voltage value is reached. The cut-off voltages for charge and for discharge are set at specific values in order to avoid triggering detrimental reactions of the battery components.

GCPL resembles the standard constant-current constant-voltage protocol (CCCV) used for charging Li-ion batteries. CCCV consists in applying a constant current until the battery reaches a certain voltage at which the charging mode switches to constant voltage until the charging current drops to a low value. In this sense, GCPL provides the first insights into the charge/discharge characteristics of battery electrodes and batteries such as the voltage profiles, the capacity values, the coulombic efficiency, the reversibility, the cycle life, among other features.

The theory for the galvanostatic reduction of freely-diffusing  $O$  species that transform into  $R$ , both species being characterized by rapid electron transfer reactions in an homogeneous medium, provides a Nernstian relationship between the potential and the time as expressed in Eq. 1.

$$E(t) = E^0 - \frac{RT}{2nF} \ln \frac{D_O}{D_R} + \frac{RT}{nF} \ln \left( \frac{\tau^{1/2} - t^{1/2}}{t^{1/2}} \right) \quad (1)$$

In the above equation  $E^0$  ≡ standard redox potential,  $R$  ≡ universal gas constant,  $n$  ≡ mole number of electrons transferred,  $F$  ≡ Faraday constant,  $D_O$  ≡ Diffusion coefficient of  $O$ ,  $D_R$  ≡ Diffusion coefficient of  $R$ ,  $t$  ≡ time and  $\tau$  ≡ transition time. The transition time is related to the time during which the flux of  $O$  species can maintain the imposed current.[1] Fig. 1a shows a constant current program and the corresponding potential vs. time profiles that follow Eq. 1. The  $E$  vs.  $t$  profiles shown in Fig. 1a resemble the profiles determined by galvanostatic cycling of some rechargeable batteries, including batteries based on insertion materials. Nevertheless, the thermodynamical and the kinetic considerations needed for deducing a relationship between the potential and other time-related parameters (charge or composition) of insertion materials require models that consider features proper of the topotactic insertion/extraction reaction of a guest ion into or out of a redox-active host compound. One of such models is the lattice gas model, which considers an insertion compound  $A_yMX$  as an ideal solution composed by the guest ions  $A$  (the solute) and the host lattice  $MX$  (the solvent).[2] The

thermodynamical description of this ideal solution approximation requires the following assumptions: i) one ion occupies one random site in the host lattice, ii) electroneutrality is observed, iii) there is no strong interaction between particles, and iv) the chemical potential of electrons is constant.

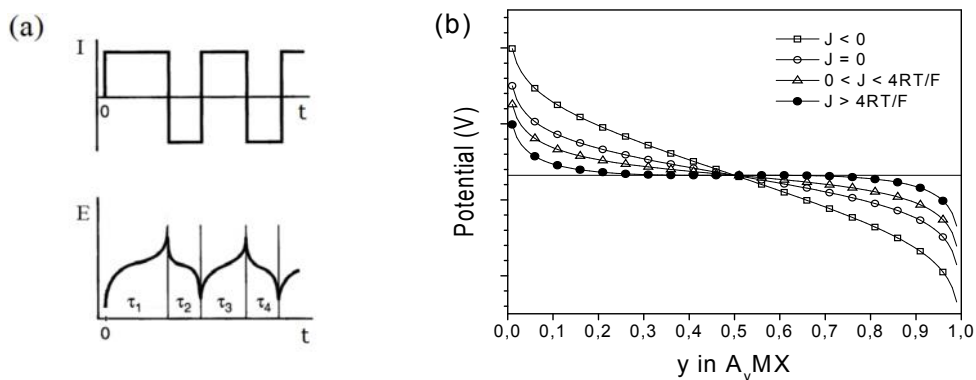


Figure 1. a) Galvanostatic cyclic programs and the corresponding theoretical potential profiles for a system composed of a freely-diffusing reactant and a product in homogeneous medium. Adapted from ref.[1] b) Theoretical variation of the potential as a function of inserted fraction  $y$  according to the lattice gas model.

Under the above mentioned assumptions, the chemical potential ( $\sim$ ) for the guest ion in the host corresponds to the change in the Gibbs free energy ( $G$ ) with the number of the intercalated ions ( $n$ ), which is related to the enthalpy ( $H$ ) variation, to the temperature ( $T$ ) and to the entropy ( $S$ ) variation, as expressed in Eq. 2.

$$\sim = \frac{\partial G}{\partial n} = \frac{\partial H}{\partial n} - T \frac{\partial S}{\partial n} \quad (2)$$

Statistical mechanics can be applied for deriving the entropy of the possible states of a fraction  $y$  of ions distributed over  $N$  available sites in the lattice. Considering the relation between the chemical potential and the electrochemical potential:  $\sim = -nFE$ , and expression of the partial entropy:  $\partial S/\partial n = -k \ln(y/(1-y))$ , where  $k \equiv$  Boltzmann constant, the potential variation as a function of the  $y$  fraction is given by Eq. 3:

$$E(y) = E^0 - \frac{RT}{nF} \ln\left(\frac{y}{1-y}\right) \quad (3)$$

For most insertion compounds, the ions inserted into the lattice may experience the energy field of neighbouring ions. To account for the ionic interactions, the term  $J(y-0.5)$ , with  $J \equiv$  interaction parameter, is considered and Eq. 3 transforms into Eq. 4.

$$E(y) = E^0 - \frac{RT}{nF} \ln\left(\frac{y}{1-y}\right) + J(y-0.5) \quad (4)$$

The intensity of the interaction, as quantified by the  $J$  parameter, has been associated to the type of transformation that the insertion compound undergoes as a function of the  $y$  fraction. It is said that the insertion/extraction reaction involve a single phase (or solid solution) in the following cases:  $J=0$  (no interaction),  $J < 0$  (repulsive interaction), or  $0 < J < 4RT/F$  (small attractive interaction). Thus, as shown in Fig. 1b, the potential varies almost constantly as a function of  $y$  for a single phase insertion reaction. For  $J > 4RT/F$ , Fig. 1b shows a composition interval of constant potential, also referred to as plateau. This feature is characteristic for a two phase system, as deduced by applying the phase rule to a system of two components (guest and host) and a degree of freedom (potential).

Regardless of its reaction mechanism, the electrochemical performance of active materials for batteries is characterized by two general features: i) the free energy change and ii) the extent of the electrochemical reaction. The change in free energy is related to the potential, which varies depending on the extent of the electrochemical reactions as the electrode delivers or accepts charge up to a degree determined by its capacity. Fig. 2 presents potential vs. capacity profiles of a half cell with  $\text{LiFePO}_4$ -based positive electrode in a battery tested using the GCPL protocol. The GCPL test parameters are indicated together with the data determined from the test, where  $Q_{\text{ch}} \equiv \text{Capacity in charge}$ ,  $Q_{\text{disch}} \equiv \text{Capacity in discharge}$ ,  $E \equiv \text{Charge/discharge polarization}$ ,  $Q_{\text{disch}50\% \text{DoD}} \equiv \text{Capacity in discharge at 50\% depth of discharge (DoD)}$ ,  $E_{\text{disch}50\% \text{DoD}} \equiv \text{Potential in discharge at 50\% DoD}$  and  $\text{Energy}_{50\% \text{DoD}} \equiv \text{Energy density in discharge at 50\% DoD}$  ( $\text{Energy}_{50\% \text{DoD}} = Q_{\text{disch}50\% \text{DoD}} \times E_{\text{disch}50\% \text{DoD}}$ ).

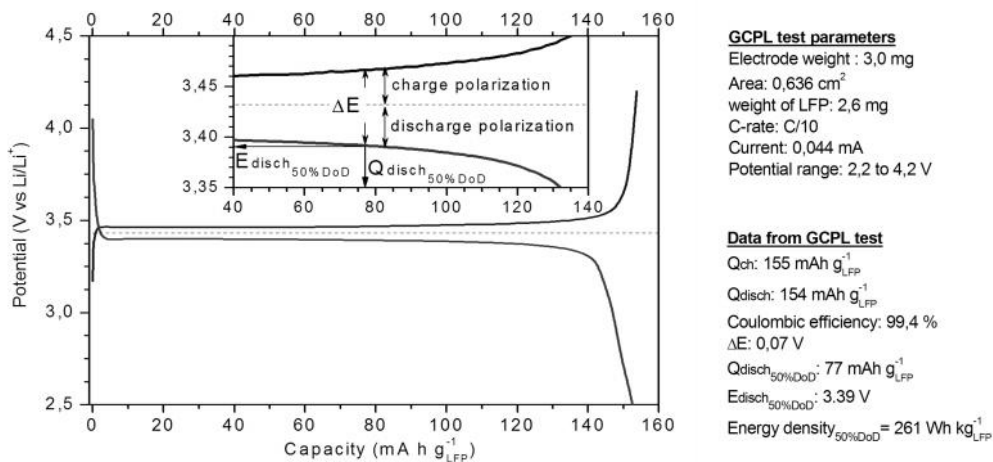


Figure 2. Test parameters and determination of different parameters used for describing and comparing the performance of a battery electrode from its charge/discharge plots.

## 2. Electrochemical impedance spectroscopy

Electrochemical Impedance spectroscopy is an analytical technique used for characterising the electrical properties of bulk materials and/or the interphases that these form as part of an electrochemical system. By analysing the response of the system upon excitation by a periodical voltage or current signal over a wide range of frequencies in a single experiment, it is possible to gain insight into the kinetics of charge transfer, the reaction mechanisms, the mobility of charge carriers, the dynamics of charge transport, among other properties and processes. EIS has been used for studying materials (solids, liquid or gels) that may be electronic conductors, ionic conductors, mixed electronic-ionic conductors, semiconductors or even insulators. In recent years, the application of EIS to the analysis of electrochemical devices such as batteries, fuel cells, capacitors or solar cells has led to a better understanding of some of the crucial physicochemical phenomena that affect the energy storage and conversion effectiveness of such devices.

The components of electrochemical systems (electrode materials, current collectors, electrolyte, membranes, coatings, etc.) resist to the flow of charge depending on their intrinsic properties and on external conditions. The parameter that quantifies the extent to which a material opposes a direct current is the resistance ( $R$ ), defined by Ohm's law as the ratio between the potential and the current:  $R = E/I$ . Nevertheless, this definition is valid only for ideal resistors. A more general concept of resistance, the impedance ( $Z$ ), extends to systems that show a frequency-dependant electric response to periodic, alternating current or potential stimuli, as well as a phase difference between the stimulus and the response signals.

The most common way to measure the impedance of an electrochemical system is by applying an alternating potential  $E(t)$  and then measuring the phase-shifted current  $I(t)$ . For an excitation of potential with known frequency, the ratio between the potential stimulus and the current response defines the impedance in the time domain, as expressed in Eq. 5.

$$Z(t) = \frac{E(t)}{I(t)} = \frac{E_0 \sin(\omega t)}{I_0 \sin(\omega t + \varphi)} = Z_0 \frac{\sin(\omega t)}{\sin(\omega t + \varphi)} \quad (5)$$

In Eq. 5 the zero sub-indexes refer to the amplitude,  $\omega \equiv$  angular frequency ( $\omega = 2\pi f$ , where  $f$  is the frequency),  $t \equiv$  time, and  $\varphi \equiv$  phase shift. Deducing electrical properties of a system from its time variant response to periodic voltage or current stimuli often involves the solution of intricate differential equations. Fourier transformation can be used to convert the voltage and current functions from the time domain into the frequency domain. This mathematical treatment provides reliable data if the system under study satisfies the conditions of linearity, causality and stability. Linearity, or pseudo-linearity, are promoted by applying stimuli of low amplitude (eg. a



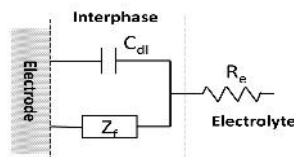
potential <10 mV) in order to produce a response with a high signal/noise ratio, but without altering the steady state. Causality means that the response of the system must be triggered only by the applied electrical stimulus, whereas stability implies that the system may preserve its composition, dimensions, temperature and other properties during the analysis. Eq. 6 expresses the impedance in the frequency domain, where  $j$  is the imaginary number. In this way, the impedance can be represented as a vector that may be plotted in polar or in rectangular coordinates.

$$Z(\%) = \frac{E_0 \exp(j\omega t)}{I_0 \exp(j\omega t - W)} = Z_0(\cos(W) + j \sin(W)) = Z' + jZ'' \quad (6)$$

There are two general approaches for analysing experimental EIS data. One approach consists in using or developing models based on physical theories that lead to the mathematical expression of the impedance function. The other approach considers that the physical processes and behaviour of the components of the system under study can be related to the individual or to the collective behaviour of idealized circuit elements (resistors, capacitors, inductors) arranged in different ways to constitute an equivalent circuit. For any of the two approaches, experimental impedance data are to be fitted in order to extract physicochemical parameters and to propose models that describe the properties and processes of the whole electrochemical system or its components.

The equivalent circuit approach is the most common one for fitting experimental EIS data. The general method for developing or using an equivalent circuit consists in recognizing the analogies between the behaviour of certain circuit elements and the nature of the physicochemical processes of the electrochemical system. For instance, resistors may account for the conductivity of a material or for the ease of charge transfer associated to an electrode reaction, whereas capacitors and inductors can be associated to space charge polarization and to adsorption phenomena, respectively.[3] Circuit elements are arranged depending on the known or hypothetical nature of the current paths and potential drops of the whole electrochemical system or its interacting components. Thus, when the total current is the sum of individual current contributions the circuit elements are arranged in parallel. If the total potential drop is the sum of individual contributions, then the circuit elements are arranged in series. A simple electrochemical system formed by an electrode in contact with an electrolyte can be modelled by the circuit shown in Fig. 3.

Figure 3. Equivalent circuit representation for an electrode in contact with an electrolyte.



In the circuit above  $R_e \equiv$  resistance of the electrolyte,  $C_{dl} \equiv$  double layer capacitance and  $Z_f \equiv$  faradaic impedance. For a single electron reaction on a uniform electrode where

mass transport is relevant (*i.e.* mixed kinetic and diffusion control), the faradaic impedance is considered as a charge transfer resistance ( $R_{ct}$ ) connected in series to the so-called Warburg impedance ( $Z_w$ ). Additional circuit elements and their combinations are required for more complex systems that involve multistep reactions, adsorption phenomena, growth of passivating layers, etc. Besides, real systems have microscopic features that are distributed in space, which may be the case for non-uniform, rough surfaces or for polycrystalline electrodes with grain boundaries. In such cases, the ideal capacitor can be replaced by a constant phase element (CPE). The systems with space-distributed properties show a distribution of relaxation time (also known as time constant  $\tau$ ), which can be related to a distribution of activation energy barriers for charge transfer, hopping, diffusion, among other thermally activated processes.[4]

Fig. 4 shows different graphic representations of the simulated impedance of an electrochemical system characterized by two different relaxation time constants fitted by the equivalent circuit abbreviated as  $R_0+(R_1/C_1)+(R_2/C_2)$ . The resistance values can be obtained from the intercept of the semicircles at the  $Z'$ -axis, whereas capacitance at the characteristic frequency can be calculated as shown in Fig. 4a. These values can be useful as initial input for fitting the whole impedance spectrum using methods such as complex nonlinear least squares (CNLS) or deconvolution, both of which consider simultaneously a larger range of data.

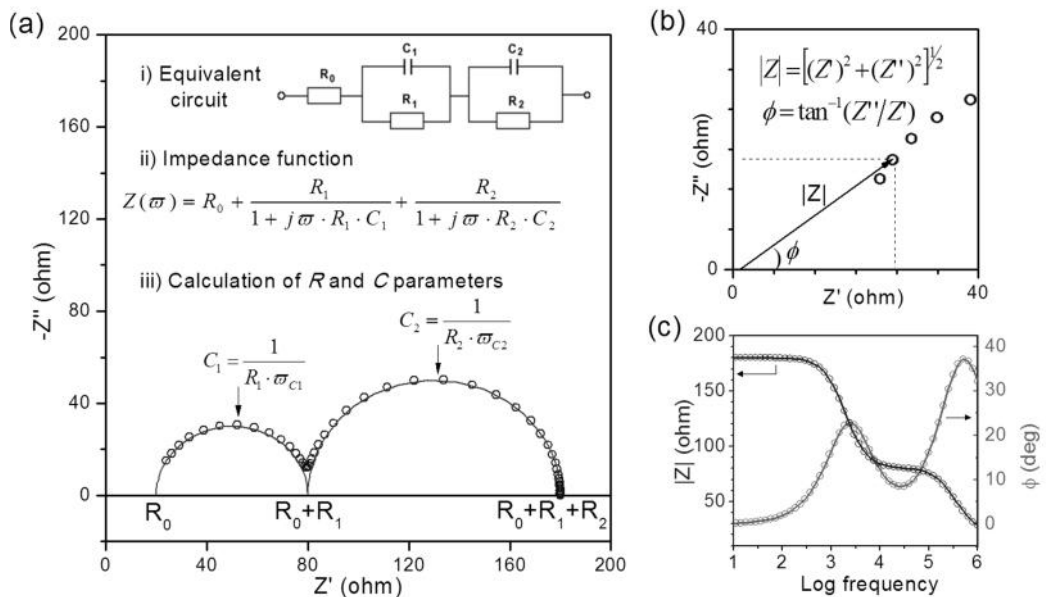


Figure 4. (a) Simulated data (blue) and individual semicircles (red) determined from fitting to the equivalent circuit (i) defined by its impedance function (ii). The calculation of  $R$  and  $C$  parameters is shown (iii). Frequency range: 1 Mhz-1mHz.  $R_0=20\Omega$ ,  $R_1=60\Omega$ ,  $R_2=100\Omega$ ,  $C_1=1E^{-8} F$ ,  $C_2=1E^{-6} F$ . (b) Nyquist plot of simulated impedance data, (c) Bode plots of the modulus and phase.

### 3. X-ray photoelectron spectroscopy

X-ray photoelectron spectroscopy (XPS) is a technique useful for the elemental analysis of the surface of materials such as metals, ceramics, semiconductors, polymers, among others with diverse forms including foils, thin films, powders etc. XPS is based on the analysis of the electrons emitted by the atoms in a sample upon excitation by X-ray photons from a source. The incident and the emitted radiation have characteristic, discrete energy values, which allow calculating the energies of the electronic states of the elements in the sample, and to relate these states to certain chemical configurations (oxidation state, partial charge, hybridization, etc.) of the atoms that compose surface layers of the sample. This technique has a detection limit of about 0.1 atom % at a depth of 1 to 10 nm, which corresponds to approximately 10 to 100 monolayers.

The ejection of X-ray photoelectrons from a material is caused by absorption and emission processes. When X-ray photons of characteristic energy pass through a sample, the incident photons can transfer energy to the electrons of the atoms by absorption processes that excite the electronic states. When excited electrons do not return to their initial state, the excess energy can cause photoelectrons to escape from the material leaving an electron vacancy (hole). X-ray absorption and photoelectron emission processes are depicted in Fig. 5a, together with the so-called Auger process, which is a relaxation mechanism consisting in the occupation of the inner electron vacancy by an electron lying in a state of lower binding energy. The energy released by the Auger process causes ejection of a second electron, so-called Auger electron. Other processes such as fluorescence, auto-ionization or direct two-electron ejection can lead to the emission of X-rays and electrons of characteristic energy.

Regarding the photoelectron emission, the kinetic energy (K.E.) gained by the electrons can be calculated from the energy conservation equation shown below:

$$K.E. = h\nu - B.E. - \phi \quad (7)$$

Where  $h\nu$   $\equiv$  energy of the incident photon,  $B.E.$   $\equiv$  binding energy of the electron in a given state and  $\phi$   $\equiv$  work function of the spectrometer. Fig. 5b presents a scheme of the energy barriers that the electron surmounts upon photoemission, and how the binding energy value may be deduced as:  $B.E. = h\nu - K.E. - \phi$

1 1

In general, XPS is considered as a non-destructive method of analysis, although some samples can undergo degradation due to charging or heating upon X-ray irradiation. Modern XPS apparatuses are equipped with Al and Mg X-ray sources that provide characteristic energies ( $K\alpha$  lines) of 1.4866 and 1.2536 keV, respectively. Electron and ion guns are also available in most spectrometers for Auger Electron Spectroscopy and for depth profiling analysis, respectively. The XPS experiment is

carried out under vacuum ( $< 10^{-8}$  mbar) in order to avoid gas molecules to contaminate the surface of the sample or to scatter the ejected electrons, which are focused onto an analyser, where they are counted as a function of their kinetic energy at certain time intervals. Thus, the X-ray photoelectron spectrum plot displays peaks at discrete energy values due to the emission of electrons from states of specific binding energies

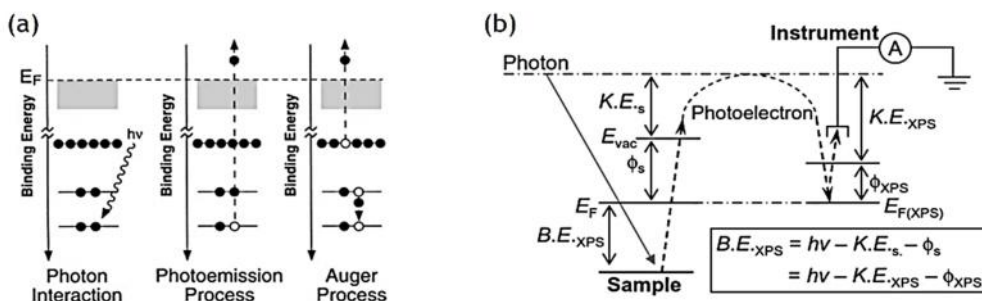


Figure 5. (a) Schematic representation of the main absorption/emission processes in XPS. (b) The relation between binding energy (B.E.), kinetic energy (K.E.) and work function ( $w$ : between the sample ( $s$ ) and the instrument (XPS)). Taken from ref.[5]

A routine XPS analysis consist in recording a survey spectrum that covers a broad interval of binding energy values, and then scanning specific regions depending on the elements and their electronic transitions of interest. Fig. 6 shows an XPS survey spectrum of a  $\text{LiFePO}_4$ -based electrode as those described in Chapter 5.

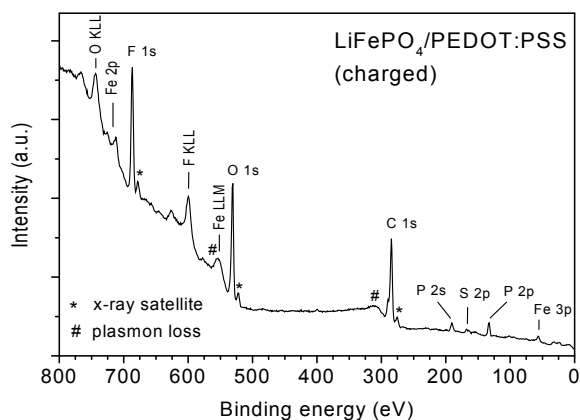


Figure 6. XPS survey spectrum of the surface of a charged composite electrode based on  $\text{LiFePO}_4$  and PEDOT:PSS.

Several databases and handbooks list binding energy values of photoelectron lines and Auger lines that can be used as reference. Nevertheless, expected shifts towards higher or lower binding energy values with respect to the reported reference values are indicative of the chemical environment of the atom due to variations in the oxidation state, substitution, proximity to electron donating or electron withdrawing atoms or

fragments, or due to effects related to the particle size or to the position of the atoms relative to the surface.[6] Thus, identification of elements and qualitative analysis is mostly based on the position of the peaks (both photoelectron and Auger) and on the shape of the peaks, which may be a sum of components due to overlapping of individual peaks from different contributions of the same element in different chemical states. Furthermore, for electronic transitions involving *p*, *d* or *f* orbitals, coupling between the electron spin and the orbital angular momentum causes splitting into two energy levels of different occupancy. For instance, in *p* orbitals, spin-orbit coupling totals an angular momentum of either 1/2 or 3/2, which in the emission spectrum results in a doublet of relative intensity 1:2. Additionally to the photoelectron and Auger lines, the XPS spectrum contains low background signals, as well as other features caused by inelastic scattering through interaction of the ejected electron with phonons (plasmon loss). Signals of lower intensity than the principal XPS lines (X-ray satellite) are present due to the non-monochromatic nature of the X-ray source. Other energy-loss processes, so-called, shake-up and shake-off satellites, may appear, respectively, due to excitation of a valence electron to unfilled higher energy levels and due to the excitation of a valence electron to an unbound, continuum state.

Quantitative analysis in XPS to obtain the composition of the sample mainly requires fitting, de-convoluting and integrating the XPS peaks, as well as background subtraction. Peak analysis is carried out using specialized software that considers theoretical or empirical models for the peak characteristics and applies constraints to the parameters of the signal, which include: position, line shape, area, FWHM and the sensitivity factor (*S*). For a homogeneous sample, considering a given photoelectron transition, the atomic concentration of an element is proportional to the peak intensity *I* as defined by Eq. 8:

$$n = \frac{I}{f \cdot \sigma \cdot \theta \cdot y \cdot \lambda \cdot A \cdot T} = \frac{I}{S} \quad (8)$$

where *n* ≡ number of atoms per cm<sup>3</sup>, *f* ≡ the X-ray flux irradiated on the sample,  $\sigma$  ≡ the photoelectric cross section for the atomic orbital of interest,  $\theta$  ≡ the angular efficiency factor for the instrument, *y* ≡ the efficiency of primary photoelectron production,  $\lambda$  ≡ the mean free path of the photoelectrons in the sample, *A* ≡ analyzed area of the sample and *T* ≡ the detection efficiency.[5] The sensitivity factor depends both on the type of photoelectron transition and the instrument, and can be calculated or determined empirically by using standard samples. If the constituent elements and the chemical formula of an analyte are known, the fractional atomic concentration of an element *A* (*C<sub>A</sub>*) can be estimated considering the sum of the ratios between peak intensities and sensitivity factors from all elements in the sample being analyzed [ $\sum_i (I_i/S_i)$ ], as expressed in Eq. 9:

$$C_A = \frac{I_A/S_A}{\sum_i (I_i/S_i)} \quad (9)$$

## 4. Scanning electron microscopy

Scanning electron microscopy (SEM) is an electron beam technique, which take advantage of the possibility of focusing and tuning the energy of an electron beam in order to probe different depths of a sample and provide 3-D images of its surface. The different signals generated through the interaction of the electron beam and the sample may provide information related to the sample's topography, its morphology, its elemental composition, phase distribution, crystal orientation, among other properties. SEM has three major advantages over optical microscopy: (i) a wide range of magnification from 3-10x to 150000x, (ii) a depth of field ca. 300 times higher than that of the optical microscope, and (iii) resolution of 1-10 nm. Although non-conducting samples may require a conducting coating of gold or carbon for SEM analysis, typically no special preparation is required other than adjusting the size or shape for fitting the specimen to the sample holder.

Due to its versatility scanning electron microscopes are used in diverse fields, including materials science, biologic and medical sciences, metallurgy, semiconductor industry, forensic-science, among others. The applications of SEM for investigating batteries span over a multi-scale range, from the materials level (elemental mapping, primary particle size and shape distributions, etc.) to the cell level (grains, pores, interphases, etc.), complementing other analytical techniques for providing insight on the synthesis, reactivity and failure mechanisms of battery materials.

In a scanning electron microscope the primary beam of electrons is generated by a thermionic (Tungsten) gun or by a field emission gun (LaB<sub>6</sub> or Shotky emitter). Electromagnetic condenser and objective lenses are used, respectively, for reducing the crossover diameter of the primary beam and for forming an electron probe with a nanometric diameter (1-10 nm). A beam deflection system (scan coils) incorporated close to the objective lens moves the probe over the surface of specimen in a rectangular pattern of parallel scanning lines. A fraction of the backscattered or emitted electrons from the specimen are collected by a detector, amplified, and used for generating an image on a display. Fig. 4a shows a diagram of the main components of a scanning electron microscope. The depth of field and resolution of the SEM images relies on the correct setting of the operational variables such as: acceleration voltage, probe current, working distance and aperture, which determine the diameter or the electron probe, its brightness and its convergence angle, respectively.[7]

The signals analysed in SEM are generated or triggered by the interaction of the incident, primary electrons with the atoms of the sample by elastic or inelastic scattering mechanisms, thus creating different signals depending on the penetration and interaction depth, as shown in Fig. 4b. Elastic interaction generates a signal of so-called backscattered electrons (BSE), characterized by changes in the trajectory ( $\theta > 90^\circ$ ) with almost no energy loss, as compared to the primary electrons. The intensity of the BSE signal is a function of the atomic number (Z), and heavier, denser elements will produce

more BSEs. Inelastic interaction generates secondary electrons (SE) by energy transfer from the incident beam to valence or conduction electrons of the sample. A fraction of the transferred energy raises the potential energy of the secondary electrons and these may leave the sample if created from within a small depth below the surface. Secondary electrons created deeper within the sample interact with other atomic electrons and are scattered inelastically.[8]

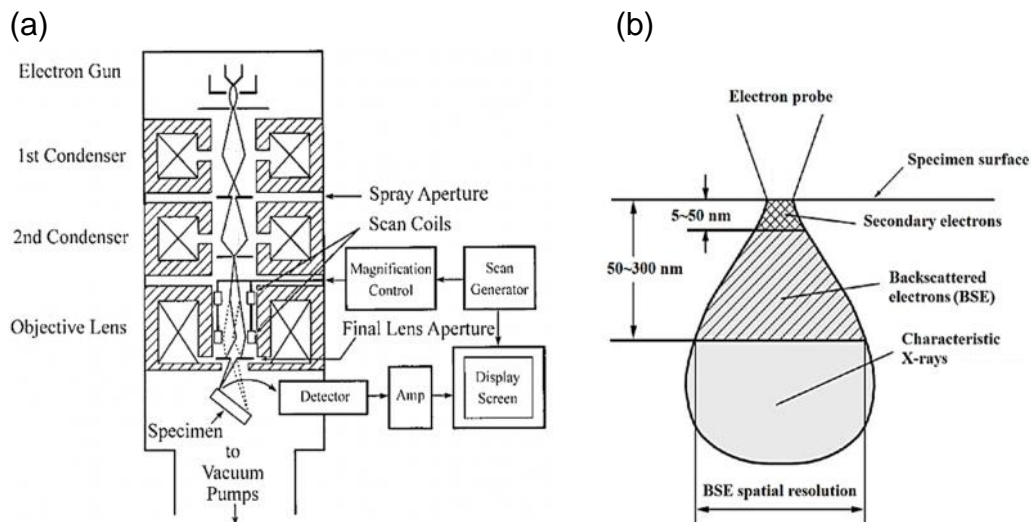


Figure 4. a) Illustration of the components of the scanning electron microscope, and b) the interaction zone of electrons and specimen atoms below a specimen surface. Figures taken from ref. [7].

The simultaneous elastic and inelastic interaction of electrons take place within a defined interaction volume of the sample and provide information from a sampling volume. Thus, the BSE signal may be used for generating SEM images that show brightness contrast due to variations in the chemical composition of the specimen, whereas the SE signal show contrast of the surface structure. Characteristic X-rays and Auger electrons are other kind of signals which are generated by inelastic interaction of the primary electrons with inner shell electrons from the sample. In this type of interactions ionization of the sample is a consequence of relaxation processes in which a higher energy, outer shell electron fills the hole created at the inner shell, thus causing the emission of Auger electrons or X-ray photons. X-ray photons are detected by an energy-dispersive detector and processed for obtaining an energy spectrum from the characteristic x-rays of different elements. In this way, Energy-Dispersive Spectroscopy (EDS) can be used for identifying and quantifying the elements within a sampling spot of a few microns as shown in Fig. 5a-c, and for creating elemental composition maps over

a wider area as shown in Fig. 5d for a composite  $\text{LiFePO}_4$ -based electrode with PEDOT obtained by in battery electropolymerization in one-step.

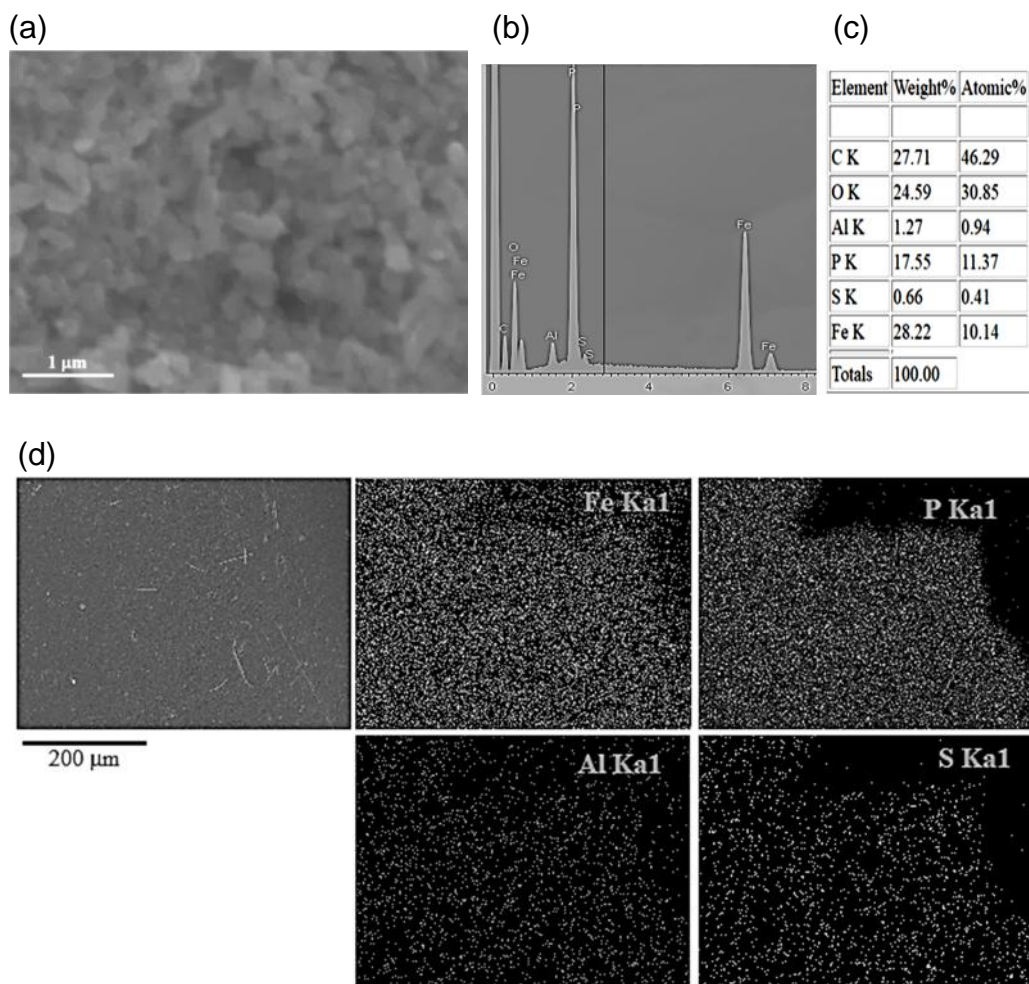


Figure 5. SEM images and EDS analysis of a composite electrode based on  $\text{LiFePO}_4$  with PEDOT obtained by one-step in battery electropolymerization as described in chapter 5. (a) SEM image at 20000x and its corresponding EDX spectrum (b) with the quantification for a set of elements (c). Elemental maps for Fe, P, Al and S (d).



## 5. Mössbauer spectroscopy

Mössbauer spectroscopy (MS) is a resonance method useful for investigating the valence state, spin state, magnetic moment, among other electronic, magnetic and structural properties of certain elements in solid compounds. This technique is based on the nuclear, recoil-free, resonant emission-absorption of  $\gamma$ -rays by certain elements. This effect was initially observed by R. L. Mössbauer in  $^{191}\text{Ir}$ , and it was later described for other elements such as K, Fe, Ni, Zn, Ge, Kr, I, Xe, Cs; among other metallic elements heavier than iron. By recording the spectrum of energies at which so-called Mössbauer nuclei absorb  $\gamma$ -rays of specific energy due to nuclear transitions and perturbations of the nuclear states, valuable information is obtained about the chemical, structural or magnetic environments that surround a nucleus.

The qualitative and quantitative applications of MS in chemistry, physics, material science, biology, as well as in industry are diverse, especially for samples that contain  $^{57}\text{Fe}$  and  $^{119}\text{Sn}$ . For battery-related materials, MS may provide valuable information about compounds with Fe, Ni, Zn, Ge, Ag, Sn, Sb, among other elements, that are either used in commercial Li-ion batteries or that have been tested as components of positive and/or negative electrodes that may undergo insertion, intercalation, conversion or alloying reactions.[9]

Nuclear transitions that concern to Mössbauer spectroscopy are associated to the emission and absorption of  $\gamma$ -rays. For instance, for  $^{57}\text{Fe}$ , the transition from the ground state ( $I = 1/2$ ) to the first excited state ( $I = 3/2$ ) requires an energy of 14.41 keV, which may be provided by a  $^{57}\text{Co}$  source when the later undergoes  $\beta$ -decay. However, one of the limitations for achieving a resonant emission-absorption process is the attenuation of the emitted and the absorbed energy due to the thermal vibrations and to the recoil energy dissipated by momentum transfer upon emission or absorption of  $\gamma$ -rays. The energy values associated to thermal vibrations and recoil are about  $10^6$  times higher than the uncertainty ( $\Delta E = 4.7 \times 10^{-9}$  eV) of the energy associated to the first excited state of  $^{57}\text{Fe}$ , thus the probability for resonant emission-absorption is very small.[10]

The approach followed by R. L. Mössbauer for increasing the efficiency of the resonant emission-absorption consisted in modulating, both through thermal Doppler broadening and Doppler shift, the  $\gamma$ -radiation from the emitter in order to compensate for the energy lost by recoil. Thus, the resonant absorption is increased when both the emitter and the absorber are cooled to liquid nitrogen temperature, and also when either the emitter or the absorber is subjected to mechanical motion. Furthermore, when the atoms of the emitter and the absorber are embedded in a solid lattice, the energy loss by recoil is minimized and resonant absorption takes place to an extent determined by the recoil-free fraction, also known as Lamb-Mössbauer factor. The energy precision of the recoil-free emitted and  $\gamma$ -rays provides enough resolution for triggering and

measuring the nuclear transitions and the hyperfine Interactions, namely: isomer shift (IS), electric quadrupole splitting (QS) and hyperfine magnetic field (HMF).

The isomer shift is related to the electron density close to the nucleus, where the excited state nuclear energy levels are perturbed by the s-electrons, due to variations of the nuclear radius and due to screening effects of valence electrons. For  $^{57}\text{Fe}$ , an increase in the number of 3d-electrons lowers the s-electron density at the nucleus, thus shifting the energy to positive values.[11] Other contributions related to changes in bond length or coordination number also play a significant role in the variation of the isomer shift as shown in Fig. 7.[12]

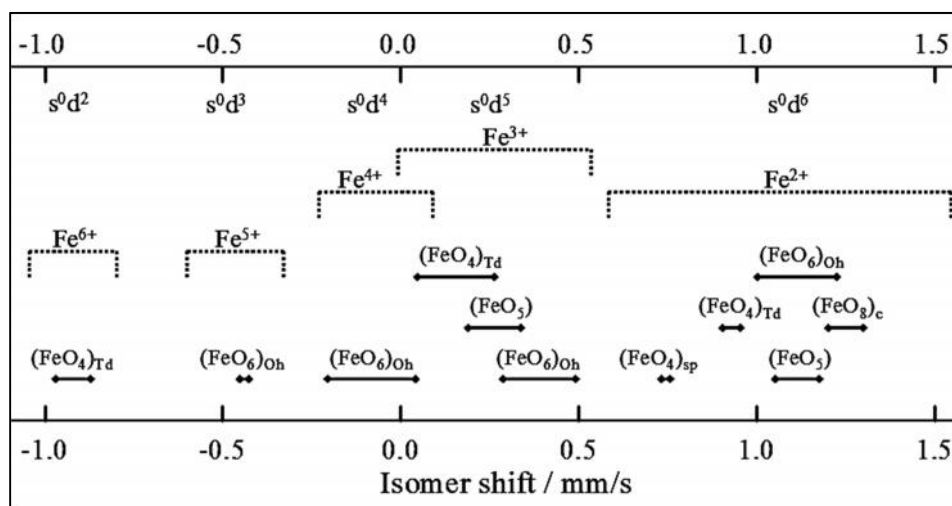


Figure 7. Isomer shifts for  $^{57}\text{Fe}$  in different oxidation states and coordination configurations. Adapted from ref. [12].

The isomer shift is often correlated to the electric quadrupole splitting in order to gain insight into the local atomic arrangement. The electric quadrupole of the nucleus originates from its asymmetry, which varies depending on the nuclear spin in the ground and in the excited state. In a symmetric arrangement of atoms, (e.g. a cubic structure), the nuclear charge distribution has a constant Coulomb energy and a corresponding single line in the Mössbauer spectrum (see Fig. 8a). On the contrary, an electronic distribution of reduced symmetry generates an electric field gradient, which will have different interaction for different alignment of the electric quadrupole moment of the nucleus. Thus, the excited state ( $I=3/2$ ) splits in two levels, which are associated to two lines in the Mössbauer spectrum (see Fig. 8b).

In the presence of a magnetic field, the nuclear spins can be oriented by virtue of its magnetic dipole moment. This magnetic interaction is also known as Magnetic Zeeman

Effect. In  $^{57}\text{Fe}$ , this effect causes the splitting of the ground state into two sub states, and also the splitting of the excited state into four sub states, which together account for the six lines (allowed transitions) in the Mössbauer spectrum shown in Fig. 8c. The relative intensity of the six lines can indicate the orientation of magnetic field with respect the direction in which the  $\gamma$ -rays propagate. The value of the magnetic field splitting provides a measure of the effective magnetic field acting on the nucleus, which may be composed of an externally applied magnetic field or of an internal magnetic field, the later caused primarily by the influence that unpaired 3d electrons valence electrons have on the density of s electrons.

Mössbauer spectra are typically recorded in transmission geometry, the sample being the absorber that contains a stable Mössbauer isotope. The reduced variety of isotopes that can be analyzed by MS is determined by the limited availability of relatively long half-life  $\gamma$ -radiation sources, as the emitter must decay to the same isotope as those to be studied in the sample in order for the nuclear resonance to occur. For the most common Mössbauer nucleus:  $^{57}\text{Fe}$ , the radiation source consists of  $^{57}\text{Co}$  embedded in a rhodium matrix of fcc crystal lattice. The energy modulation of the  $\gamma$ -radiation by Doppler Effect is typically achieved by moving the source in periodical back and forth oscillations, usually of constant acceleration ( $\sim 10$  mm/s for a  $^{57}\text{Co}$  source). Thus, the Mössbauer spectrum displays a count of the x-rays transmitted through the absorber recorded as a function of the Doppler velocity, where the velocity zero is defined as the center of the calibration spectrum.

Recording a Mössbauer spectrum may take hours or days depending on the abundance of the Mössbauer nucleus and the thickness of the sample, which may be in the range of  $1.0 \text{ mg/cm}^2$  of natural iron and less than  $50 \text{ }\mu\text{m}$ , respectively, in order not to cause distortion of the lines. Attenuation of the x-rays from the source is caused by recoil-free resonant absorption in the absorber, although effects such as Compton scattering, mass absorption or other non-resonant absorption processes contribute to the recorded signal that constitute the background and noise

Extraction of Hyperfine parameters from Mössbauer spectra is carried out by using software that analyzes the data through deconvolution and fitting algorithms considering Lorentzian line shapes, Gaussian distribution of Lorentzian or Voigt profiles. Special care must be paid as different types of hyperfine distributions are simultaneously present in a single spectrum. For example, a spectrum that has been broadened by an EFG distribution, or even an HMF distribution, can be fit perfectly with an IS distribution. In such cases it may be necessary to consider correlations between the hyperfine parameters, the use standards or modifying the experimental conditions in order to discern line contributions.[10]

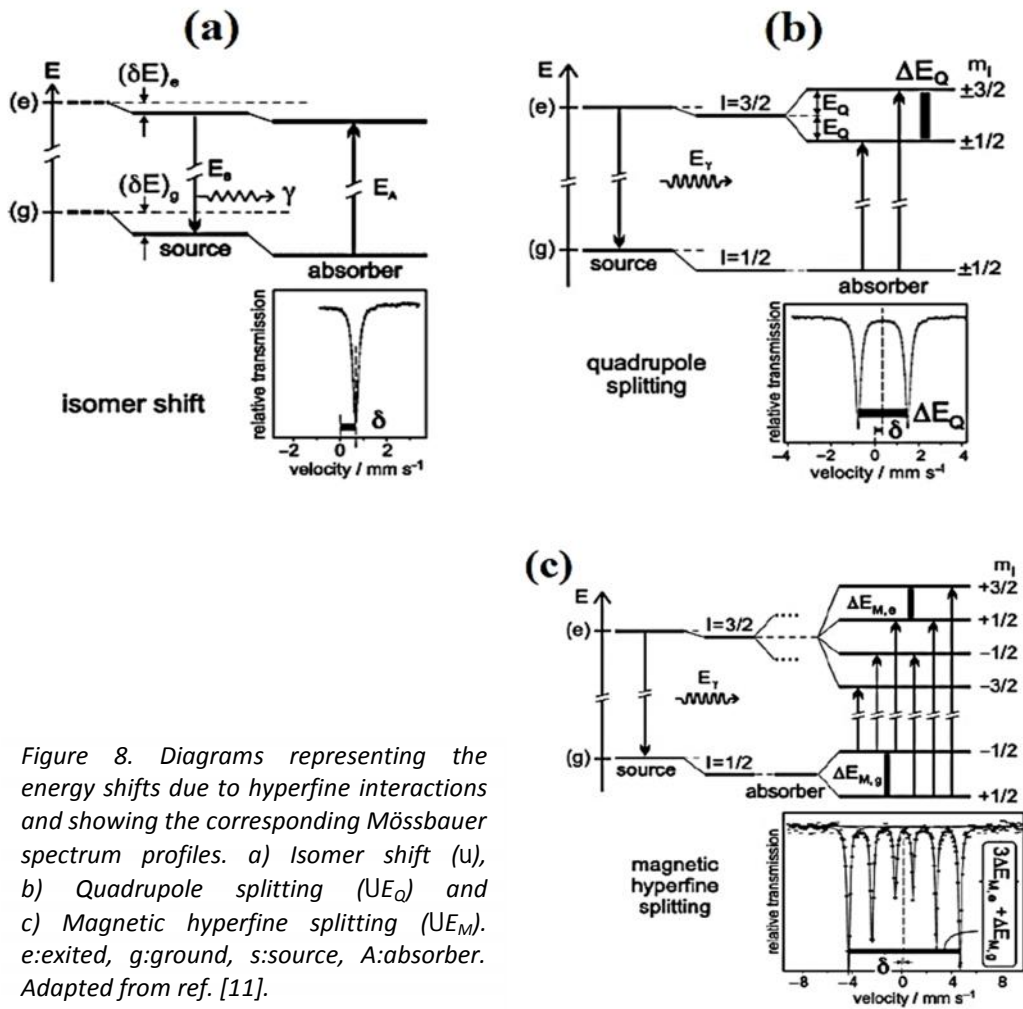


Figure 8. Diagrams representing the energy shifts due to hyperfine interactions and showing the corresponding Mössbauer spectrum profiles. a) Isomer shift ( $\delta$ ), b) Quadrupole splitting ( $\Delta E_Q$ ) and c) Magnetic hyperfine splitting ( $\Delta E_M$ ). e: excited, g: ground, s: source, A: absorber. Adapted from ref. [11].

## References

1. A. J. Bard and L. R. Faulkner, Electrochemical methods fundamentals and applications. 2<sup>nd</sup> edition, New York, NY: John Wiley & Sons, 2001. pp. 307-314.
2. P. Lavela, J. L. Tirado, Baterías Avanzadas. Córdoba: Servicio de publicaciones de la Universidad de Córdoba, 1999, pp. 158-159.
3. J. R. Macdonald and W. B. Johnson, Fundamentals of Impedance Spectroscopy. In: *Impedance Spectroscopy Theory, Experiment, and Applications*. E. Barsoukov and J.R. Macdonald (Eds.), New York, NY: John Wiley & Sons, Inc., 2005, p 13.
4. M.E. Orazem and B. Tribollet, Electrochemical impedance spectroscopy. New York, NY: John Wiley & Sons, Inc., 2008, p 233.
5. J. J. Weimer, X-ray photoelectron spectroscopy. In: *Characterization of materials*, E. N. Kaufmann (Ed.). 1<sup>st</sup> edition, Hoboken, NJ: John Wiley & Sons, Inc., 2003.
6. C. C. Chusuei and D. W. Goodman, X-ray photoelectron spectroscopy. In: *Encyclopedia of physical science and technology*, R. A. Meyers (Ed.). 3<sup>rd</sup> edition, San Diego: Academic Press, 2003.
7. Y. Leng, Materials Characterization—Introduction to Microscopic and Spectroscopic Methods. Singapore: John Wiley & Sons (Asia) Pte Ltd., 2008, pp. 122, 129, 134.
8. B. Fultz, Electron techniques—Scanning electron Microscopy. In: *Characterization of materials*, E. N. Kaufmann (Ed.). 1<sup>st</sup> edition, Hoboken, NJ: John Wiley & Sons, Inc., 2003, pp. 1050-1052.
9. R. Alcántara, P. Lavela, C. Pérez Vicente and J. L. Tirado, Applications of Mössbauer spectroscopy in the study of battery materials. In: *Mössbauer Spectroscopy: Applications in Chemistry, Biology, Industry, and Nanotechnology*, V. K. Sharma, G. Klingelhofer and T. Nishida (Eds.). Somerset, NJ: John Wiley & Sons, 2013. 552-555.
10. B. Fultz, Mössbauer spectrometry. In: *Characterization of materials*, E. N. Kaufmann (Ed.). 1<sup>st</sup> edition, Hoboken, NJ: John Wiley & Sons, Inc., 2003, pp. 818, 820, 831.
11. P. Gütlich, E. Bill and A. X. Trautwein, Mössbauer Spectroscopy and Transition Metal Chemistry, New York, NY: Springer-Verlag Berlin Heidelberg, 2011, pp. 79, 93, 103.
12. F. Menil, Systematic trends of the <sup>57</sup>Fe Mössbauer isomer shifts in (FeOn) and (FeFn) polyhedra. Evidence of a new correlation between the isomer shift and the inductive effect of the competing bond T-X (→ Fe) (where X is O or F and T any element with a formal positive charge), J. Phys. Chem. Solids, 1985, 46(7), 763–789.

# Appendix IV

## Conference abstracts and posters

- Improved cycling performance of  $\text{LiFePO}_4$  cathode material by coating with PEDOT conducting. Presented at the 64th ISE Meeting, Quéretaro, México, 2013.



- Polimerización electroquímica de alquilendioxitiofeno sobre fosfato de litio y hierro para cátodos de baterías de iones litio. Presented at Nano UCO V, Córdoba, España, 2015.



- Judicious design of lithium iron phosphate electrodes with poly(3,4-ethylenedioxythiophene):polystyrene sulfonate for high performance battery. Presented at ABAA8, Bilbao, España, 2015.



## Improved cycling performance of $\text{LiFePO}_4$ cathode material by coating with PEDOT conducting polymer

D. Cíntora-Juárez<sup>a</sup>, C. Pérez-Vicente<sup>a</sup>, Shahzada Ahmad<sup>b</sup>, J. L. Tirado<sup>a</sup>

<sup>a</sup>*Laboratorio de Química Inorgánica, Campus de Rabanales, Universidad de Córdoba 14071 Córdoba, Spain*

<sup>b</sup>*Campus Palmas Altas, C/ Energía Solar, Abengoa Research  
41014-Sevilla, Spain  
z02cijud@uco.es*

Lithium-ion batteries incorporating  $\text{LiFePO}_4$  or other  $\text{LiMPO}_4$  (M= Mn, Co, Ni) olivine compounds as cathode material are very attractive in terms of safety, energy and power density, general performance and cost. Unfortunately, these olivine compounds have low electronic conductivity and poor ionic diffusivity, which cause bad cycling performance in Li-ion batteries. Strategies to improve their electrochemical activity include the use of carbon or conducting polymers, the control of the particle size and morphology, blending with carbon or metallic additives, ionic doping or substitution in the crystalline lattice, among other approaches [1-2]. Within this context, we explored different routes to prepare PEDOT [Poly(3,4-ethylenedioxythiophene)] conducting polymer coatings on  $\text{LiFePO}_4$ .

We have observed that electropolymerization over the cathode improves the cycling performance of bare  $\text{LiFePO}_4$ . The reasons for this improved performance could be attributed to enhanced electronic and ionic conductivities, as reflexed from the low charge/discharge polarization and the impedance of the battery. Optimization of the cathode's composition and implementation of the different preparation methods to obtain composites with other  $\text{LiMPO}_4$  olivine compounds are under progress.

### References

1. B. Kang, G. Ceder, Nature Letters 1 (2009) 190.
2. L. X. Yuan, Z. H. Wang, W. X. Zhang, X. L. Hu, J. T. Chen, Y. H. Huang, J. B. Goodenough, Energy Environ Sci. 4 (2011) 269.

## Improved cycling performance of LiFePO<sub>4</sub> cathode material with poly(3,4 ethylenedioxythiophene)

ABENGOA  
RESEARCH

D. Cíntora-Juárez<sup>a</sup>, C. Pérez-Vicente<sup>a</sup>, Shahzada Ahmad<sup>b</sup>, J. L. Tirado<sup>a</sup>  
<sup>a</sup>Laboratorio de Química Inorgánica, Campus de Rabanales, Universidad de Córdoba  
 14071-Córdoba, Spain.  
<sup>b</sup>Campus Palmas Altas, C/ Energía Solar, Abengoa Research  
 41014-Sevilla, Spain



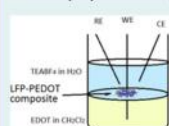
### 1. INTRODUCTION

Lithium-ion batteries incorporating LiFePO<sub>4</sub> or other LIMPO<sub>4</sub> (M= Mn, Co, Ni) olivine-related compounds are very attractive in terms of **safety, energy and power density, general performance and cost**. However, these compounds have **low electronic conductivity and poor ionic diffusivity**, which cause bad cycling performance in Li-ion batteries. **Improvement of the electronic conductivity** and the general electrochemical performance can be achieved by **incorporating conducting polymers** to the electrode. **LiFePO<sub>4</sub> composites with poly(3,4-ethylenedioxythiophene) [PEDOT]** are specially attractive in terms of high electronic conductivity, mechanical stability and the ability to improve Li-ion transport [1-4].

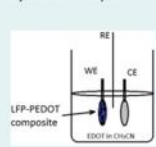
### 2. METHODS

#### Preparation of LFP-PEDOT and LFP/C-PEDOT composites

#### a) Three phase Electro-polymerization[4]



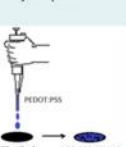
#### b) Electro-deposition



#### c) Blending

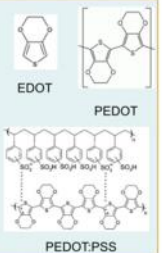


#### d) Deposit



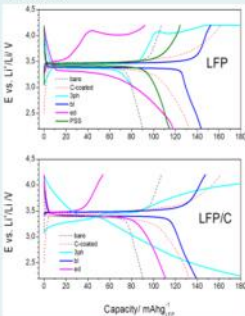
#### Samples

Sample	LFP/PEDOT weight ratio
LFP	100:0
LFP-3ph	70:30
LFP-bl	80:20
LFP-ed	78:22
LFP-PSS	80:20
LFP/C	100:0
LFP/C-3ph	70:30
LFP/C-bl	80:20
LFP/C-ed	87:13



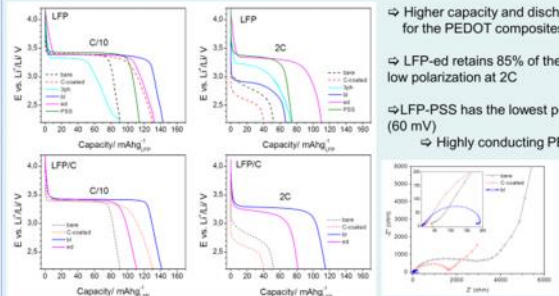
### 3. RESULTS

#### 1st charge/discharge profiles at C/10



- ⇒ Abnormal charge profiles for LFP-bl and LFP-ed composites
- ⇒ Oxidation of LFP
- ⇒ Redox activity of EDOT/PEDOT at ca. 4 V
- ⇒ LFP-bl performs well **without carbon coating and any additives**.
- ⇒ Optimization still needed to achieve higher capacity

#### Discharge at low and high rate

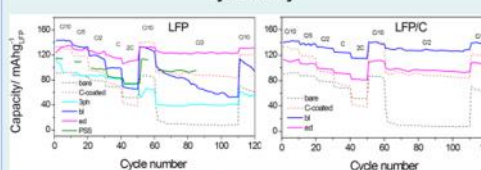


- ⇒ Higher capacity and discharge voltage for the PEDOT composites
- ⇒ LFP-ed retains 85% of the initial capacity with low polarization at 2C
- ⇒ LFP-PSS has the lowest polarization at 2C (60 mV)
- ⇒ Highly conducting PEDOT:PSS

#### Cell impedance

- ⇒ Lower impedance for the LFP-bl composites
- ⇒ PEDOT improves the total conductivity

#### Cycleability



- ⇒ LFP-ed outperforms LFP/C
- ⇒ good reversible capacity at 2C
- ⇒ notable capacity retention and
- ⇒ low charge/disch. polarization
- ⇒ LFP/C-bl has excellent performance without CB and PVDF additives

### 5. REFERENCES

- [1] A.K. Padhi, K.S. Nanjundaswamy, J.B. Goodenough, J. Electrochem. Soc. 144 (4) (1997) 1188.
- [2] A. V. Murugan, T. Muraligarthi, A. Manthiram, Electrochem. Commun. 10(2008) 903.
- [3] K. Abe, Y. Ushigoe, H. Yoshitake, M. Yoshio, J. Power Sources 153 (2006) 325.
- [4] N.D. Trinh, M. Saunier, D. Lepage, S.B. Schougaard, J. Power Sources 221(2013) 284.

### 4. CONCLUSION

The LiFePO<sub>4</sub>/PEDOT composite obtained by electro-deposition over the cathode showed the best cycling performance, with a reversible capacity of ca. 110 mAh g<sup>-1</sup> at 2C, a notable capacity retention at C/2 (125 mAh g<sup>-1</sup> after 50 cycles) and low charge/discharge polarization. The improved performance is ascribed to an enhanced electronic and ionic conductivity emerging from the polymer. The combination of carbon coating and PEDOT coating is not necessary to improve the performance of the phosphate.



## POLIMERIZACIÓN ELECTROQUÍMICA DE ALQUILENDIOXITIOFENO SOBRE FOSFATO DE LITIO Y HIERRO PARA CÁTODOS DE BATERÍAS DE IONES LITIO

**Daniel Cíntora-Juárez<sup>a</sup>, Carlos Pérez-Vicente<sup>a</sup>, Shahzada Ahmad<sup>b</sup> y José Luis Tirado<sup>a</sup>**

<sup>a</sup> *Laboratorio de Química Inorgánica, Campus de Rabanales, Universidad de Córdoba, 14071, España.*

<sup>b</sup> *Abengoa Research, C/ Energía Solar 11, Campus Palmas Altas, 41014, España.*

Hoy en día las baterías de iones litio se emplean en los dispositivos electrónicos portátiles más comunes y en años recientes se ha planteado su uso en vehículos eléctricos. Entre los diferentes compuestos disponibles para el electrodo positivo (cátodo), el fosfato de litio y hierro (LiFePO<sub>4</sub>), inicialmente propuesto por Padhi et al.<sup>1</sup>, ofrece ventajas por su estabilidad térmica y su buen desempeño electroquímico. Para obtener la mayor capacidad del LiFePO<sub>4</sub> a cinéticas de descarga rápidas es necesario incrementar su conductividad iónica y electrónica, lo cual es posible mediante la nanoestructuración y la formación de recubrimientos de carbón sobre nanopartículas de LiFePO<sub>4</sub>.<sup>2,3</sup> Respecto a la formación de recubrimientos de carbón, el método más común consiste en la calcinación de azúcares a temperaturas entre 500-800° C.<sup>4</sup> Desafortunadamente, tales métodos implican un alto consumo energético, además de la generación directa de gases contaminantes.

Se ha demostrado que al incorporar polímeros conductores producidos por vía química o electroquímica a electrodos basados en LiFePO<sub>4</sub> y otros materiales activos se mejora notablemente el desempeño. Cuando la polimerización se efectúa en ausencia del material activo y posteriormente se mezcla con éste, el contacto no es óptimo, lo que limita la utilización de toda la capacidad del electrodo. Por otra parte, en los métodos de polimerización directa sobre LiFePO<sub>4</sub> o Li<sub>1-x</sub>FePO<sub>4</sub> se emplean disolventes y oxidantes que pueden generar subproductos que afecten a los componentes de la batería.<sup>5,6</sup>

Recientemente hemos propuesto un método sencillo para polimerizar 3,4-alquilendioxitiofeno directamente sobre LiFePO<sub>4</sub> durante la primera carga dentro de una batería de prueba.<sup>7</sup> La polimerización se efectúa en presencia de Li<sub>1-x</sub>FePO<sub>4</sub> (conteniendo Fe<sup>3+</sup>) que actúa como oxidante y sustrato. De esta forma se crea un cableado a nivel del electrodo que facilita la transferencia de carga y la movilidad iónica entre partículas del material activo. El cambio de estado de oxidación del hierro y la variación de la impedancia del electrodo a diferentes estados de carga se estudiaron mediante espectroscopía Mössbauer e impedancia electroquímica, respectivamente. Cuando la polimerización se lleva a cabo dentro de la propia batería, se obtienen de manera fácil electrodos con valores de capacidad más altos y de mejor fiabilidad al ciclar respecto al material de referencia.

<sup>1</sup> Padhi, A.K.; Nanjundaswamy K.S.; Goodenough J.B., *J. Electrochem. Soc.*, **2007**, 144(4), 1188.

<sup>2</sup> Yamada, A.; Chung, S.; Hinokuma, K., *J. Electrochem. Soc.*, **2001**, 148, A224.

<sup>3</sup> Ravet, N.; Chouinard, Y.; Magnan, J.F.; Besner, S.; Gautier, M.; Armand, M., *J. Power Sources*, **2001**, 97, 503.

<sup>4</sup> Chen Z.; Dahn, J. *J. Electrochem. Soc.*, **2002**, 149, A1184.

<sup>5</sup> Trinh, N.D.; Saulnier, M.; Lepage, D.; Schougaard, S.B.; *J. Power Sources*, **2013**, 221, 284.

<sup>6</sup> Lepage, D.; Michot, C.; Liang, G.; Gauthier, M.; Schougaard, S.B.; *Angew. Chem. Int. Ed.* **2011**, 50, 6884.

<sup>7</sup> Cíntora-Juárez, D.; Pérez-Vicente, C.; Ahmad, S.; Tirado, J.L., *Phys. Chem. Chem. Phys.*, **2014**, 16, 20724.

## POLIMERIZACIÓN ELECTROQUÍMICA DE ALQUILENDIOXITIOFENO SOBRE nano-LiFePO<sub>4</sub> PARA CÁTODOS DE BATERÍAS DE IONES LITIO



**D. Cíntora-Juárez<sup>a</sup>, C. Pérez-Vicente<sup>a</sup>, Shahzada Ahmad<sup>b</sup>, J. L. Tirado<sup>b</sup>**  
<sup>a</sup>Laboratorio de Química Inorgánica, Campus de Rabanales, Universidad de Córdoba  
 14071-Córdoba, Spain.  
<sup>b</sup>Campus Palmas Altas, C/ Energía Solar, Abengoa Research, 41014-Sevilla, Spain



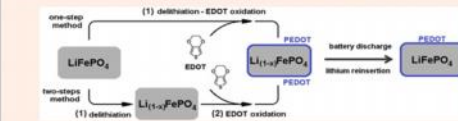
### 1. INTRODUCCIÓN

La incorporación de polímeros conductores a electrodos basados en LiFePO<sub>4</sub> u otros materiales activos se mejora notablemente el desempeño en carga/descarga.<sup>1-3</sup> Cuando la polimerización se efectúa en ausencia del material activo y posteriormente se mezcla con éste, el contacto no es óptimo, lo que limita la utilización de toda la capacidad del electrodo.

Se propone un método sencillo para polimerizar alquilandioxitiofeno directamente sobre nanopartículas de LiFePO<sub>4</sub> durante la primera carga dentro de una batería de prueba.<sup>4</sup> La polimerización se efectúa en presencia de Li<sub>1-x</sub>FePO<sub>4</sub> que actúa como oxidante y sustrato. De esta forma se crea un cableado a nivel del electrodo que facilita la transferencia de carga y la movilidad iónica entre partículas del material activo, resultando en un notable aumento de la capacidad.

### 2. MÉTODOS

Polimerización sobre Li<sub>1-x</sub>FePO<sub>4</sub> en una o en dos etapas

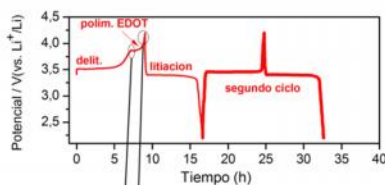


**Técnicas de caracterización:**

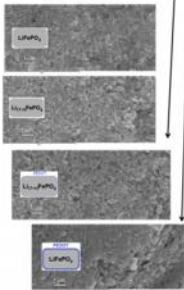
- Microscopía electrónica (SEM)
- Espectroscopia Mössbauer
- Carga/descarga a diferentes valores de corriente (C-rate)
- Espectroscopia de impedancia

### 3. RESULTADOS

#### a) Polimerización de EDOT sobre Li<sub>1-x</sub>FePO<sub>4</sub>

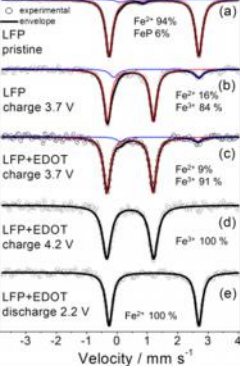


Evolución de la superficie del electrodo

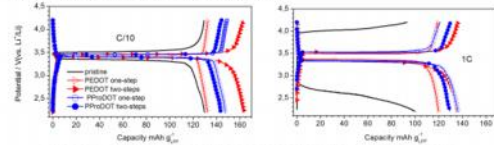


➢ Recubrimiento de polímero conductor sobre nano LiFePO<sub>4</sub>

Variación de estado de oxidación del hierro en función de estado de carga

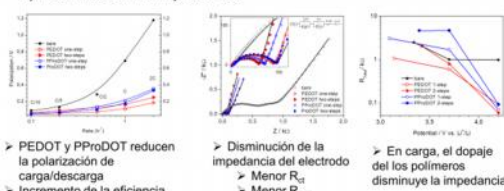


#### b) Ciclado inicial lento y moderado



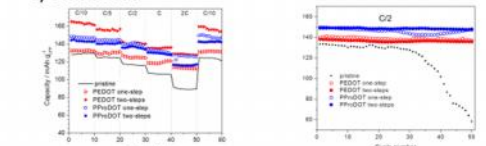
- Mayor capacidad y potencial de descarga más alto para los composites
- Hasta 97 % de la capacidad teórica (170 mAh/g) a C/10

#### c) Polarización e impedancia



- PEDOT y PProDOT reducen la polarización de carga/descarga
- Incremento de la eficiencia energética
- Disminución de la impedancia del electrodo
- Menor R<sub>ct</sub>
- Menor R<sub>SEI</sub>
- En carga, el dopaje de los polímeros disminuye la impedancia

#### d) Ciclabilidad



- Mejor ciclabilidad para los composites con PEDOT y PProDOT
- Descarga de hasta 136 mAh/g a C con PEDOT
- Mayor retención de capacidad con PEDOT y PProDOT
- Hasta 150 mAh/g a C/2 con PProDOT

### REFERENCIAS

1. Lepage, D.; Michot, C.; Liang, G.; Gauthier, M.; Schougaard, S.B.; *Angew. Chem. Int. Ed.* **2011**, *50*, 6884.
2. Huang, Y. & Goodenough, J. B.; *Chem. Mater.* **2008** (3), 7237–7241.
3. Cíntora-Juárez, D., Pérez-Vicente, C., Ahmad, S., & Tirado, J. L. *RSC Advances*, **(2014)** 4(50), 26108.
4. Cíntora-Juárez, D.; Pérez-Vicente, C.; Ahmad, S.; Trado, J.L., *Phys. Chem. Chem. Phys.*, **2014**, *16*, 20724.

### 4. CONCLUSIÓN

Es posible polimerizar EDOT o ProDOT sobre nano-LiFePO<sub>4</sub> dentro de una batería de prueba. El polímero conductor se forma tras la primera carga de la batería y proporciona un cableado molecular entre nanopartículas de LiFePO<sub>4</sub> disminuye la resistencia a la transferencia y transporte de carga. El resultado es una mayor capacidad a corrientes elevadas y una ciclabilidad superior comparada con el LiFePO<sub>4</sub> sin recubrimiento conductor. Los métodos propuesto constituyen una estrategia sencilla y escalable para preparar electrodos más eficientes a temperatura ambiente.

## Judicious design of lithium iron phosphate electrodes with poly(3,4 ethylenedioxythiophene):polystyrene sulfonate for high performance battery

Daniel Cíntora Juárez<sup>1</sup>, Carlos Pérez Vicente<sup>1</sup>, Samrana Kazim<sup>2</sup>, Shahzada Ahmad<sup>2</sup>, José Luis Tirado<sup>1</sup>

<sup>1</sup>Laboratorio de Química Inorgánica, Campus de Rabanales, Universidad de Córdoba, 14071, Spain.

<sup>2</sup>Abengoa Research, Abengoa, C/ Energía Solar nº 1, Campus Palmas Altas, 41014, Spain.

Lithium-ion batteries are the most advanced energy storage technology for portable electronics and are also considered for electric-vehicle applications. Different materials are available for the cathode and anode in a lithium-ion battery, however, due to safety and performance reasons, some of them are unsuitable for use in electric vehicles. LiFePO<sub>4</sub> (LFP), firstly described by Padhi *et al.*<sup>1</sup>, offers advantages as a cathode active material in terms of power and energy density, as well as lower cost and reduced environmental impact compared to lithium transition metal oxides.<sup>2</sup> The synthesis and optimization efforts around LFP have focused mainly on decreasing the particle size and creation of conducting coatings in order to achieve fast lithiation kinetics and electronic conductivity, which are paramount for high charge/discharge currents.<sup>2</sup> LFP composite electrodes are mainly composed of carbon-coated LFP mixed with PVDF-based binders and carbon particles as electron conducting additive. However in such formulations the electrical contact between active particles is limited by the homogeneity of the carbon coating over LFP and by the amount of carbon additive. Thus an additive able to extend the electronic communication between LFP particles and the current collector is most sought after. For this purpose, common cathode active materials have been combined with conducting polymers due to their mechanical stability and their ability for charge transport.<sup>3</sup>

Here we describe the preparation of LFP-based electrodes with different architectures using poly(3,4-ethylenedioxythiophene)-polystyrene sulfonate (PEDOT:PSS) as mixed conductor additive. We found that the discharge capacity and potential of LFP electrodes at fast rates can be substantially improved by the presence of the conducting polymer within the bulk of the electrode and more notably when the polymer is coated over the aluminium current collector (Figure 1). Further to increase the conductivity small amounts of ethylene glycol or dimethyl sulfoxide were added to PEDOT:PSS. The superior electrochemical performance was ascribed to the low initial impedance and load resistance of the composite electrodes with conducting polymer. Furthermore <sup>57</sup>Fe Mössbauer and XPS spectroscopies were used, respectively, to follow the bulk transformation of the LFP active material and the surface changes of the composite electrodes upon lithiation.

### References:

1. A.K. Padhi, K.S. Nanjundaswamy and J.B. Goodenough. *J. Electrochem. Soc.* 1997, **144**, 1188.
2. Yuan, L.-X., Wang, Z.-H., Zhang, W.-X., Hu, X.-L., Chen, J.-T., Huang, Y.-H., & Goodenough, J. B., *Ener. Environ. Sci.*, 2011, **4**, 269.
3. Cíntora-Juárez, D., Pérez-Vicente, C., Ahmad, S., & Tirado, J. L., *RSC Advances*, 2014, **4**, 26108.

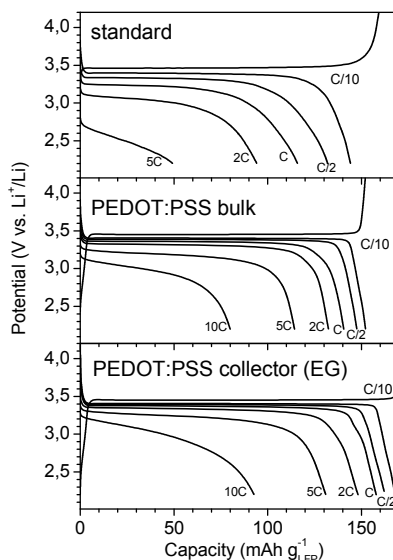


Figure 1. Electrochemical performance of the standard electrode and two composite electrodes with conducting polymer.

**ABAA8**  
Bilbao 2015

**Judicious design of lithium iron phosphate electrodes with poly(3,4-ethylenedioxythiophene):polystyrene sulfonate for high performance battery**

**D. Cíntora-Juárez<sup>a</sup>, C. Pérez-Vicente<sup>a</sup>, Samrana Kazim<sup>b</sup>, Shahzada Ahmad<sup>b</sup>, J. L. Tirado<sup>a</sup>**

<sup>a</sup>Laboratorio de Química Inorgánica, Campus de Rabanales, Universidad de Córdoba, 14071-Córdoba, Spain.

<sup>b</sup>Campus Palmas Altas, C/ Energía Solar, Abengoa Research, 41014-Sevilla, Spain



**ABENGOA  
RESEARCH**

### 1. INTRODUCTION

$\text{LiFePO}_4$  (LFP) offers better thermal stability and power density compared to  $\text{LiCoO}_2$ . LFP composite electrodes are mainly composed of carbon-coated LFP mixed with binders and carbon as electron conducting additive.<sup>1</sup> However, in such formulations the **electrical contact between active particles is limited by the homogeneity of the carbon coating over LFP** and by the amount of carbon additive. Thus, other strategies to extend the **electronic communication between LFP particles and the current collector** are most sought after.<sup>2a-b</sup> Here we describe the preparation of LFP-based electrodes with different architectures using **poly(3,4-ethylenedioxythiophene)-polystyrene sulfonate (PEDOT:PSS) as mixed conductor additive.**<sup>3</sup>

### 2. APPROACHES AND METHODS

#### ➤ Different electrode architectures

#### ➤ Conductivity enhancement of PEDOT:PSS by secondary doping with ethylene glycol (EG)

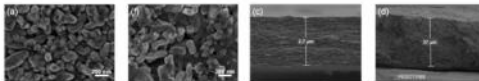


#### Characterization techniques:

- Electron microscopy (SEM)
- Galvanostatic cycling
- Mössbauer spectroscopy
- Impedance spectroscopy
- XPS

### 3. RESULTS

#### a) SEM



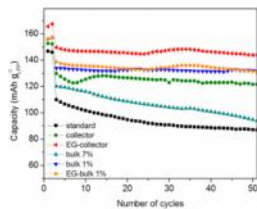
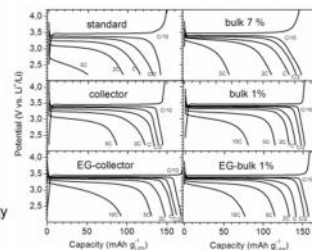
#### ➤ Coating and network of PEDOT:PSS

#### b) Galvanostatic cycling

#### ➤ Higher capacity and/or voltage for all samples with PEDOT:PSS

#### ➤ bulk 1% PEDOT:PSS increases both voltage and capacity

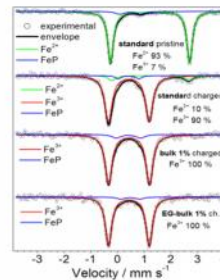
#### ➤ Doping with ethylene glycol boost voltage and/or capacity



- EG-doped PEDOT:PSS coating over current collector (EG-collector) shows the best performance, 145 mAh/g @ 2C
- Undoped bulk 1% PEDOT:PSS shows practical rate capability and cycle stability

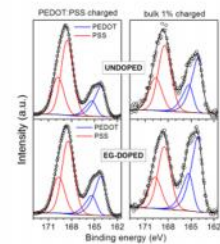
#### c) Mössbauer spectroscopy

- 1 % w PEDOT:PSS promotes higher efficiency of  $\text{Fe}^{2+}$  to  $\text{Fe}^{3+}$  oxidation



#### d) XPS

- Ethylene glycol increases the fraction of the conducting PEDOT phase in PEDOT:PSS

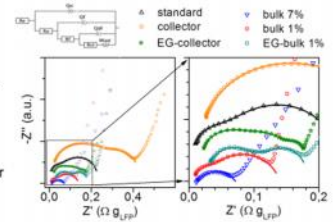


#### e) Impedance spectroscopy

#### ➤ Comparison of impedance in charged state

#### ➤ PEDOT:PSS lowers the impedance of most electrodes

#### ➤ PEDOT:PSS coating over the current collector affects the high freq. impedance



### REFERENCES

1. Yuan, L.-X., Wang, Z.-H., Zhang, W.-X., Hu, X.-L., Chen, J.-T., Huang, Y.-H., & Goodenough, J. B., *Ener Environ Sci*, **2011**, 4, 269.
2. a) D. Cíntora-Juárez, C. Pérez-Vicente, S. Ahmad and J. L. Tirado, *RSC Adv.*, **2014**, 4(50), 26108. b) D. Cíntora-Juárez, C. Pérez-Vicente, S. Ahmad and J. L. Tirado, *Phys. Chem. Chem. Phys.*, **2014**, 16(38), 20724.
3. D. Cíntora-Juárez, C. Pérez-Vicente, S. Kazim, S. Ahmad and J. L. Tirado, *J. Mater. Chem. A*, **2015**, 3, 14254.

### 4. CONCLUSION

**PEDOT:PSS** was successfully mixed with  $\text{LiFePO}_4$ , carbon black and PVDF for preparing **composite electrodes** that showed **mechanical stability and improved electrochemical activity** for the insertion/extraction of lithium. **1 % w of PEDOT:PSS** additive within the bulk is enough in order to form an **electrode that outperforms the standard. Ethylene glycol boosts the conductivity of PEDOT:PSS** coated over the electrode's current collector or present within the bulk of the electrode. Thus, it seems that the interphase of the electrodes that limits high rate performance is the **interphase between the active material particles and the current collector.**



# Appendix V

## Author's biodata

**DANIEL CÍNTORA JUÁREZ, 1984, Mexico City, Mexico.**

- MSc. Materials for Energy Storage and Conversion, Aix-Marseille Université, Warsaw University of Technology, Université de Picardie Jules Verne and Universidad de Córdoba, 2011.
- BSc. Chemistry, Universidad Nacional Autónoma de México (UNAM), 2008.

### *RESEARCH INTERESTS*

Electroanalysis, synthesis and characterization of energy-related materials: conducting polymers, polymer electrolytes, inorganic compounds, composite electrodes; and their application in devices for energy storage & conversion.

### *BIOGRAPHIC STATEMENT*

As an undergraduate student, I participated in short internships in the fields of electroanalysis, environmental pollution and synthesis of materials. I majored in electrochemistry and synthesized and characterized catalysts for methanol fuel cells at the Electrochemical Engineering Lab. at UNAM, under the supervision of Dr. Pedro Roquero. These early experiences provided me a first contact with the work in scientific research, and sparked my interest for enrolling in a master's program on energy technology. I was awarded an Erasmus Mundus Scholarship in the MESC master's program, and I followed courses in three different European universities, where I learnt fundamental and practical aspects of materials and technologies for energy storage and conversion from experts in the field. Under the supervision of Dr. Renaud Bouchet at MADIREL Lab. (Aix-Marseille Université), my master's thesis focused on the measurement of transport and mechanical properties of block co-polymer electrolytes and their application in lithium metal batteries, with lithium iron phosphate or sulfur as cathode materials.

I also have deep interest in technology transfer and I have completed several introductory courses on intellectual property and business management. This training has allowed me to carry out my work having always in mind that applied research not only has to be acknowledged and promoted, but also that it entails the responsibility of contributing to social progress.

I have co-authored 9 research papers, a book chapter and a patent application.







